AD-779 400

PREDICTION OF HAZARDS OF SPILLS OF ANHYDROUS AMMONIA ON WATER

ARTHUR D. LITTLE, INCORPORATED

PREPARED FOR
COAST GUARD

MARCH 1974

Technical Report Documentation Page

1. Report No.	2. Government Accession No.	3. Recipient's Catalog No.
CG-D-74-74		AD 779400

4. Title and Subtitle	5. Report Date
Prediction of Hazards of Spills of Anhydrous Ammonia on Water	March 1974
	6. Performing Organization Code
7. Author(s)	8. Performing Organization Report No.
Raj, P.K., Hagopian, J., and Kalelkar, A.S.	Report No. 74763
9. Performing Organization Name and Address	10. Work Unit No. (TRAIS)
Arthur D. Little, Inc. Acorn Park Cambridge, Massachusetts 02140	3125.11
	11. Contract or Grant No. DOT-CG-22, 182-A
12. Sponsoring Agency Name and Address	13. Type of Report and Period Covered
U.S. Coast Guard Office of Research and Development Marine Safety Technology Division Washington, D.C. 20590	Final Report
	14. Sponsoring Agency Code
15. Supplementary Notes	

16. Abstract During the past decade, maritime transport of liquid anhydrous ammonia (LNH_3) on the Inland and Coastal waters of the United States[1] has increased rapidly. Anhydrous ammonia is carried on barges as a high-pressure, liquefied cargo in heavy-wall steel tanks, and as a low-temperature cargo in essentially atmospheric-pressure refrigerated tanks. The frequent movement of bulk quantities of LNH_3 on United States waters poses a potential hazard to the public, to aquatic life, and to other shipping should there be an accidental surface or underwater release of ammonia. Although the explosion and fire hazard of such a spill is limited[2,3], the health and pollution hazard is not insignificant. The United States Coast Guard (USCG) recognized the need to evaluate large accidental spills of LNH_3 and, in April 1972, asked Arthur D. Little, Inc. (ADL) to study the phenomena associated with surface and underwater ammonia spills. The purpose of the study was to develop a thorough understanding of the physio-chemical behavior of ammonia/water reactions, develop analytical models, and conduct a scaled experimental program to verify and modify the models for use in predicting the potential hazards due to spills of one up to 3,000 tons of LNH_3.

This report contains the results of an experimental and analytical program aimed at evaluating the hazards presented by a 3,000 ton release of liquid anhydrous ammonia on water. Test spills were conducted in the laboratory (up to 1/2 gallons), in a swimming pool (5 gallons) and in a lake (50 gallon size) and the fraction of released ammonia dissolving in water and the amount vaporizing were determined. The dispersion of vapor in air was measured and a theory was developed to predict the movement. Analytical models to predict water dispersion are also presented.

17. Key Words	18. Distribution Statement
Hazardous Materials Anhydrous Ammonia Vapor Clouds	Document is available to the public through the National Technical Information Service, Springfield, Va 22151

19. Security Classif. (of this report)	20. Security Classif. (of this page)	21. No. of Pages	22. Price
Unclassified	Unclassified	257	$6.50

Form DOT F 1700.7 (8-72) Reproduction of completed page authorized

ACKNOWLEDGMENTS

In the course of conducting this study, substantial contributions were made by James C. Burke and W. David Lee of Arthur D. Little, Inc. In addition, Professor Robert C. Reid of the Massachusetts Institute of Technology provided several valuable technical inputs.

This work was performed under contract with the Office of Research and Development, U. S. Coast Guard, under the technical supervision of Dr. John Cece.

TABLE OF CONTENTS

TABLE OF CONTENTS (cont)

TABLE OF CONTENTS (cont)

TABLE OF CONTENTS (cont)

TABLE OF CONTENTS (cont)

LIST OF TABLES

LIST OF TABLES

(Continued)

LIST OF FIGURES

LIST OF FIGURES

(Continued)

LIST OF FIGURES

(Continued)

LIST OF FIGURES

(Continued)

1. SUMMARY

1.1 PURPOSE

During the past decade, maritime transport of liquid anhydrous ammonia (LNH_3) on the Inland and Coastal waters of the United States [1] has increased rapidly. Anhydrous ammonia is carried on barges as a high-pressure, liquefied cargo in heavy-wall steel tanks, and as a low-temperature cargo in essentially atmospheric-pressure refrigerated tanks. The frequent movement of bulk quantities of LNH_3 on United States waters poses a potential hazard to the public, to aquatic life, and to other shipping should there be an accidental surface or underwater release of ammonia. Although the explosion and fire hazard of such a spill is limited, [2,3] the health and pollution hazard is not insignificant.

The United States Coast Guard (USCG) recognized the need to evaluate large accidental spills of LNH_3 and, in April 1972, asked Arthur D. Little, Inc. (ADL) to study the phenomena associated with surface and underwater ammonia spills. The purpose of the study was to develop a thorough understanding of the physio-chemical behavior of ammonia/water reactions, develop analytical models, and conduct a scaled experimental program to verify and modify the models for use in predicting the potential hazards due to spills of up to 3,000 tons of LNH_3.

1.2 SCOPE

To achieve the objectives of this investigation, ADL established and conducted a program consisting of four major tasks.

Task I -- Study LNH_3 Spills on Water
Task II -- Model LNH_3 Spills on Water
Task III - Study LNH_3 Release Underwater
Task IV -- Recommend Neutralization Methods

Both Task I and Task III were conducted in three stages. First, a series of laboratory tests was conducted with spills of up to 2.5 liters of liquid ammonia. Second, tests were conducted in the open in a small swimming pool, with one gallon and five gallon spills. Finally, quantities of up to 50 gallons were spilled on the water in a pond. For underwater

release, there were 0.4 gallon laboratory tests, one gallon intermediate scale tests, and five gallon large-scale tests. Discharge depths varied from 4.5 inches to 60 inches.

1.3 FINDINGS

The objective of this work was to predict the vapor and water dispersion hazards of up to 3,000 ton LNH_3 spills on water. These predictions are given in Appendix C.

1.3.1 Laboratory Experiments

1.3.1.1 Surface Spills

The mean partition ratio, the fraction of the total weight of spilled ammonia that goes into solution with water, was about 0.73. In over 90% of the experiments, the partition ratio was between 0.65 and 0.82; was insensitive to quantity, rate, and orientation of spill; and was independent of the water salinity (up to 3.5% NaCl) and air or water motion. In addition, restricting the reaction area on the water surface did not cause any great variation in the partition ratio. A slight change in the partition ratio was observed with changes in water temperature.

Surface spills reacted with water in a small area, and the ammonium hydroxide formed spread out along the water surface at about 2.5 inches/second. The NH_4OH temperature was about 5° to 15°F above the ambient water temperature.

The partition ratio results and the water temperature data can be adequately explained by a thermodynamic mixing model.

1.3.1.2 Underwater Release

When the release of LNH_3 was at shallow depths and at low velocity, there was no substantial difference in the partition ratio compared to the surface spill mean value. In general, when the release was at depths greater than about 10 pipe diameters, the partition ratio was between 0.85 and 0.95.

1.3.2 Intermediate-Scale Experiments

1.3.2.1 Surface Spills

The average value of the partition ratio was about 0.56 for both one gallon and five gallon spills, and increased to about 0.66 for continuous spills. The water temperature rise at the surface was about 5° to 10°F, although in some tests a change of as much as 22°F was observed. The elevated temperature lasted for about five to ten minutes.

Liberated vapor dispersed as a cloud and passed across the instrument rake, 15 feet downwind. This was indicated by a momentary dip in the air temperature recorded at the rake, which implies that the core of the cloud was still cold and unmixed. Distribution of the vapor mass collected by the impingers on the instrument rake could be reasonably fit with Gaussian profiles. The partition ratios measured by analyzing the pool water samples were close to those calculated from vapor samples collected in the impingers.

1.3.2.2 Underwater Release

At an average value of 0.85 to 0.90, the partition ratio values were considerably higher than those for surface spills. No vapor liberation could be observed. Water surface agitation was minimal for release depths greater than about 15 inches and release rates less than 15 m²/sec (about 0.25 gal/min). A maximum water temperature rise of about 10°F was recorded by a set of thermocouples five inches off the axis of the discharge pipe.

1.3.3 Large-Scale Experiments

1.3.3.1 Surface Spills

The partition ratio, calculated from tests that had good impinger data, was between 0.53 and 0.63. The partition ratio date shows a wide scatter because the vagaries of the wind often caused the vapor cloud to miss the instrument rafts. In low wind, the vapor rose rapidly. The water temperature in the spill zone (recorded by thermocouples at 0.5 inch to 1 inch depth) showed substantial heating of the surface layer, with up to 50°F increase noted. The temperature rise was very gradual, and reached peak temperature in six to eight minutes. The average diameter of the surface boiling zone was about 20 to 25 feet.

Vapor cloud behavior in the wind is adequately explained by a plume theory of vapor dispersion, and it has been shown that the water temperatures observed could result form an adiabatic mixing of water and liquid ammonia.

1.3.3.2 Underwater Release

The results in this series of underwater tests are not much different from those obtained in the intermediate size tests. A 10° to 15°F rise in

water temperature was noticed. The temperature rise was in phase with the duration of the spill, with the peak temperature being reached just at the end of the spill. No substantial vapor release was observed, but violent agitation of the water was observed directly above the release pipe when the release depth was 36 inches.

1.4 CONCLUSIONS

The following major conclusions can be drawn from the results of the experimental test program and the data analysis:

1. The partition ratio is highest in the case of underwater release and is as high as 0.95. Very little vapor liberation occurs in the case of underwater release at depths from 10 inches (for small quantities) to five feet (for five gallon releases).

2. For large surface spills, the partition ratio depends on the spill dynamics and varies between 0.5 and 0.6 (closer to the latter) for instantaneous release on the surface. For slow, continuous release on the surface, partition ratio values tend to be as high as 0.66. However, for small spills, under controlled laboratory conditions the partition ratio values are between 0.7 and 0.75, with a mean of 0.735.

3. In the case of large surface spills, the reaction is extremely rapid and liberates a dense, white fog of vapor, probably containing a large fraction of aerosols, in low wind conditions.

4. The vapor puff formed is very buoyant and rises into the air as it travels downwind. The rate of rise depends on the wind velocity. Under low wind conditions the cloud forms a characteristic mushroom cloud before dispersing. The path of the cloud can be estimated with reasonable accuracy by existing plume theories. Because of the rapid rise in low wind, the toxic hazard at ground level is smaller for low wind than for high wind.

5. The boiling zone is reasonably small — about 25 feet in diameter for a 50 gallon spill. The diameter of the boiling zone

increased as the 0.8th power of the quantity of spill for the tests conducted. However, based on the analysis of spread of other cryogens on water, we expect that a 0.375 power relation with quantity is more appropriate for really massive "instantaneous" spills.

6. The ammonium hydroxide formed at the boiling zone stays close to the top of the water surface and spreads radially at about 0.2 ft/sec. The depth of this layer is of the order of a few inches (at best one foot). Because of this layered spreading of NH_4OH, the hazard to aquatic life just beneath a spill site is small.

In short, we conclude that a reasonable estimate of the partitioning for a massive spill on the water surface would be 0.6 into water and 0.4 into vapor. The downwind vapor hazard at ground level is not as severe as earlier believed because of the buoyant nature of ammonia vapor.

The main achievements of the program have been to:

1. Show that the LNG_3/water surface reaction is rapid and confined to a reasonably small area;

2. Show that the ammonia vapor liberated is buoyant and rises rapidly;

3. Develop a thermodynamic model that accurately predicts the upperbound of the partition ratio for surface spills. We feel that, though the reaction is thermally limited, the dynamics of the spill do affect the partitioning;

4. Develop a method for indirectly calculating the partition ratio from vapor sample measurements.

5. Develop a model that indicates that under certain accident situations, the present design of refrigerated ammonia tanks for barging is inherently safe even if the barge sinks; and

6. Show that the continuous underwater release of LNH_3 at depths greater than ten pipe diameters results in all the liquid dissolving in water with very little vapor production.

1.5 UNRESOLVED QUESTIONS

Though much has been achieved in the present program, questions have remained unanswered, either because of the size of the tests conducted or due to the difficulties in measurement. The important unknowns are:

1. The amount of aerosol in the vapor liberated in a surface spill and its relationship to the mode of spill (instantaneous, continuous, etc.) and the rise of the vapor cloud;
2. The rapid rise of the vapor cloud for a water spill as against the ground-hugging clouds, possibly due to greater aerosol formation in land spills reported in the literature;
3. The possibility of underwater explosions in the case of instantaneous underwater release of large quantities of LNH_3. (The present program experiments were limited to a continuous release of a maximum of five gallons, and it is difficult to extrapolate to the consequences of a large instantaneous release); and
4. Validation of scaling laws for the determination of the maximum radius of the boiling zone (pool radius).

1.6 RECOMMENDATIONS FOR ADDITIONAL TESTS

As a result of this test program, we are now in a position to extrapolate the findings of this work to predict the hazard presented by a 3,000 ton release of ammonia on water. Appendix C of this report contains the predictions of hazards for a 3,000 ton (about one million gallons) release of LNH_3 on water. However, because of some of the unresolved questions discussed above and the initial buoyant behavior of the ammonia vapor cloud, we feel that further experimentation on a much larger scale would serve to increase confidence in the analytical models and provide optimum benefits from the overall test program. We recommend, therefore, that a final series of tests be conducted utilizing 3,000 gallon releases in a

300-500 ft. diameter pond. A test program with spill quantity at least two orders of magnitude greater than the largest tests in the present series would provide an excellent data base with which to test the scaling laws and improve confidence in theories of vapor movement.

2. INTRODUCTION

2.1 BACKGROUND

During the past decade, maritime transport of liquid anhydrous ammonia (LNH_3) on the Inland and Coastal waters of the United States has increased rapidly. Anhydrous ammonia is carried on barges as a high-pressure cargo in heavy-wall steel tanks, and as a low-temperature cargo in atmospheric-pressure refrigerated tanks. There has been very rapid growth of refrigerated transport, motivated largely by the substantial savings in capital costs associated with onshore refrigerated storage compared to pressure storage.

The frequent movement of bulk quantities of LNH_3 on United States waters poses a potential hazard to the public, to aquatic life, and to other shipping, should there be an accidental release of ammonia either on or underwater. Although the explosion and fire hazard of such a spill is limited, the health and pollution hazard is not insignificant.

There is a definite need, therefore, to study the hazards associated with large accidental spills of LNH_3 and to develop emergency procedures to neutralize the effects of such spills.

The United States Coast Guard (USCG) recognized the hazards presented by a spill of LNH_3 on the inland waterways and felt the need to evaluate the potentialities of such a hazard. USCG therefore initiated a research program to study the important physical aspects of LNH_3 spill on and underwater. The main objectives of the study were to conduct scale experiments and develop theoretical models so that the results of small-scale experiments could be extrapolated to predict the hazard caused by spills of up to 3,000 tons of LNH_3.

At atmospheric pressure, liquid ammonia (LNH_3) boils at about -28°F; at a vapor pressure of about 108 psia, it boils at 60°F. The ammonia can be as a liquid either refrigerated or at ambient temperature (under the associated vapor pressure)[1]. Ammonia is very soluble in water, and dissolution process is exothermic.

Releases of ammonia are harmful for two primary reasons: first, the vapor is toxic; and second, a solution of ammonia in water (ammonium hydroxide) is deadly to both flora and fauna.

In general, spills of ammonia will result in both dissolution and vapor evolution, and the relative percentage of both forms depends largely on the manner in which LNH_3 and water combine. For example, a water surface spill leads to rapid boiling of some ammonia, and simultaneous mixing of the remainder with the water. Thus, in some ways, the process is similar to spills of cryogens on water -- with the added complication of an exothermic reaction occurring at the LNH_3/water interface.

2.2 HAZARDS OF AMMONIA

2.2.1 Fire Hazard

Ammonia is not highly combustible. Its flammability limits in dry air are 15 to 28% (by volume). It is not known how the presence of water vapor affects these limits, but most likely it will tend to quench a flame and reduce the fire hazard. Furthermore, the ignition temperature of ammonia is relatively high (1500°F in a quartz bomb and 1204°F in an iron bomb).

If liquid ammonia remains on the water surface for any reasonable length of time before it evaporates, and is accidentally ignited, it may burn. Tests by Husa and Buckely [2] in which LNH_3 was poured into a 3-ft by 3-ft by 2-inch deep pan and ignited showed that brief flashes occurred when the ignition source was brought near the liquid surface, but that the flames could not be sustained.

There are no similar experiments with ammonia on water. Even if we assume that LNH_3 burns on water, existing correlations [3] show that ammonia flame heights should be lower than those calculated for organic liquid fuel fires of the same diameter. Furthermore, ammonia fires should not be luminous because no carbon is present. Thus, with less height and nonluminousity, ammonia fires should not radiate as much as organic fuel fires.

2.2.2 Explosion Hazard

The accumulation of flammable NH_3 vapor in an enclosure (such as a house on the shore or in a vessel) and its subsequent ignition may lead to an explosion. Ammonia explosions are known to have occurred in industry. The force of such an explosion depends on the degree of confinement. Buckley and Husa[4] found that the magnitude of the pressure ratios observed in ammonia explosions is roughly three-quarters that found for common hydrocarbon fuels under similar conditions. Attempts by the same authors to detonate ammonia/air mixtures at atmospheric pressure have failed.

2.2.3 Toxicity Hazard

The major hazard from an ammonia vapor cloud is its toxicity, because ammonia is an extremely irritating gas and is toxic in relatively small concentrations. Exposure to 0.25-0.65% NH_3 in air for 30 minutes is sufficient to cause death or serious injury, and most deaths from ammonia spill accidents on the ground have been attributed to toxicity. The American Conference of Governmental Industrial Hygenists recommends a threshold limit value (TLV) of 50 ppm in air (18 mgm/m^3 of air) for eight-hour exposures. Fortunately, the human olfactory system is capable of detecting the presence of ammonia at 20 ppm. long before the toxic limit is reached[5].

In the case of excessive exposure, reaction of anhydrous ammonia occurs in the upper respiratory tract and spasms, inflammation, or edema of the larynx results. LNH_3 can cause severe caustic skin burns. Current practices of first aid include removal to uncontaminated regions, breathing pure oxygen for short periods, and flushing skin burns and clothes with water [5]. In case of after effects (usually laryngeal spasms) medical examination is recommended.

2.2.4 Hazards Due to Dispersion in Water

The short-term effects of large quantities of ammonia dissolving in water are the rise in temperature and pH level of the water. Both of these can cause severe harm to aquatic life in the vicinity of the

the spill. The water temperature increase could also cause pressure buildup in sunken, slowly leaking low-pressure refrigerated tanks.

2.2.5 Explosion Hazard Due to Large Underwater Release

Small-scale experiments[6,7] on the release of LNH_3 and other cryogens under water have determined that there is a possibility of pressure explosions occurring underwater. The physical aspects of such explosions are not fully understood at this time, but a possible explanation lies in the hypothesis of extensive superheating of the cryogen.

2.3 PREVIOUS INVESTIGATIONS

Few academic studies have been carried out in which one liquid is boiled by contacting it with another hot liquid. Those that have been reported involve steady state experiments with organic liquids over hot mercury. They are summarized briefly in a paper by Nakanishi and Reid[6]. In this same paper, the available experience involving liquid natural gas (LNG) spills is also discussed and pertinent references given. The LNG spill studies were carried out primarily by industrial concerns[8,9] and by the Bureau of Mines[10]. The major objective was to ascertain the rapidity of boil-off should LNG (b.p. ≈ -258°F) be spilled in an accident. Such data could be used as input to a vapor dispersion program to predict downwind concentrations. However, another significant objective was to clarify an unusual phenomenon first observed by the Bureau of Mines; i.e., in a few cases where LNG was spilled on water, a pressure explosion resulted. The subsequent studies by Shell[11] and Esso[12], as well as by Nakanishi and Reid[6], indicated that such explosions might be expected if the cryogen could superheat and initiate vaporization by homogeneous nucleation.

A major investigation using ammonia is reported by Resplandy[13]. The tests, conducted in France, studied releases on land for three situations; namely, liquid released from a pressurized tank, the dispersion of vapor released from a pressurized tank, and the spill of liquid ammonia into earthen dikes. The results from these tests

indicated that for pressurized releases (up to 300 kg/min from a 6-atmosphere pressure tank) a large fraction of the vapor was in the form of aerosols of 10 to 30-micron droplets. It was also reported that up to 40% of the liquid released flashed, resulting in the formation of stable aerosols. It is not very clear from the paper what fraction of the vapor formed was in the aerosol phase.

At low wind conditions, the cloud rose initially to a height of about 20 meters in a 0.5 m/sec wind, then fell to the ground and dispersed at ground level. The visible vapor cloud traveled just about 100 meters before vanishing. Further, the cloud boundary and the boundary of the odorous region were very close. In the case of liquid ammonia spill into earthern dykes, aerosol formation is said to have been noticed in the first few seconds after spill. However, within a few minutes, the vapor generation ceased, leaving a stagnant pool of LNH_3. The paper also describes the tests to contain the vapor by water spray resulting in no major improvements in the cloud travel. Also described was a test to ignite the cloud, which failed.

Small scale tests[6] involving the pouring of cryogenic liquids such as nitrogen, ethane, LNG, etc. on a water surface indicate the occurrence of agitated boiling at the water surface. However, when small quantities of methane were poured on ethylene glycol (antifreeze), there was a hiss/crack noise and evaporation was quickly over. Laboratory tests conducted by Reid et al.[7] show that the LNH_3 water interaction resembled more the methane/glycol case than the methane/water case. The vapor produced did not contain any water fog.

These results suggest that the vapor cloud from a spill of LNH_3 on water may differ from the results reported by Resplandy[13], Ball[14], et al., for the experiments in which ammonia land spills were studied. For a spill of the same quantity of ammonia, the vaporization rate on water is much greater than for a land spill. This could give a shorter, high-concentration "puff" which might travel further downwind before dispersing safely even though the total fraction of ammonia vaporized might be less because of solution of ammonia in the water phase. Further, limited observations[15] of land spills

indicate the presence of a thick white fog for large spills, which was missing in the small-scale experiment[7]. The fog is caused by cooling the surrounding air below its dewpoint. This phenomenon depends largely on the relative humidity of the air, and once the water vapor in air precipitates out, it dissolves the gaseous ammonia in the vapor cloud. This may result in a fog which can be "heavy" enough to stay close to the ground.

A few small scale underwater release test results have been reported[6,7]. The results show that most of the ammonia dissolved in water, under suitable conditions (4 to 5 inches release depths for 4 ml LNH_3). However, it is reported that in one test with 15°C water, a violent explosion destroyed the glass vessel containing the water. Based on Apfel's[16] superheat explosion theory, it was found that LNH_3 may be superheated to a temperature of 342°K, corresponding to a vapor pressure of 460 psia. This pressure is high enough to cause an explosion.

Very little theoretical analysis is available in the literature concerning the ammonia-water interaction. For the dispersion of vapor in air and NH_4OH in water, the usual air dispersion and water dispersion models are used.

2.4 PRESENT PROGRAM

The present program was undertaken with a view to answering certain basic questions such as: how much spilled LNH_3 dissolves in water? what is the relationship of the dissolution fraction (called the partition ratio) to the dynamics and the quantity of spill, if any? and what are the features of the vapor dispersion in the atmosphere and ammonium hydroxide dispersion in water?

To achieve the objectives of the program indicated in Section 1.2, and to obtain answers to the above questions, a three-stage experimental program was undertaken. The primary parameter of interest in all the experiments was the partition ratio (that is, the fraction of the LNH_3 spilled that goes into solution with water). The dispersion of vapor in the atmosphere was also studied.

First, a laboratory program was completed in which up to 2.5 liters (0.7 gallons) of LNG_3 were spilled on the water in a small aquarium tank. Both surface spills and underwater releases were conducted. The details of the experiments and the results are given in Chapter 3. Second, spills were conducted in the open atmosphere. A small swimming pool was used to contain the water. The vapor dispersion was measured by sampling the ammonia vapor in air. In this series, up to 18 liters (5 gallons) of LNH_3 were spilled. Chapter 4 contains the details of the second stage of testing. Chapter 5 describes the final part of the experimental program. The tests were conducted in a pond and quantities of up to 180 liters (50 gallons) of LNH_3 were spilled on the water surface. The partition ratio was estimated using the measured vapor concentration in the air.

Several theoretical analyses have been made to describe or predict the various phenomena that occur following a spill of LNH_3. Chapter 6 deals with particular aspects of the LNH_3 spill problem. Section 6.2 gives a vapor flash model, useful for calculating the amount of vapor produced by flashing when liquid ammonia leaks from a pressurized container. Section 6.3 describes a therodynamic model for the mixing of LNH_3 and water. It can be seen that the two liquids can react in three different ways, leading to three different answers. In reality, all three reactions may take place simultaneously. In fact, some of the experimental results tend to confirm this. Section 6.4 presents a detailed heat-transfer model, to predict the pressure rise inside an ammonia tank that is submerged in water. Section 6.5 and 6.6 treat the problem of dispersion in air and water of ammonia vapor and ammonium hydroxide. Section 6.7 discusses two theories of the rise of buoyant vapor in the atmosphere. It is found that one of these theories describes quite well the rise of ammonia vapor in the atmosphere. Section 6.8 gives an order-of-magnitude type analysis for underwater release.

Chapter 7 is devoted to the steps to be taken to neutralize an ammonia spill area. Various methods are discussed from containing the area with booms, to air sparging.

3. LABORATORY EXPERIMENTS

3.1 PURPOSE AND SCOPE

The main purpose of the laboratory testing was to study the liquid ammonia-water interaction, under controlled conditions, and to develop an analytical model to explain such interaction. The key experimental result was the partition ratio, i.e., the fraction of the total weight of spilled ammonia that goes into solution with water. However, in addition to studying the dependence of the partition ratio on the test variables, we also tried to develop an understanding of the physical mechanisms involved.

The basic experimental steps were to:

1. Spill a predetermined quantity of LNH_3 on water;
2. Allow the reaction to complete, and the vapor to disappear, then thoroughly mix the water; and
3. Titrate the water samples to obtain the amount of ammonia dissolved in water (and hence the partition ratio).

3.2 APPARATUS AND PROCEDURES

3.2.1 Test Facility

Figure 3-1 is a schematic of the laboratory test apparatus. The system consisted mainly of an LNH_3 transfer system, a spill system, and a test tank. Ammonia was transferred as a two-phase fluid from a storage cylinder to a separator. The vapor formed was vented out through a hood and the saturated liquid was collected in a spill dewar. The ammonia dumping system consisted of a pivoted spill dewar, a tipping lanyard, and a funnel under the dewar that had interchangeable discharge tubes for controlling delivery of LNH_3 to the water tank. The testing section was a six-foot-long glass tank, 18 inches wide and 20 inches high, half filled with water.

Both the separator and the test tank were enclosed in a vented laboratory hood having glass doors to permit observation of the spill

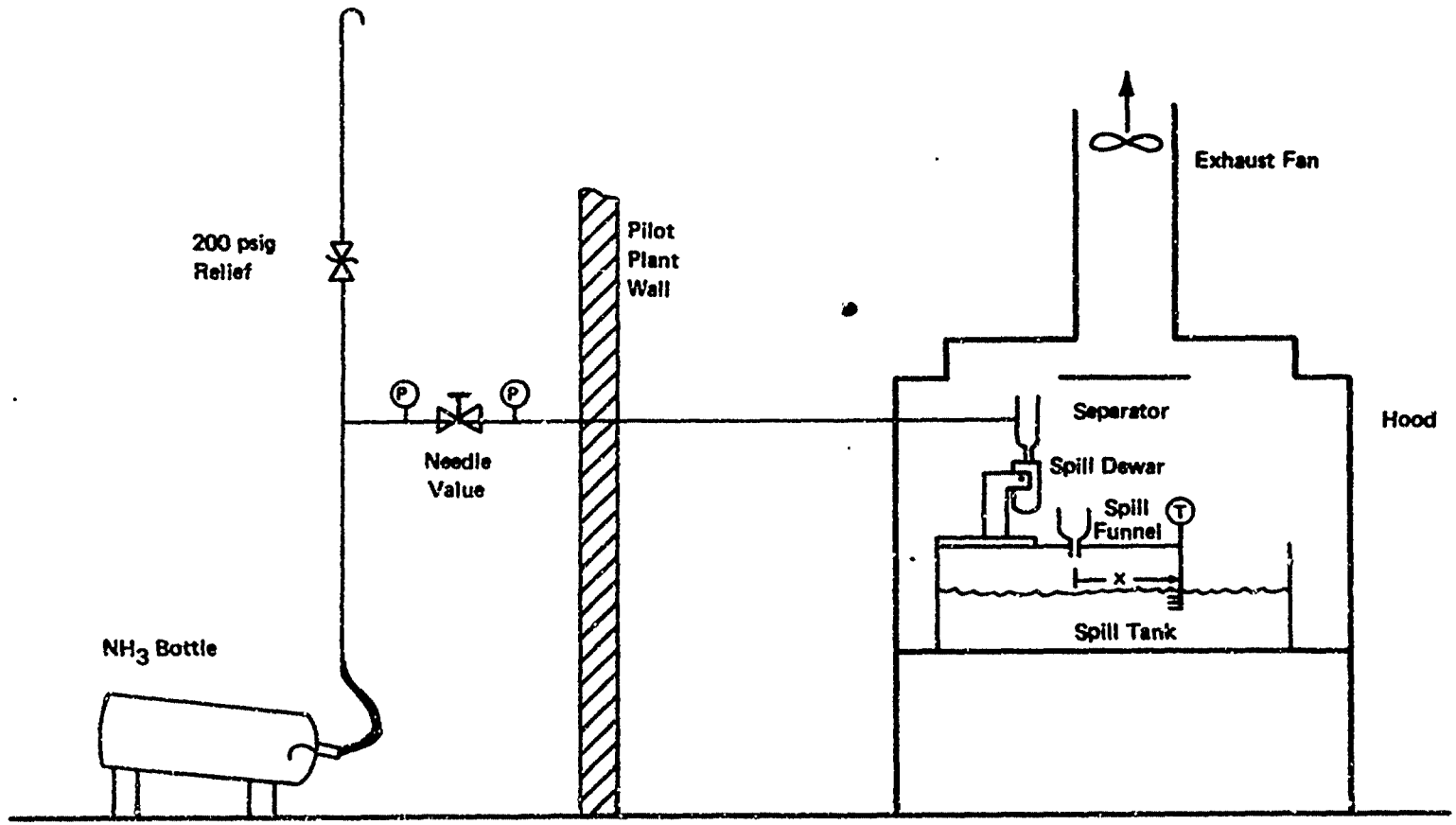

FIGURE 3–1 LNH_3 LABORATORY TEST FACILITY

tests. A circulating pump (not shown in Figure 3-1) was provided for rapid mixing and draining of water in the tank.

3.2.2 Instrumentation and Measurement

A listing of the techniques used and the parameters measured during the tests is in Table 3-1. Phenolphthalein was added to the water to obtain a qualitative indication of ammonia concentration and its extent in the test volume. In several of the tests, concentration gradients in the water were measured with pH probes. Following each test, the partition ratio was obtained by titrating samples of the final mixed solution from the tank.

Temperature profiles for both the liquid and vapor phases were recorded, through four high-speed thermocouple channels (about 20 milliseconds response) and three slower-speed channels, on a multi-point recorder. (The time between printing of each point was about 3.6 seconds.) One high-speed channel was attached to the spill discharge nozzle to provide a spill initiation reference. A second high-speed channel was attached to thermocouple Rake A, and the remaining two high-speed channels were attached to Rake C. For some tests, Rake A and Rake C were combined to form Rake D, a three-thermocouple rake with three high-speed channels. The three-thermocouple read-out on the multi-point recorder was attached to a common Rake B.

Photography has provided a permanent visual record. Many tests were recorded with real-time movies, while for others the high-speed Fastex camera was used. A series of 35 mm stills was taken of each test, particularly during the latter stages of the test program.

3.2.3 Test Procedures

Preceding each test, the water tank was flushed several times to remove any residual traces of ammonia and then a phenolphthalein solution (typically 15 ml of a solution of 2.5 g of phenolphthalein to 100 ml of ethanol) was added to the clean water.

After the thermocouples were checked, the exhaust hood was secured,

Table 3-1

Laboratory Test Techniques and Parameters

CONCENTRATION

- Gradients - Phenolphthalein Indicator, pH Probe
- Final Mix - Titration

TEMPERATURE - LIQUID (VAPOR)

- Nozzle - 1 Hi-speed
- Rake A - 1 Hi-speed
- Rake B - 3 Multi-point
- Rake C - 2 Hi-speed
- Rake D - Rake C + Rake A

PHOTOGRAPHY

- Real-Time Color Movies
- Slow-Motion Color Movies
- Ultra-Slow-Motion (Fastex) Color Movies
- 35 mm Color Stills

and the area cleared of non-test personnel, ammonia was transferred from the storage bottle outside the test building into the spill dewar. This transfer was accomplished by opening a valve in the neck of the LNH_3 bottle and, controlling the flow with the needle valve in the transfer line, filling the graduated spill dewar to a predetermined level. With the dewar filled, a countdown was begun and the thermocouple recorders and cameras were started at predetermined intervals before the actual spill.

Each test was initiated by tipping the spill dewar with a lanyard, so that the LNH_3 dumped into the spill funnel flowed through a discharge tube onto the surface of the water. The rates and angles of LNH_3 discharge were controlled by the size and angle of the discharge tube below the spill funnel. Temperature recording and photographic surveillance were usually maintained for about five minutes following completion of the spill. (Depending on spill tube size and spill quantity, a spill was normally completed within 15 to 45 seconds.)

At five minutes into each test, mixing of the tank was initiated. A mixing period of two minutes was allowed - although visual observation of the dye and temperature measurement indicated that mixing was, in fact, essentially complete after about 40 seconds - then analysis by titration.

The total quantity of ammonia dissolved in the water was determined from the measured concentration of ammonia in the final mixed solution and the known volume of the final mixed solution. This, in turn, was divided by the initial spill quantity to obtain the partition ratio.

3.3 SURFACE TESTS

Eight groups of tests were conducted to determine the dependency of the partition ratio on various physical parameters. Figure 3-2 shows the relationship of the five test categories in the laboratory test program. Several test parameters were varied for each category to study possible influence on the partition ratio.

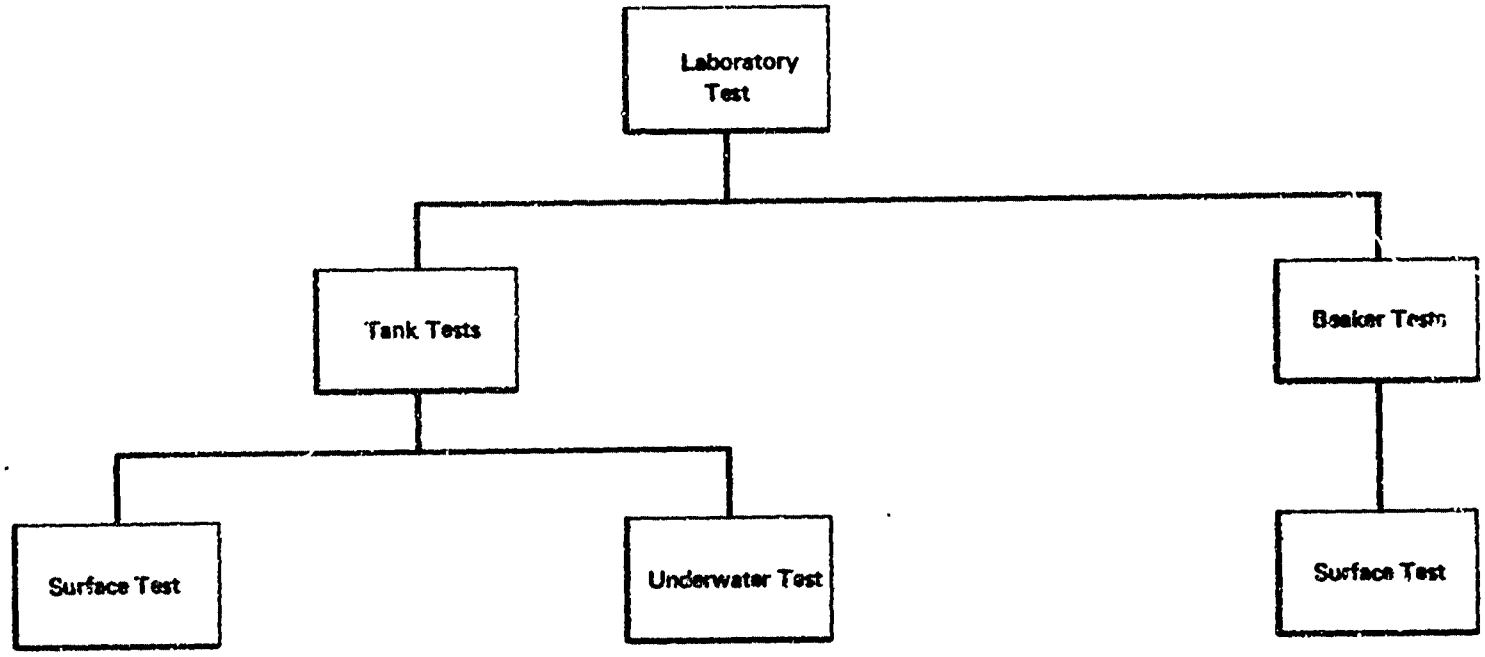

Group I: Quantity, Rate
Discharge Angle (22 tests)

Group II: Water Temperature (3 tests)

Group III: Contained Area (2 tests)

Group IV: Air Velocity and R.H.,
Water Velocity
Surface Isolation (4 tests)

Gravity feed low depth discharge
(2 tests)

Pressurized low depth discharge
(4 tests)

Pressurized high depth discharge
(3 tests)

Group III: Confined area
(4 tests)

FIGURE 3–2 SCHEMATIC DIAGRAM OF THE LABORATORY TESTS

3.3.1 Group I - Basic Effects

The Group I tests were conducted to investigate the basic effects of spill quantity, rate, and method of delivery. The tests are listed in Table 3-2. In this group, spill quantity ranged from 800 to 2400 ml; spill rates were varied from a nominal 50 ml/sec (from a 3/8-inch diameter discharge tube) to a nominal 100 ml/sec (from a 1/2-inch diameter discharbe tube); and the spill angle was either parallel with, or vertical to, the liquid surface. We felt that Group I would be the key to establishing good base data and understanding the liquid-ammonia/water-surface interaction. Thus, a relatively large number of tests (22) were conducted in this group.

Table 3-2 lists calculated partition ratios that are plotted in Figure 3-3 as a function of spill quantity and plotted in Figure 3-4 as a function of spill rate. The results show that the partition ratio is essentially independent of spill size, spill rate, or angle of delivery. With two exceptions, all experimentally determined partition ratios fell between 0.65 and 0.82, or within ± 0.11 of the 0.74 mean value. The two tests that did not fall in this range were rerun and then did fall within the expected values.

The fact that considerable difference in the ammonia delivery method seemed to have little effect on partition ratio suggested that the partition ratio might be limited more by thermodynamic considerations than by surface reaction rates.

Test observation and the test movies indicated that ammonia evaporation occurred in a rather small boiling zone, the diameter of which could be roughly measured by observing surface waves and the location of the vapor cloud leaving the surface. Outside of this small zone, which typically seemed to be about eight inches in diameter, little vapor generation was noted. Surface temperature measurements and the phenolphthalein dye both indicated a warm layer of fluid, evidently aqueous ammonium hydroxide, propagating along the surface away from the boiling zone. Typical values for the thickness of the

Table 3-2

Group I Spill Tests

Date	Spill No.	Spill Quantity (ml)	Small Tube Diameter (in)	Spill Angle	Partition Ratio
10/19	1	805	3/8	0	0.70
10/24	2	770	3/8	0	0.65
	3	810	3/8	0	0.67
10/26	4	800	3/8	0	0.72
	5	800	3/8	90°	0.76
	6	900	3/8	0	0.66
	7	750	3/8	0	0.72
11/1	8	810	3/8	0	0.68
	9	900	1/2	0	0.72
11/6	10	1,00	3/8	0	0.75
	11	1600	1/2	0	0.80
11/8	12	1550	3/8	0	0.81
	13	1560	1/2	0	0.95
	14	1740	3/8	90°	0.61
11/13	15	1600	3/8	90°	0.76
	16	1590	3/8	0	0.74
11/15	17	2600	1/2	0	0.73
11/16	18	2300	3/8	0	0.78
	19	2350	3/8	90°	0.82
12/6	20	1650	Trip Pan		0.68
12/7	21	1700	3/8	90°	0.75
	22	1700	3/8	90°	0.72

mean = 0.735

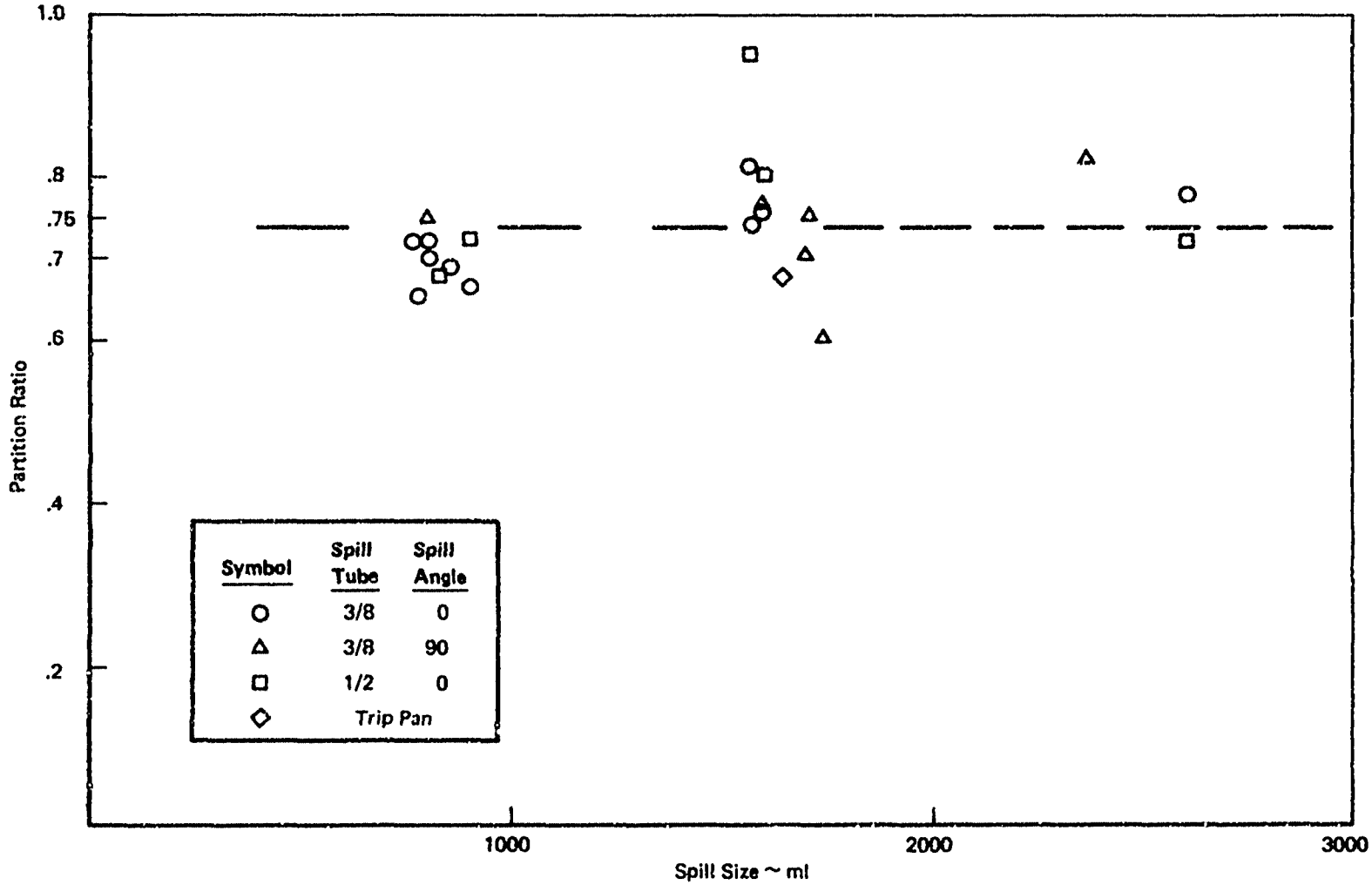

FIGURE 3–3 PARTITION RATIO VERSUS SPILL SIZE

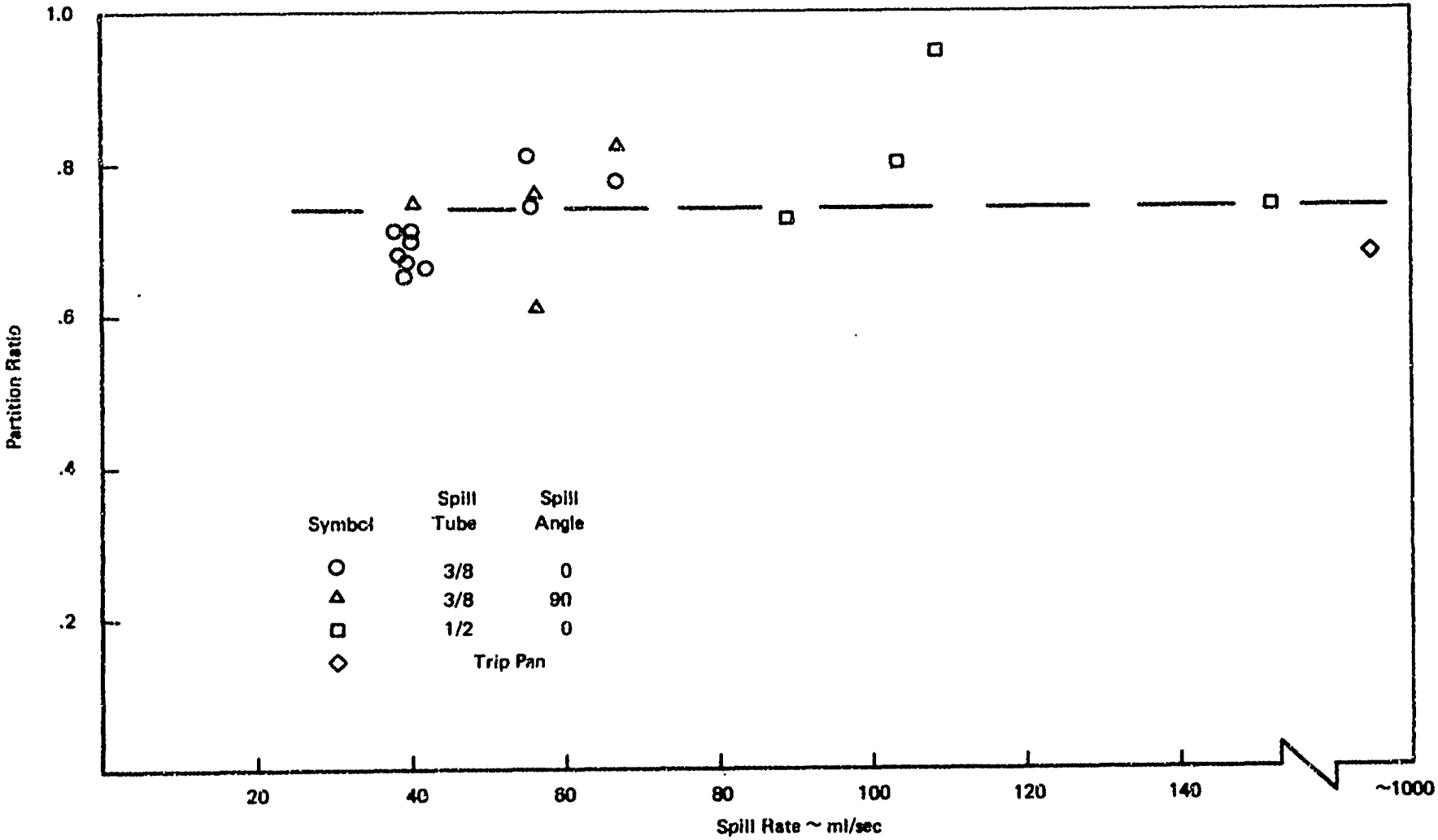

FIGURE 3–4 PARTITION RATIO VERSUS SPILL RATE

layer ranged from two to four inches. The dye propagated much faster horizontally than vertically. Figure 3-5 shows two photographs of a spill. The dye dispersion and the boiling zone can both be clearly seen.

Temperatures were measured for all tests in the liquid near the surface, and also in some instances in the vapor space. Figure 3-6 shows a typical liquid temperature vs. time history at 1/8, 3/8, and 7/8 inch below the liquid surface. The plotted test had 1550 ml of ammonia spilled through the 3/8-inch diameter flow nozzle parallel to the liquid surface. The measurement point was 23.5 inches downstream from the spill point (downstream implies the injection direction of the spill). As shown by the plot, a rather abrupt rise in surface temperature occurred approximately three seconds after spill initiation. High-frequency temperature variations occurred during the spill (about 25 seconds), particularly near the surface.* This phenomenon appears to be associated with wave motion induced by the spill. After completion of the spill, the temperature variations were much smoother, which suggested a much smoother NH_4OH flow. Typically, a maximum 5° to 10°F surface temperature rise was noted following a spill.

It was possible to plot the propagation of the leading edge of the warm ammonium hydroxide layer leaving the spill zone from photographic and thermocouple records. Figure 3-7 shows that the front had a mean propagation velocity of about 0.22 foot per second. This plot seems to roughly correlate with other observations indicating the radius of the boiling zone to be about eight inches (at zero seconds).

---

*The temperature trace for the 7/8-inch depth was manually replotted from another chart. In this process, some of the high-frequency components may have been lost; however, in general, temperatures measured at greater depths exhibited less change and less high-frequency oscillation.

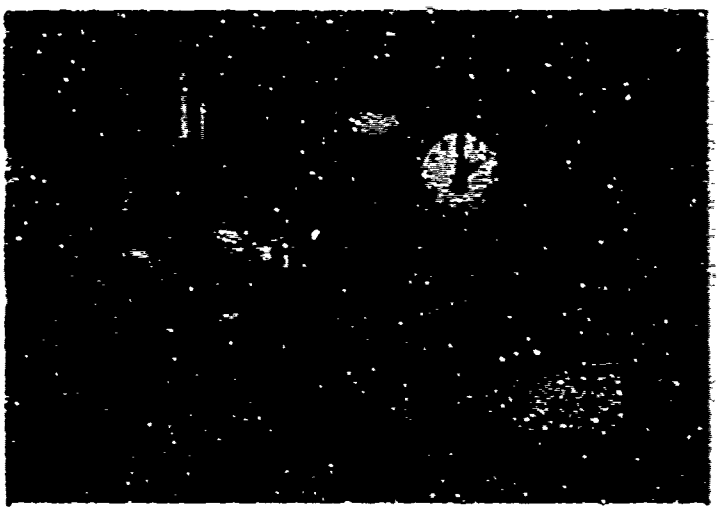

FIGURE 3–5 PHOTOGRAPH SHOWING THE BOILING ZONE AND THE SPREADING OF THE AMMONIUM HYDROXIDE. [Experiment 18, 11/16/72]

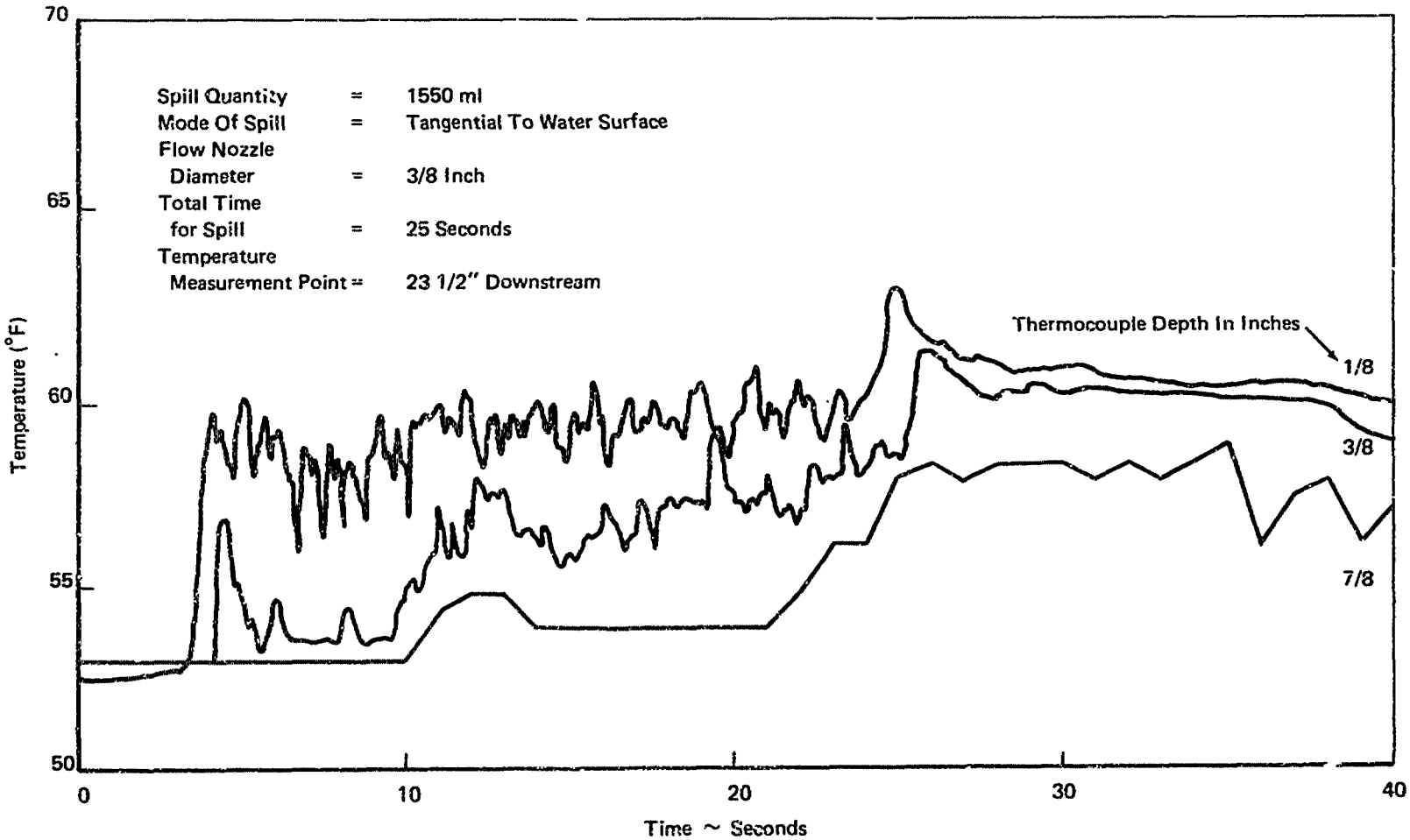

FIGURE 3–6 TYPICAL WATER TEMPERATURE RECORD

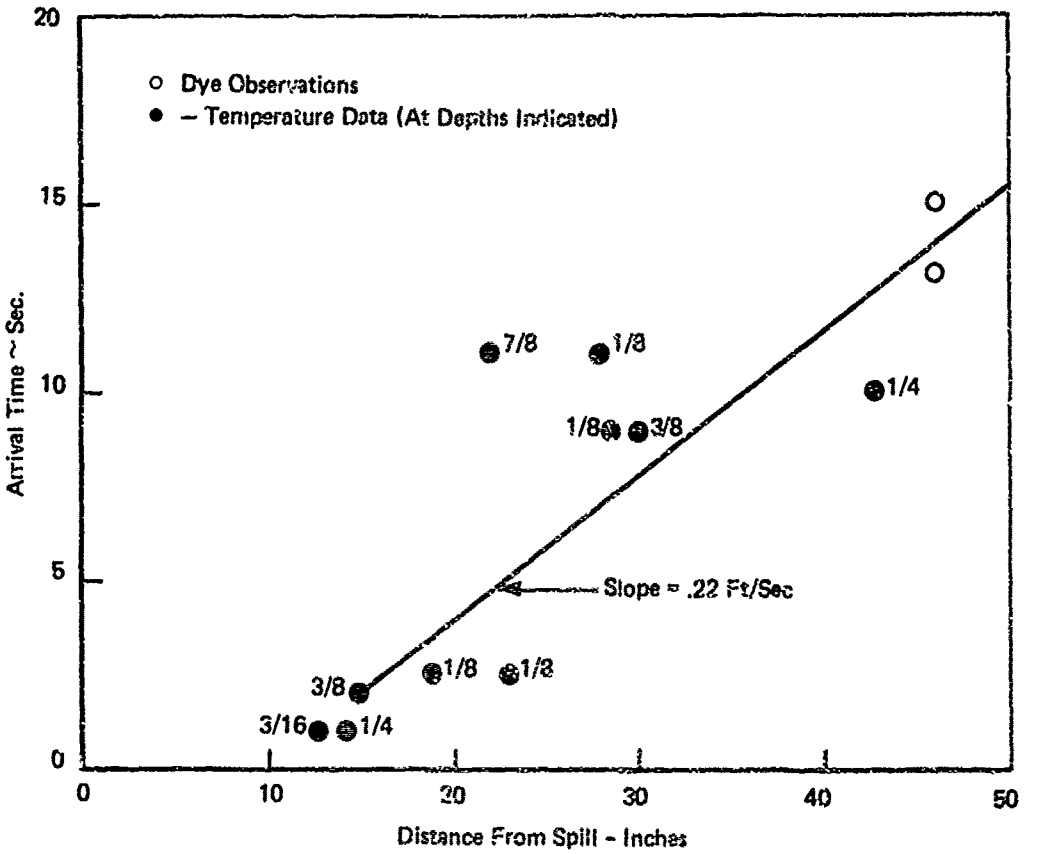

FIGURE 3–7 HORIZONTAL PROPAGATION OF NH_4OH SOLUTION

3.3.2 Group II - Temperature and Salinity Effects

The Group II tests were conducted to investigate the influence of water temperature and salinity. Table 3-3 lists the three tests of this group - two to investigate the influence of water temperature, and one to investigate the influence of salinity. Before each high-temperature test, the water was nominally* at 94°F; prior to the low-temperature test, the water was 37°F. In previous tests, water temperature had varied between 45° and 60°F. Common salt (NaCl) was added to the test water to achieve a salinity comparable to sea water (3.5%).

Figure 3-8 shows the partition ratios obtained in this set of tests. Note that the partition ratio was not significantly affected by either water temperature or salinity. However, high temperature water tended to give a slightly lower partition ratio. This observation is in keeping with theoretical calculations. (See Section 6.2.) Although water temperature had no major effect on the partition ratio, the surface temperature rise (in the propagating NH_4OH solution) outside the boiling zone was much less at higher water temperatures. This result, shown in Figure 3-9, also correlates with predictions of the theoretical analysis.

3.3.3 Group III - Containment Effects

The Group III tests were conducted to investigate the influence of containing the spilled ammonia (and/or propagating ammonium hydroxide layer) on both the liquid-ammonia/water-surface reaction and the partition ratio. Containment was achieved by: 1) restricting the spread of NH_4OH to a fraction of the total tank surface area with a plywood baffle across the water tank; and 2) conducting spill tests

---

*Nominal water temperatures for each test were measured with a mercury in glass thermometer prior to closing the hood and transferring the ammonia into the spill dewar. Typically, about five minutes might elapse between measuring nominal water temperature and the actual spill. During the high-temperature test, some surface temperature drop occurred between measurement of the nominal temperature and the actual spill time (so the surface temperature at the spill initiation was closer to 90°F than to 94°F).

Table 3-3

Group II Spill Tests

Date	Expt. No.	Spill Quantity (ml)	Spill Tube Diameter (in)	Spill Angle	Additional Variable	Partition Ratio
12/19	23	1575	3/8	0	water @ 94°F	0.63
	24	1700	3/8	0	water @ 37°F	0.69
12/20	25	1700	3/8	0	3.5% NaCl	0.72
					mean =	0.68

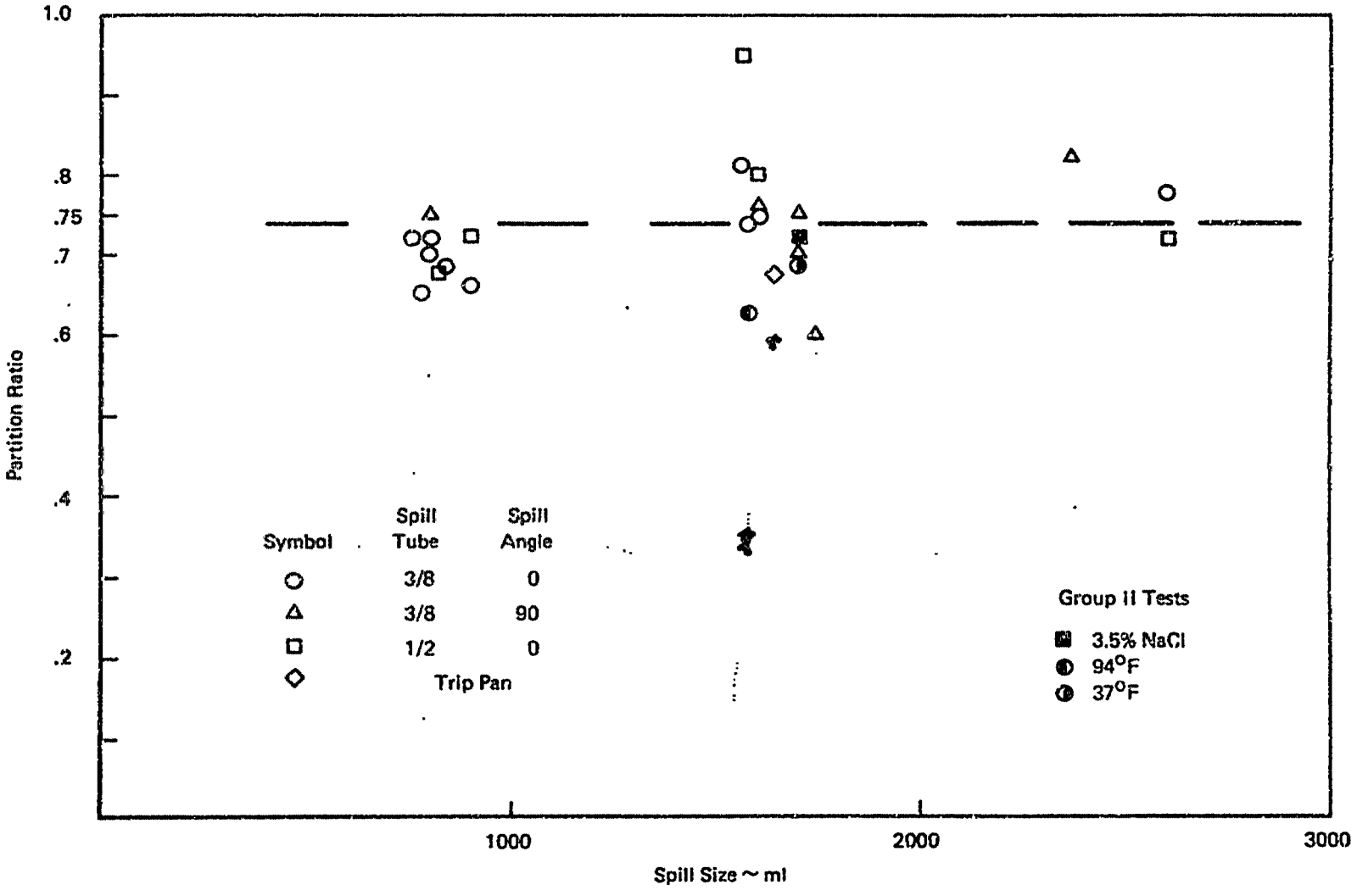

FIGURE 3–8 PARTITION RATIO VERSUS SPILL SIZE FOR DIFFERENT WATER TEMPERATURES AND SALINITY

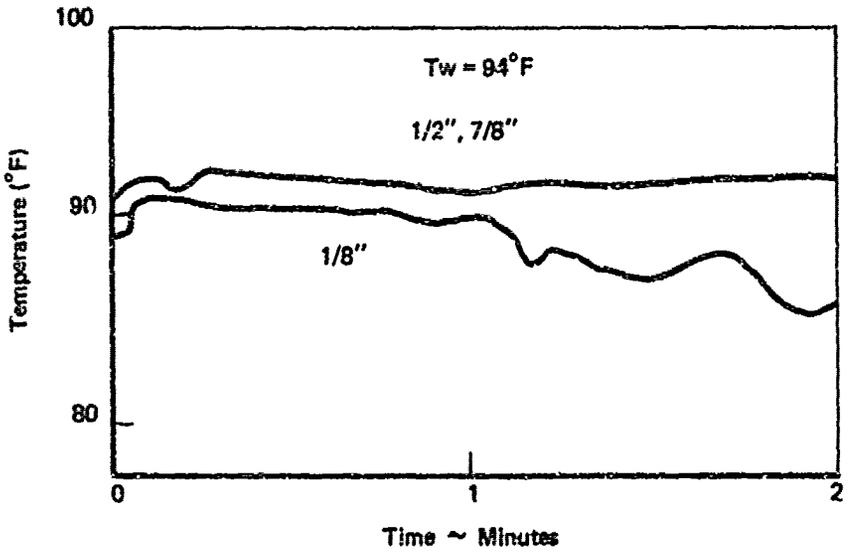

FIGURE 3–9a

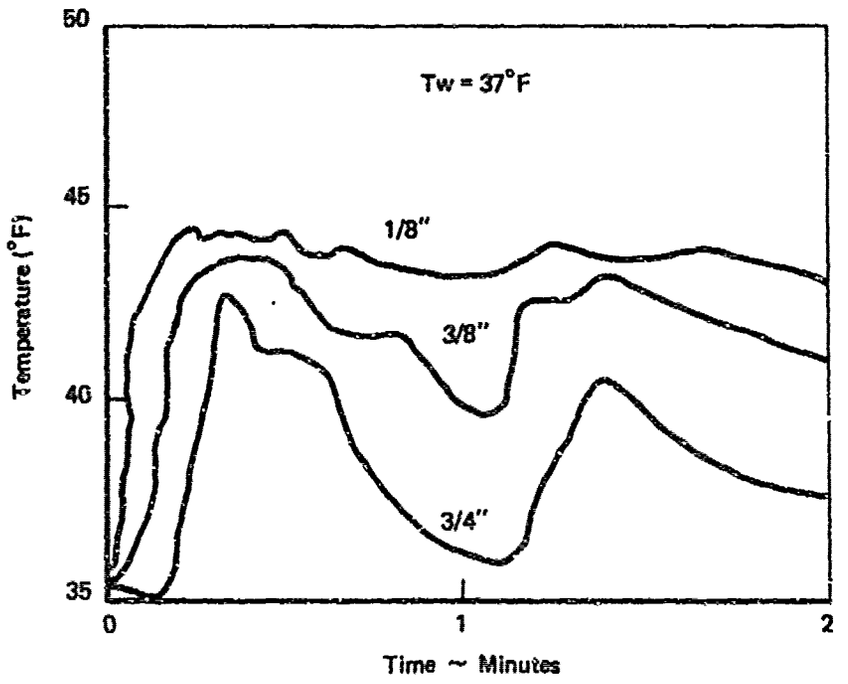

FIGURE 3–9b

FIGURES 3–9 EFFECT OF WATER TEMPERATURE ON THE MAXIMUM RISE OF TEMPERATURE IN THE NH_4OH SUBLAYER

in a six-inch diameter beaker. Table 3-4 lists the data for the six tests conducted in this group.

Figure 3-10 shows the partition ratio data, which indicates that putting a baffle at either station 27 (37% of the tank left available to the spill) or at station 42 (58% of the tank left available to the spill) had no appreciable effect on the partition ratio. A beaker test, with a total area even smaller than that previously observed as the boiling zone in the tank, also did not significantly influence the partition ratio. However, the reproducibility of the beaker spills was not as good as it had been in the larger tank.

Figure 3-11 shows the temperature data from one of the beaker tests. Note that during the test the temperature measured in the vicinity of the surface was colder than the initial water temperature; while below the surface the temperature was somewhat warmer than the initial temperature; and at about the midway level in the beaker the temperature is uninfluenced by the superimposed layer of ammonia and/or ammonium hydroxide. This type of vertical temperature profile probably occurs because of stable stratification of the liquids, with the layer of coldest LNH_3 at the top, followed by a slightly warmer (but nevertheless heavier) NH_4OH solution, overlaying the water. The vertical diffusion of the NH_4OH solution is very slow, as can be seen by the photographs in Figure 3-12.

3.3.4 Group IV - Interface Reactions

The Group IV tests were conducted to study the influence of water and air motion on the ammonia/water-surface reactions and the resulting partition ratio. Another variable studied in these tests was the effect of isolating the liquid surface downstream of the spill to determine if any appreciable portion of the dissolved ammonia resulted from vapor/liquid reactions remote from the actual spill zone. Table 3-5 lists the tests and data of this group.

Figure 3-13 shows the test facility modifications required for

Table 3-4

Group III Spill Tests

Date	Spill No.	Spill Quantity (ml)	Spill Tube Diameter (in)	Spill Angle	Containment	Partition Ratio
10/27	26	810	3/8	0°	Baffle at Station 42	0.66
12/29	27	1675	3/8	90°	Baffle at Station 27	0.74
12/27	28	500	3/8	90°	4000 ml beaker	0.78
	29	1000	3/8	90°	4000 ml beaker	0.94
12/28	30	750	3/8	90°	2000 ml beaker	0.58
2/6	31	1000	3/8	90°	4000 ml beaker	0.695

mean = 0.733

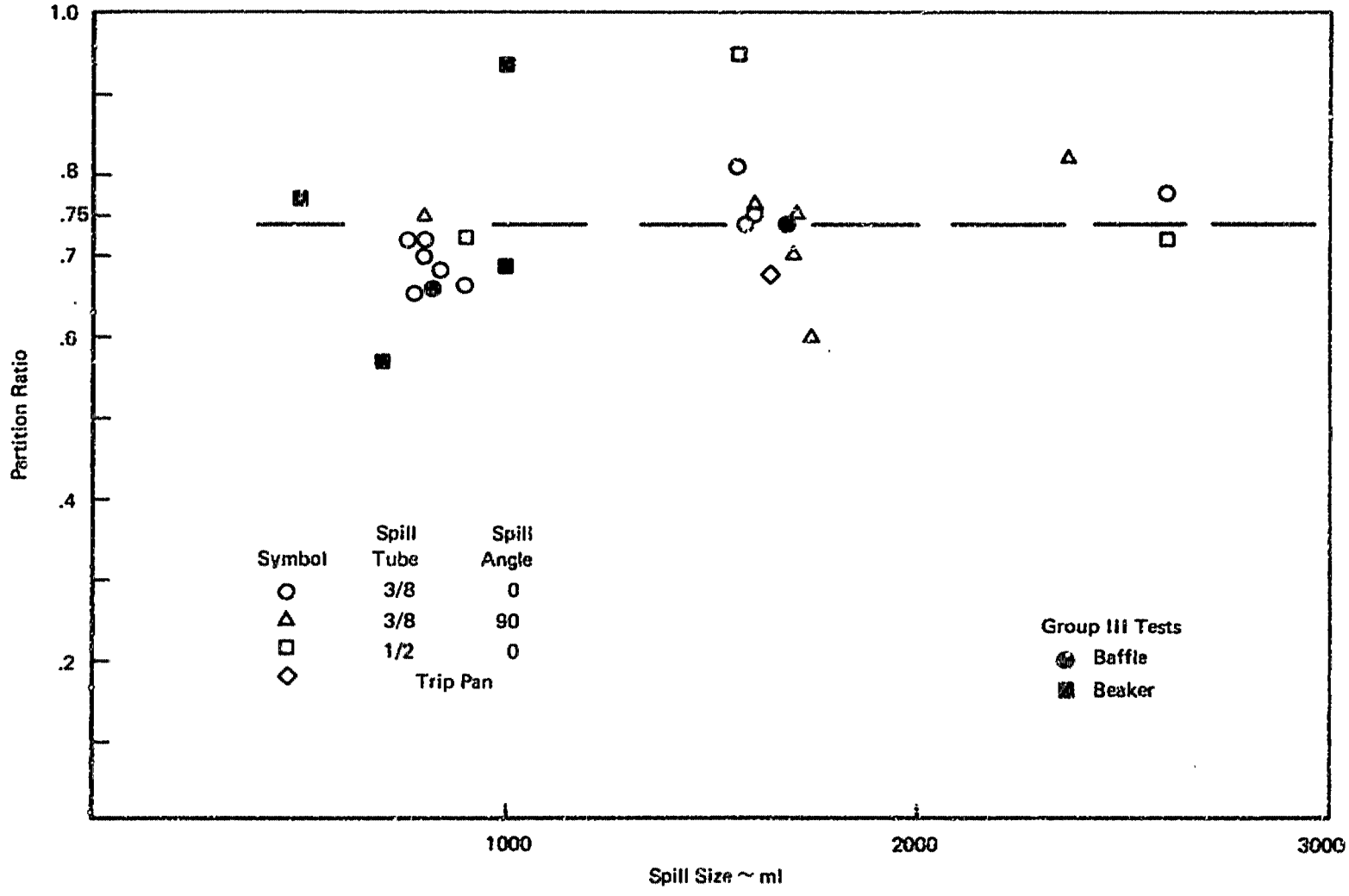

FIGURE 3-10 EFFECT OF SPREAD CONTAINMENT ON THE PARTITION RATIO

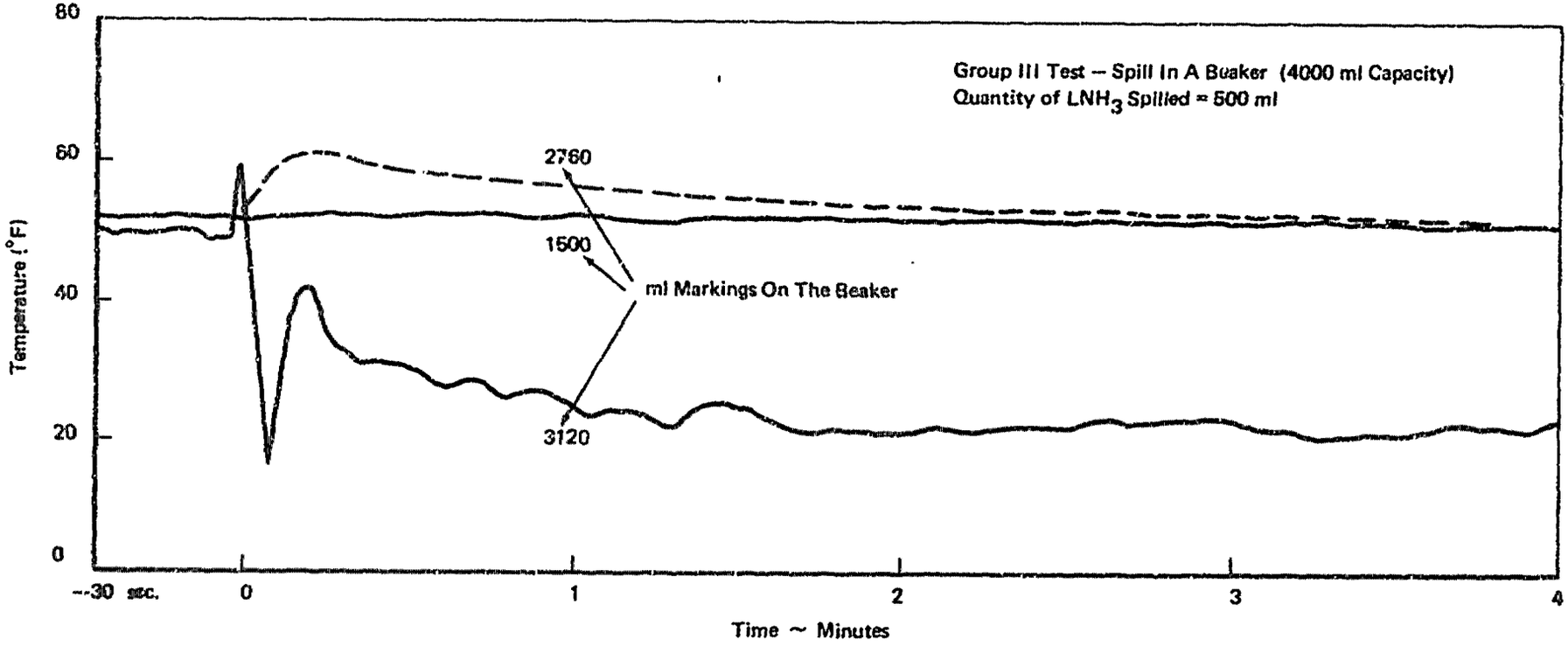

FIGURE 3–11 TEMPERATURE HISTORY IN NH_4OH LAYER FOR SPILL IN A BEAKER

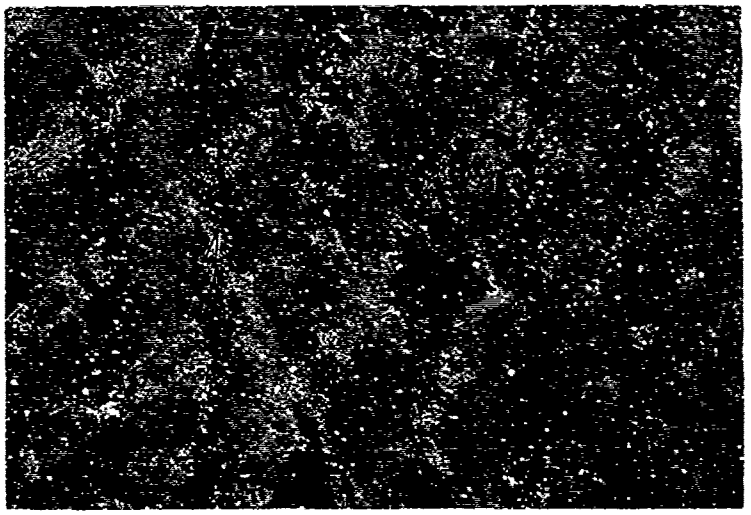

Figure 3 –12a 12 Seconds After Spill

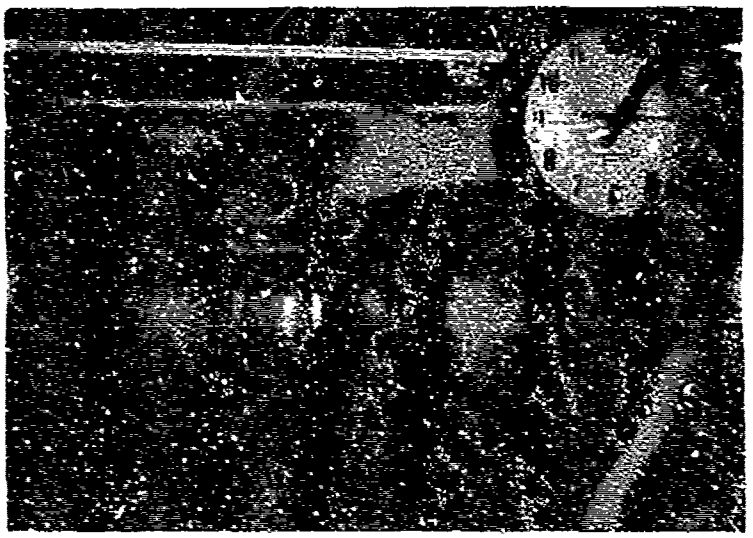

Figure 3 –12b 375 Seconds After Spill

FIGURE 3–12 PHOTOGRAPHS ILLUSTRATING THE SLOW DIFFUSION RATE OF NH_4OH SOLUTION IN THE VERTICAL DIRECTION

Table 3-5

Group IV Spill Tests

Date	Spill No.	Spill Quantity (ml)	Spill Tube Diameter (in)	Spill Angle	Additional Variables	Partition Ratio
1/30	32	1350	3/8	0	water velocity only	0.675
2/6	33	1550	3/8	0	water & air velocity only	0.675
2/9	34	1250	3/8	0	air velocity only	0.660
1/13	35	1450	3/8	0	surface isolation only	0.675

mean = 0.671

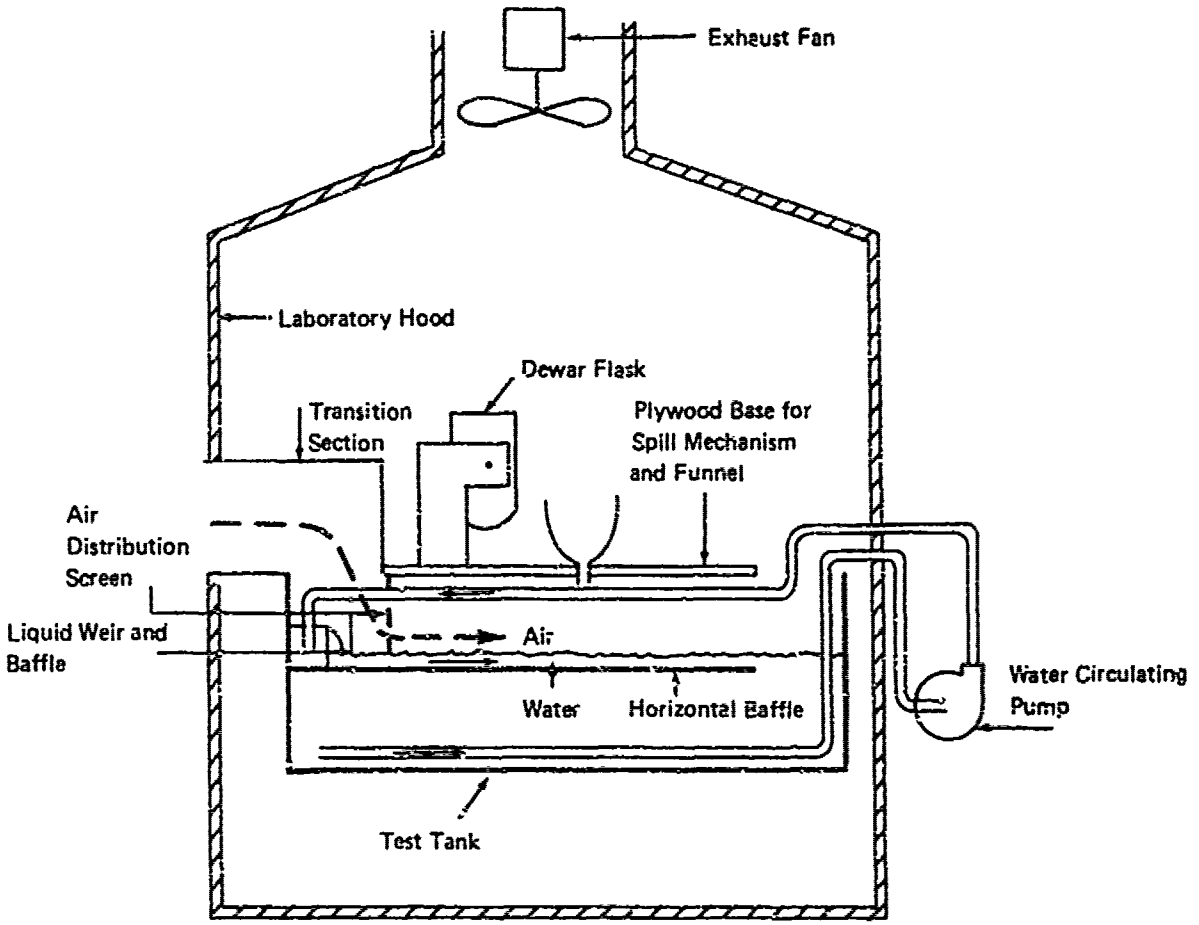

FIGURE 3–13 TEST FACILITY AS MODIFIED FOR AIR AND WATER VELOCITY

the Group IV spill tests. A transition section was placed in the vent hood, so that the air flow induced by the exhaust fan would pass directly over the water tank and tend to purge the surface of ammonia vapor. (In prior tests, air flow had been around the tank, but not across, the water surface.) A horizontal baffle was placed approximately one inch below the liquid surface, and the inlet and suction lines from the circulation pump were modified to induce water motion at the surface. With these modifications, it was possible to achieve an air velocity of about 15 feet per second and a water velocity of about 0.5 foot per second. The water surface outside the spill zone was isolated from the test area by placing plywood sheets on the water, except for about eight inches on either side of the spill zone.

Figure 3-14 shows the partition ratios obtained in these tests. Note that almost all of the experiments had a partition ratio of 0.67. This is slightly less than the mean of 0.74 obtained in the unmodified experiments. However, neither air motion, nor water motion, nor surface isolation affected the partition ratio to any substantial degree when considered separately.

3.4 UNDERWATER TESTS

Nine underwater tests were conducted to determine the influence of submergence and spill mode on the partition ratio. Table 3-6 lists the data for these tests.

A gravity head device was used for two tests, and a pressurized transfer device was used for the other tests. Figure 3-15 shows schematics of both pieces of apparatus. The gravity head device was an extension of the spill tube used in the previous surface tests. However, it was limited to shallow depths, because boiling in the submerged portion of the tube resulted in slow discharge response (i.e., rapid subsurface ammonia discharge did not occur for about 30 to 45 seconds after liquid ammonia had been dumped into the spill funnel). Further, to ensure a consistent outflow of liquid ammonia, it was necessary to bend the nozzle upward so that bubbles forming near the

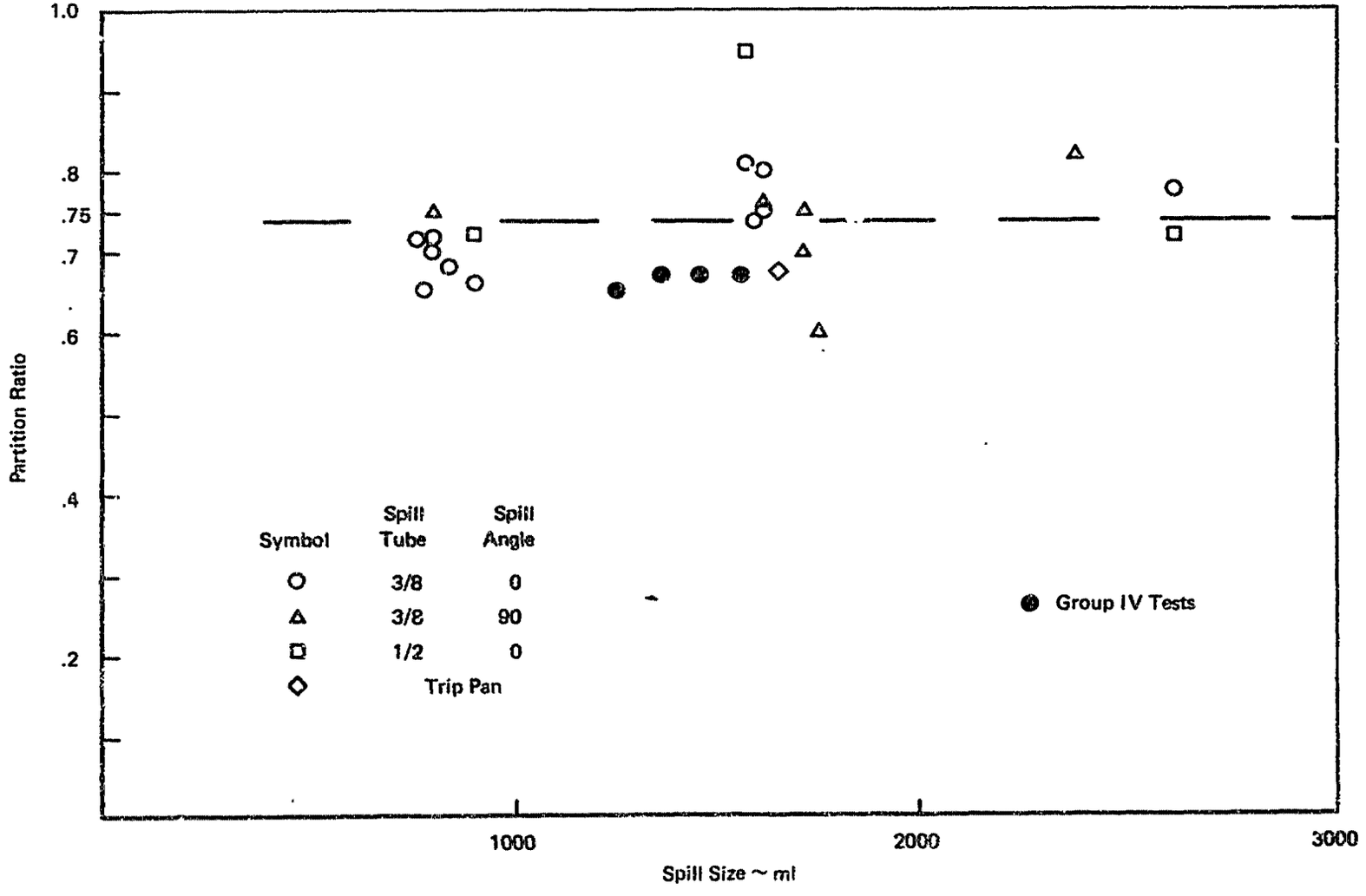

FIGURE 3–14 EFFECT OF AIR VELOCITY AND WATER VELOCITY ON THE PARTITION RATIO

Table 3-6

LNH_3 Underwater Spill Test Data

Date	Spill No.	Spill Quantity (ml)	Initial Discharge Pressure (psig)	Approximate Spill Time (seconds)[b]	Nozzle Direction	Submergence Depth (inches)	Partition Ratio
2/22	36	1300	0	--	Up	5	0.79
	37	1500	0	20	Up	5.5	0.76
2/27[c]	38	~776[a]	20	20	Down	9.5	>1
3/16	39	~530[a]	25	15	Down	9.5	0.73
3/19	40	~685[a]	5	25	Down	4.5	0.88
3/27	41	710	25	30	Horizontal	9	0.94
3/29	42	735	21	20	Horizontal	4	0.91
	43	424	22	165[d]	Horizontal	4	0.95
3/30	44	836	21	90[e]	Horizontal	4	0.93
						mean =	0.86

(a) Quantity estimated by frost line on discharge vessel.

(b) Spill time refined after viewing test movies.

(c) Very preliminary test - incomplete data.

(d) .03 orifice in discharge line.

(e) .05 orifice in discharge line.

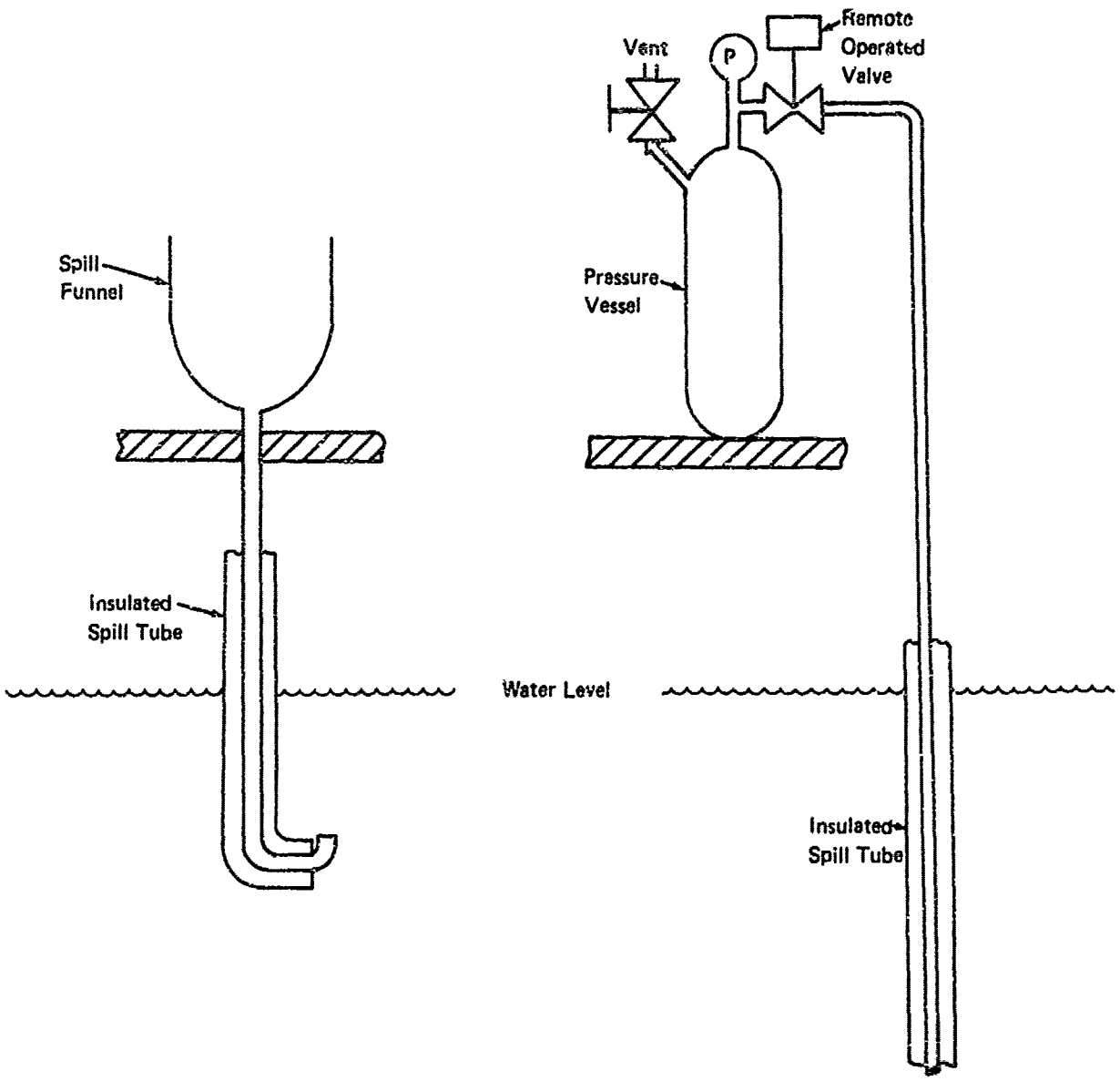

Gravity Head

FIGURE 2-15a

Pressurized Transfer

FIGURE 2–15b

FIGURE 3–15 LNH_3 UNDERWATER SPILL APPARATUS

end of the nozzle would enter the water rather than back up into the discharge tube. The pressurized discharge apparatus was not depth limited, nor was it necessary to bend the discharge tube upward to ensure positive outflow.

Note that the partition ratios obtained with gravity discharge (at a depth of 5.5 inches below the water surface) are not very different from the partition ratios obtained with the surface spills. This agreement may be due to the shallow release depth, because the ammonia vapor may not have had time enough to dissolve. Thus, the results may be similar to those with surface boiling. However, with deep discharge, most of the ammonia vapor was dissolved by the water. Table 3-6 lists the increased partition ratios obtained for pressurized releases under water. Note that the partition ratio is high for pressurized release even at relatively shallow depths (except for one test). This may be due to better mixing caused by the high velocity jet that issues from the end of the pipe during such releases.

3.5 FINDINGS

3.5.1 Surface Spills

The partition ratio seems to be essentially a constant, not influenced by changes in a number of physical variables. Specifically, we observed that:

- In over 90% of the tests, the partition ratio was between 0.65 and 0.82. In almost all instances, where data was outside this range, test reruns resulted in ratios within the expected range.
- Observation of the test tank indicates that evaporation seemed to be confined to an eight-inch zone surrounding the spill. Phenolphthalein dye and temperature measurements showed that a warm layer of ammonium hydroxide propagated from the spill zone along the water surface. The layer was about an inch thick, and its surface temperature was about 5° to 10°F above the initial water temperature.

- Within the range of the experiment, the water temperature did not seem to have a strong effect on the partition ratio, although for higher water temperatures a smaller temperature rise was measured in the propagating layer of ammonium hydroxide.
- Neither the partition ratio nor the physical model just described seemed to be strongly affected by variables which might be expected to influence interface heat and mass transfer, such as: spill quantity, spill rate, spill delivery angle, air and water motion, or salinity.
- Restricting the total area of the spill site did influence propagation of the ammonium hydroxide layer, but if the evaporation zone remained unobstructed, there did not seem to be any marked affect on either the evaporation process or the partition ratio.
- When the area available to the spill was reduced to less than the nominal eight-inch boiling zone (such as in the beaker tests), the upper layers of the ammonium hydroxide solution underwent a temperature reduction rather than the temperature rise previously noted. However, although the partition ratio varied more in these tests, the average value was not greatly affected.

3.5.2 Underwater Release

We observed that:

- When the release was at low velocity and close to the water surface, there was no substantial change in the partition ratio compared with the mean value for the surface spills.
- When the release was at high velocity, and at depths of four and nine inches, the partition ratio values increased and were much closer to 1.0. This may be a consequence of increased turbulence and hence better mixing caused by the high velocity jet of liquid ammonia exiting from the tube. Also, the

increased residence time of the vapor in the water (due to great depth) results in redissolution of vapor in water, giving a higher partition ratio.

3.6 DISCUSSION

It appears that the partition ratio for small-scale tests is not very dependent on the physical or dynamic variables in the experiment and remains nearly constant - within a reasonable experimental scatter - at an average value of 0.735. The mode or total quantity of surface release do not seem to influence the partition ratio. This holds true even when the spread of NH_4OH is restricted (as during the beaker and baffle tests). On the other hand, underwater release below a certain depth seems to increase the dissolution of NH_3 vapor and thereby increase the partition ratio.

In the Group IV tests conducted with slightly changed apparatus, the partition ratio was consistently at 0.67. It is not clear whether this was due to airflow over the water surface, or water motion, or both. However, the 6% decrease in partition ratio from that of the surface tests might very well represent some experimental problems rather than any physical phenomenon.

The analytical model presented in Section 6.2 predicts a partition ratio of 0.735 for a 70°F water. Most of the experiments were carried out with 50°F to 70°F water, and the agreement between experiment and theory is remarkable. This indicates that the reaction between small quantities of ammonia and water is purely a thermodynamic phenomenon and is independent of other kinetic and dynamic variables.

The maximum temperature of the NH_4OH solution measured is a function of the initial temperature of the water. The temperature rise is about 15°F for water at 35°F and almost zero for water at 90°F. Note, however, that the temperatures were measured at about three to four reaction-zone diameters from the center of the spill. Temperature measurements made in the reaction zone did not

give very meaningful results due to the extremely noisy data stream caused by violent boiling and agitation. The thermodynamic model predicts that the temperature rise of NH_4OH (14°F for 32°F water, and no rise for 70°F water) is a function of the water temperature. The measured and predicted values agree fairly closely.

Visual observation of the NH_4OH layer spread indicates that it spreads horizontally with a mean velocity of about 0.22 foot per second, as shown in Figure 3-7. The vertical propagation of NH_4OH is minimal. Based on visual observation of the vertical diffusion of a dye marker during the first few seconds after a spill, we calculate that diffusion coefficient for NH_4OH is between 0.1 and 0.2 cm^2/sec (0.4 to 0.8 ft^2/hr).

4. INTERMEDIATE SIZE EXPERIMENTS

4.1 PURPOSE AND SCOPE

The purpose of the intermediate-scale tests was to measure both the partition ratio and vapor concentration in air, simultaneously, on as large a scale as possible. By doing so, we intended to see if the partition ratio could be predicted by measuring the integrated vapor concentration in air.

The small spill quantities and unnatural environment of the laboratory tests (a constricting of the hood and vertical air movement in the vent) precluded meaningful measurement of vapor concentrations in the gas phase. Conversely, during any large-scale spill it is not possible to directly measure the partition ratio, because of the difficulty in obtaining a uniformly mixed water sample. Therefore, indirect methods were needed to determine the partition ratio.

These experiments were based on the premise that it would be possible to estimate total vapor flow by obtaining vapor samples over a specified time interval with collecting devices at a few locations downwind of the spill. Comparing the estimated total vapor mass liberated during a spill with the quantity of LNH_3 spilled on water would allow calculation of the partition ratio. This value of the partition ratio can then be compared with the value obtained by titrating samples of the thoroughly mixed water on which the LNH_3 was spilled.

4.2 APPARATUS AND PROCEDURE

4.2.1 Test Facility

Figure 4-1 shows the essential features of the test facility: a swimming pool, a vapor-sampling instrument rake, and a spill bucket. The aluminum-sided, plastic-lined swimming pool - 20 feet in diameter and 2 feet deep - was buried in the ground so that its top was just above ground level and the pool water surface was at about ground level. The LNH_3 transfer system, tipping mechanism, discharge nozzle, water circulating pump, and drain loop were very similar to those used in the

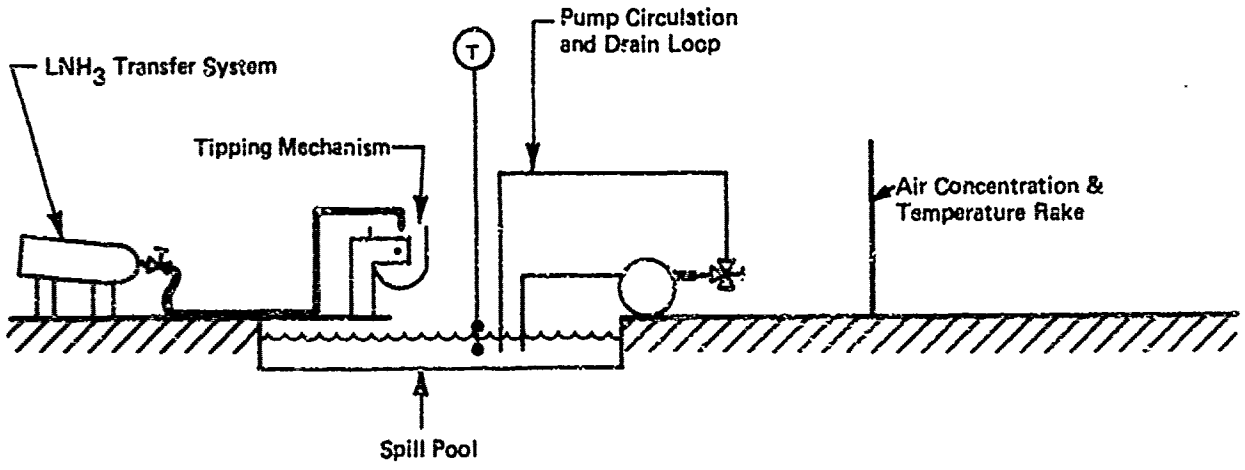

FIGURE 4-. SCHEMATIC OF INTERMEDIATE SIZE (FIELD) TEST FACILITY FOR SURFACE SPILLS

laboratory test facility. The pool was generally filled with water using a fire hose connected to the city water supply. However, the water from an adjacent pond was used for some of the early tests. The test facility was located on the testing grounds of Arthur D. Little, Inc.

4.2.2 Instrumentation:

Vapor concentration measurements were made with impinger (sniffer) devices mounted on a cross-shaped rake, as shown in Figure 4-2, generally placed about 15 feet downwind of the pool center. The rake also contained thermocouples to measure ammonia vapor temperature. Pool water temperatures were also recorded.

The impinger, shown in Figure 4-3, draws a metered flow of air through a boric acid solution, which dissolves aspirated ammonia vapor. The mass of dissolved NH_3 can be determined later by laboratory titration techniques. A steady air flow of 2.3 liters per minute through the device was maintained - at least for the duration of the ammonia vapor flow over the rake - by connecting the impingers outlets to vacuum tanks.

In addition to the above general arrangement of apparatus and instruments, the following modifications were made to perform the surface and underwater releases of liquid ammonia.

4.2.2.1 Surface Spills

Both one-gallon and five-gallon surface spills were performed. The spill bucket and tipping arrangement used in the one-gallon tests is shown in Figure 4-1. This arrangement was identical to that used in the laboratory tests. (See Figure 3-1.) A special bucket, shown in Figure 4-4, was fabricated for the five-gallon surface spill tests. The bucket had a faucet to facilitate slow release of LNH_3 (continuous spills).

As shown in Figure 4-5a, three liquid temperatures and two vapor temperatures were measured approximately two feet downstream of the

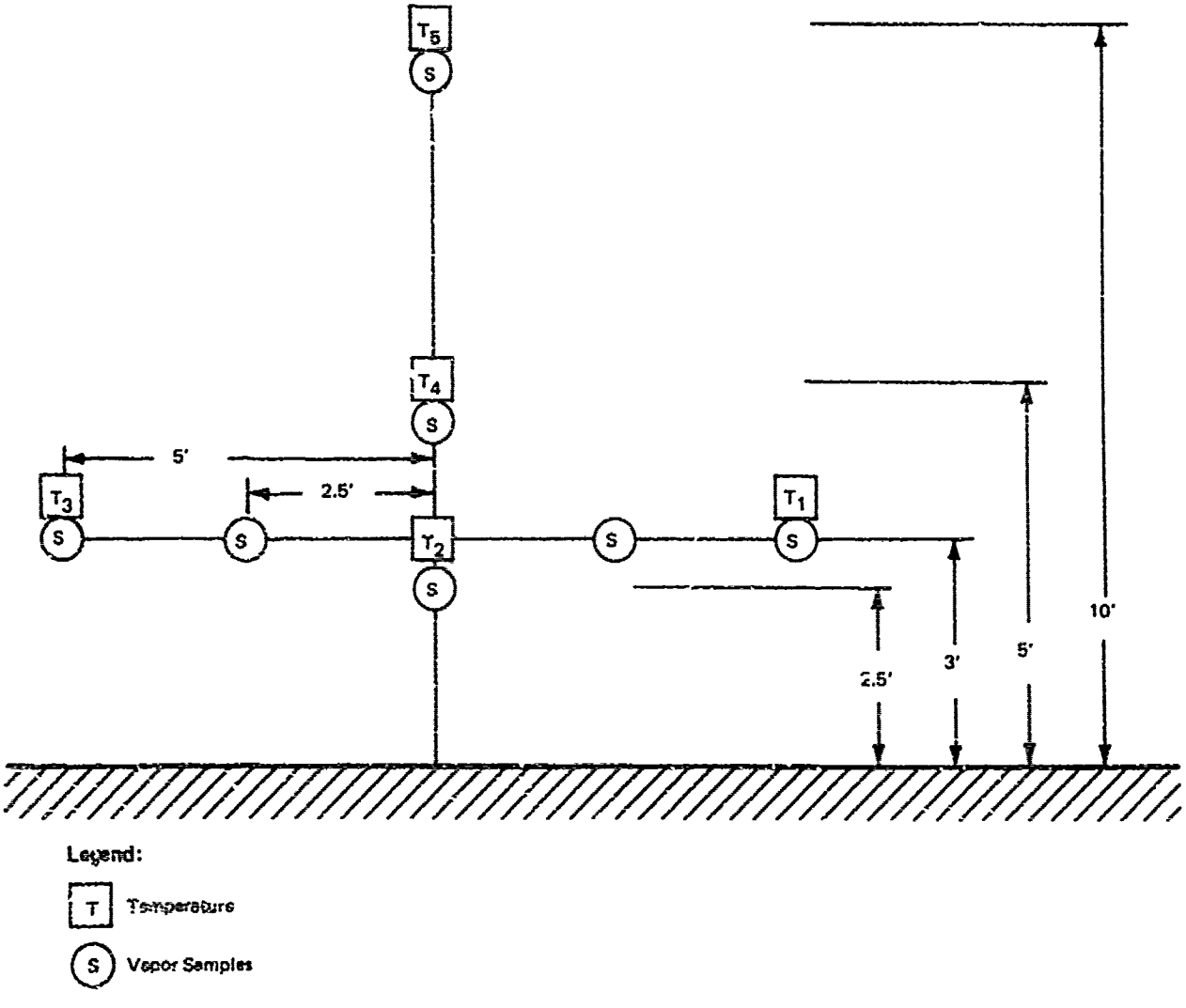

FIGURE 4–2 INSTRUMENT LOCATIONS ON THE RAKE

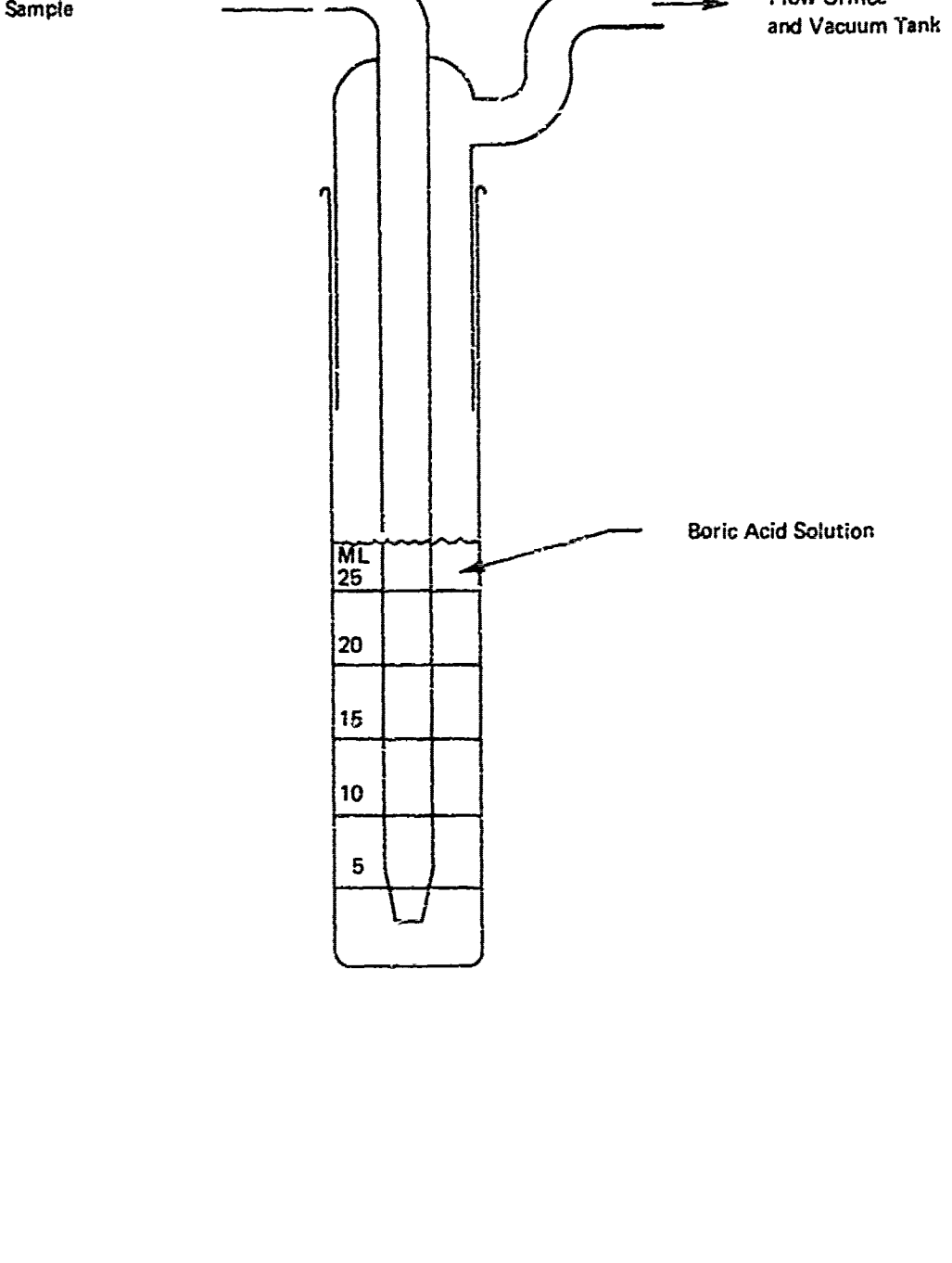

FIGURE 4–3 SKETCH OF IMPINGER DEVICE FOR VAPOR SAMPLING

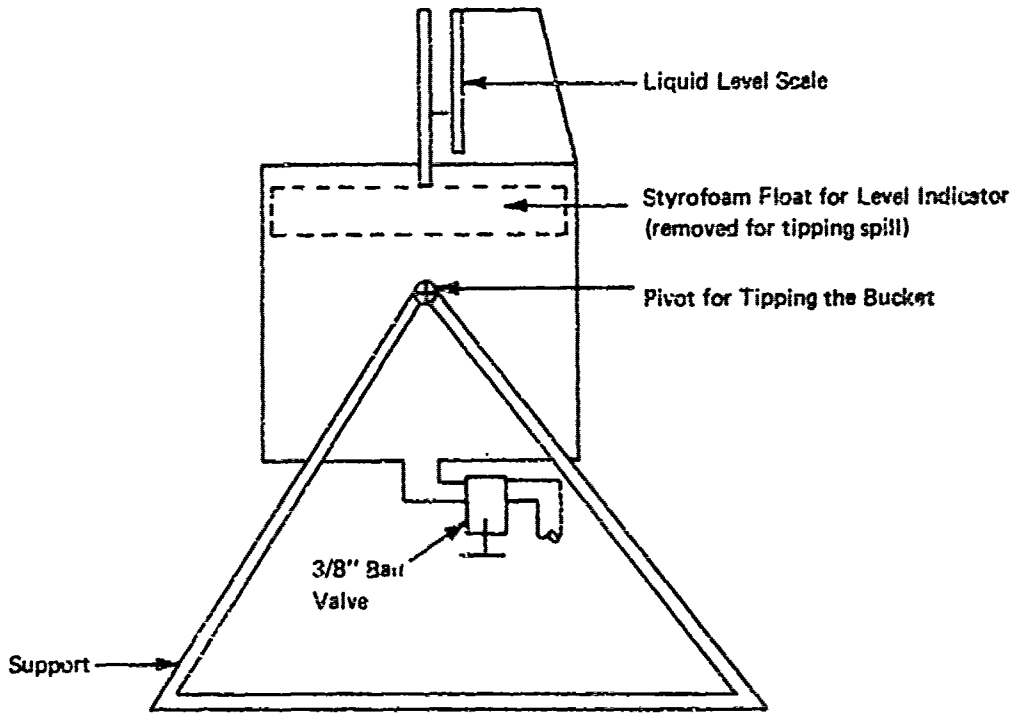

FIGURE 4–4 5-GALLON TIPPING AND CONTINUOUS FLOW BUCKET

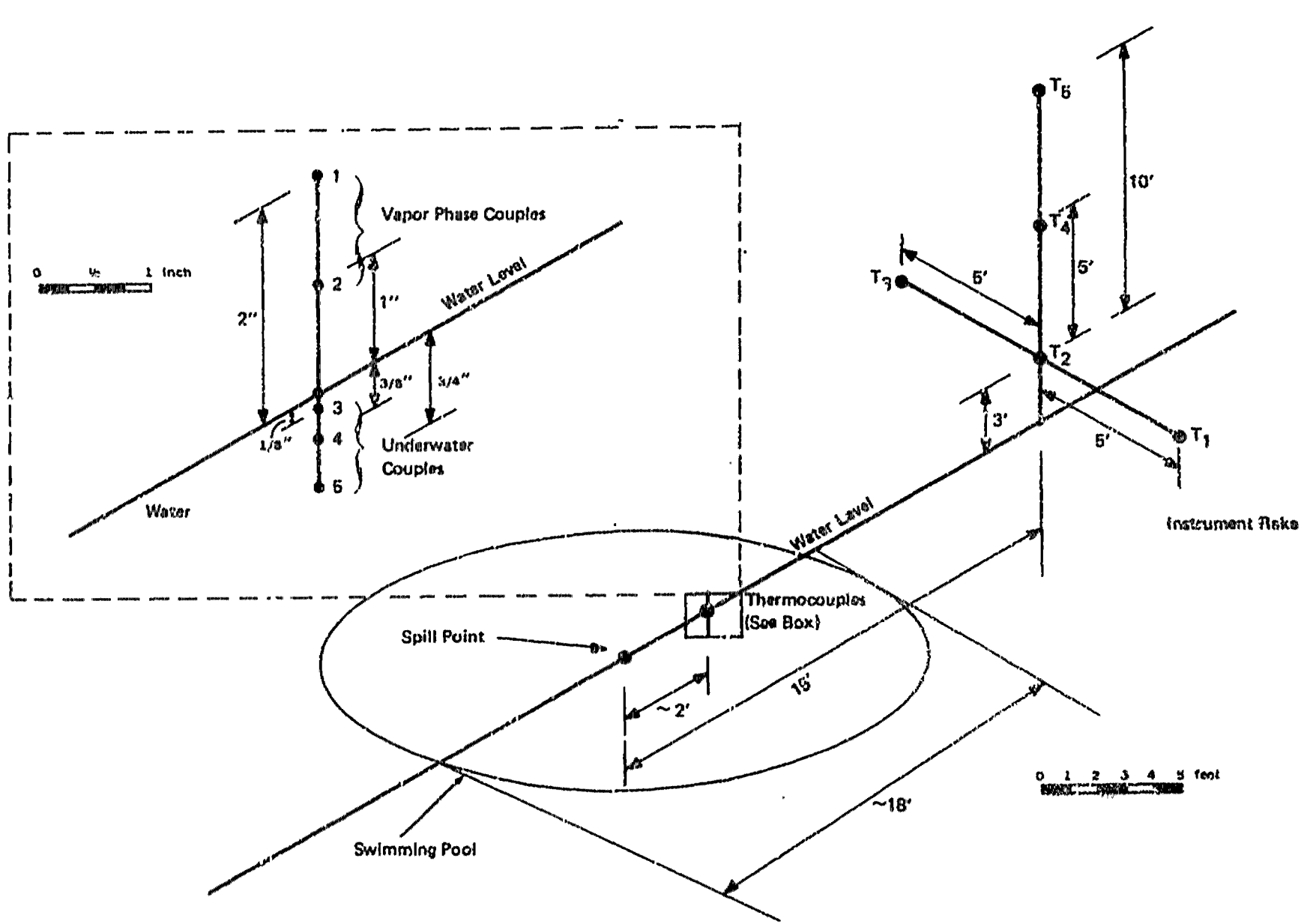

FIGURE 4–5n SCHEMATIC DIAGRAM OF THE ARRANGEMENT OF THERMOCOUPLES FOR THE SURFACE SPILLS

spill point. Pool temperatures were measured at 1/8 inch, 1/2 inch, and 3/4 inch below the water surface. Vapor temperatures were measured at about one inch and two inches above the water surface during the one-gallon spills, and at three inches and 12 inches above the surface during the five-gallon spills. In addition, five vapor temperatures were measured at the downstream rake.

4.2.2.2 Underwater Release

Figure 4-5b shows the thermocouplearrangement used during the underwater release experiments. Figure 4-6 shows the special release system built utilizing a one-gallon pressure vessel (stainless-steel fire extinguisher), a 3/8-inch stainless-steel ball release valve, and 0.5-inch ID stainless-steel submerged release tube. A similar system employing a smaller release valve and a 0.364-inch ID submerged release tube was also fabricated.

The pressure vessel was filled through a T-fitting attached to the release valve, and once the tank was filled to the desired liquid level, the supply was valved off at the T. The release valve was also closed to allow a pressure rise in the tank. At about 15 psig, ammonia was released through the submerged tube into the pool. The depth at which the liquid was released was varied by raising or lowering the submerged pipe.

Nine underwater thermocouples were placed 1.75-inch apart at the spill site, and were monitored during the underwater releases. One thermocouple above the water surface was also used. (See Figure 4-5b.)

For all tests, wind velocity and wind direction were measured, adjacent to the pool, with an anemometer and a direction vane. However, only graduated-dial readouts were available, rather than graphical strip recordings. Colored movies and 35 mm stills were made of all tests. Some tests were recorded on infrared film. Underwater color movies were made of certain subsurface tests.

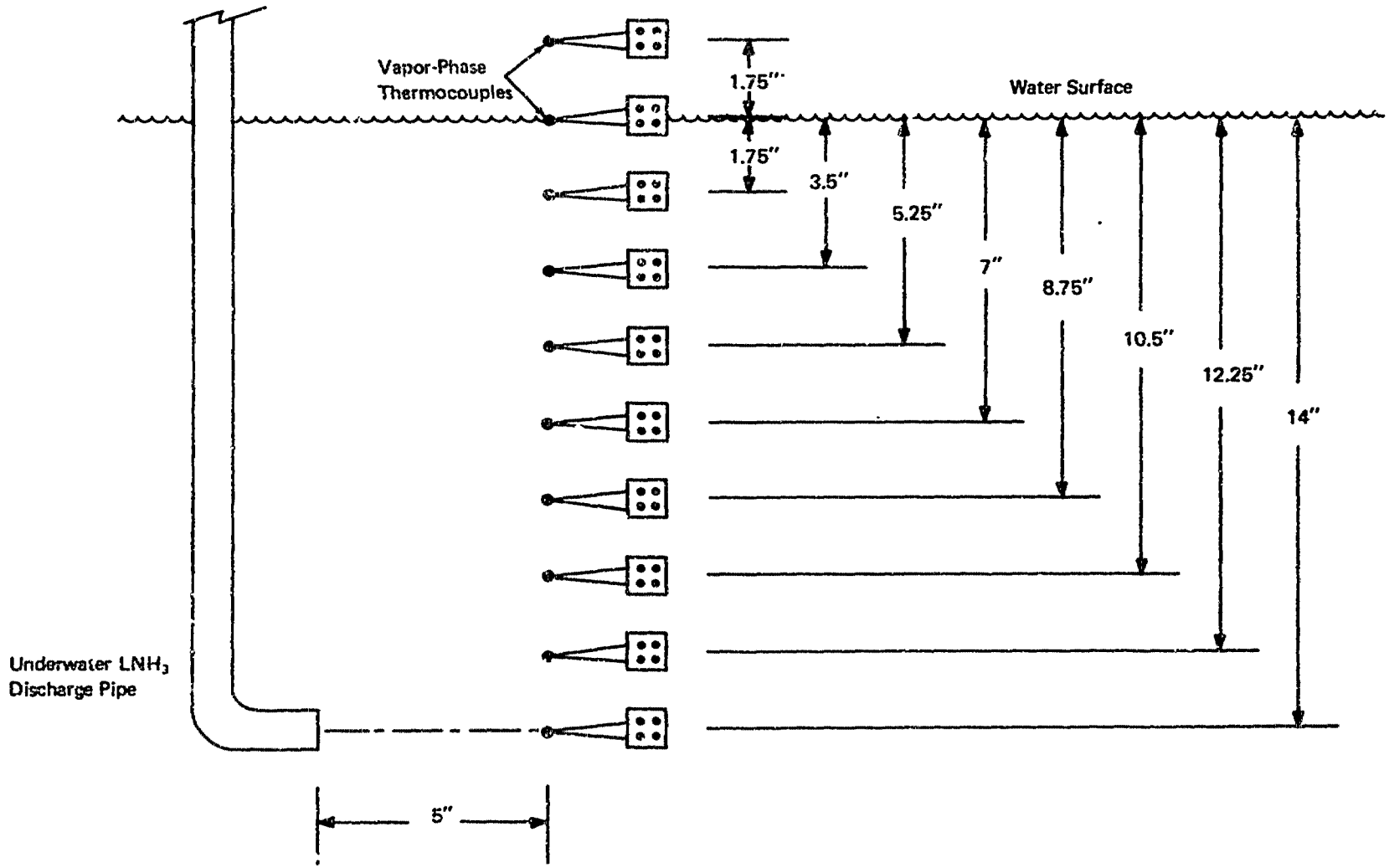

FIGURE 4–5b ARRANGEMENT AND POSITION OF THE THERMOCOUPLE BANK FOR WATER TEMPERATURE MEASUREMENT DURING UNDERWATER RELEASE OF LNH_3

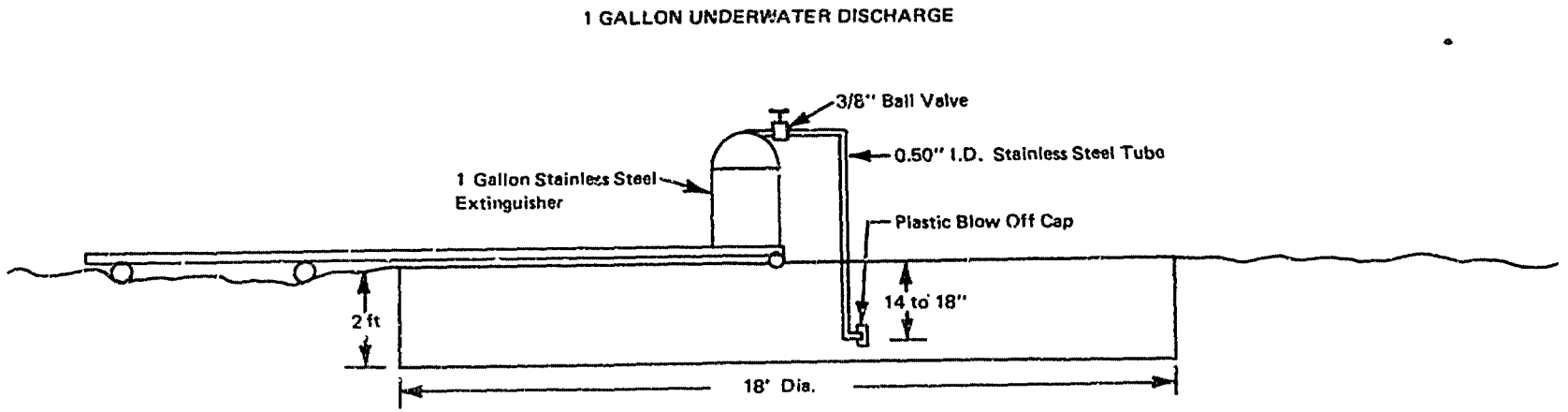

FIGURE 4–6 SCHEMATIC OF THE INTERMEDIATE SIZE TEST FACILITY FOR UNDERWATER RELEASES OF LNH_3

Table 4-1 lists the techniques and numbers of parameters measured during these tests.

4.2.3 Procedures

4.2.3.1 Surface Spills

After the pool was filled with water, the thermocouple assembly was placed in position, and the impinger rake was positioned downwind along the mean wind direction. The vacuum tanks were evacuated, and liquid ammonia was transferred to the spill bucket. When the proper volume of liquid had been transferred, and the wind was in the proper direction, the test countdown was begun.

About 60 seconds before the spill, the temperature recorders were started, and at five seconds before the spill, the impinger suction was started with a solenoid-operated valve. The LNH_3 in the spill bucket was emptied onto the water surface, all at once in the case of instantaneous spills, and slowly through the faucet in the case of continuous spills. After the vapor cloud had disappeared and about 10 minutes had elapsed, the water in the pool was mixed thoroughly by operating the water recirculating pump for about 15 minutes. Five water samples were taken, each from a different point in the pool, for laboratory analysis of dissolved ammonia content. The ammonia vapor dissolved in the impinger boric acid solutions was also analyzed.

4.2.3.2 Underwater Release

The procedure was similar to that used for surface spills, but LNH_3 was transferred to a pressure tank. The tank and contents were weighed continuously and when a pre-set weight of LNH_3 (15 to 18 lbs) had been transferred, the transfer was terminated. Because the pressure tank was uninsulated, the pressure would immediately start to rise. When the pressure inside the tank reached about 15 psig, the test countdown was begun. When the wind was oriented correctly, the vessel's valve was opened and LNH_3 was released underwater. The impingers were

Table 4-1

Intermediate Size Techniques and Parameters

	Surface Tests	Underwater Tests
Concentrations		
Mixed Liquid in Pool	5	5
Downstream Vapor Samples	7	7
Temperatures		
Liquid	3	9
Vapor over Pool	2	1
Downstream Vapor	5	-
Photography		
Color Movies		
Infrared Movies		
35 mm Stills		
Wind		
Velocity		
Direction		

switched on at the same time, and the rest of the procedure was similar to that described for surface tests.

4.3 SURFACE TEST FINDINGS

4.3.1 One-Gallon Surface Spills

Only instantaneous spills were tested in this category. The data and results are shown in Table 4-2. The average partition ratio is 0.5 (0.552 if only the results with city water are used) compared to the 0.735 obtained with laboratory spills of comparable spill quantity. (Figure 4-8 shows these partition ratios plotted against spill quantity. A discussion of the above results is deferred to Section 4.6.)

The temperature data obtained in the tests are given in Table 4-3. Note that within about a second after the spill the temperature recorded by the immersed thermocouples dropped to nearly the LNH_3 temperature and then began to rise. The temperature increase (of 5° to 10°F above water temperature) continued for three to five minutes. For one test, 22°F above water temperature was reached. The vapor phase thermocouples followed a similar pattern. However, in many cases the maximum temperatures indicated by the vapor phase thermocouples were 20° to 40°F above the air temperature. Such values are considerably higher than the increases shown by the water thermocouples. The thermocouples on the instrument rake (15 feet downwind) recorded ambient temperature except when the ammonia cloud passed over the rake. This occurred in many tests, and the temperature in the cloud was indicated to be between 15° and 20°F lower than air temperature. Such low temperatures lasted for only about one to two seconds, indicating rapid passage of the cloud past the rake. (Unfortunately, the recording instrument to which rake couples T_1, T_2, and T_3 were connected did not record the event because of its slow response time and noncontinuous printing.) For all cases when the cloud passed through the rake the temperature indicated by a thermocouple at a higher elevation lower than the temperature indicated by the one beneath it. (This phenomenon is shown better for the five-gallon spills.)

Table 4-2

One-Gallon Surface Spill Tests

Date	Spill No.	Spill Quantity (liters)†	Spill Funnel	Partition Ratio	Water Source
6/1	1	3.25	-	-	-
6/8	1	3.50	-	0.30	Pond
6/11	1	2.50	-	0.45	Pond
6/14	1	3.50	-	0.51	City Water
6/14	2	3.50	1/2"	0.49	City Water
6/14	3	3.50	-	0.65	City Water
6/15	1	3.50	-	0.56	City Water
6/15	2	3.50	-	0.55	City Water
			mean =	0.5	
			mean for City water =	0.552	

†Note: 1 gallon = 3.6 litres

Table 4-3

One-Gallon Spill

Date	Expt.	Mean temp. of Water °F	Mean temp. of Air °F	Maximum Temperature Rise (°F) Registered by the Thermocouples Above their Initial Ambient Values: Couples at 2 ft. from spill — Vapor Phase 1"	Vapor Phase 2"	Water Phase 1/8"	Water Phase 3/8"	Water Phase 3/4"	Couples on the Rake T_1	T_2	T_3	T_4	T_5	Remarks
6/11	1	80	90	No data		22	16	16	No change					
6/14	1	73	75	82	107	10	6	5	No change					The vapor phase temperatures indicated seem to be in error; this may be due to some equipment malfunction.
6/14	2	75	78	20	45	3	3	3	No change					The readings of air TCs over spill area increase slowly reaching peak at about 5 min. after spill. The high temp. persists for a long time (5–8 min).
6/14	3	75	77	30.5	48	6	6	6	No data					1/8" depth water TC shows a small dip in temperature first before increasing. High temperature indicated by the vapor phase TCs lasts for over 2 1/2 min.
6/15	1	72	73	29	39	4	4	4	No observed change		-19	-15		1" TC in vapor phase first dips to about -10°F and then within the next 2 min. rises to 101°F. The 2" high TC in the vapor also dips to about 23°F and then rises steadily to 110°F in about 2 min. The dip in the rake temp. - for a very few secs. (about 1) - indicates the passage of cloud. It is possible that the recorder used for T_1, T_2 and T_3 could not register this brief event. The water temp. first dips momentarily to 59°F and then rises.

Table 4-3 (cont'd)

One-Gallon Spill

Date	Expt.	Mean temp. of Water	Mean temp. of Air	Maximum Temperature Rise (°F) Registered by the Thermocouples Above their Initial Ambient Values: Couples at 2 ft. from spill — Vapor Phase 1"	Vapor Phase 2"	Water Phase 1/8"	Water Phase 3/8"	Water Phase 3/4"	Couples on the Rake T_1 T_2 T_3 T_4 T_5	Remarks
6/15	2	75	71	32	53	6	6	5	No change	The water TCs dip a few degrees for a brief period and then rise. The no change in rake TC readings indicate that probably the bulk of the cloud missed the tree. The vapor TC 1" values first dips to 14°F (for 1 sec.) and then rises to about 104°F in 2 1/2 min. The hot temp. persists for about 3-4 min. The TC at 2" dips to 32°F and then rises to 125°F. The hot temp. persists for over 4 min. total.

Figure 4-7 shows plots of the total mass of the NH_3 vapor collected in each impinger. Figure 4-7a shows the distributions of vapor collected along the horizontal beam three feet off the ground, and Figure 4-7b shows vertical distributions. The figure also shows the best possible Gaussian profiles that pass through the experimental points in each experiment.

4.3.2 Five-Gallon Surface Spills

A set of eight experiments were conducted with spills of about five gallons; six were instantaneous spills, and two were continuous spills at 65 ml/second. Table 4-4 gives the details of the tests in this category, such as spill quantities, partition ratio measured, etc. Note that the average partition ratio for an instantaneous spill is less than that for a continuous spill. Figure 4-8 shows these partition ratios, together with those obtained for the one-gallon spills.

Table 4-5 shows the temperature data obtained for the five-gallon tests. Note that the vapor phase thermocouples were three inches and 12 inches above the water level. The temperature data are very similar to those obtained for one-gallon spills. The large increase in vapor-phase temperature, compared to a relatively small change in water temperature, can be clearly observed.

Figure 4-9 is a plot of both vapor-concentration impinger data and best-fit Gaussian curves. Note that for the vertical distribution the maximum concentration occurred, in two experiments, at an elevated level rather than at ground level. This corresponds well with the temperatures recorded by the vertical array of thermocouples. The lowest temperature was recorded by the 10-foot-high thermocouple during passage of a cloud. This seems to indicate that NH_3 vapor rises rapidly in the atmosphere during dispersion.

4.4 UNDERWATER RELEASES

Seven underwater tests were conducted, each releasing about one

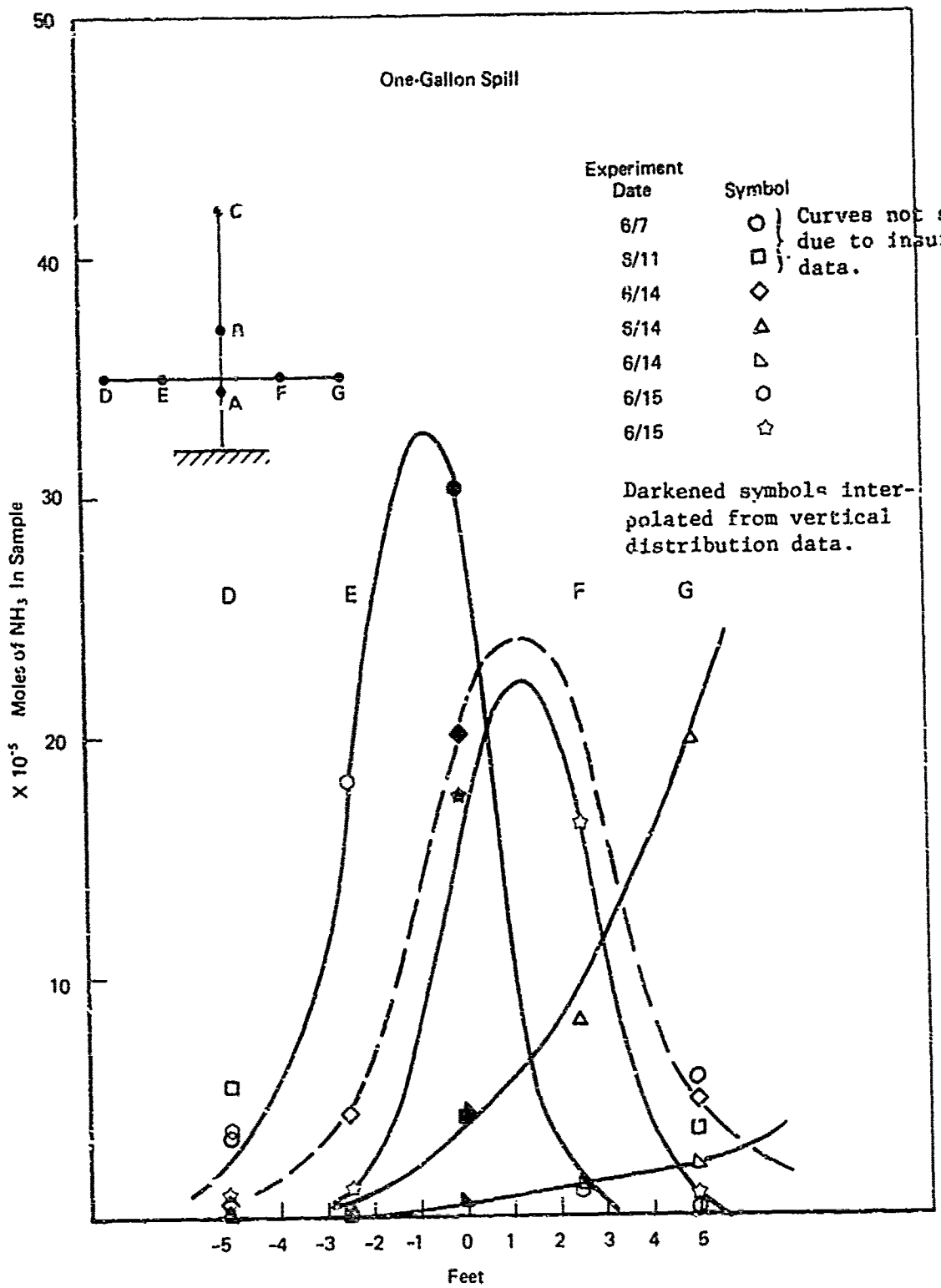

FIGURE 4–7a HORIZONTAL ARRAY ASPIRATOR DATA (D, E, F, G)
(3 Ft. Above Ground)

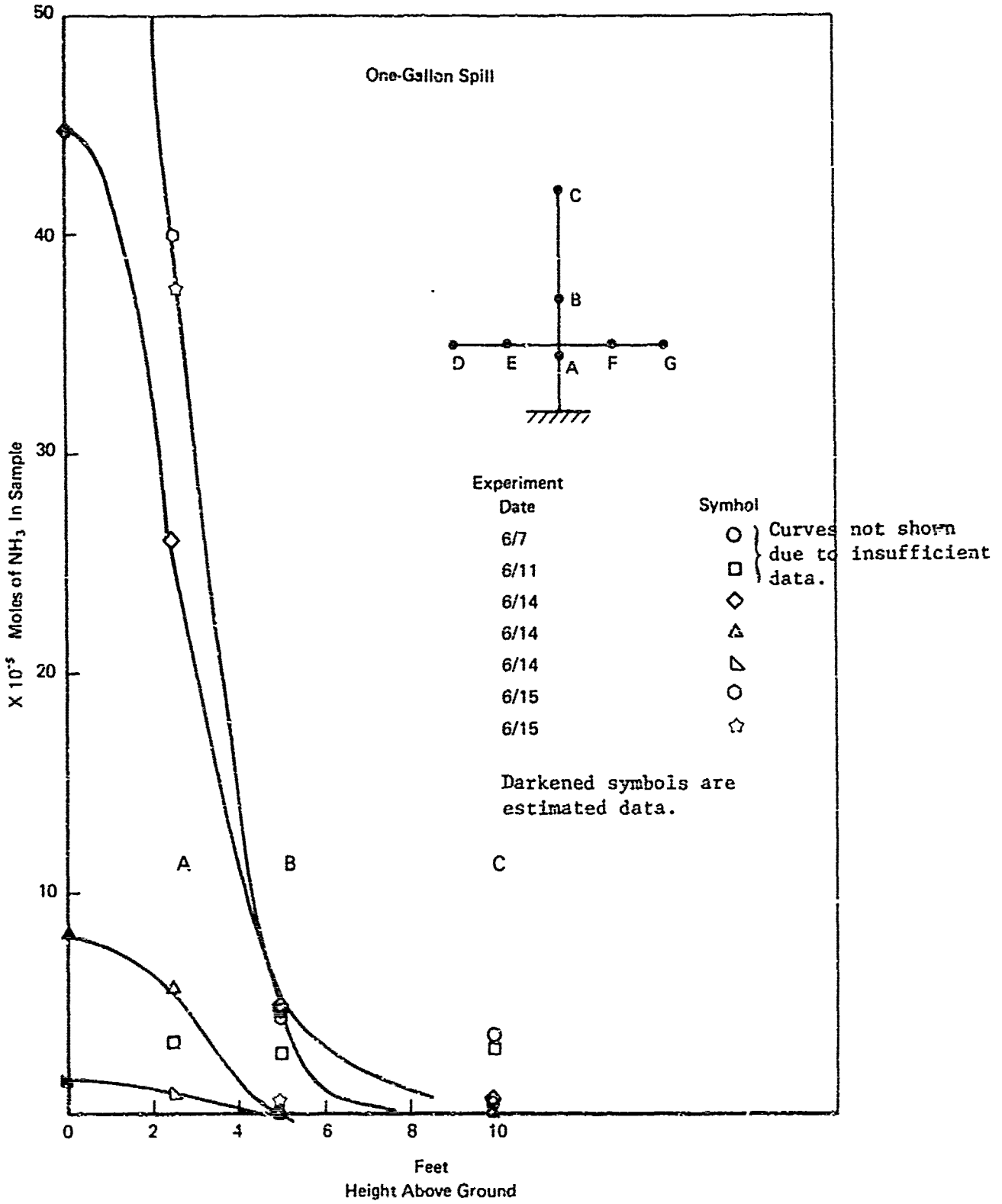

FIGURE 4–7b VERTICAL ARRAY ASPIRATOR DATA (A, B, C)

Table 4-4

Small Scale Tests Above Water

Test	Spill Quantity (litres)	Partition Ratio	Avg. Spill Rate in ml/sec	Wind Speed in mph	Type
7/19-1	17.55	0.592	Instantaneous	5-6	Above
7/19-2	21.45	0.707	Instantaneous	5-6	Above
7/20-1	19.50	0.637	61.5	0-5	3/8" pipe
7/20-2	21.45	0.686	61.5	0-5	3/8" pipe
7/23-1	17.06	0.543	Instantaneous	10	Above
7/23-2	19.50	0.526	Instantaneous	10	Above
8/3-1	21.00	0.597	Instantaneous	0-5	Above
8/3-2	21.00	0.430	Instantaneous	0-1	Above
	mean =	0.59			

Mean for instantaneous spill only = 0.566

Mean for continuous spill only = 0.662

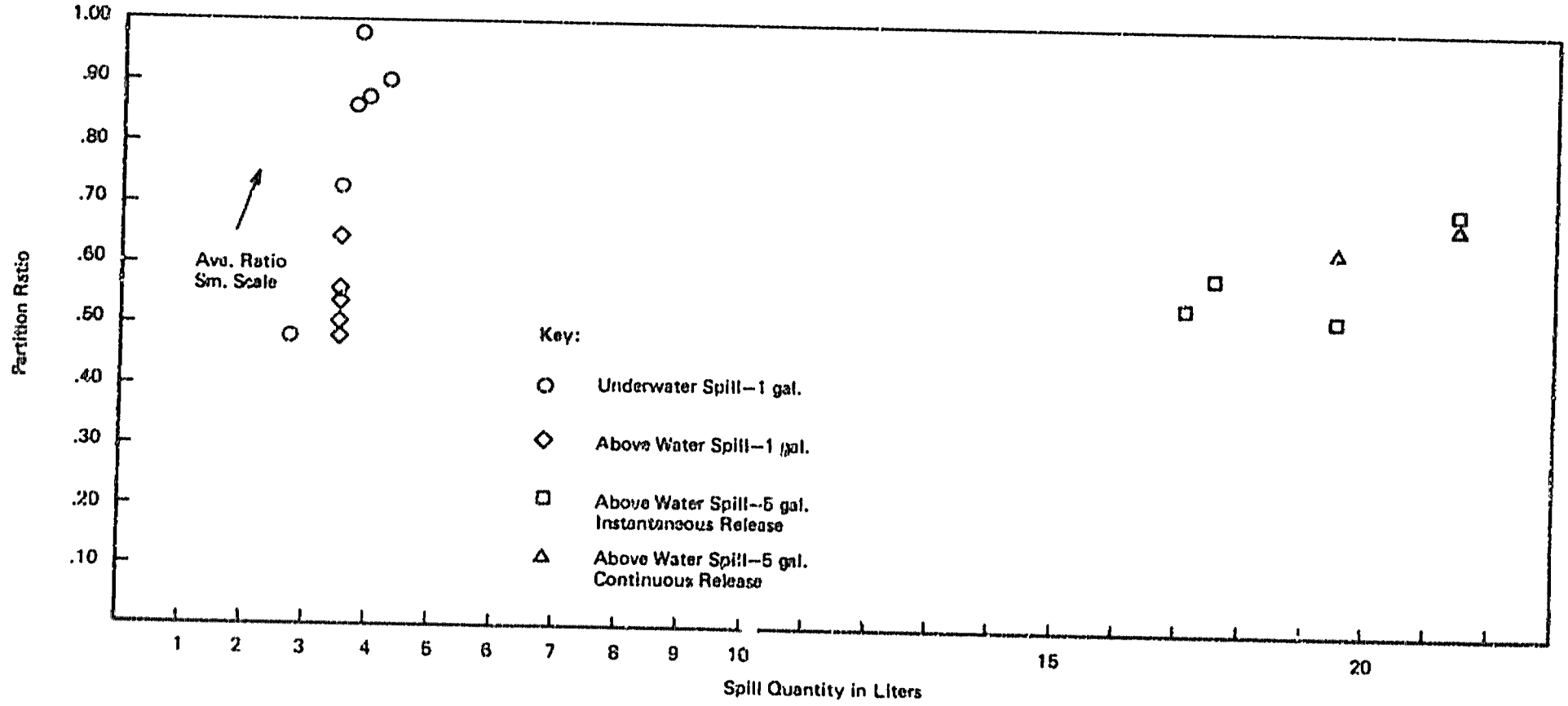

FIGURE 4–8 PLOT OF PARTITION RATIO VERSUS QUANTITY

Table 4-5

Five-Gallon Surface Spill

Date	Expt.	Mean temp. of Water °F	Mean temp. of Air °F	Maximum Temperature Rise (°F) Registered by the Thermocouples Above their Initial Ambient Values: Couples at 2 ft. from spill — Vapor Phase 1"	Vapor Phase 2"	Water Phase 1/8"	Water Phase 3/8"	Water Phase 3/4"	Couples on the Rake T_1	T_2	T_3	T_4	T_5	Remarks
7/19	2	76	83	19	19	5	2	2	No change registered			-13.5	-27.3	The air TCs on the rake indicate that a cloud passed by. That the higher TC (#5) shows a lower temp. indicates that the cloud is rising. The dip in temp. lasts only for about 1 1/2 - 2 secs. The lowest reading by water TC is 70°F. T_1, T_2 and T_3 do not show any change in reading because of the large response time of the recorder. The minimum temps. attained by vapor phase TKS are respectively -27°F and -40°F.
7/19	1	73	80	29	30	5	3	3	No change registered			-17	-21	All comments similar to above.
7/20	2	75	79	9	17	0	0	0	No change					Continuous release. The vapor phase readings are very noisy; may be due to continuous dissolution of LNH_3. Water temp. dips to about 62°F and then rises to initial temp. This rise takes about 6 to 7 mins. Note that total time for release = 5 1/2 mins.

Table 4-5 (cont'd)

Five-Gallon Surface Spill

Date	Expt.	Mean temp. of Water °F	Mean temp. of Air °F	Maximum Temperature Rise (°F) Registered by the Thermocouples Above their Initial Ambient Values: Couples at 2 ft. from spill — Vapor Phase 1"	Vapor Phase 2"	Water Phase 1/8"	Water Phase 3/8"	Water Phase 3/4"	Couples on the Rake T_1	T_2	T_3	T_4	T_5	Remarks
7/20	2	76	82	22	22	4	2	2	No change					Continuous release. Vapor TCs behavior same as above. Water temp. dips to 53°F and then rises in about 5 to 6 mins. to final value. Note total time for release = 6 mins.
7/23	1	75	78	22	18	2	2	2	No change		−13		−27	Water temp. = 50°F
7/23	2	76	76	0	8	1	1	1	No change					Water temp. dips to 54°F and then rises. Cloud probably missed the rake.

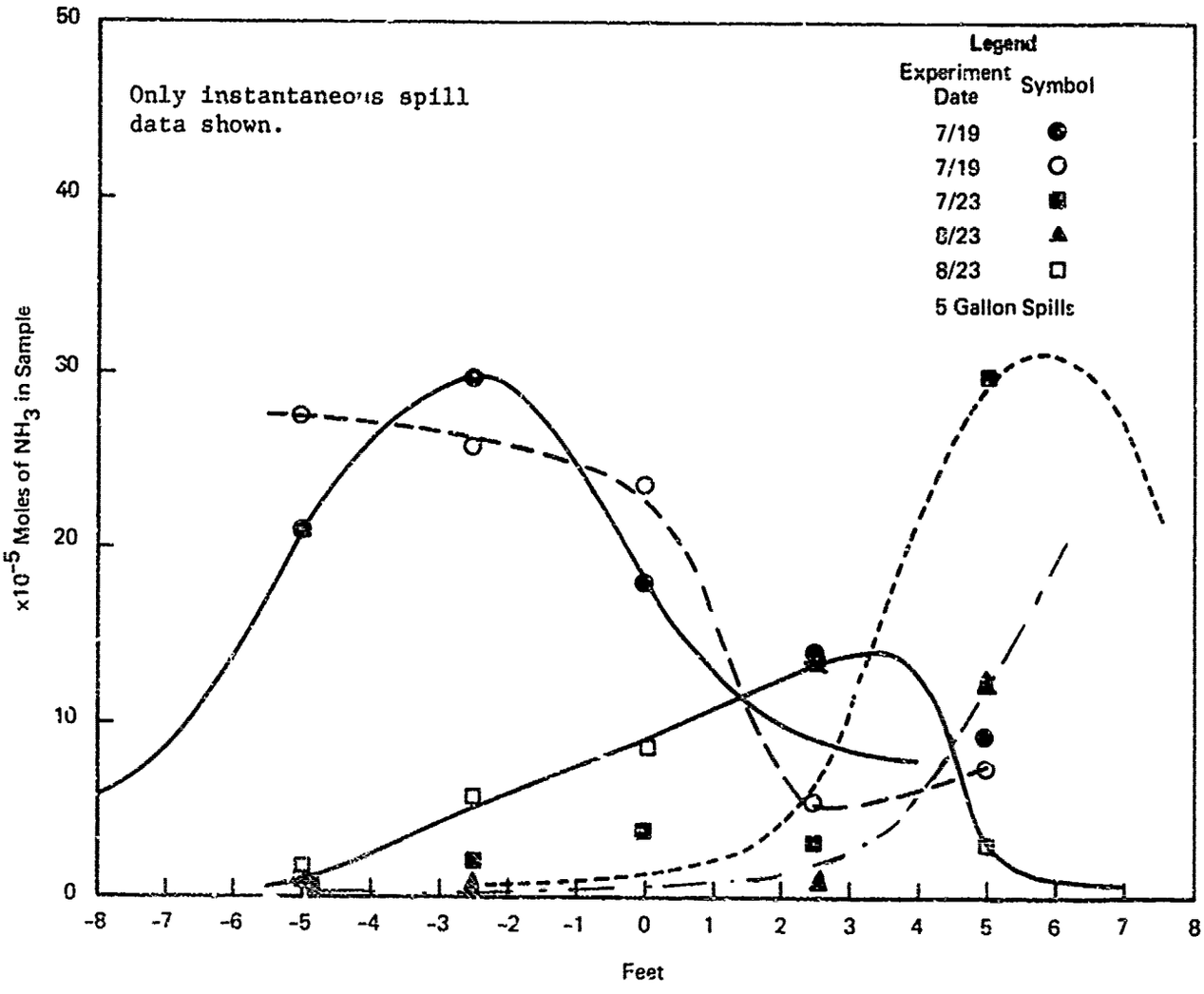

FIGURE 4–9a HORIZONTAL ARRAY ASPIRATOR DATA (D, E, F, G)
(3 feet above ground)

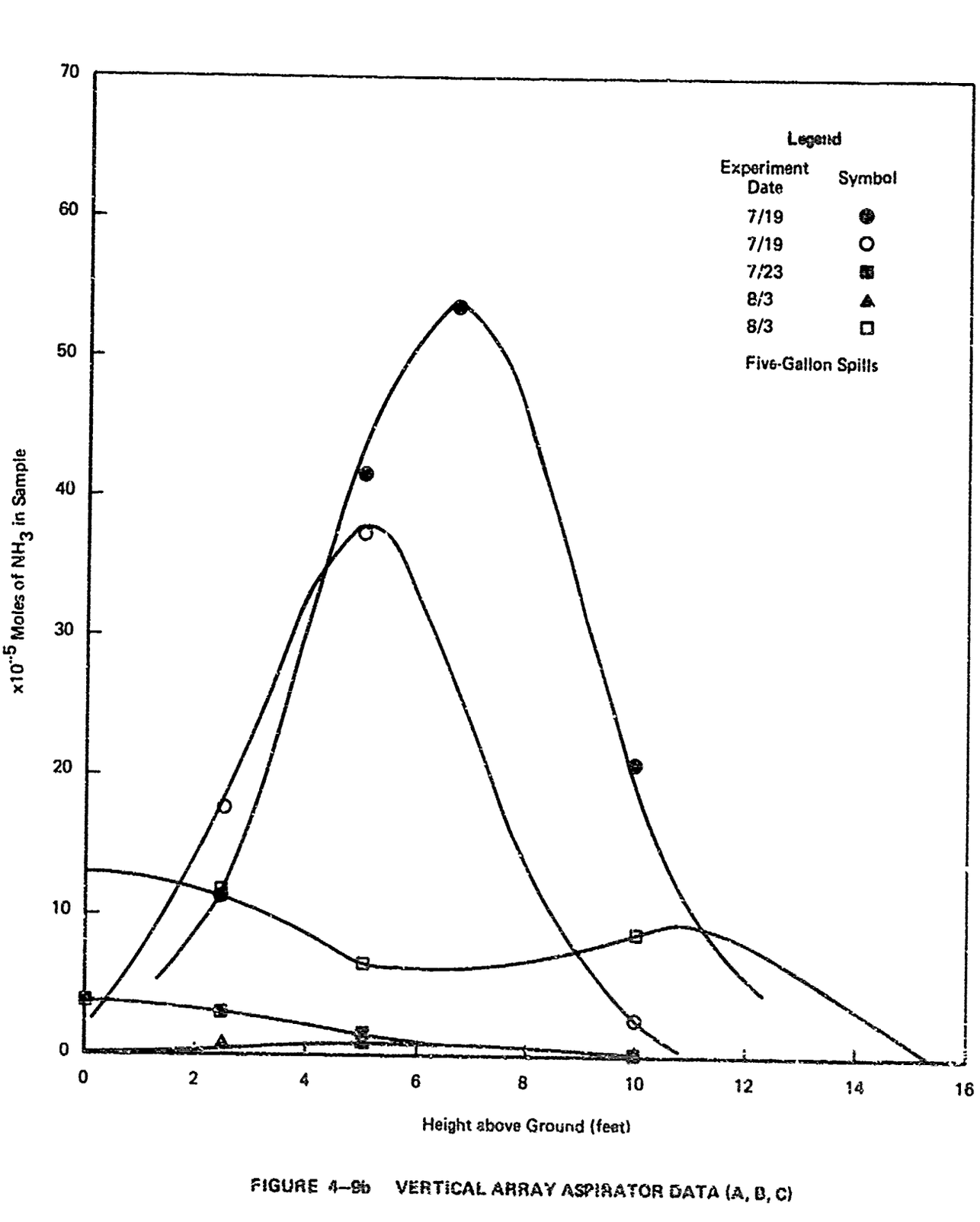

FIGURE 4–9b VERTICAL ARRAY ASPIRATOR DATA (A, B, C)

gallon of LNH_3 at depths between 14 and 18 inches below the water surface. Table 4-6 gives the details of the tests. During the process of release, only minimal agitation of the water surface was noticed, except when the release was at seven inches. In that case the water surface was punctured with mini fountains (four to five inches high), which were almost directly over the release point. Some "crackling" sound was recorded and the ground very close to the edge of the pool rattled, as if there were a small earthquake. The recordings of the crackling noises, made with a hydrophone in the pool, have not provided any useful information.

Note that the measured partition ratios are all very high, indicating almost total dissolution of the LNH_3 in water. In fact, in the first two tests, he impingers did not register any ammonia vapor at all. Therefore, in subsequent tests, no impinger data were taken. The low values of the partition ratio obtained for the first two tests were probably due to incorrect sampling of the water after the test. (The pool water was not mixed well before samples were obtained for those tests.)

The water temperature was measured using a bank of thermocouples along a vertical line about five inches from the exit of the underwater discharge pipe. (See Figure 4-4b.) Figure 4-10 shows typical records of the temperatures for 14-inch release depth and 7-inch release depth. These indicate that, close to the point of release, large temperature variations occurred. Although very low temperatures were recorded close to the release point, the high temperatures occurred only above the release point. Also, the maximum increase in temperature at any point seemed to be not mor than about 10°F, while up to 30°F drops have been seen. The latter temperatures may be due to cold LNH_3 being released in the vicinity of the thermocouple. No particular pattern can be ascribed to the temperature variations with time. However, there is a definite decrease in the effect as one goes farther from the release point. The thermocouple in the air recorded a more disturbed temperature profile that varied as much as 15°F.

The spread radius was estimated from movies.

Table 4-6

Underwater Swimming Pool Tests

Test	Spill Quantity (litres)	Tank pressure before release psig	Depth of release -inches-	Partition Ratio	Avg. Spill Rate in ml/sec	Wind Speed in mph	Type
6/22-1	2.69	10	18	0.484	-	1.0 mph	.364 ID
6/22-2*	3.40	15	18	0.330	-	0 - 1.0	.364 ID
6/26**	3.80	20	-	-	5.5	0 - 1.0	.364 ID
7/6-1	3.77	17	14	0.864	9.2	0.5	.466 ID
7/6-2	3.51	20	14	0.725	11.0	10.0	.466 ID
7/12-1	3.90	23	14	0.875	12.6	8 - 10	.466 ID
7/12-2	4.235	12	7	0.903	14.6	5 - 8	.466 ID

* Pool water not mixed well

** Test with hydrophone

mean for last four tests = .842

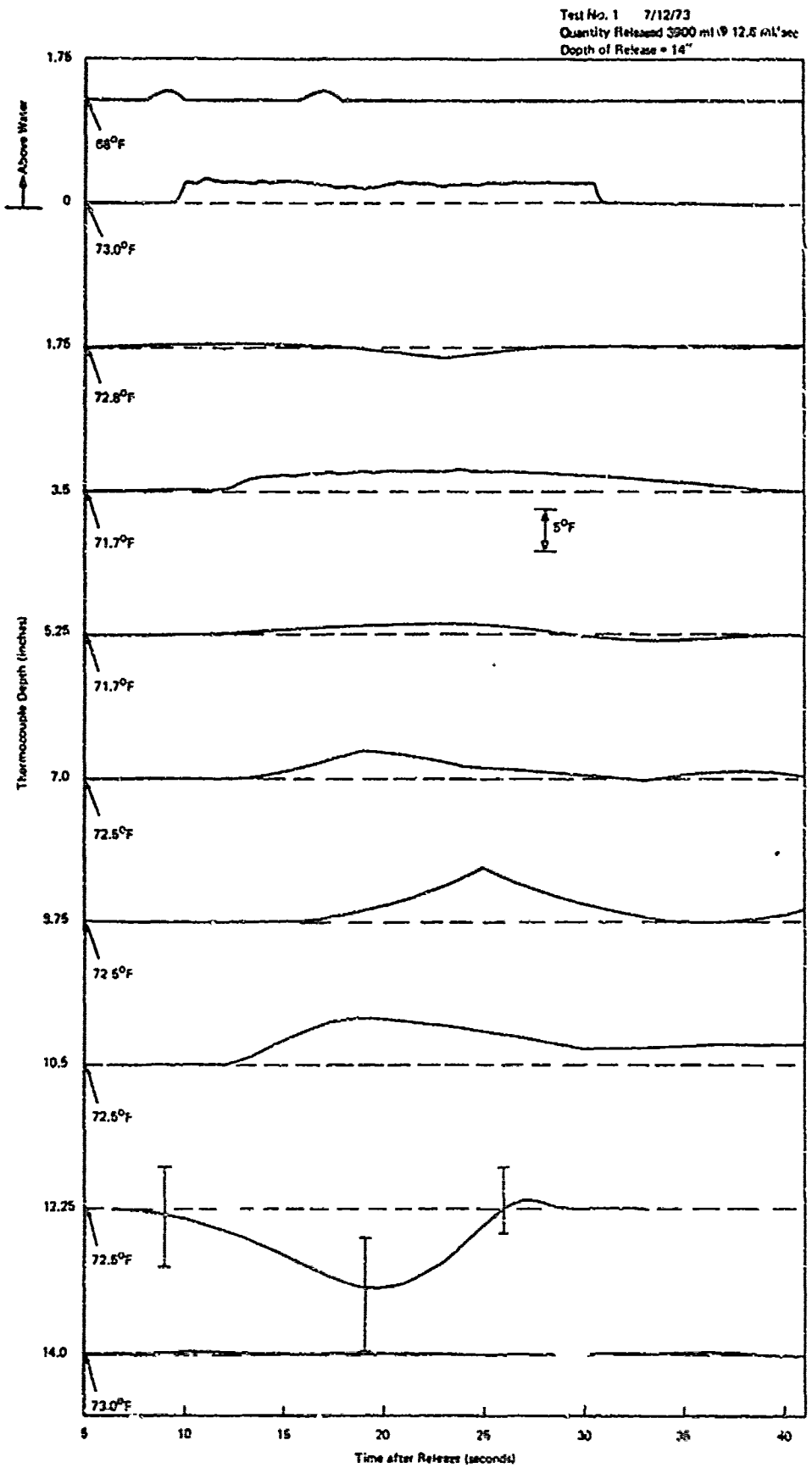

FIGURE 4-10a WATER TEMPERATURE RECORD DURING UNDERWATER RELEASE

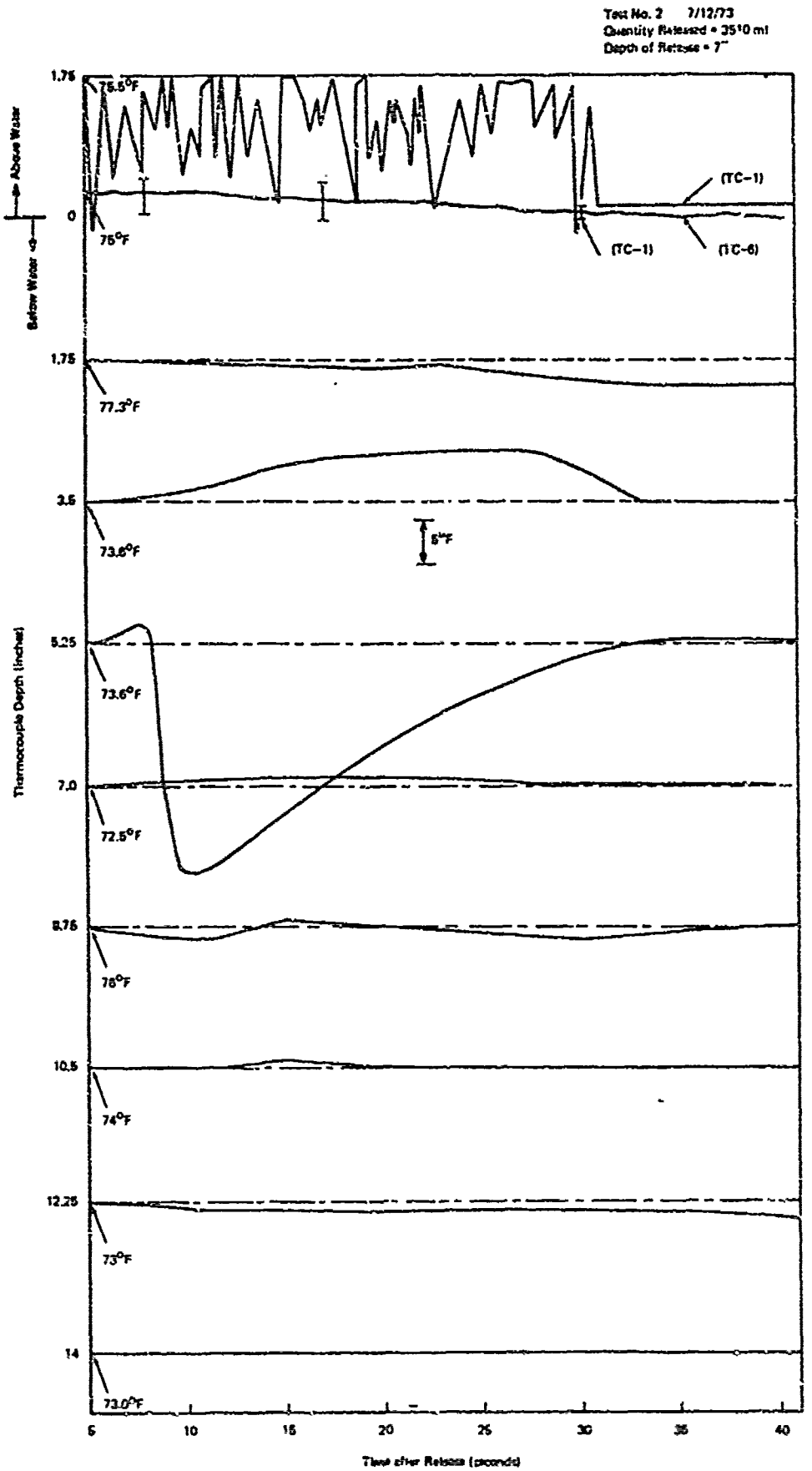

FIGURE 4–10b WATER TEMPERATURE RECORD DURING UNDERWATER RELEASE

4.5 ANALYSIS

From the impinger data, we can calculate the total vapor mass as follows:

If

$m(y,z)$ = moles of vapor collected at the location y,z on the instrument rake at distance x

where

y = direction normal to the wind direction and parallel to the ground

z = vertical direction

and

A_y = Area under the measured y-molar distribution = $\int_{-\infty}^{+\infty} m(y,z)\, dy$

A_z = Area under the measured z-molar distribution = $\int_{-\infty}^{+\infty} m(y,z)\, dz$

Assuming that the distributions in other regions of the y-z plane are similar to the measured distributions, it can be easily shown that the total mass of vapor liberated is

$$M_v = \mu \frac{U}{q} \frac{A_y A_z}{m(y_o,z_o)} \qquad (4\text{-}1)$$

μ = molecular weight of NH_3

q = constant suction rate

U = wind velocity

In Eq. 4-1, $m(y_o,z_o)$ represents the value of moles of NH_3 vapor collected by the impinger at the common point between the vertical and horizontal arrays, Once the mass of vapor is calculated, then the partition ratio can be calculated with

$$P = 1 - \frac{M_v}{M_{LNH_3}} \qquad (4\text{-}2)$$

Table 4-7 shows the calculated values of the partition ratio, made using the impinger data of selected tests by the above method. These are compared with the partition ratio values obtained from water sampling. Note that for the tests where the cloud hit the instrument rake squarely, the mass of vapor liberated in the spill could be estimated fairly accurately. A comparison of the values of the partition ratios both calculated and measured indicates that in most cases they agree reasonably well.

Note that the mass of vapor calculated by Eq. 4-1 is quite sensitive to wind velocity. During the pool experiments, wind velocity was not measured accurately. The numbers for wind velocity given in Table 4-7 are best estimates, based on readings from a meter. It is, however, encouraging to note that even if the wind velocity was actually slightly different from the above-quoted values, the mass of vapor estimated would be correct within a factor of 2 for the worst case.

Table 4-8 indicates the same vapor concentration data in terms of the standard deviations of the best Gaussian profiles that fit the distribution data. The mean values of the horizontal standard deviations (σ_y) are 1.7 feet and 3.7 feet for the one-gallon and five-gallon spills, respectively. Similarly, the values in the vertical direction (σ_z) are 2.2 and 2.9 feet respectively. These values are compared with the values of σ's estimated from Pasquill-Gifford curves for a distance of 15 feet from the source. (See Figure 6-17.) Table 4-9 lists both of these values. The agreement is reasonably good. This indicates that probably the regular vapor dispersion models could be used to describe the NH_3 vapor dispersion. (This subject is discussed better in Section 5.5 in the light of large-scale experimental data.)

No systematic and meaningful analysis of the temperature data could be made. A general discussion of the implications of the results of temperature measurements is given in the next section.

4.6 DISCUSSION

There is a definite pattern to the partition function results.

Table 4-7

Reduced Data - Intermediate Size Test

Expt. Date	Expt.	Wind Velocity (mean) mph	$A_z = 10^{-5}x$ Measured areas from impinger data distribution curves Mole-ft	$A_y = 10^{-5}x$	Vapor collected by the common impinger $n(y_o, z_o)$ Moles = $10^{-5}x$	Volumetric suction rate litre/min.	Calculated mass of vapor kg	Mass of LNH_3 spilled kg	From vapor measurement Partition Ratio From water sample		Remarks
						1 GALLON SPILLS					
6/11	1	4.0	104	46.0	4.0	2.25	0.90	1.705	0.47	0.45	Cloud missed the instrument rake
6/14	1	5	123.3	134.0	20.0	2.25	0.778	2.387	0.67	0.51	
6/14	2	5	190	24.4	4.0	2.25	1.09	2.387	0.54	0.49	
6/15	1	7	122.9	215.8	34.0	2.25	1.028	2.387	0.57	0.56	
6/15	2	4	89.36	204.54	17.4	2.25	0.79	2.387	0.67	0.55	
						5 GALLON SPILLS					
7/19	1	6	203.8	344	18	2.25	4.4	11.97	0.632	0.592	
7/19	2	7	390	200	23.2	2.25	4.43	14.63	0.697	0.707	
7/23	1	10	190	20	4	2.25	1.79	11.63	0.846	0.543	Cloud missed the instrument rake
8/3	1	0-5	-	-	-	2.25		14.32	-	0.597	Cloud missed the instrument rake
8/3	2	3	88	124	8.8	2.25	0.7	14.32	0.95	0.430	Not enough good data

Table 4-8a

Vapor Concentration Data (Reduced), One-Gallon Spill

Date	Estimated Value of Standard Deviations (feet)		Molar Masses Estimated ($\times 10^{-5}$)		Remarks
	σ_y	σ_z	m_z^{max}	m_y^{max}	
6/14	2.05	2.38	45	24	
6/14	?	2.4	8.1	?	Cloud out of instrument range
6/14	?	2.4	1.4	?	
6/15	1.4	2.05	84	32.7	
6/15	1.55	1.6	102	23	

Table 4-8b

Vapor Concentration Data (Reduced), Five-Gallon Spill

Date	Estimated Standard Deviations (feet)		Location of maximum concentration		Molar Mass Estimated ($\times 10^{-5}$)		Remarks
	σ_y	σ_z	y Direction (feet)	z Direction (feet)	m_y^{max}	m_z^{max}	
7/19	2.71	2.4	-2.72	6.72	30	53.5	Instantaneous Spill
7/19	5.59	2.14	-2.95	5.12	27.6	37.76	"
7/20	4.43	3.5	4.68	0.75	50.33	37.9	Continuous Spill Not shown in Figure 4-9.
7/20	?	2.2	?	3.59	?	42.7	
7/23	2.2	4	5.7	0	30.8	4	Instantaneous Spill

Table 4-9

σ_y and σ_z Values

at 15 Feet from Source

Standard Deviations	Arithmetic Mean of Experimental Data (from Tables 4-8a and 4-8b)		Extrapolation of Pasquill Curves**	
	1 Gallon	5 Gallons	Formula	Value
σ_y in feet	1.5	2.5	$0.165\ X$	2.475
σ_z in feet	2.5	2.5	$0.318\ X^{0.8}$	2.78

**X is in feet. Formula obtained by extrapolating the Pasquill Curves (Figures 6-17a and 6-18b) for Atmosphere B to small distances.

The partition function is high, close to 0.9, when the LNH_3 is released underwater and is low, about 0.57, when a large quantity is released instantaneously on the water surface. When the release is continuous and on the water surface, the partition function ranges from 0.66 to 0.7. These results conform to what one might expect, based on the physics of the release problem.

In the case of underwater release, the LNH_3 and the vapor generated have enough time to completely dissolve in water. The vapor that is generated at the point of release dissolved during its travel upward through the water. Hence, the partition function is high.

In the case of a large instantaneous release on the surface, two phenomena may be occurring simultaneously. One is the boiling of saturated LNH_3 to produce saturated ammonia vapor, while the LNH_3 and water reaction also contributes vapor. The other phenomenon is the aerosol formation, as fine drops of ammonia are thrown up into the air by the brief but violent agitation that occurs during the surface boiling process. Because of this, the total quantity of liquid that goes into solution with water is low and the partition ratio is small. We observed that the mean partition ratio of the surface spills was quite below that obtained in the laboratory experiments. We speculate that in the laboratory experiments the confining walls of the test tank may have allowed liquid ammonia droplets to condense from the vapor and return to the liquid, resulting in an increased partition ratio.

The very low partition ratios obtained when pond water was used in the pool may be due to the initial high pH of the water (resulting in lower amounts of LNH_3 in solution). However, because the pond water was not analyzed before the tests, it is hard to give any definitive reasons for the observed low values. In the continuous release case, the partition ratio value is between the underwater and surface spill values, for obvious reasons. In fact, the partition ratio for the continuous release is closer to the predicted value (see Section 6.2) of 0.73 based on the thermodynamic mixing model.

Immediately after a surface spill, the thermocouples in the water showed a marked temperature decrease, with the one nearest the surface indicating the lowest temperature. Within 15 seconds, the temperature was everywhere above the ambient and slowly rising. A maximum temperature was reached in two to three minutes, with the top thermocouple again showing the maximum value. In many experiments, the maximum was about 120°F, a value very close to the maximum (122°F) predicted by the second adiabatic mixing model (see Section 6.2). The observable reaction was complete within about 5 to 10 seconds, whereas the rise in water temperature continued for about two to three minutes and stayed at the high temperature for over five minutes before starting to decrease. This slow increase in water temperature is probably the result of a slow reaction of concentrated NH_4OH solution at the water surface with the layers of pure water below. Once the boiling had stopped, the mixing was brought about by molecular diffusion, and this is a long-term process. The persistence of the high water temperature at the surface is due to the slowness of natural cooling. It is interesting to see that not much lateral mixing takes place, even though hot water (or the NH_4OH solution) is less dense than the surrounding water.

The temperature rise recorded by the thermocouples in the vapor phase seems to be more or less in phase with water thermocouple results. Initially there was a sudden decrease in temperature - to almost -27°F - and then a steady rise. The low temperature was indicated only for about 1 to 1.5 seconds. This is probably the result of the passage of NH_3 vapor past the thermocouple. However, the maximum temperature registered by these thermocouples is far above the value registered by the water thermocouples, though the maximum readings occur at about the same time and persist as long. Also, in many cases the thermocouple farther away from the water surface (two inches above or 12 inches above) indicated higher temperatures than the one nearer to the water. The reasons for this behavior are not known precisely, but there are various possibilities. One possibility is that a small drop of NH_3,

water, or concentrated NH_4OH solution thrown up into the air by the boiling process lodged itself on the thermocouples and the reaction between the various radicals was completed on the thermocouple bead. Though the temperature rise can be explained by this "model," the duration of temperature rise cannot be explained because LNH_3 and water react rapidly any time they are mixed together. A more likely possibility is that of a reaction between a droplet of water on the thermocouple bead and a continuous stream of vapor that is being liberated from the water surface during the slow reaction process in the water mass. In this case, one cannot only explain the high temperatures recorded (adiabatic reaction of NH_3 vapor dissolving in water results in very high mixture temperatures) but also the duration to attain these maximum values. It is, however, noteworthy that in all experiments, except one, the maximum temperature rise above the ambient value recorded by the vapor phase thermocouples was never more than 52°F. This value is the maximum rise possible by the adiabatic mixing of LNH_3 and water (see Section 6.2, Model 2). However, for the adiabatic dissolution of gaseous ammonia (GNH_3) in water, theoretically the mixture temperature can almost reach the temperature of boiling water (212°F). Though the exact nature of the reaction that brings about such a high temperature reading of the vapor phase thermocouple is not known, we experimentally verified that is is <u>not</u> due to any ionization phenomenon caused by charged NH_3 vapor flow over the dry thermocouple bead.

The temperatures indicated by the thermocouples on the instrument rake are useful to the extent that they indicate the passage of the cloud past the rake. The entire cloud passed the rake within a matter of two seconds. (Because one of the recorders used for measuring these temperatures was of the integrating type, with duration of integration considerably longer than two seconds, no temperature change was registered by the printout of this recorder.) For many tests, the temperature indicated by the highest thermocouple was less than the temperature read by the couple beneath it. In the same tests the vapor-concentration impinger dats also indicated a maximum at

the top impinger. These results indicate that the center of the cloud was far above the ground surface and was still fairly cold (indicating the presence of partially mixed GNH_3). It also indicates that the cloud rises rapidly during the process of dispersion.

The relative agreement between the vapor mass flow estimated from the impinger data and that obtained from water sampling indicate that it is possible to estimate the partition ratio from measurements of vapor concentration in air. However, note that the calculation of the partition ratio is very sensitive to the accuracy of the wind velocity data and that the instrument rake be hit squarely by the cloud. Therefore, while in principle it is possible to obtain the mass of vapor flow by time-integrated concentration measurements, cooperation by nature is very essential to assure success in this method. Results shown in Section 4.5 also indicate that the standard deviations (or dispersion parameters) for the measured concentrations could be reasonably predicted from existing methods in the literature. A complete discussion on the dispersion results is given in Section 5.

The temperature results of the underwater tests indicate that the maximum temperature change occurs near the exit section. The maximum increase in water temperature is not more than about 10°F, whereas no temperatures were less than 30°F below water temperature. Since no details of the NH_4OH concentration could be measured, the temperature data by itself does not give much quantitative information. However, the partition ratio was not very affected by the release at 7 inches or 14 inches depth. In both cases the release is at a depth greater than 10 times the diameter of the discharge pipe. The result is in qualitative agreement with the result of the simple order-of-magnitude theoretical analysis presented in Section 6.8.

5. LARGE-SCALE EXPERIMENTS

5.1 PURPOSE AND SCOPE

The purpose of the large-scale field test program was to obtain downwind ammonia-vapor concentration data from as large a test as practical in an unconfined, natural environment. It was hoped that such data (in addition to that collected from the intermediate size experiments) would allow extrapolation to, and prediction of, the downwind vapor concentrations to be expected from releases of LNH_3 amounts ranging up to and including 3,000 tons.

These experiments were based on the premise that a certain portion of the NH_3 vapor cloud might dissolve in water as the cloud traveled considerable distances downwind over open stretches of water. In addition, it was assumed that the vapor-sampling devices (which provided adequate data for indirectly calculating the partition ratio for the intermediate-scale experiments) could also be relied on to provide adequate data for large-scale tests.

5.2 APPARATUS AND PROCEDURES

5.2.1 Test Facility

The large-scale experimental program was conducted on a pond, located at Space Research Corporation headquarters, along the United States-Canada border. Seven 8-foot by 8-foot instrumentation rafts and an 8-foot by 8-foot spill platform, with 25-foot by 4-foot walkways, were constructed on the pond and anchored in the configuration shown in Figure 5-1. A partial side view of spill platform and raft A are shown schematically in Figure 5-2. The instrumentation rafts were outfitted with cross-shaped instrument rakes that supported eight impinger devices, as shown in Figure 5-3. As for the intermediate-scale tests, the impingers on any one rake were connected to a set of vacuum tanks with vacuum tubing containing in line limiting orifices. The use of solenoid-operated valves and underwater power connections to each raft allowed the entire system to be remotely activated from

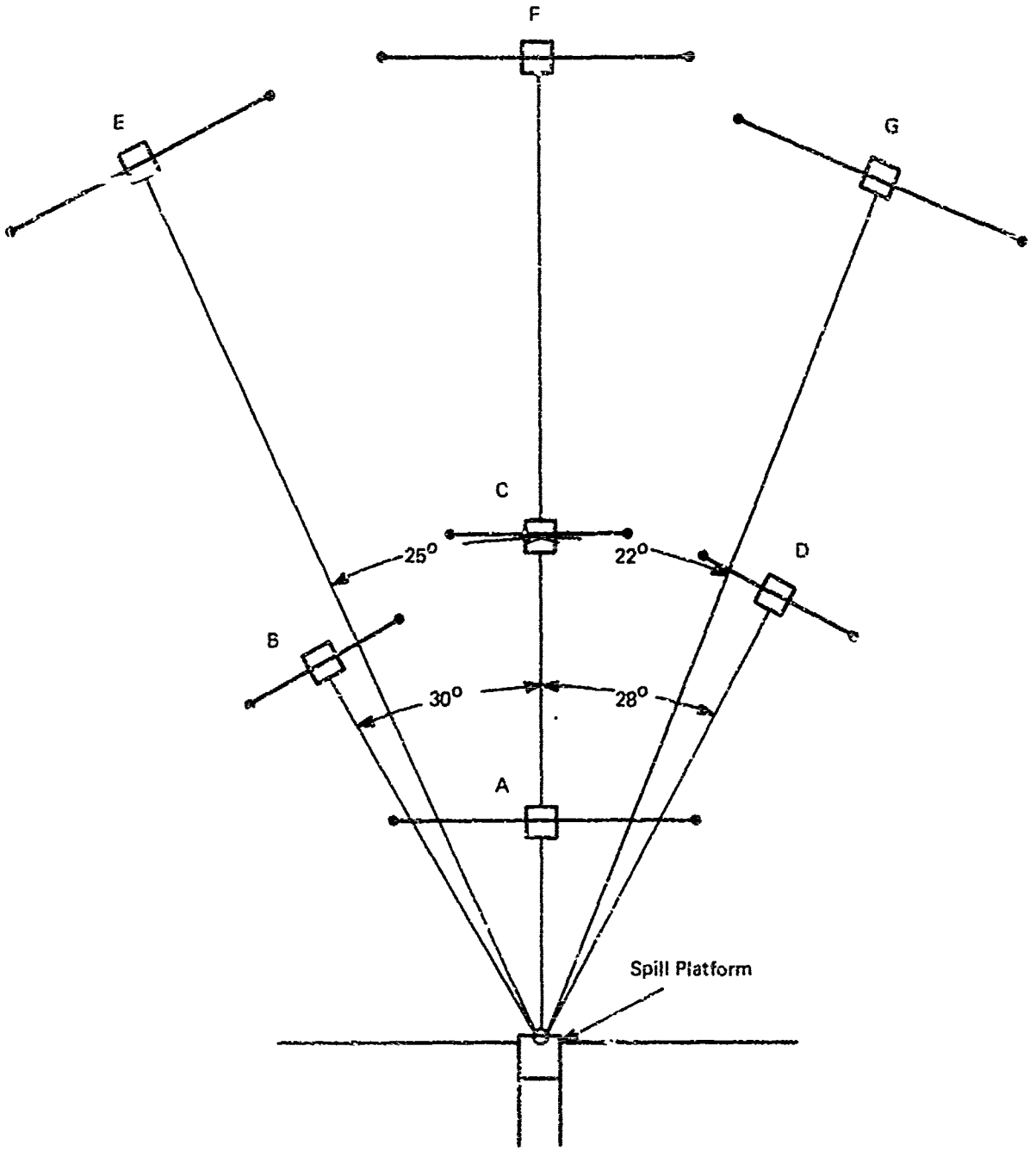

MEAN LOCATIONS OF RAFTS

RAFT #	A	B	C	D	E	F	G
Distance to Raft Center from Edge of Spill Platform – Feet	26	52	60	60	115	117	111
Bearing Angles	0°	–30°	0°	28°	–25°	0°	22°

Scale 1" = 20'

FIGURE 5–1 MEAN LOCATION OF RAFTS

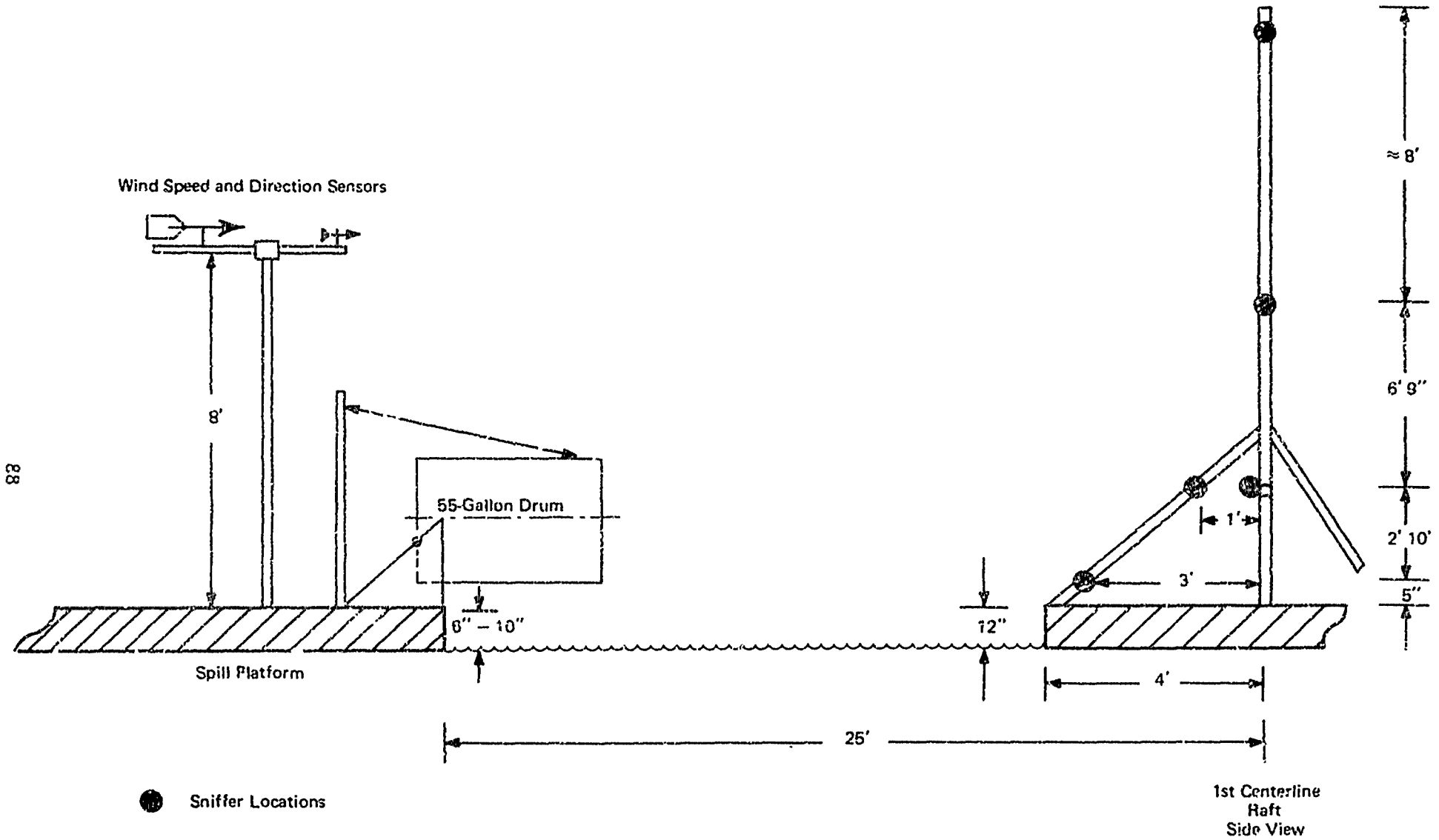

Note: Spill Platform and Raft A Set-up for Tests Nos. 3–18.

FIGURE 5–2 PARTIAL SIDE VIEW OF THE SPILL PLATFORM AND RAFTS

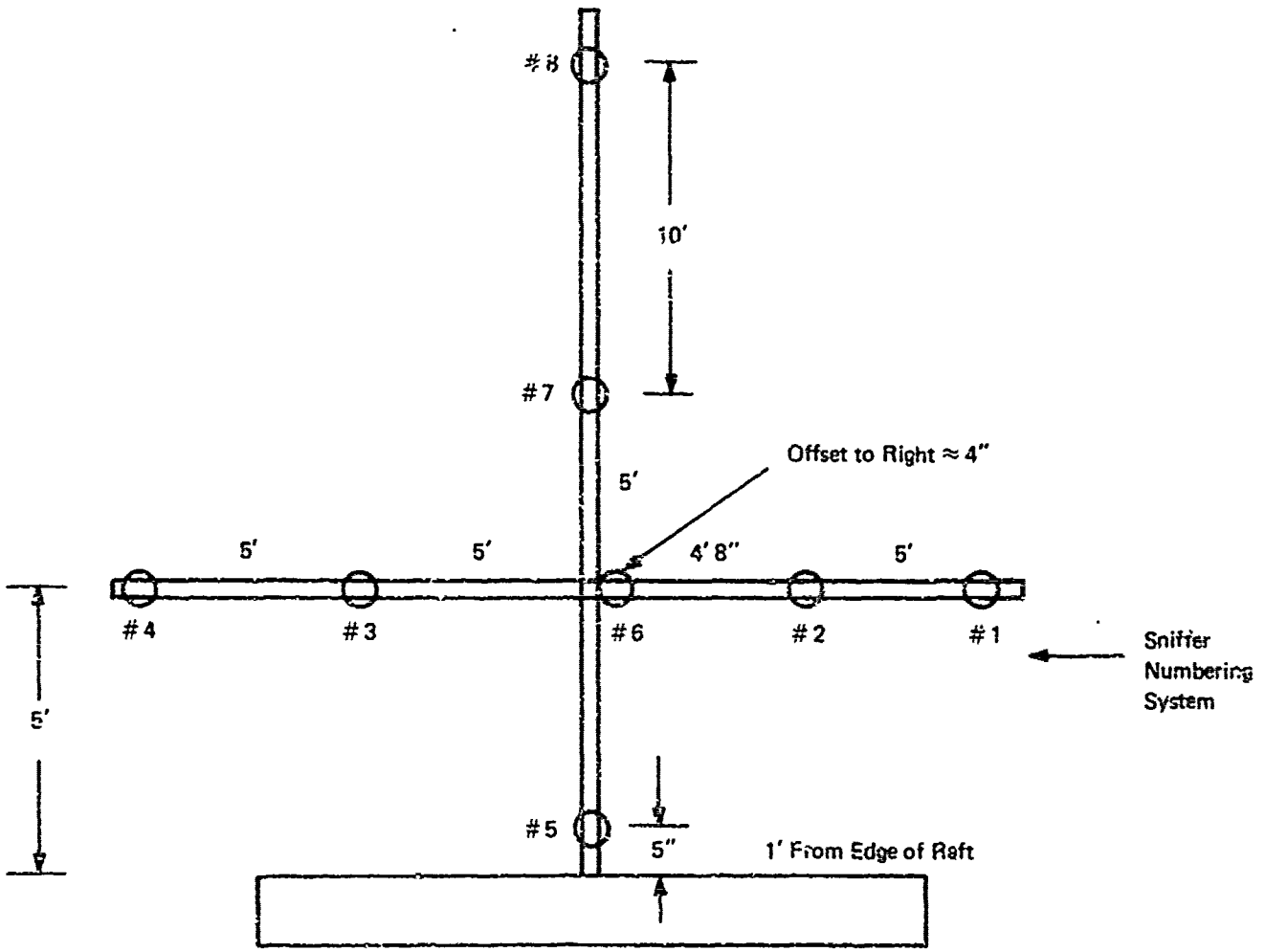

Note: Rafts B, C, and D; Rafts E–G were similar but had 36' cross-pieces with horizontal separations = 9'.

FIGURE 5–3 SNIFFER POSITIONS ON THE RAFTS AND THE SNIFFER IDENTIFICATION NUMBERS

shore just prior to an LNH_3 release.

5.2.2 Instrumentation

Figure 5-3 shows the details of the vapor sampling instrumentation set-up for the seven rafts (designated rafts A-G as in Figure 5-1). In addition to this arrangement of vapor sampling apparatus, the following additions and modifications of instrumentation were made to perform the surface and underwater releases of LNH_3.

5.2.2.1 Surface

In all, ten surface releases of LNH_3 were performed. Three five-gallon spills were made to correlate the data with that obtained from the intermediate-scale tests, and seven were 50 gallon spills, made to provide additional data for this phase of the project.

The five gallon spill tests used the specially fabricated bucket from the intermediate-scale tests. The details of this bucket and its associated mechanisms were shown in Figure 4-4.

The 50 gallon spill tests were conducted with a similar apparatus, using a 55 gallon-capacity insulated steel drum. A support rope held the drum during filling, and a rubberized cable was added to lessen the shock to the drum during the sudden tipping and dumping of the contents. The floating foam block previously used to indicate the volume of fluid in the spill vessel was replaced by a yardstick, so that the depth of liquid could be noted just prior to a spill.

In addition to the vapor-concentration measurements, five liquid-temperature measurements and two vapor-temperature measurements were made during some of the experiments. Liquid temperatures were measured 0.5 to 1.0 inch below the water surface. Vapor temperatures were measured six feet above the water surface approximately 60 feet and 117 feet downwind of the edge of the spill platform. Figure 5-4 is a schematic of the underwater thermocouple position during the surface release tests.

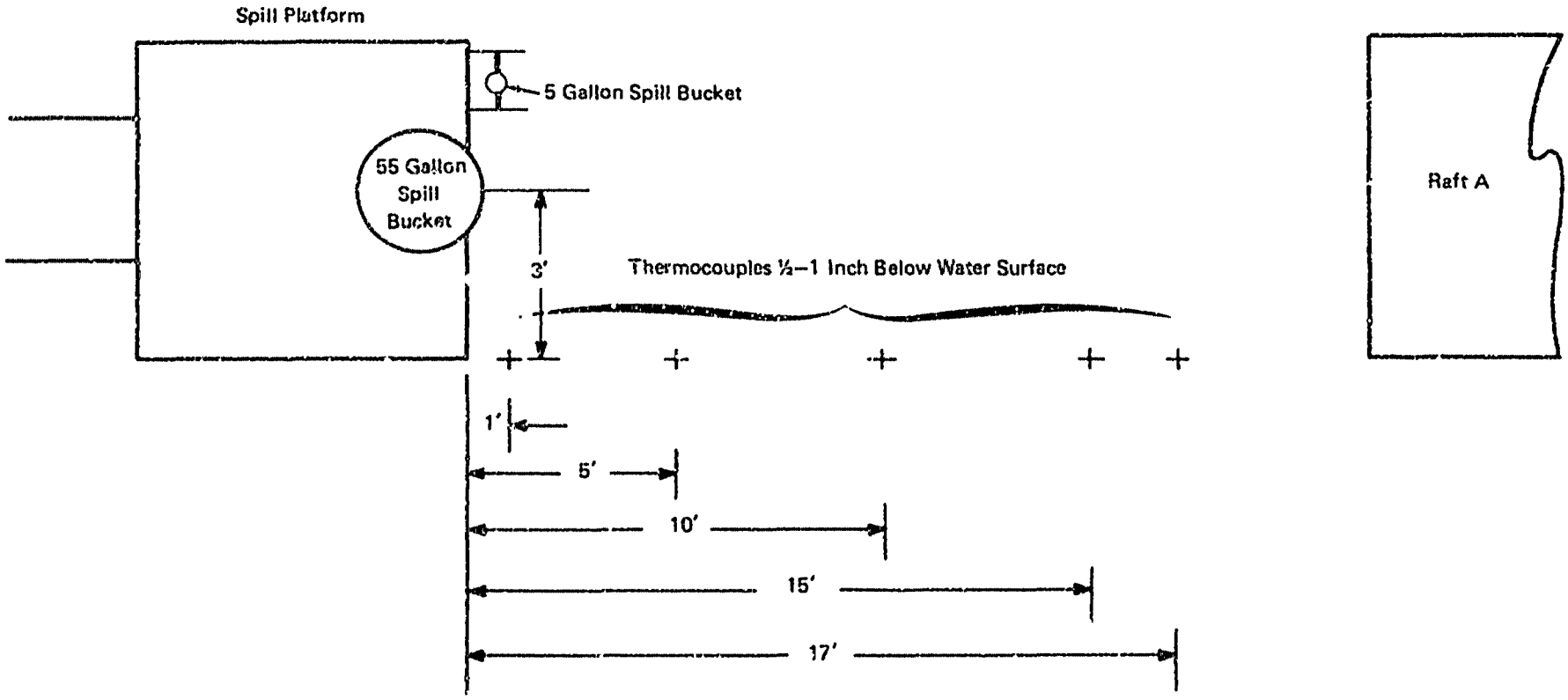

FIGURE 5–4 PLACEMENT OF WATER TEMPERATURE THERMOCOUPLES FOR LARGE-SCALE TESTS

5.2.2.2 Underwater

Four underwater releases of five gallons of ammonia were made with a specially fabricated 2.5-cubic-foot capacity welded-steel pressure vessel and appropriate plumbing. Figure 5-5 shows the layout of the underwater release system, including a 1.5-inch ID PVC pipe connected to a 1.5-to-0.5-inch reducer, to which a length of 0.5-inch ID pipe is attached at a depth of five feet. Similar systems with discharge depths of three or five feet were also fabricated with pipes of constant 1.5 inch diameter.

The spill vessel was filled by placing it, minus external plumbing, on a scale and adding LNH_3 until the desired weight was reached. The vessel was then positioned and connected to the piping system and allowed to warm until the internal pressure had increased to about 20 psig. Then, the ball valve was remotely opened and LNH_3 was released.

5.2.2.3 Other Instruments

Wind velocity and direction were measured during all tests with an accurate, sensitive anemometer and direction-vane sensor system calibrated and connected to a high-speed strip-chart recorder. All but two spills were recorded with 16 mm color movies (during one test the camera power system malfunctioned, and during another the camera jammed). In addition, 35 mm color stills were taken. Table 5-1 lists the test measurements.

5.2.3 Procedures

The test procedures for both surface and underwater releases were similar to those used in the intermediate size experiments. Only minor changes - dictated by the location and size of the experiments - were made. These primarily were because the pond water could not be thoroughly mixed and sampled as the swimming pool water had been.

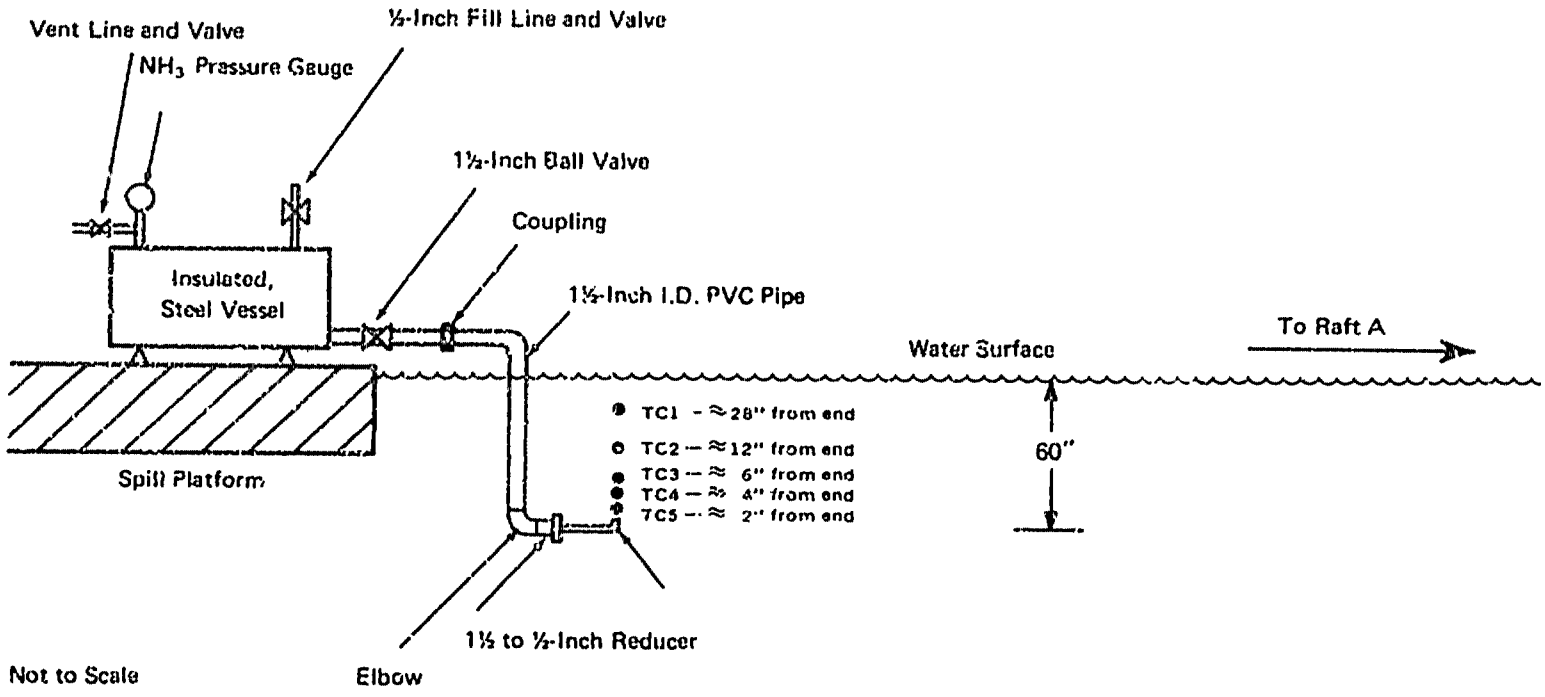

FIGURE 5–5 UNDERWATER RELEASE APPARATUS AND INSTRUMENTATION

Table 5-1

Large-Scale Test Measurements

	Surface Tests	Underwater Tests*
Concentrations		
Downstream Vapor Samples	8-56	8
Temperatures		
Liquid	5	5
Downstream Vapor	2	-
Sound	1	1
Photography		
Color Movies		
Infrared Movies		
35 mm Stills		
Wind		
Velocity		
Direction		

*Not all measurements were made for every test.

5.3 TEST RESULTS

5.3.1 Surface Spills

In all, three five gallon and seven 50 gallon instantaneous spill tests were conducted in this series. Table 5-2 summarizes the test data, ambient conditions, and vapor cloud behavior during the tests. Wind velocity data were obtained by timing the vapor cloud movement in the movies, as also from the chart records. Table 5-3 shows the wind characteristics obtained from strip-chart records of wind velocity and direction (measured by the anemometer and the direction vane). The table indicates the variable character of the wind.

Figure 5-6 shows typical water-temperature data obtained during a 50 gallon test. The water temperature was considerably higher than was observed during the intermediate-scale tests. However, during the five gallon spills of the large-scale tests, the maximum temperature increase over the initial water temperature recorded by the same set of thermocouples was about 5° to 6°F. Note, however, that the line of the thermocouples for the latter case was about five feet from the center of the five-gallon spill bucket. Therefore, it is likely that the thermocouples were not within the boiling zone.

The radii of the boiling zones were measured primarily by scaling from the movies. Figure 5-7 shows a plot of boiling zone radius as a function of the spill quantity. Because of the difficulty of exactly locating the edges of the boiling region (due to vapor-cloud overlap) a range of values has been given. The plot shows that the estimate of a five gallon spill spread from the large-scale tests does not seem to agree with that from the intermediate-scale size tests.

The impinger data from several typical tests (5,6,8, and 13) are shown plotted in Figure 5-8 through 5-10. These represent the data from 50 gallon (nominal) spills obtained under both very high and very low wind velocity conditions. Figures 5-8a and 5-8b show the horizontal and vertical distributions of the vapor mass collected at

Table 5-2

Details of Five-Gallon and 50-Gallon Surface Spills

Test Date	Test Number	Spill Quantity Liters	Pond water temp. °F	Atmospheric Temp. °F	Atmospheric RH %	Ambient weather condition	Wind velocity* during the cloud travel mph	Duration of vapor evolution secs.	Maximum pool radius during vapor evolution ft	Remarks on vapor cloud travel
						5 - G A L L O N				
10/9	7	17.25	57	69	60	clear and sunny	6-7	4-6	3-4	Cloud center passes through raft A, between sniffers 2 and 6. Cloud disappears within 17-18 secs i.e., before reaching the 2nd row of rafts
10/22	10	18.9	47	57	78	clear and sunny	10	3-4	4-5	Cloud traveled close to the water surface. Hits raft A dead center. Cloud can be seen up to the 2nd row of rafts. Last traces disappear at about 40 secs after spill
10/22	11	18.9	47	57	78	clear and sunny	6	4-5	4-5	Cloud hit raft A dead center and then veered to the right. It disappears in about 40 secs.
						50 - G A L L O N				
9/21	13	151.5	45	50	60	clear sky	5	8	8-10	Experiment aborted due to the sticking of the barrel release latch. Cloud traveled almost right angles to the center line of rafts, missing all of them. No sniffer data.
9/26	4	155.0	60	63	75	Cloudless sunny and wind direction very unsteady	2.75-3.25	5	10-12	Cloud hits squarely, rises and heads between rafts B and E. Pool seems to extend all the way to the front of raft A.

Table 5-2 (cont'd)

Details of Five-Gallon and 50-Gallon Surface Spills

Test Date	Test Number	Spill Quantity Liters	Pond water temp. °F	Atmospheric Temp. °F	Atmospheric RH %	Ambient weather condition	Wind velocity* during the cloud travel mph	Duration of vapor evolution secs.	Maximum pool radius during vapor evolution ft.	Remarks on vapor cloud travel
						50 · G A L L O N				
9/27	5	144	60	72		Blue sky but slightly hazy condition	1.5-2	11	12-13	Full height of raft A is enveloped in cloud. Shape of cloud somewhat like a mushroom. Sniffers 7 and 8 were in the thick top of the cloud. Cloud moved to the right of A. Visible top part traveled mostly on top of C and disappeared before reaching the last row of rafts.
10/4	6	170	60	61	91	Cloudy day with fog. Very light wind	2-2.5			Because of low wind, cloud stays low and spreads over water enveloping raft A. A classic mushroom cloud forms Major portion of cloud passed over raft C. The stem of the mushroom hits C. Cloud invisible by the 3rd row. Wind velocity died down immediately after spill.
10/17	8	174	46	44	78	Completely overcast sky	11.5	6-7	8-10	About 10 gallons LNH_3 spilled during the charging of the barrel. (1 hr. before test) Cloud hit raft A, with the main portion passing by sniffer 1. Cloud is still visible as it goes off into the woods behind the pond. Cloud does not seem to rise very much.
10/18	9	189	46	49.5	.62	medium overcast	2-3	-	-	Cloud hit centre of raft A, veered to left and hit C. Third row of raft solution did not turn green.

Table 5-2 (cont'd)

Details of Five-Gallon and 50-Gallon Surface Spills

Test Date	Test Number	Spill Quantity Liters	Pond water temp. °F	Atmospheric Temp. °F	Atmospheric RH %	Ambient weather condition	Wind velocity* during the cloud travel mph	Duration of vapor evolution secs.	Maximum pool radius during vapor evolution ft.	Remarks on vapor cloud travel
						50 G A L L O N				
10/23	13	155	46	71	42	Sunny and clear, about 15% clouds. Steady wind.	7.5-8	4-5	12-13	Cloud passed through the middle of rafts A and C but slightly to the right of E. A peculiar horseshoe cloud is generated. Raft A is passed by the gap of the horseshoe. This shape degenerates to an elongated puff heading upward and to the left of raft center line.

Table 5-3

Wind Characteristics

Experimental Date	Experimental Number	Average for 15 min. trace before test: Mean velocity mph	Average for 15 min. trace before test: Peak to peak mph	Wind at the moment of spill mph	Wind velocity about 2 mins. after spill mph	Mean cloud velocity measured from movies mph	Remarks based on graphical trace of wind velocity and direction
10/9	7	4	6	5	7	6-7	Wind speed data recorded on low speed recorder and hence may not be very accurate.
10/22	10	5	5	4.5	2	5	Mean wind varies sinusoidally with a period of 40 mins. Wind died down from 4.5 mph at the moment of spill to about 2 mph in 25 seconds.
10/22	11	4	4	4.5	2.5	6	Wind velocity drops to 2.5 mph within 5 seconds and holds steady thereafter.
9/26	4	3.5-4	4	2.5	0.5	2.75-3.25	Mean wind velocity varies sinusoidally but at the same time decreasing.
9/27	5	2.5	3	1.0	2.5	1.5-2	Mean wind velocity increasing. After the spill wind direction is steady.
10/4	6	1.0	2.0	2.0	2.5	2-2.5	Wind died out immediately after spill from about 1.5 mph to 0.5 mph. Direction was quite steady.
10/17	8	10	10	13	10	11.5	Wind velocity quite steady. Direction was right along the raft center line.
10/18	9	2.5	5	4.5	0	?	Wind decreased to zero within about 1 min. Direction changed to the left of raft center line about 10 secs. after spill.
10/23	13	6	9	7.5	6	7.5-8	Velocity very steady for over 30 seconds after spill

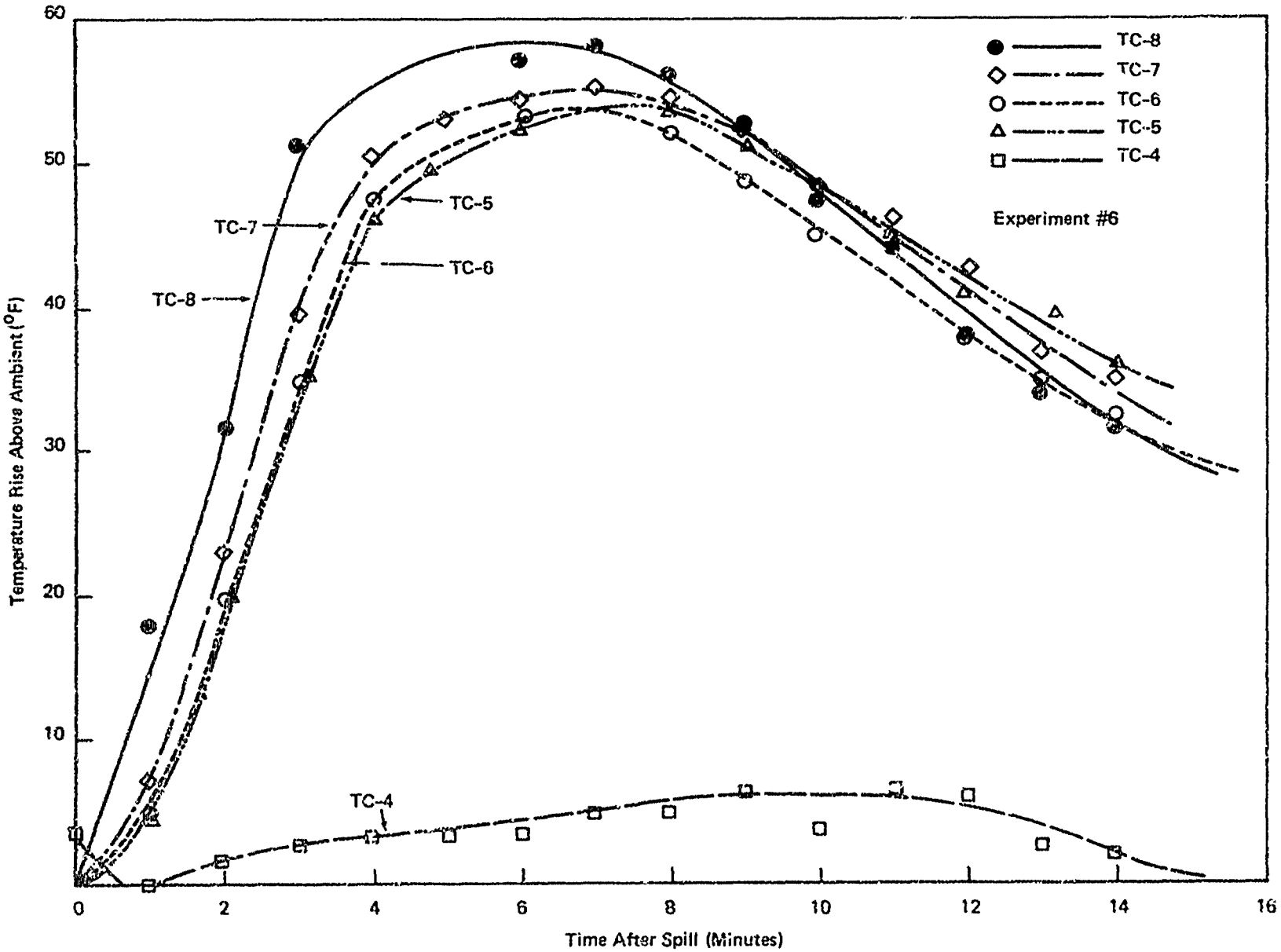

FIGURE 5--6 TEMPERATURE VARIATION OF WATER IN THE SPILL ZONE FOR A 50 GALLON SPILL

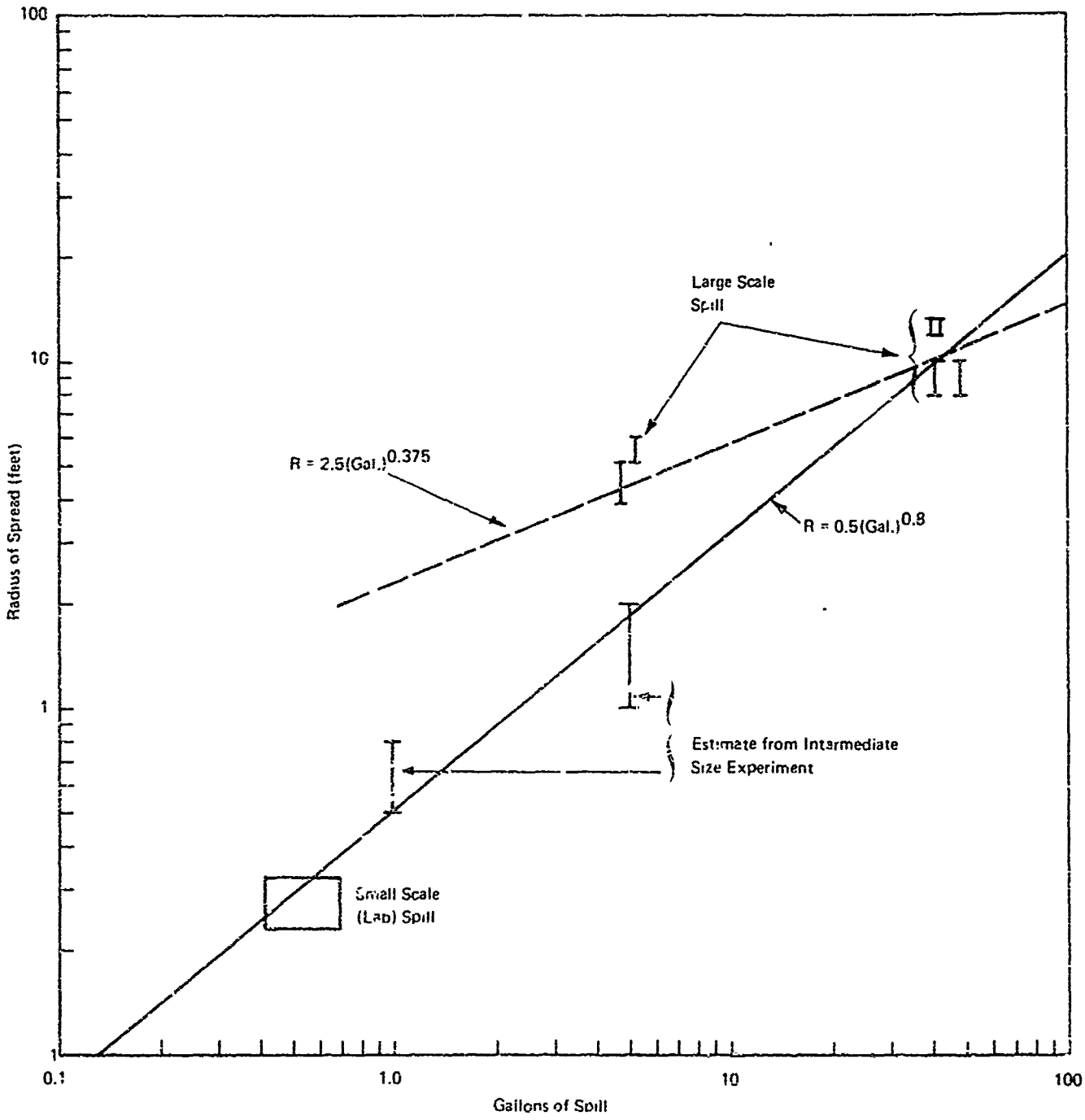

FIGURE 5-7 MAXIMUM RADIUS OF LNH_3 BOILING AREA AS A FUNCTION OF SPILL VOLUME

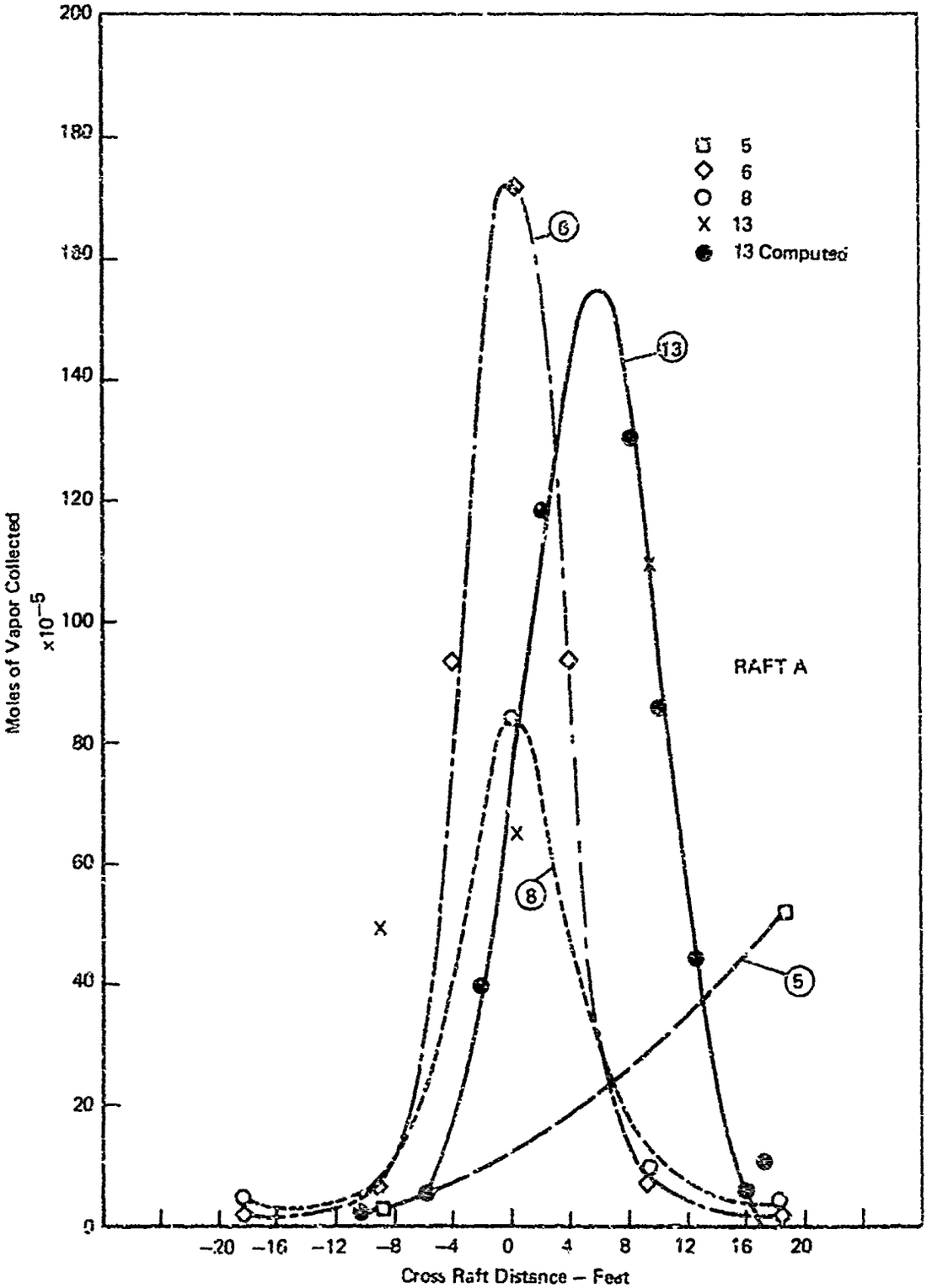

FIGURE 5–8a HORIZONTAL IMPINGER DATA ON THE FIRST ROW RAFT A

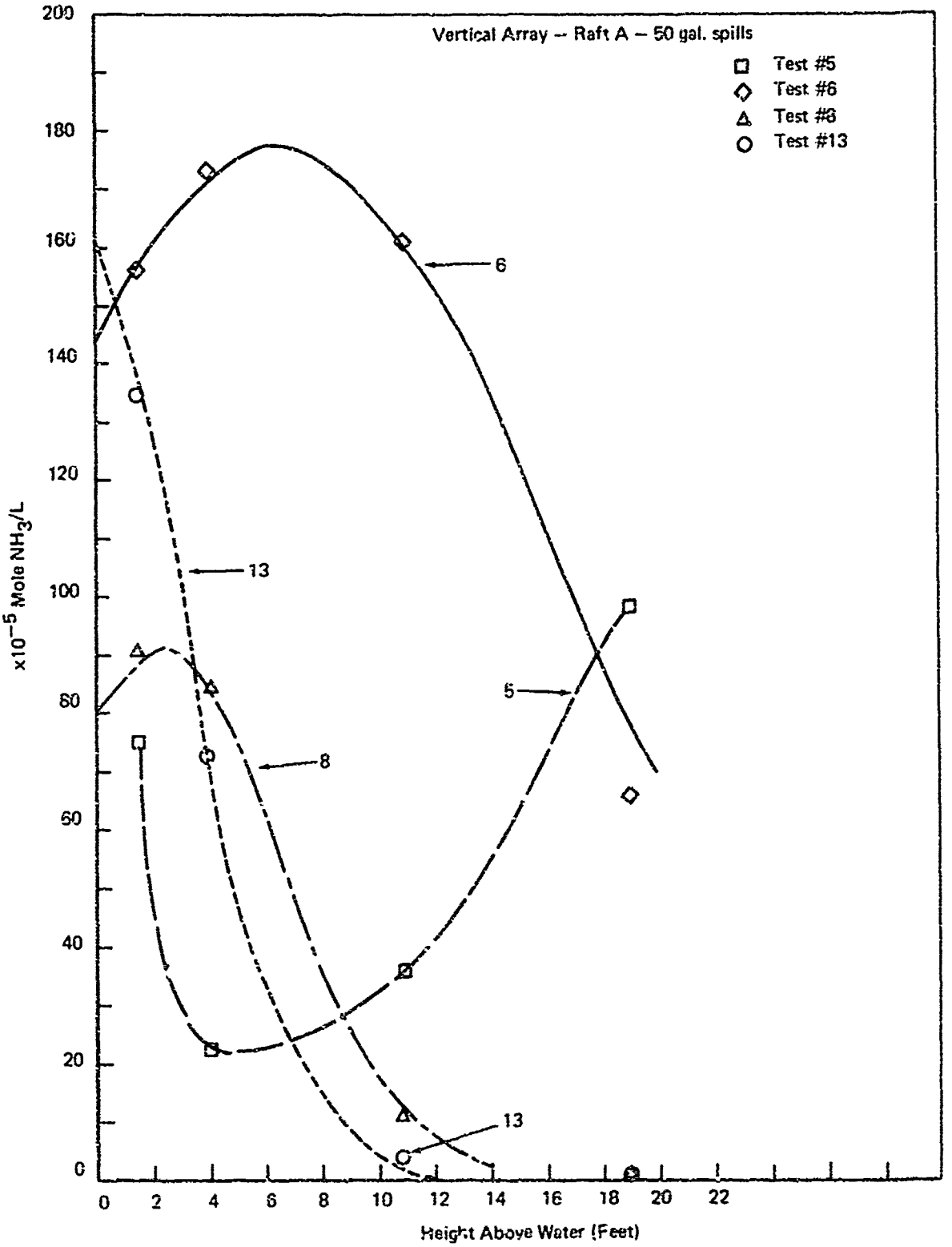

FIGURE 5–8b VERTICAL IMPINGER DATA FOR FIRST ROW RAFT A

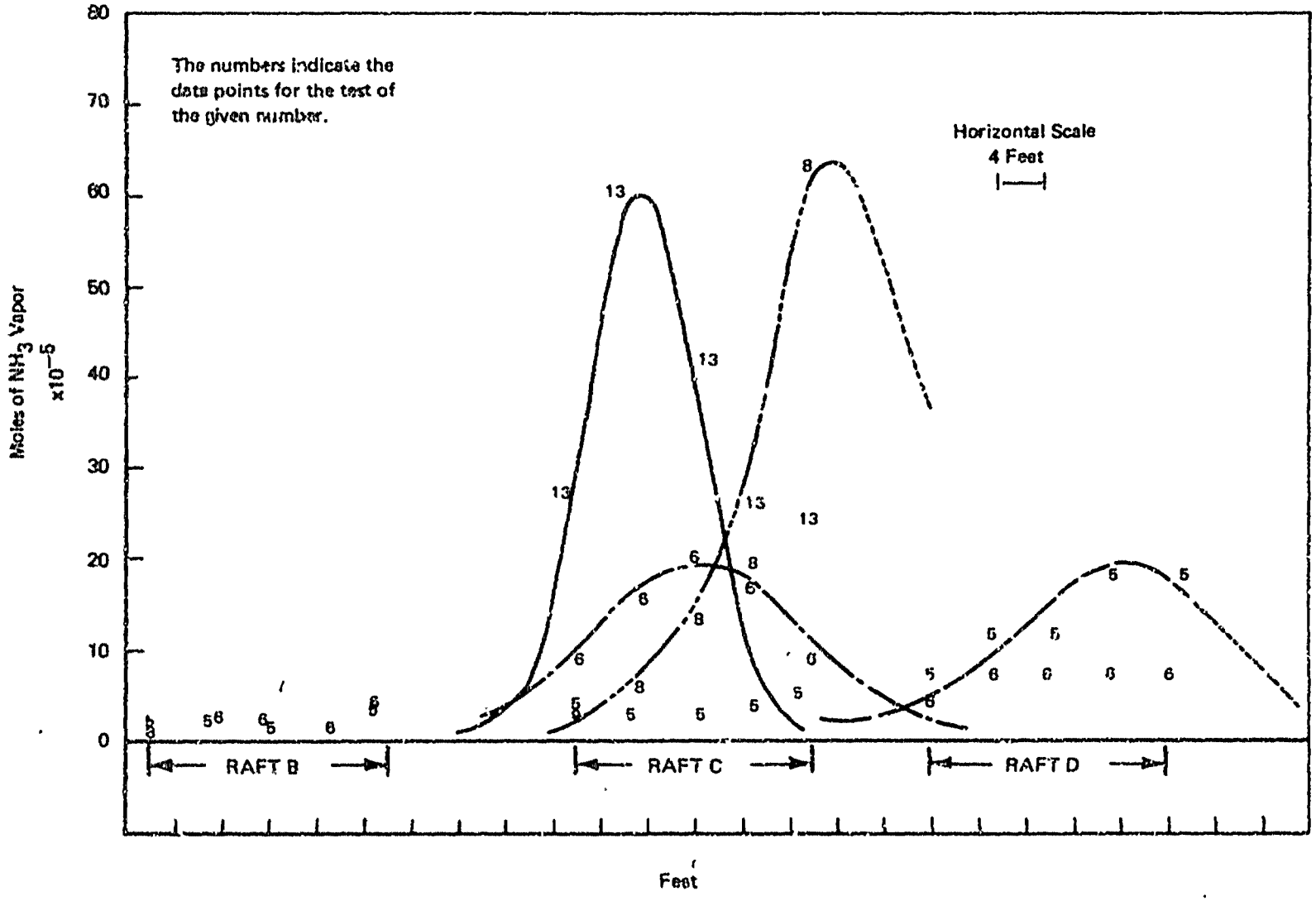

FIGURE 5-8a HORIZONTAL IMPINGER DATA ON THE SECOND ROW OF RAFTS

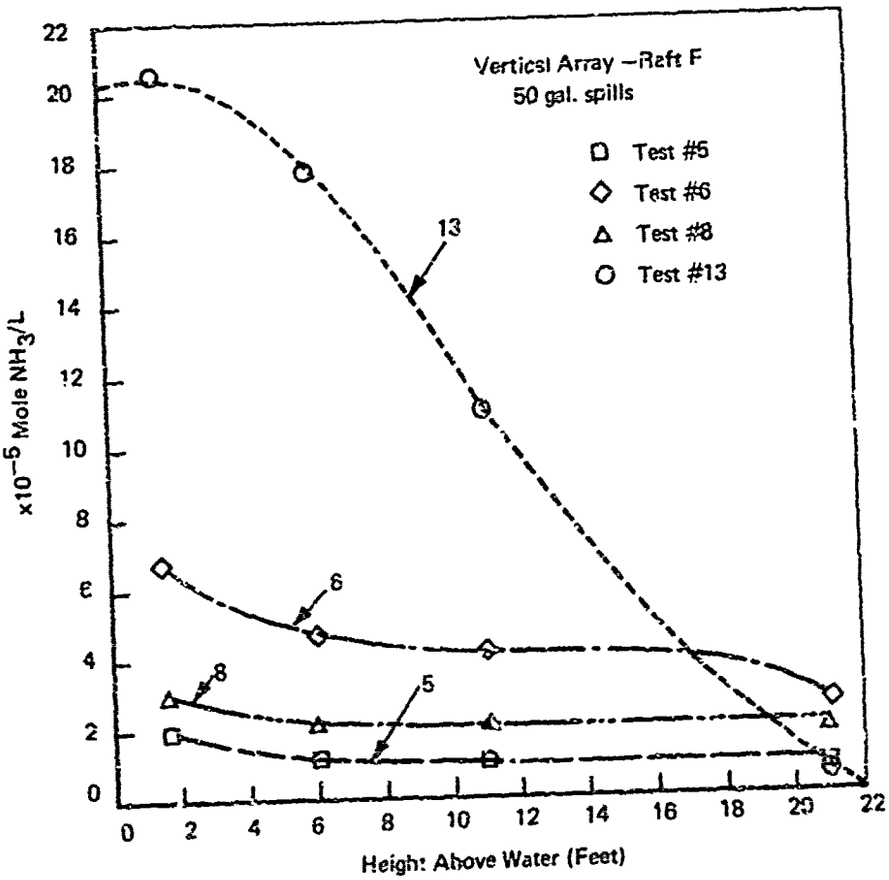

FIGURE 5–9b VERTICAL ARRAY IMPINGER DATA FOR SECOND ROW RAFT (C)

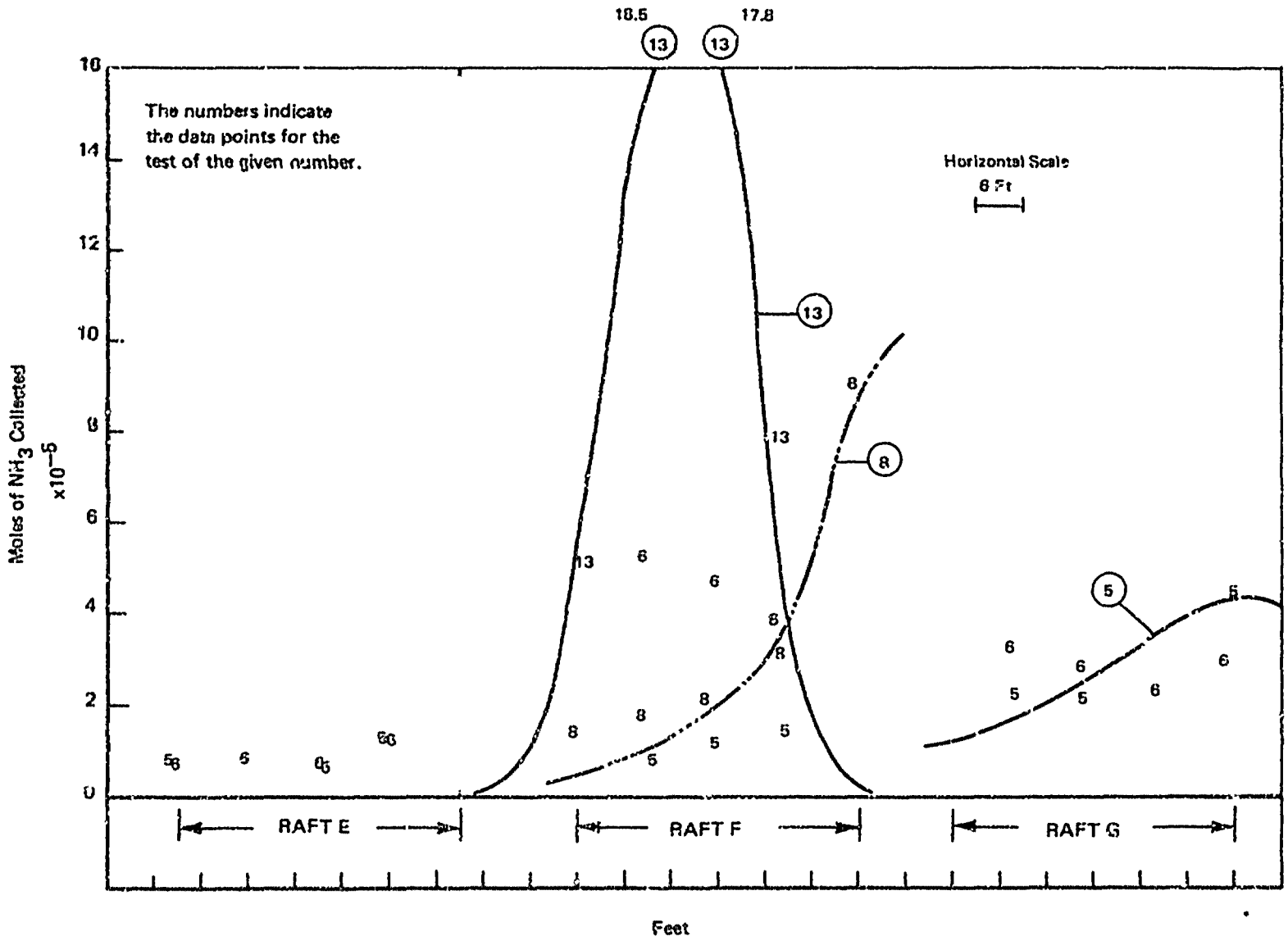

FIGURE 5–10a HORIZONTAL IMPINGER DATA ON THE THIRD ROW OF RAFTS

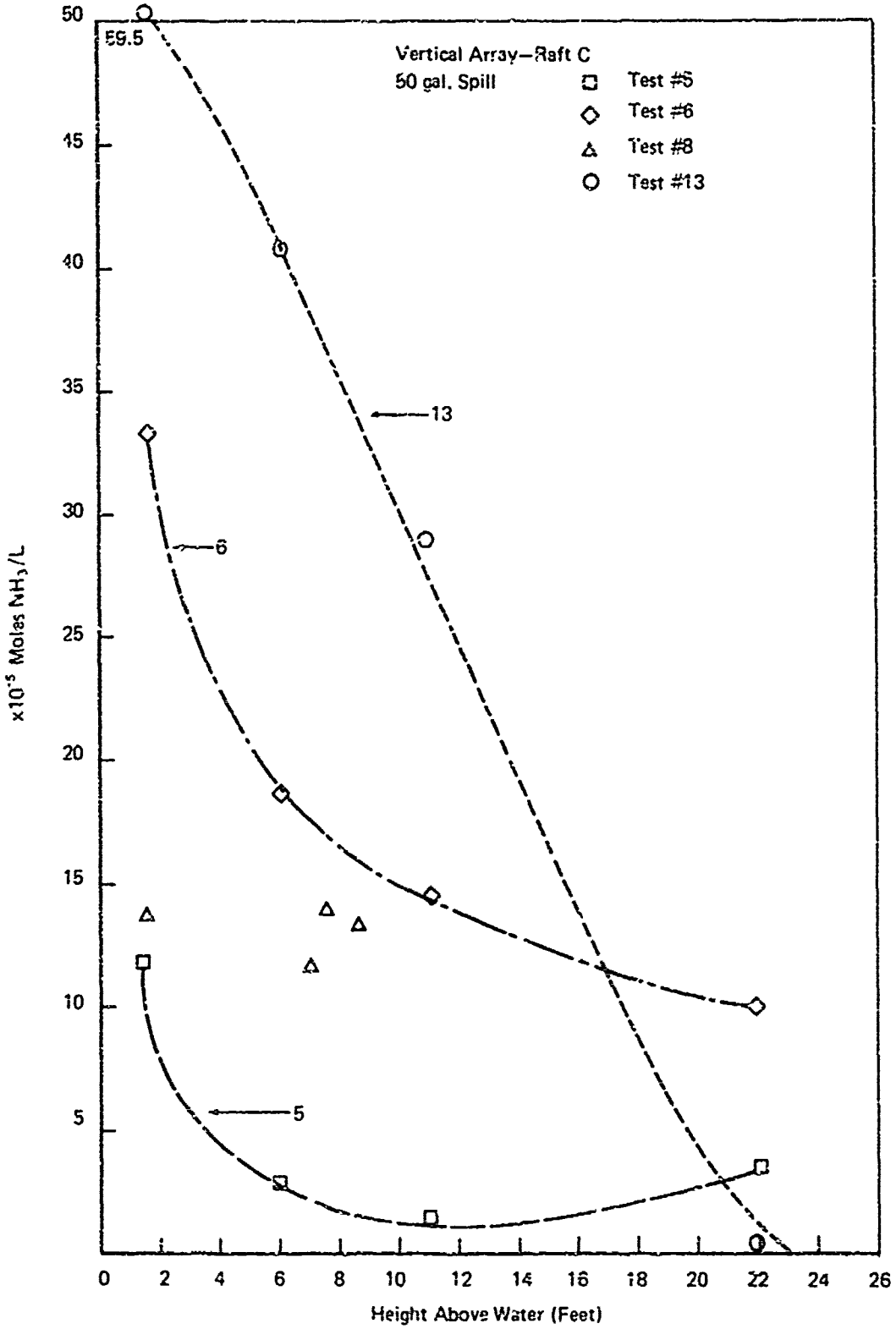

FIGURE 5–10b VERTICAL ARRAY IMPINGER DATA FOR THIRD ROW RAFT (F)

raft A. (The figures also show the best-fit Gaussian curves, wherever possible.) Similarly, the other figures show the horizontal distributions for the second and third row of rafts. Figures 5-9a and 5-9b show the vertical distribution data just of those rafts in the second and third row through which the vapor cloud passed. The figures indicate that for the tests in which the wind velocity was high (tests 8 and 13) the horizontal distributions can be reasonably represented by Guassian profiles. For low wind velocity (tests 5 and 6) the distribution seems to be quite different from Gaussian, and tends to be more uniform for the rafts at the same distance from the source. Also, in general, the concentrations of NH_3 vapor collected were much lower for the tests with low wind that those with high wind. The vertical distributions show that during high wind velocities the peak concentration occurred at a lower altitude than during low wind. However, non-uniform distributions also occurred, especially at low wind speeds. (See test 5 in Figure 5-8b.)

It is clear from the vertical concentration distribution data, obtained during the present series of experiments, that the ammonia vapor plume rises above the water surface as it disperses downwind. This has also been confirmed by observation of the visible vapor cloud movement in the test movies. The rate of rise of the plume also seems to depend on the wind velocity and the size of the spill. Figure 5-11a shows the positions of peak concentration values obtained from the vertical distribution of Raft A impinger data, plotted against wind velocity. (The values from other rafts in the second and third row have not been plotted because of the uncertainties in their "peak" values.) The theoretical predictions based on plume theory are also shown. (The details of this theory are given in Section 6.7. Figure 5-11a suggests that to explain the observed variation of the peak concentration position with height, allowance has to be made for the possible presence of aerosols in the vapor cloud. However, there is considerable data scatter. The cloud motions were observed from the movies and the motion of each puff center over the different rafts

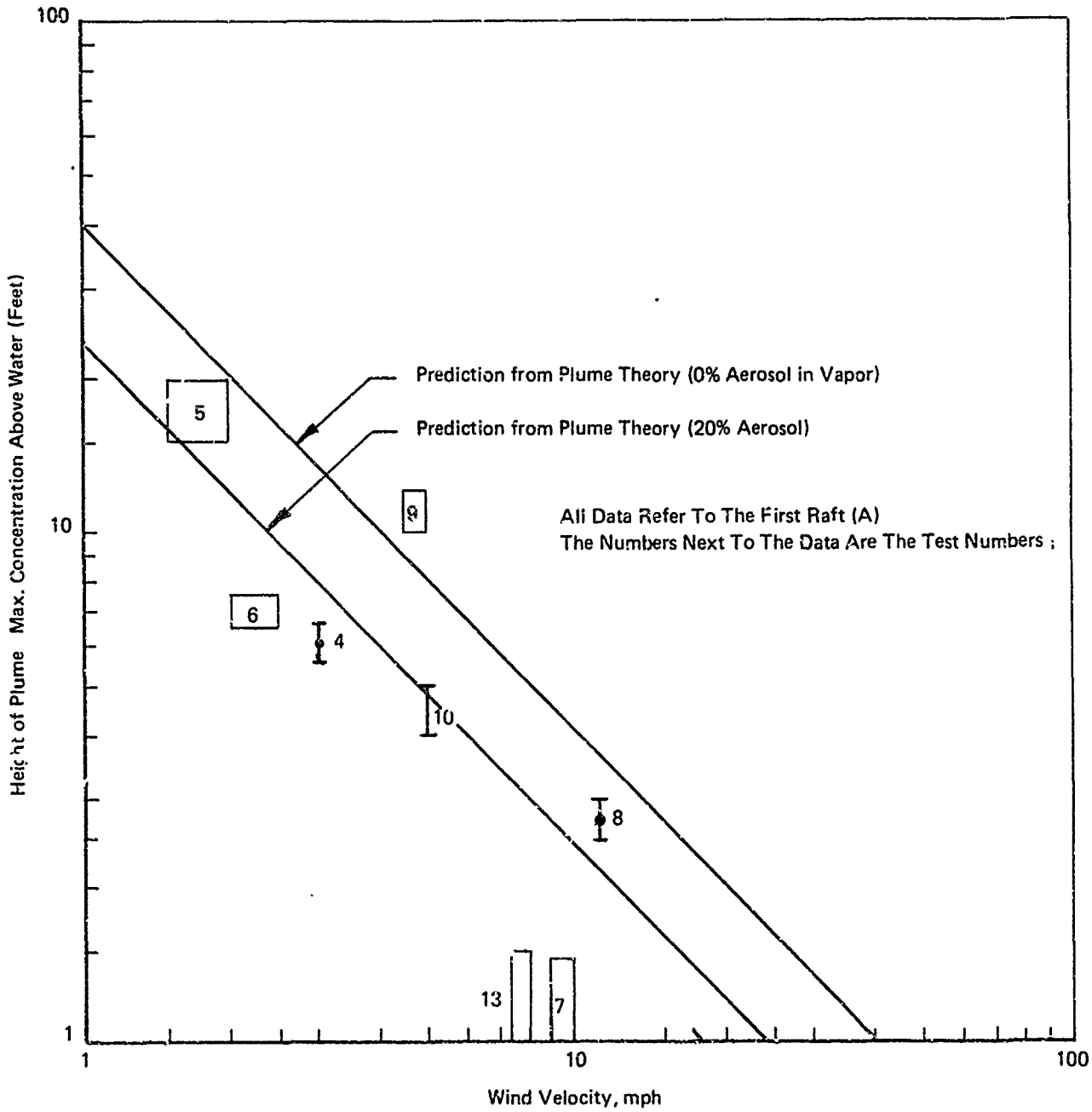

FIGURE 5–11a HEIGHT OF PEAK CONCENTRATION OF VERTICAL ARRAY IMPINGER DATA AS A FUNCTION OF WIND VELOCITY

was noted. Figure 5-11b shows the heights of the cloud centers over the three rows of rafts. The theoretical predictions based on plume theory are shown on the same plot. (A discussion on the results is given in Section 5.5.)

Some general qualitative observations made from the movies can be summarized as follows:

- In quite a few tests, during the spread of LNH_3 on the water surface an uneven spread could be observed; that is, the spreading pool edge was not a uniform convex front, but had long elongated "fingers." This may have been caused by the dynamics of the spilling process.
- The cloud formation was rapid, and in all cases the cloud hit the first raft. Characteristic mushroom cloud formation was seen under low wind conditions. The clouds dispersed by a rapid rise at the top of the mushroom, followed by a stretching of the stem of the mushroom. The stretched cloud seemed to pass over the rafts.
- The vapor cloud was visible for a longer duration (further distance traveled downwind) when the atmospheric humidity was high.
- The vapor cloud did not exhibit any special affinity for water by dispersing close to its surface. In fact, the tendency for the cloud to rise in the atmosphere was very evident.
- After the vapor had completely disappeared, a distinctly visible pool spread on the water surface at the spill position. This pool was distinguishable from the surrounding water by the lack of small surface waves and slightly different optical reflective properties. It is very likely that this represented the spreading NH_4OH solution.

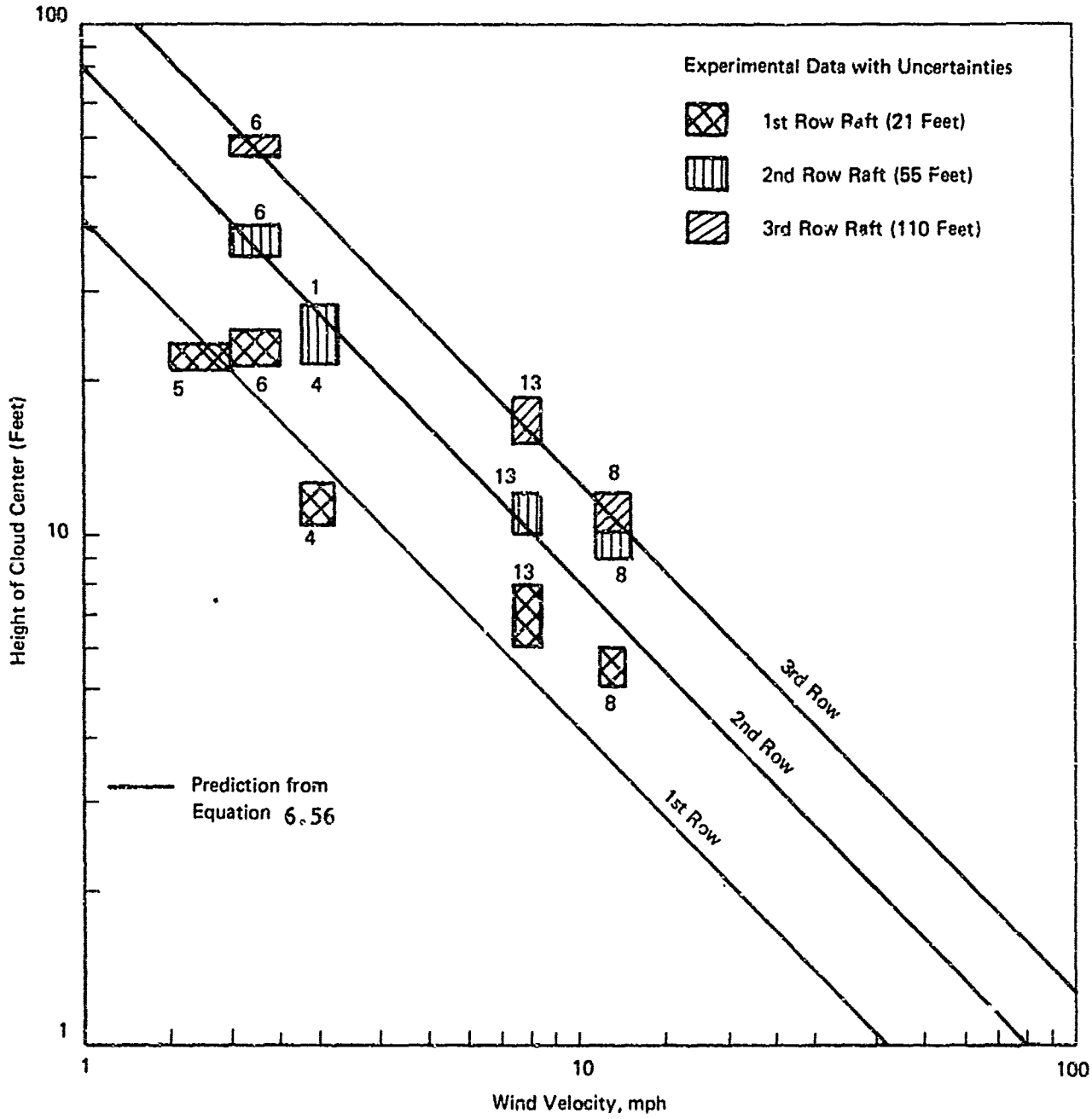

FIGURE 5–11b HEIGHTS OF CLOUD CENTERS OVER THE THREE ROWS OF RAFTS. DATA FROM MOVIE FILMS.

5.3.2 Underwater Release

Four underwater tests were conducted. Approximately five gallons of LNG_3 were released in each of the tests about four feet below the water surface. The temperature in the water was measured at five locations. Figure 5-5 shows a schematic of the thermocouple locations relative to the mouth of the discharge pipe, as well as the general arrangement of the underwater release apparatus.) Both 0.5-inch and 1.5-inch discharge pipes were used, each in two experiments.

Table 5-4 lists the experimental data, together with some observational remarks, for this test series. Note that water temperature could increase by as much as 50°F (though in one case it was about 70°F), and that for the smaller-diameter pipe discharge, the maximum temperature observed was much lower than when the discharge was from a large pipe diameter. This may indicate that the rate of discharge is important for the type of reaction that can occur between water and LNH_3. No vapor was sensed by the sniffers in the first raft, nor did observations of the area directly above the release point indicate any vapor clouds. Only violent bubbling and agitation of the water in these regions were noticed. The thermocouples close to the release pipe seemed to first indicate temperatures as low as 0° to -3°F (probably liquid ammonia) and then begin to indicate increased temperatures.

5.4 ANALYSIS

5.4.1 Partition Ratio

Partition ratios were calculated from the impinger data of each raft over which the vapor cloud passed, using the method described in Section 4.5. Table 5-5 lists the calculated partition ratios and dispersion variance parameter values for the impinger data. The latter were obtained by fitting the best Gaussian curves, wherever possible, to the impinger data for the horizontal and vertical arrays. It can be seen from the table that the partition ratios are far from being unique. In fact, in some cases the vapor masses calculated from

Table 5-4

Underwater Release Test Data

Experiment Date	Experiment Number	Water temp. before test °F	Quantity of LNH_3 released lbs.	Release pressure psig	Duration of release secs.	Depth of release inches	Maximum Temperature Increase Recorded Above Initial Water Temperature					Remarks on Temperature Data	Remarks on the Experiment
							T_1	T_2	T_3	T_4	T_5		
9/13	1	60	26	30	40	33	9-10	9-10	broken	15	broken	T_1 reaches maximum and comes down within 1 min. Remains at about 6-7°F above ambient for a long time. T_2 and others reach maximum and come down to ambient value within 1 min.	Small bubbles noted on the surface for few seconds only. After that only water agitation noticeable with continuous circular wakes. Audible sound during discharge which lasted for about 35 secs. Discharge pipe size at the mouth = 1/2" dia. Acid in the sniffers did not turn green. T_1 is 33" about the mouth.

Table 5-4 (cont'd)

Underwater Release Test Data

Experiment Date	Experiment Number	Water temp. before test °F	Quantity of LNH_3 released lbs.	Release pressure psig	Duration of release secs.	Depth of release inches	Maximum Temperature Increase Recorded Above Initial Water Temperature					Remarks on Temperature Data	Remarks on the Experiment
							T_1	T_2	T_3	T_4	T_5		
9/13	2	62	23.75	35	18-20	28	14	8-9	broken	broken	broken	T_1 keeps rising even at 4 mins. T_4 showed a dip in temperature initially.	Up to about 17 secs. observations similar to those noted above. After this the pipe union broke, discharging remaining LNH_3 on water surface. The vapor formed was of considerable size, bit first left, but did not turn any solutions green. 1/2" dia. pipe at the mouth of release. T_1 is 28" above the mouth.

Table 5-4 (cont'd)

Underwater Release Test Data

Experiment Date	Experiment Number	Water temp. before test °F	Quantity of LNH_3 released lbs.	Release pressure psig	Duration of release secs.	Depth of release inches	Maximum Temperature Increase Recorded Above Initial Water Temperature					Remarks on Temperature Data	Remarks on the Experiment
							T_1	T_2	T_3	T_4	T_5		
10/23	12	63	25.75	16	about 60	30	18	70		45	40	All temp. reached maximum and came down to steady values of about 3° above ambient within 1 min. except for T_2. T_2 reaches max. value quickly but reaches steady values after 2 mins. The steady value = 16°F above ambient.	No vapor was observed at the surface. Water surface extremely agitated above release pipe mouth. Regular papping sound heard; 1 1/2" dia. pipe at the mouth of release.

Table 5-4 (cont'd)

Underwater Release Test Data

Experiment Date	Experiment Number	Water temp. before test °F	Quantity of LNH_3 released lbs.	Release pressure psig	Duration of release secs.	Depth of release inches	Maximum Temperature Increase Recorded Above Initial Water Temperature					Remarks on Temperature Data	Remarks on the Experiment
							T_1	T_2	T_3	T_4	T_5		
10/24	14	59	27.5	10	30	30	14	29-30	45	5-7	25	T_4 shows very low temp. (about 3°F) for over 50 secs. All other temp. increase. T_2, T_3 and T_4 were connected to high response recorders. The temp. trace indicates high frequency temp. variation with amplitude as high as 50°F.	All comments similar to that in test 12. The high response recorders indicate highly varying temp. structure. The values quoted are the mean values. The slow response recorder values (T_1 and T_5) are subject to error because of the way in which the records integrate the noise and print the data.

Note: The thermocouples T_1, T_2, T_3, T_4 and T_5 are respectively at vertical distances 24", 12", 6", 4" and 2" vertically above the mouth of the release pipe underwater.

Table 5-5

Partition Function and Dispersion Parameters from Impinger Data

Test Number	Mean wind velocity (m/s)	Areas under the impinger data mole-ft $A_x=10^{-5}x$	$A_y=10^{-5}x$	Vapor collected by the common impinger $a(y_o,z_o)$ moles = $10^{-5}x$	Calculated mass of vapor (kg)	Mass of NH_3 spilled (kg)	Partition Ratio	Dispersion values for the best-fit Gaussians (feet) σ_y	σ_z	Atmospheric class	Dispersion Values from Gifford curves (feet) σ_y	σ_z	Remarks
7	6	330	71.3	4.5	5.92	11.76	0.477	4.3	-	B	3.5	2.7	1st row raft
		240	54.0	3.5	4.2		0.633	5.3	-		9.5	7.0	2nd row raft
10	5	221	250	25.7	2.0	12.9	0.843	5.5	4.5	B	4.0	3.0	
11	6	223	220	14.8	3.75	12.9	0.709	5.1	-	B	4.0	3.0	
4	3	1650	1959	137	13.37	105.7	0.874	4.0	6.0	A	4.6	3.6	1st row raft
		2300	662	18	47.9		0.547	7.0	-		12.0	8.0	2nd row raft
		138	147	2.9	4.0		0.962	12.3	-		24.0	17.5	3rd row raft
5	2	1340	1909	22.6	42.8	98.2	0.564	6.4	-	B	3.5	2.7	
		400	134	11.3	1.79		0.981	8.0	-		9.0	6.5	
		432	37.2	2.8	2.95		0.970	17.0	-		17.3	12.2	
6	2	1690	3174	172.8	37.8	116.0	0.674	3.6	10.0	D	1.8	1.6	
		600	429	18.7	5.2		0.955	9.0	-		4.6	3.7	
		440	101.6	4.7	4.88		0.958	19.0	-		9.4	6.7	
8	12	1000	731.6	84.5	19.6	118.7	0.835	4.2	4.3	C	4.3	2.6	
		1300	266.0	14.0	56.0		0.528	5.5	-		8.6	5.0	
		408	55.0	2.2	31.44		0.735	-	-		16.0	9.5	
9	5	915	595	10.8	47.7	129	0.630	6.4	-	B	4.8	3.6	
		360	40.0	2.5	5.4		0.958	-	-		8.2	6.0	
		96	30.0	1.5	2.47		0.981	19	-		19.7	13.9	
13	8	2239	710	73.1	32.73	105.7	0.690	4.2	4.0	B	4.5	3.4	
		900	672	40.8	22.40		0.788	5.0	8.3		10.0	7.3	
		400	250	17.8	11.54		0.890	7.5	8.6		19.5	13.7	

the impinger data are very small compared to the mass of liquid spilled. In general, high partition ratios were obtained for those experiments in which the wind velocity was very low. This indicates that, for such cases, the major portion of the cloud missed passing by the impingers and the readings obtained by the impingers were due to the residual vapor that passed by them. (See the remark about the passage of the stem of a mushroom cloud in Section 5.3.1.)

Table 5-5 also indicates that the partition ratio values calculated from the data of the first raft seem to be within reasonable limits (between about 0.5 and 0.7 for a majority of the experiments), but no definite pattern can be ascribed to the data of the second- and third-row rafts. It is known from observational data that in almost all the tests the cloud hit the first raft, almost squarely, yet did not necessarily hit the rafts in the second and third rows. This information, coupled with the large differences in the partition ratio obtained from second- and third-row raft data, is a further indication of the rapid rise of the vapor cloud in the atmosphere.

5.4.2 Impinger Concentration Distribution

Most of the horizontal distributions could be reasonably fit by Gaussian profiles. The variances obtained from these profiles are given in Table 5-5, along with the dispersion parameter (σ) values obtained from the Gifford-Pasquill curves (see Figure 6-17) for the appropriate atmospheric type and the downwind raft distance. A comparison of the measured σ_y values and those obtained from the Gifford-Pasquill data are shown in Figure 5-12. Note that the measured σ_y's tend to be slightly higher for the near raft and smaller for the second row raft than the Gifford σ_y's. For larger distances, this difference seems to be reduced. Also note that the latter values were obtained by extrapolating the Gifford curves, which have σ values listed only for distances greater than 100 meters. Hence allowance must be made for possible errors in extrapolation. Considering this uncertainty, the agreement seems to be quite good.

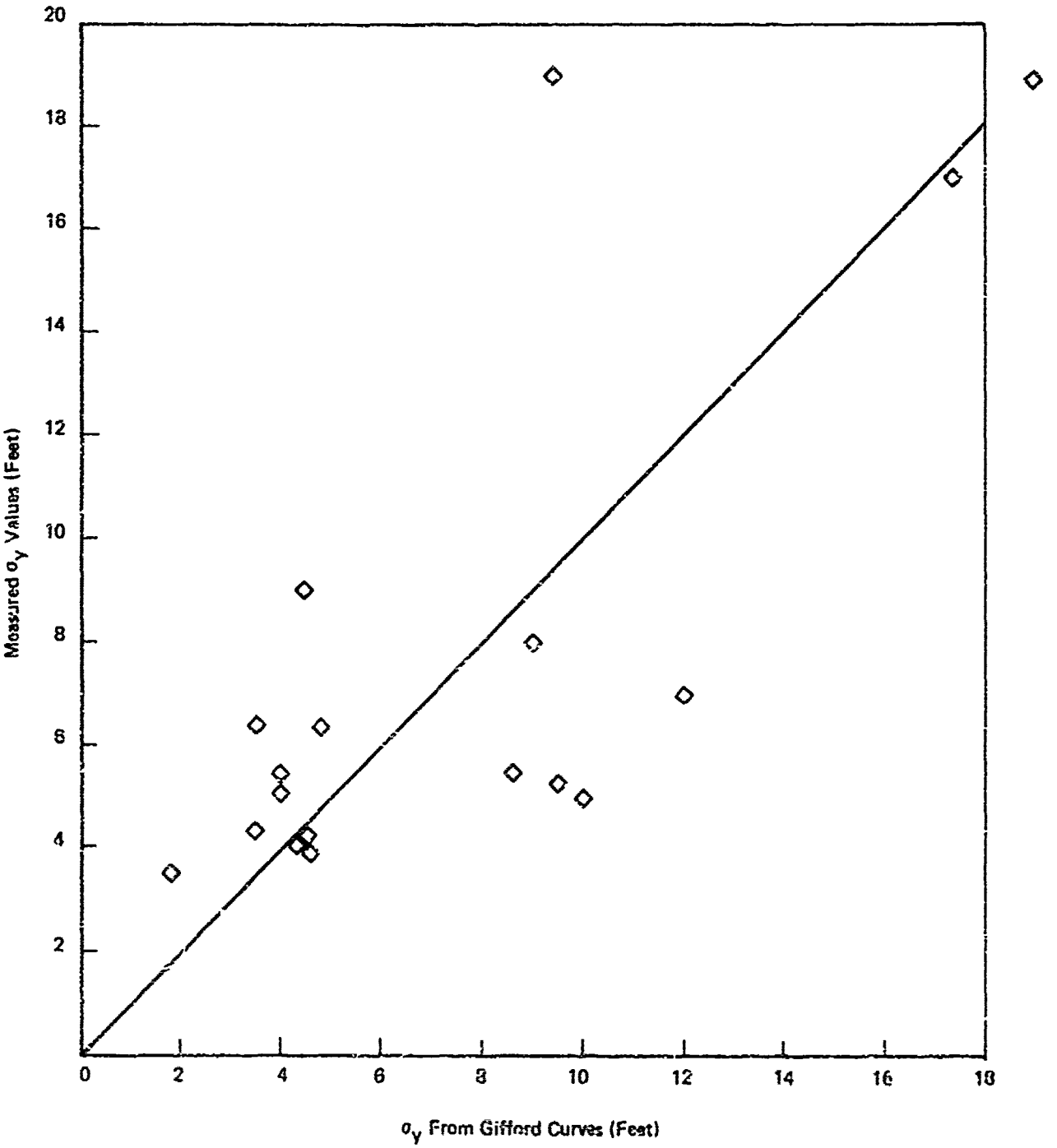

FIGURE 5–12 COMPARISON OF MEASURED σ_y VALUES WITH GIFFORD σ_f VALUES

In the case of vertical distribution of the measured impinger data, the Gaussian profile seems to be more an exception than the rule. The most likely explanation for this behavior is the rapid rise of the cloud at low wind velocities. In fact, note that in Table 5-5, the agreement between measured and Gifford σ_z values is good only for tests in which the wind velocity was high (about 10 mph).

5.4.3 Ammonia Vapor Rise

The path of the center of the vapor cloud, liberated by the LNH_3 spill on water, can be described by the theories of vapor cloud dispersion in the atmosphere discussed in detail in Section 6.7. Essentially, the cloud can be treated either as a maintained plume or as a puff of vapor. Both theories are applied to describe the ammonia vapor cloud dispersion, and their results are then compared with the experimental observation.

For comparing the predictions and experimental values of vapor cloud rise, the following experimental values are used:

M = mass of liquid ammonia spilled = 284.5 pounds

p = partition ratio

R_{max} = maximum radius of spread = 12 feet

t = duration of evaporation = 10 seconds

T = ambient temperature (60°F)

x = distances to the rafts = 21, 55, and 110 feet

g = acceleration due to gravity = 32.2 feet/second^2

The physical property values for both liquid ammonia and the saturated vapor are taken from Appendix A. The following atmospheric conditions are assumed for the sake of calculations:

U = wind velocity = 8 mph = 11.73 feet/second

$\frac{\partial \theta}{\partial z}$ = potential temperature gradient = 0.01 °K/meter

ρ_a = density of air = 0.07488 lbm/ft^3

ρ_v = density of saturated ammonia vapor at atmospheric pressure = .05556 lbm/ft^3

Hence, we have, assuming no aerosol formation,

$$\Delta = 1 - \frac{\rho_v}{\rho_a} = \text{density defect} = 0.258$$

V = total volume of vapor generated = 18 x 0.4 x 284.5 = 2050 ft^3

5.4.3.1 Predictions from Plume Theory (See Section 6.7.2.1.)

Because of the expanding character of the pool source of ammonia vapor, we assume

$$b_i = R_{max}\sqrt{\sqrt{2}}$$

$$F = \text{buoyancy flux} = \frac{Vg\Delta}{\pi t}$$

$$\ell_p = \text{buoyancy length} = \frac{542}{11.73^2} = 0.336 \text{ feet}$$

using equation 6-56 we have, with β=1,

$$z = 0.795\ x^{2/3}.$$

The heights of the vapor cloud predicted by this theory for x values of 21, 55, and 110 feet are 6, 11.5, and 18.3 feet.

$$\omega = \left[\frac{g}{T}\ \frac{\partial\theta}{\partial z}\right]^{1/2} = \text{Brunt Vaisalla frequency} = 0.0185 \text{ radians/second}$$

$$S = \text{stratification parameter} = \frac{11.73}{.336 \times .0185} = 1891.$$

Hence, from equation 6-61

$$z_\infty = \text{maximum plume rise height} = 0.336 \times 1891^{2/3} = 51.4 \text{ feet.}$$

Approximate downwind distance within which this height is reached is

$$x^* = 443 \text{ feet}$$

5.4.3.2 Predictions from Puff Theory (See Section 6.7.2.2)

B_i = buoyancy volume released = $Vg\Delta$ = 17030 ft^4/s^2

ℓ_c = buoyancy length = $\frac{B_i}{U}$ = 11.12 ft

Assuming $\alpha\kappa$ = 0.3 and using equation 6-62 , we have

$$z = 6.86\ x^{1/2}$$

The heights of the vapor cloud predicted by the above equation by this theory for x values of 21, 55, and 110 feet are respectively 31.5, 51, and 72 feet.

$$S = \text{stratification parameter} - \frac{11.73}{11.12 \times .0185} = 57$$

Assuming again $\alpha = 0.093$ and $\alpha_K = 0.3$, we have from equation 6.65

$$z_\infty = 273 \text{ feet}$$

This height is reached first at a distance x* given by equation 6.66

$$x^* = 1790 \text{ feet.}$$

We compared the values predicted by the above two theories with the experimental values as shown in Table 5-6. The values in the table indicate that the continuous plume theory seems to correlate with experimental data extremely well. The experimental data plotted in Figure 5-12b (visual observation data) indicate that height decreases inversely with wind velocity. This is precisely the law for the continuous plume theory, rather than the puff theory in which the height goes down as the inverse square root of the velocity. Results computed for other wind velocities at the three raft positions, based on the plume theory, are shown in Figure 5-12b.

Similar calculations of cloud rise made with plume theory, assuming two different percentages of aerosol in vapor (0% and 20%) are shown in Figure 5-12a and are compared with those obtained from impinger data. The comparison indicates that maximum concentration data could probably be explained if we allow for aerosols in the vapor cloud.

5.4.4 Comparison of the Vapor Concentration Data with Predicted Values

In this section, we show a method of calculating the vapor concentration downwind. The analysis uses the results of a vapor dispersion model shown in Section 6.5 and the plume rise theory indicated earlier. The results obtained are then compared with the experimentally obtained NH_3 vapor concentration. For the calculations, the following data

Table 5-6

Comparison of Experimental & Predicted Cloud Height Values

Downwind Distance (Feet)	Height of the center of vapor cloud predicted by: Experiment (Feet)	Plume Theory (Feet)	Puff Theory (Feet)	Remarks
21	6-8	6	31.5	Observed values of test #13 are used.
55	10-12	11.5	51	
110	15-18.5	18.3	72	
Maximum plume rise height	-	55 at x = 1790 ft	273 at x = 443 ft	

are assumed:

Quantity of spill	=	4.0 gallons
Partition Ratio	=	0.6
Distance of raft downwind at which the vapor concentration is to be calculated	=	55 feet
Wind velocity	=	7.5 mph = 11 feet/second
Impinger suction rate	=	q = 2.25 liters/minute = 1.324×10^{-3} feet^3/second
Fraction of aerosol in vapor	=	0%

Hence mass of vapor liberated = $m_v = 40 \times 5.69 \times 0.4 = 91.04$ pounds

From Figure 5-11b, the height (z_o) of the center line of the vapor plume at 55 feet from the spill center = 15 feet

Gifford values of dispersion parameters from Figure 6-17 for atmosphere B are: $\sigma_y = 10$ feet, $\sigma_z = 7.5$ feet.

Assuming that the wind is steady, and that the maximum concentration at any downwind location occurs in the same spatial position during the passage of the cloud, we can derive the following relationship between the moles of vapor collected by an impinger at height z_i, directly downwind.

From Section 6.5, the concentration of vapor at any location (y,z) at a distance x downwind can be adequately represented by

$$c(x,y,x,t) = \frac{\dot{m}_v(t-x/U)}{\pi\, \sigma_y(x)\, \sigma_z(x)\, U}\, e^{-\frac{(y-y_o)^2}{2\sigma_y^2}} \left[e^{-\frac{(z-z_o)^2}{2\sigma_z^2}} + e^{-\frac{(z+z_o)^2}{2\sigma_z^2}} \right] \quad (5\text{-}1)$$

$$\text{and } m_v = \frac{q}{U} \int_0^t c(x,y_o,z_i,t)\, dt \quad (5\text{-}2)$$

where

m_v = moles of vapor collected by an impinger

$\dot{m}_v$ = rate of evaporation of vapor (a function of time)

c = vapor concentration (in density units)

y_o, z_o = position of the maximum concentration

t = time

q = impinger suction rate

μ = molecular weight = 17 gms/mole = 0.375 pounds/mole.

Assuming that the peak concentration occurs at the position of the center line of the cloud, we can show that

$$M_v = \frac{m_v q}{\pi \sigma_y \sigma_z \bar{U} \mu} \; e^{-\frac{(z_i - z_o)^2}{2\sigma_z^2}}$$

Substituting the values with z_i = 21 feet

$$\text{we get } M_v = \frac{91.04 \times 1.324 \times 10^{-3}}{\pi \times 10 \times 7.5 \times 11 \times 0.0375} \; e^{-\frac{(21-15)^2}{2 \times 7.5^2}} = 90 \times 10^{-5} \text{ moles} \quad (5\text{-}3)$$

This value is compared with the experimentally observed value (see Figure 5-9a) of 60×10^{-5} moles. The theoretical value is about 50% more than the experimental value. Wind direction is never steady in the atmosphere. This might be one reason for lower mass collected by the impinger. Also, because the raft is floating, the impinger direction may not have been parallel to the wind direction, leading to lower mass of NH_3 vapor collected. It is also possible that the impinger itself was sucking air at a rate less than 2.25 liters/minute (because of the long tubing in the vacuum line). Other possibilities are discussed in Section 5.5.

5.4.5 Spill Radius

The maximum spill radius measured as a function of the spill quantity is shown plotted in Figure 5-7. Note that a straight line, of slope 0.8 on the logarithmic plot, correlates most of the data. However, if the same power law with volume is assumed to hold, then the radius of a 3,000 ton spill would be about 36,000 feet - a highly improbable number. Hence care should be exercised when the small-scale test results are extrapolated to large-scale spills. A theoretical model

has been worked out and reported elsewhere [17] to predict the maximum radius of spill for the spread on water of instantaneously released liquid natural gas. The results of the analysis are as follows:

$$R_{max} = \left[\frac{V^3 G}{\dot{y}^2}\right]^{1/8} \tag{5-4}$$

$$t_e = 0.674\left[\frac{V}{G\,\dot{y}^2}\right]^{1/4} \tag{5-5}$$

where

V = volume of spill

$\dot{y}$ = linear liquid regression rate (assumed to be a constant)

G = effective gravity = $g\left(1 - \frac{\rho_{LNH_3}}{\rho_{water}}\right)$

t_e = time to complete the evaporation

The 3/8 ths power law variation of radius with spill size is also plotted in Figure 5-7. Note that the line seems to correlate the large-scale field observations. Based on equation (5-4) and the experimental results of the 50-gallon tests, we find the "liquid regression" rate ($\dot{y}$) to be 2.8 inches/minute. Using this value, the time to complete evaporation, calculated from equation (5-5) is 9.5 seconds. This time is compared to the experimental values of between five and 11 seconds. The agreement seems to be very good. Using the above formulae for prediction, a 3,000-ton instantaneous spill of LNH_3 on water would spread to a maximum radius of about 475 feet and evaporation would be complete in about 120 seconds.

5.5 DISCUSSION

The partition ratios have been calculated from the impinger data using the "mass balance" method. The validity of this method for obtaining partition ratios has already been tested in the case of intermediate-scale tests. The method gives reasonably accurate values, provided the impinger data are good and wind velocity is known with

good precision. (See Table 4-7.) In the large-scale tests, the partition ratios calculated vary from a low of 0.49? to a high of 0.98. The latter high values have been obtained in tests where either the impinger data are peculiar or visual observations indicated the passage of the vapor cloud above the rafts. The logical conclusion is, therefore, that in such cases a major mass of vapor did not pass through the impingers, resulting in high values of the partition ratios. However, in the tests where the wind was good and the bulk of vapor cloud passed through the rafts, the partition ratios are reasonable, giving credence to the method of calculating the vapor mass from just the time-integrated, spot-sampled vapor concentration data. Recall that the major assumption in this method of calculation vapor mass is that the concentration distribution profiles everywhere in space, at a given location, must be similar. This assumption should be reasonably valid for steady wind conditions. Even in cases where the wind meanders very much, the above assumption will be valid, provided the time of passage of a cloud at any given location is small compared to the period of meandering of the wind.

The Gaussian nature in the distribution of the vapor concentrations (impinger data) is clearly indicated in the sample data shown in Figures 5-8 through 5-10. The horizontal distributions conform to the Gaussian better than do the vertical distributions. In the low-wind tests, very peculiar vertical distributions have been noticed. As explained earlier, the main reason for this is the passage of the cloud well above the rafts. Another reason may be the movement of the rafts (which are floating) during the cloud passage resulting in the impinger mouths being not in line with the wind direction. While the possibility always existed that the wind direction was not always parallel to the impinger intake tube, the movement of the rafts within the duration of the passage of vapor cloud is so small as not to materially affect the impinger data.

The plume rise data has been shown in two graphs. One of them has been obtained from the peak concentration locations in the z direction distribution of impinger data. In view of the comments in the

previous paragraph, it is very likely that these peak location data are not very accurate. In fact, the z direction distributions seem to be reasonable only for the first raft. Figure 5-11a is based on this data. This plume rise data has to be compared with that obtained from observations of the visible cloud behavior (plotted in Figure 5-11b). The two figures give the impression that the maximum vapor concentration occurs below the center of the visible cloud. However, before accepting this as always being the case, note that the data are really insufficient to draw any conclusions. In fact, the impinger data are time-integrated values of concentration and therefore may not reflect the true position of the peak concentration during the cloud passage. Also, there are other uncertainties in the z direction impinger data, as discussed earlier.

The plume theory predictions agree with the observation data (Figure 5-11b) very well. In addition, the experimental data and the plume theory have the same power-law relationship with wind velocity. This agreement with "plume" theory, instead of with "puff" theory is intriguing, because in the experiments the vapor was observed to disperse in the form of a spherical cloud moving downwind rather than as a plume. However, it is likely that in spite of the fact that the vapor seems to be liberated in the form of a puff, the time duration of 10 seconds (for 50 gallons) is long enough for the vapor to move as a plume. It is quite uncertain how the vapor liberated by a really massive spill (occurring in an extremely short period) would behave. However, application of puff theory to the prediction of the movement of cloud originating from an atomic blast, has proved to be very successful[18].

Because of the location of the source at ground level, the surface boundary layer wind structure is important in the dispersion of the vapor. The wind velocity in this surface boundary layer varies from zero on the ground (small but finite value on the water surface because of water movement) to an essentially constant value at the top of the boundary layer (of height 50 to 100 meters). A plume rise model incorporating the variable character of the wind has been worked out, but

because of lack of information on the vertical velocity distribution of the wind, no comparison could be made with experimental vapor cloud rise observations. However, the simple plume theory has predicted the experimental observations quite well. In obtaining the "predictions," the mean pool radius was assumed to be 0.707 of the maximum pool radius and the partition ratio was assumed to be 60%.

To explain the results shown in Figure 5-11a by the plume theory, one has to assume a large fraction of aerosol, up to about 20% by weight, in the vapor. Even though it is likely that the vapor liberated has considerable amounts of aerosol, 20% by weight seems to be rather a large fraction. (Unfortunately there are no direct measurements of the amount of aerosol in the vapor cloud.) It is therefore concluded that visual observation data give the best indication of the location of the peak vapor concentration.

The dispersion parameter values (σ's) obtained from the experimental data and those obtained from Gifford curves are plotted in Figure 5-12.

Note that Gifford curves were developed from a large number of tracer experiments with continuous sources. Also, Gifford curves are given only for distances greater than 100 meters. For comparison with the experimental data, these curves have been extrapolated to the raft distances, which are much closer than 100 meters. Also, the atmosphere type for the days of the experiments were inferred from the sunshine data, the type of wind, kinds of clouds, etc. Since these are all subjective information, it is possible to make some errors in judgment and misconstrue the class of the atmosphere. Considering all these problems, the agreement between experimental and Gifford-dispersion parameter values are quite excellent. Therefore, for predicting the NH_3 vapor concentrations, Gifford values can be used.

A possibility exists that all the atmospheric classes indicated in Table 5-5 are incorrect. When a cold vapor such as saturated NH_3 vapor disperses over a water surface, it may create its own local inversion condition in the atmosphere. Since dispersion of the cloud

of vapor depends to a considerable extent on the local atmospheric condition, and since inversion represents a stable situation, it is feared that the vapor cloud may not disperse as quickly as expected. However, experimental observations do not seem to justify these fears.

The dispersion example worked out in Section 5.5.4 shows agreement between the predicted concentration and the experimental value. Note that a simple continuous point source formula was used in the concentration prediction. Thus, the answers are expected to be valid for distances greater than about two times the maximum pool diameter from the pool center. The example shown in Section 5.4.4 indicates an error of about 50% in prediction. Though this error seems to be high, it is not unreasonable considering the fact that we are comparing two numbers which are the time integrated values of the concentration. Experimentally, there are many variables, the important ones of which are the wind velocity and direction. The assumptions made in the dispersion model as to the steadiness of the wind may not be that accurate. However, that the predicted and experimental values agree that closely is in itself a proof of the adequacy of the dispersion model to predict reasonably accurate concentrations.

6. THEORETICAL ANALYSES

6.1 INTRODUCTION

In the previous chapters, several experimental results have been presented, analyzed, and discussed. In this chapter, several theoretical analyses are given which are relevant to the prediction of hazards presented by a spill of liquid ammonia on water. These analytical models provide a foundation for suitably extrapolating small-scale experimental data to bigger scale spills that might occur due to an accident.

Section 6.2 is a discussion of the vapor flash model, which provides a basis for calculating the amount of vapor produced when liquid ammonia from a pressurized tank leaks out to the atmosphere.

Section 6.3 presents a thermodynamic mixing model for the mixing of ammonia and water, where it can be seen that quite different answers are obtained depending on whether ammonia mixes with water or vice versa. In an actual spill, both types of mixing may take place. The results of the model are the partition ratio and the temperature of the mixed solution.

Section 6.4 contains a detailed heat transfer analysis, made to obtain the pressure-time relation for the tank pressure of a liquid ammonia tank submerged in water. Such a situation may occur following the collision of an ammonia barge and its subsequent sinking.

Sections 6.5 and 6.6 present a compendia of models for the dispersion of ammonia vapor in air and ammonium hydroxide in water; i.e., the various formulae used in different situations, rather than detailed derivations. Most of the formulae have proved accurate for predicting various other gas dispersions and water pollutant concentrations.

Section 6.7 presents the predictions of the plume and vapor puff rise theories, which are based on the analysis of the motion of a buoyant cloud of gas.

An underwater release reaction theory is presented in Section 6.8. This model is based on an anology between the behavior of turbulent flames and LNH_3 jet.

6.2 FLASH MODEL

Ammonia is transported as a liquid, either under pressure at ambient temperature, or at atmospheric pressure as a cryogenic liquid. When the pressurized liquid is released, a fraction of the liquid vaporizes very rapidly and escapes into the atmosphere. The remaining liquid cools to below its atmospheric pressure liquefaction temperature.

The present analysis is to obtain a method of calculating this fraction of vapor produced. In deriving the following equation, we have assumed that the process is adiabatic. It can be shown that the process is also isenthalpic. Thus, we can equate the initial and final enthalpies of a unit mass of LNH_3. Assuming no supercooling of the liquid, we can write the enthalpy equation as

$$h_\ell^i = f h_v^o + (1-f)\, h_\ell^o \qquad (6\text{-}1)$$

where

f = fraction of released LNH_3 that vaporizes

h = specific enthalpy (Btu/lbm)

λ^o = heat of vaporization at one atmosphere saturated condition

superscript o = final (outside the tank) value (one atmosphere pressure saturated condition)

superscript i = initial (inside the tank) value

subscript ℓ = liquid

subscript v = vapor

Hence, $$f = \frac{(h_\ell^i - h_\ell^o)}{\lambda^o} \qquad (6\text{-}2)$$

Illustrative examples have been worked out for three cases of tank conditions, and the results are given in Table 6-1. Note that the fraction of vapor formed increases as tank pressure increases.

Table 6-1

Vapor Flash Calculations for Three Tank Conditions

Ambient Temperature (°F)	Tank Pressure (psi)	(h_2^i) Enthalpy of Tank Liquid (Btu/lbm)	Heat of Vaporization λ^o at atmospheric pressure (Btu/lbm)	Vapor fraction (f) formed at 1 atm. pressure
0	30.42	42.9	589.3	0.051
40	73.32	86.8	589.3	0.126
100	211.90	155.2	589.3	0.242

A computer program has also been written to calculate the vapor fraction, given the ambient temperature. The program utilizes an "ammonia properties subroutine" to evaluate property values.

6.3 THERMODYNAMIC MODELS

6.3.1 Model Types

When LNH_3 is spilled on water, it reacts with water in a relatively small area and forms ammonium hydroxide (NH_4OH) solution and gaseous ammonia vapor (GNH_3). The reaction is quite rapid and, for all practical purposes, heat loss from the reaction can be neglected. Thus, the mixing can be considered to be adiabatic. The mixing process can be modeled, using an equilibrium thermodynamic approach.

However, depending on the details of the mixing process, different answers are obtained. This behavior is not unlike the differences found between adding drops of water to concentrated sulfuric acid and adding drops of sulfuric acid to water. In this section, the three different thermodynamic models that explain the various mixing reactions are derived and discussed. The first case is most representative of surface spills of LNH_3 on water. It can explain most of the experimentally observed phenomenon with the exception of certain temperature measurements observed in the larger size spill tests.

Case 1. A "packet" of LNH_3 mixes with increasing amounts of water, thereby undergoing dilution, and liberating ammonia vapor (GNH_3). The ammonium hydroxide (NH_4OH) formed mixes again with water, undergoing further dilution. The "packet" is assumed to be at uniform concentration throughout its volume, and the vapor produced by dilution is assumed to be removed out of the reaction zone.

A model derived on these assumptions is presented, and an expression for the maximum vapor liberated by a unit mass of LNH_3 undergoing infinite dilution is obtained. The results of the model are compared with experimental data and discussed.

Case 2. A given mass of LNH_3 reacts adiabatically with a known mass of water. The final condition obtained is an equilibrium state, with the final NH_4OH solution in equilibrium with its vapor at saturation.

The derived model presents expressions for calculating both the total mass of vapor produced, and the temperature of the final mixture (NH_4OH) for various final concentrations. The results of this model are compared with some experimental results.

Case 3. The reaction is visualized to be between a given mass of water and increasing quantities of LNH_3 (a process quite the opposite of Case 1). A model based on this premise has been worked out and its results are given.

6.3.2 Continuous Water Mixing (Case 1)

Figure 6-1a shows a schematic representation of Case 1, in which water is continuously mixed with NH_4OH solution (starting with LNH_3; i.e., 100% NH_4OH solution) under adiabatic conditions and at one atmosphere pressure. As vapor is liberated, it is removed from the liquid. The solution remains saturated at its local condition at all times.

The following equations may be written for the conditions of the solution before and after mixing with the quantity "dM" of water. Referring to the control volume (shown in Figure 6-1b) we have,

$m \equiv m(c)$ = mass of ammonia (NH_3) in the solution (NH_4OH) at any concentration

M = mass of water in the solution

c = concentration of the NH_4OH solution $= \frac{m}{(m + M)}$ (6-3)

For the addition of "dM" mass of water

Initial enthalpy of the system $= (m + M)I(c) + dM\ I_w$ (6-4)

Final enthalpy of the system after mixing $= \left\{(m + dm) + (M + dM)\right\} I(c + dc)$ (6-5)

Where I refers to the specific enthalpy of mixture at any concentration.

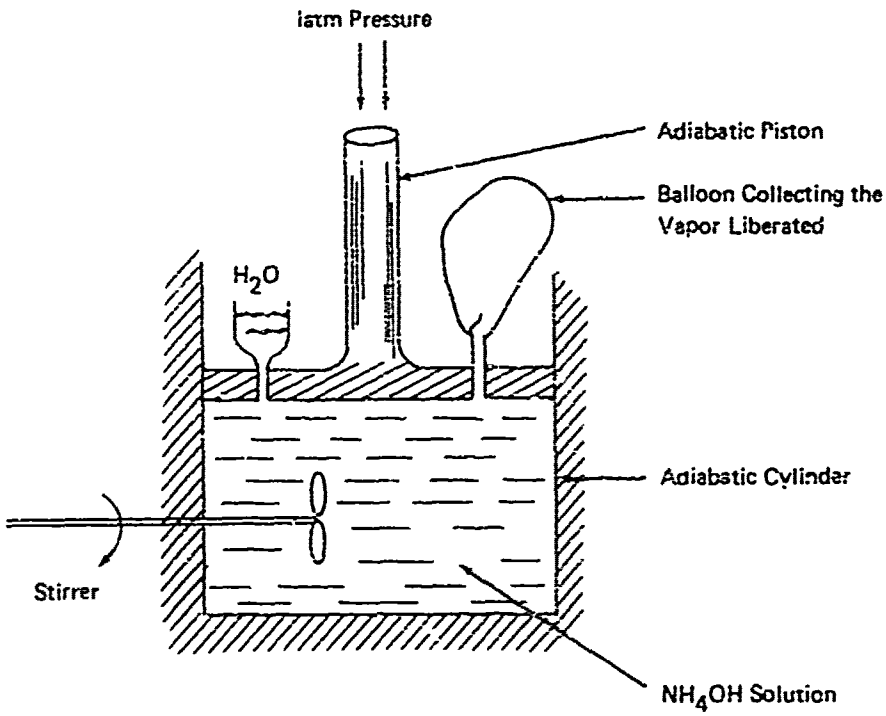

Figure 6–1a Thermodynamic Model for Mixing of LNH_3 and Water

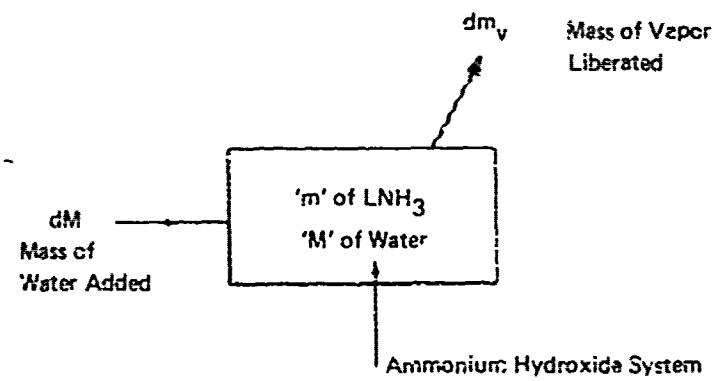

Figure 6–1b Control Volume for the Mixing of LNH_3 and Water

FIGURE 6–1 SCHEMATIC DIAGRAMS ILLUSTRATING THE THERMODYNAMIC MIXING MODEL 1

Since the mixing is isenthalpic, we can equate equations (6-4) and (6-5). Expanding I (c + dc) in Taylor series, simplifying, and rearranging using equation (6-3) gives

$$\frac{dm}{dM} = \frac{m}{c} \left\{ \frac{\left[I - c \frac{dI}{dc} - I_w\right]}{\lambda - (1 - c) \frac{dI}{dc}} \right\} \tag{6-6}$$

or alternacively

$$\frac{dm}{dc} = \frac{m}{c} \left\{ \frac{\left[I - c \frac{dI}{dc} - I_w\right]}{\left[(1-c)\ (I-I_w) - c\lambda\right]} \right\} \tag{6-7}$$

where

$\lambda \equiv \lambda(c)$ = Heat of vaporization of NH_4OH at any concentration c.

The terms within brackets on the righthand side of equations (6-6) and (6-7) are functions of only the concentration (and hence are obtainable from the NH_3--water system property data) and the condition of the water. The two equations can therefore be solved (for a given initial value of m, the mass of LNH_3) to obtain m as a function of the mass of water added (M), or the NH_4OH concentration (c).

Without loss of generality, and for the sake of a simple solution, we assume m = 1 at c = 1 for the initial condition: i.e., a unit mass of LNH_3 to begin with. Hence the <u>total mass</u> of vapor produced, by the time the LNH_3 is diluted to a concentration c, is

$$m_v = 1 - m(c) \tag{6-8}$$

The physical meaning of the term $I - c \frac{dI}{dc}$ (called "partial enthalpy of water") in the righthand side of equation (6-7) is shown in Figure 6-2; the enthalpy of the saturated NH_4OH solution at atmospheric pressure is represented by point E. Point D is the intersection of the ordinate axis and the tangent (DE) at E to the atmospheric pressure enthalpy curve, while BD represents the value of $(I - c \frac{dI}{dc})$ at the concentration c. Point A on the ordinate axis represents the condition of water.

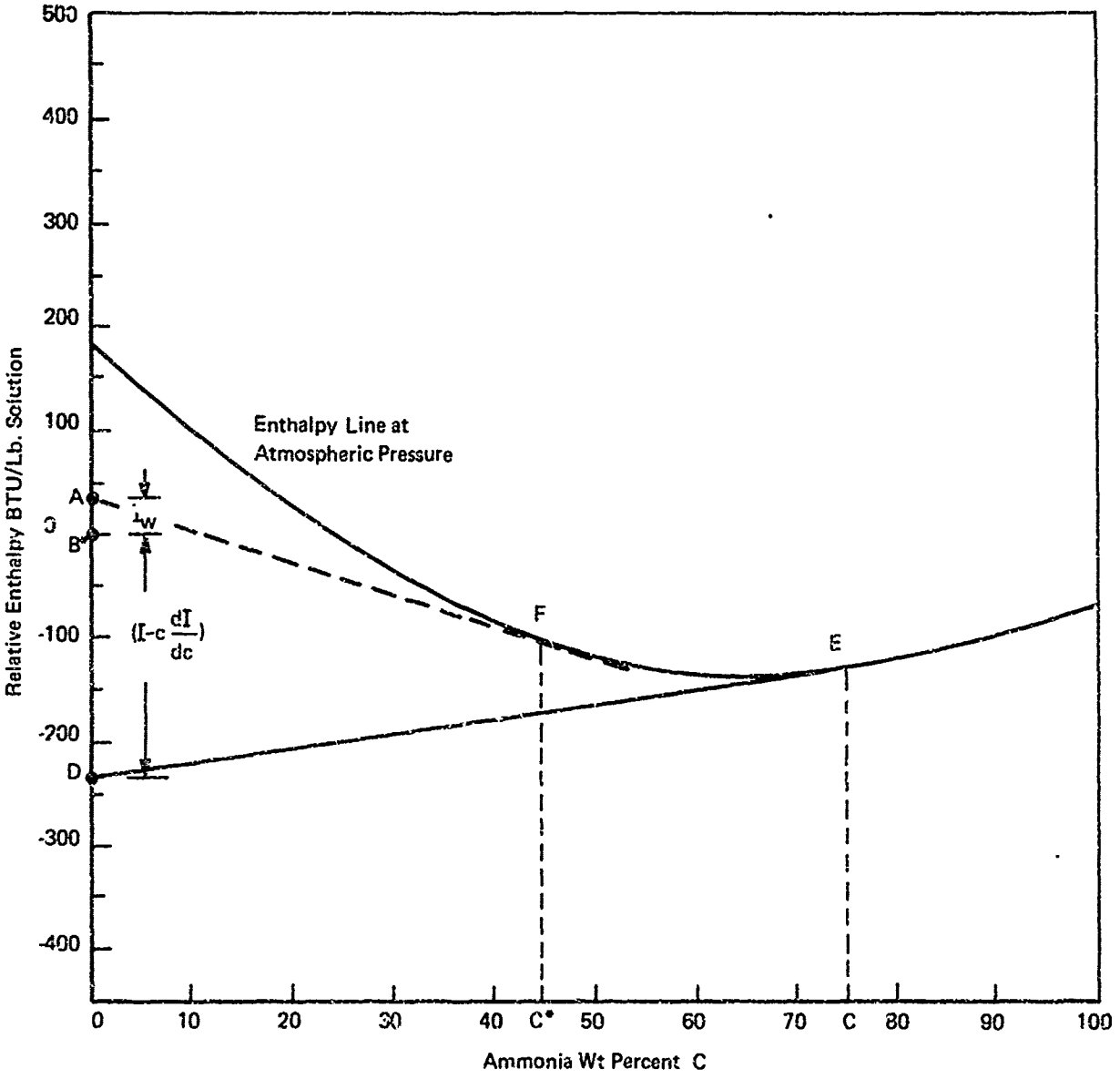

FIGURE 6–2 ENTHALPY-CONCENTRATION DIAGRAM FOR AMMONIA-WATER SYSTEM

Distance AD represents the magnitude of the term $(I - c\frac{dI}{dc} - I_w)$.

As the LNH_3 gets diluted, the intersection point of the tangent line with the ordinate moves up the ordinate until the point D coincides with point A at a "critical concentration" c*.

For $c > c^*$, $\frac{dm}{dc} > 0$, indicating thereby that a decrease in concentration (dilution) results in the liberation of vapor†.

At $c = c^*$, $\frac{dm}{dc} = 0$.

For $c < c^*$, $\frac{dm}{dc} < 0$; i.e., for a further dilution below c*, the mass of ammonia in the solution should increase.

The last case is not allowable, because for that to happen some ammonia vapor should dissolve in the solution. However, the basic assumption in the model is that any vapor produced is removed immediately and is not allowed to redissolve. Because of this stipulation, dilution of the solution below the concentration c* results in unsaturated NH_4OH solution, without, however, changing the mass of ammonia that is in the solution at concentration c*. The solution temperature is no longer given by the saturation temperature corresponding to the concentration.

Hence the maximum amount of vapor produced by the above mixing process is given by

$$\text{Total vapor produced} = m_v(c^*)$$

$$\left.\begin{aligned}\text{Therefore partition ratio } p &= \frac{\text{mass of ammonia in solution after complete mixing}}{\text{original mass of ammonia spilled}} \\ &= 1-m_v(c^*) = m(c^*)\end{aligned}\right\} \quad (6\text{-}9)$$

The solution of equation (6-7) is obtained numerically by curve fitting for the properties that occur on the righthand side. Figure 6-3 shows

---

†Note that vapor is liberated when "dm" is negative.

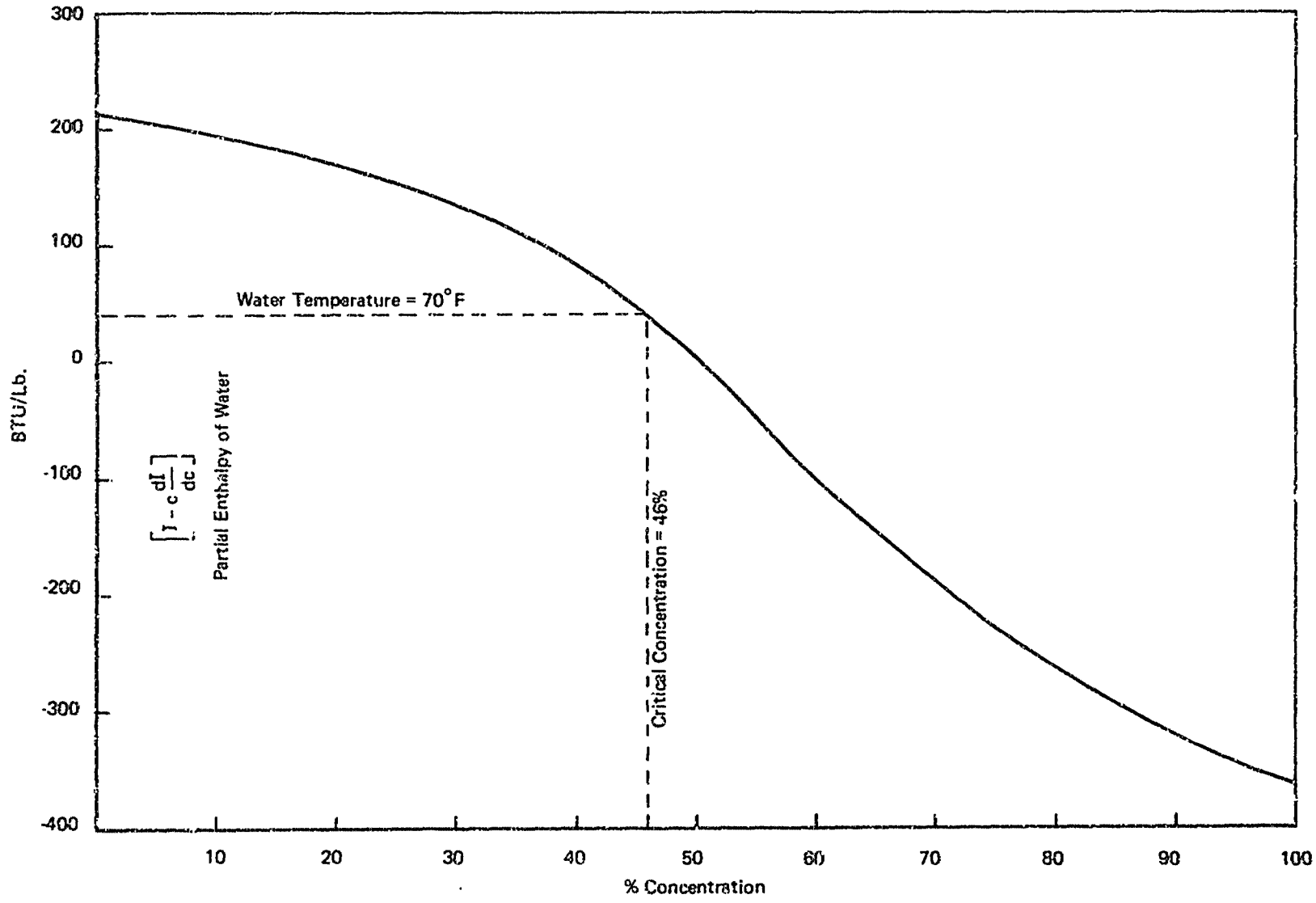

FIGURE 6–3 PLOT OF PARTIAL ENTHALPY OF WATER AS A FUNCTION OF CONCENTRATION FOR NH_3-WATER SYSTEM

the plot of the partial water enthalpy $I - \frac{dI}{dc}$ plotted against the concentration. The critical concentration is determined by equating the enthalpy defect and the initial water enthalpy (for 70°F water, $c^* = 0.46$). The solution obtained in terms of total mass of vapor liberated is plotted in Figure 6-4 for two values of water temperature. The partition ratios given in Table 6-2 were obtained for two different water temperatures.

For any concentration c below c*, the temperature of the NH_4OH solution is not equal to the saturation temperature corresponding to the concentration c. The following analysis indicates the method used for calculating the temperature solution below c*.

As before, the enthalpies of the system before and after the addition of a "dM" mass of water are equated. Hence we get

$$(m^* + M)\,[I(c) - c_p\,(T^{sat}\,(c) - T)] + dM\,I_w$$

Initial Enthalpy of System

$$= (m^* + M + dM)\,[I(c + dc) - c_p\,T^{sat}(c + dc) - (T + dT)\,]$$

Final Enthalpy of the mixture (6-10)

where

m^* = mass of ammonia in the solution when the concentration is c* (This value remains a constant during the subsequent dilution.)

c_p = specific heat of NH_4OH solution (assumed independent of temperature and concentration)

$T^{sat}(c)$ = saturation temperature at concentration

T = temperature of the solution at concentration c

$$\text{Also } c^* = \frac{m^*}{m^* + M}$$

$$\text{and } dM = -\frac{m^*}{c^2}\,dc \qquad (6\text{-}11)$$

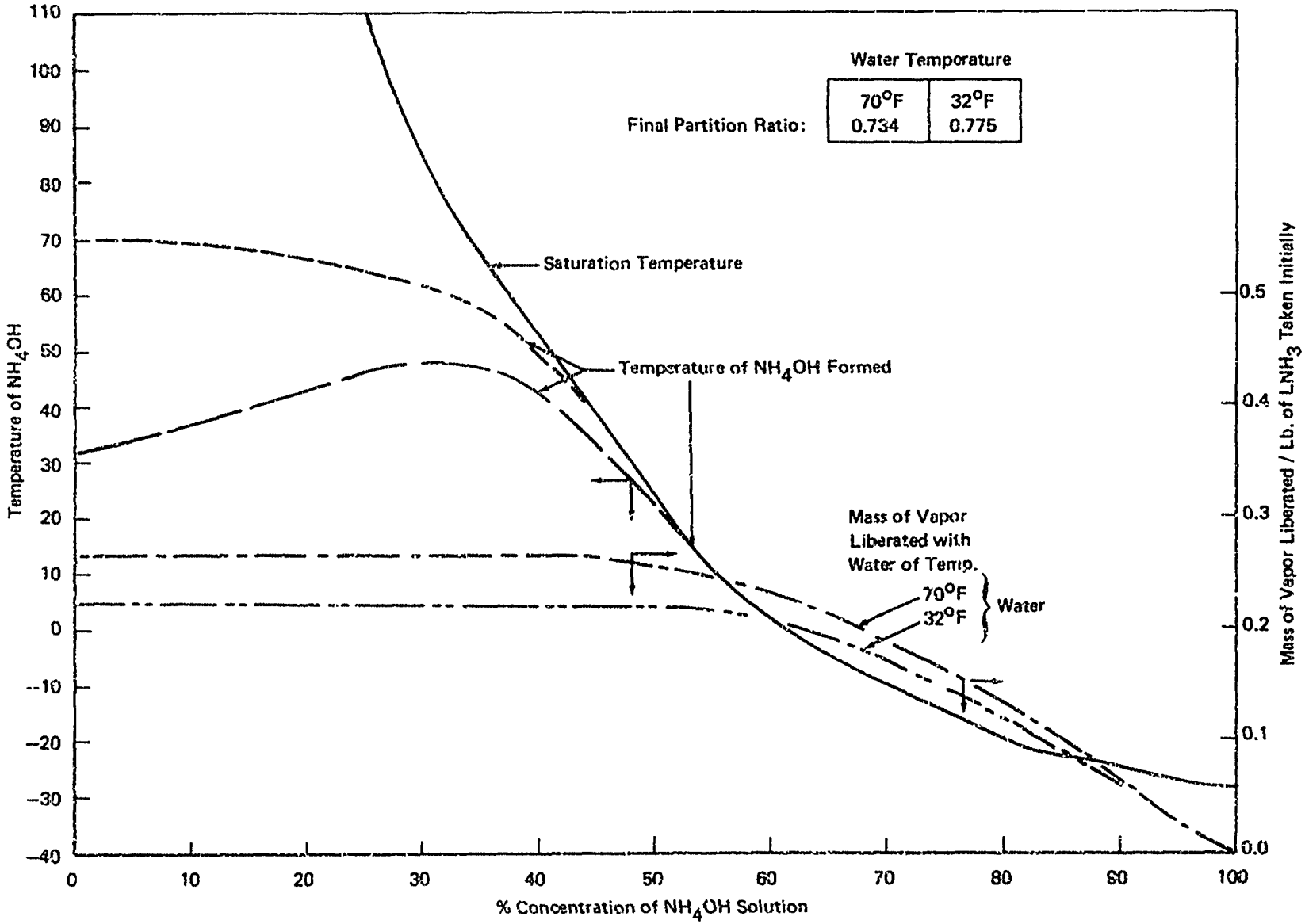

FIGURE 6-4 RESULTS OF THE THERMODYNAMIC MODEL 1

Table 6-2

Theoretically Predicted Partition Ratios and Maximum NH_4OH Solution Temperature

Mixing Water Temperature °F	Critical Concentration %	Partition Ratio	Maximum Temperature of NH_4OH Solution °F	Concentration at which Maximum Temperature Occurs %
32	50.5	0.775	48	≈30
70	46.0	0.735	70	0.0

Expanding the terms on the righthand side of equation (6-10) in a Taylor series, then rearranging and simplifying using equation (6-11), it can be shown that equation (6-10) reduces to

$$-\frac{dc}{c} + \frac{d\,(I - c_p(T^{sat} - T) - I_w)}{(I - c_p(T^{sat} - T) - I_w)} = 0 \qquad (6\text{-}12)$$

Integrating the above equation and substituting the initial condition that,

$$T = T^{sat}(c^*) \text{ at } c = c^*$$

we obtain the following solution for the temperature

$$T(c) = T^{sat}(c) + \frac{1}{c_p}\left[(I_w - I(c)) + \frac{c}{c^*}\,(I\,(c^*) - I_w)\right] \qquad (6\text{-}13)$$

This result is plotted in Figure 6-4 for two water temperatures - 32°F and 70°F - along with the saturation temperature as a function of the concentration. The result indicates that when cold water is used, the maximum temperature attained by the solution is higher than the water temperature, and that for moderate and high water temperatures no temperature rise is observed.

6.3.3 Complete Adiabatic Mixing (Case 2)

In this model we again discuss the adiabatic mixing of LNH_3 and water, but the feature that distinguishes this model from that of Case 1 is its complete equilibrium between vapor (if produced) and the final NH_4OH solution. The results are independent of the "path" in which the final situation is attained.

The basic aspects of the model may be seen in the idealized experiment shown in Figure 6-5.

A certain mass of LNH_3 at saturation (atmospheric pressure) and a unit mass of water at given temperature are kept inside an adiabatic cylinder, separated by an ideal membrane as shown in Figure 6-5a with

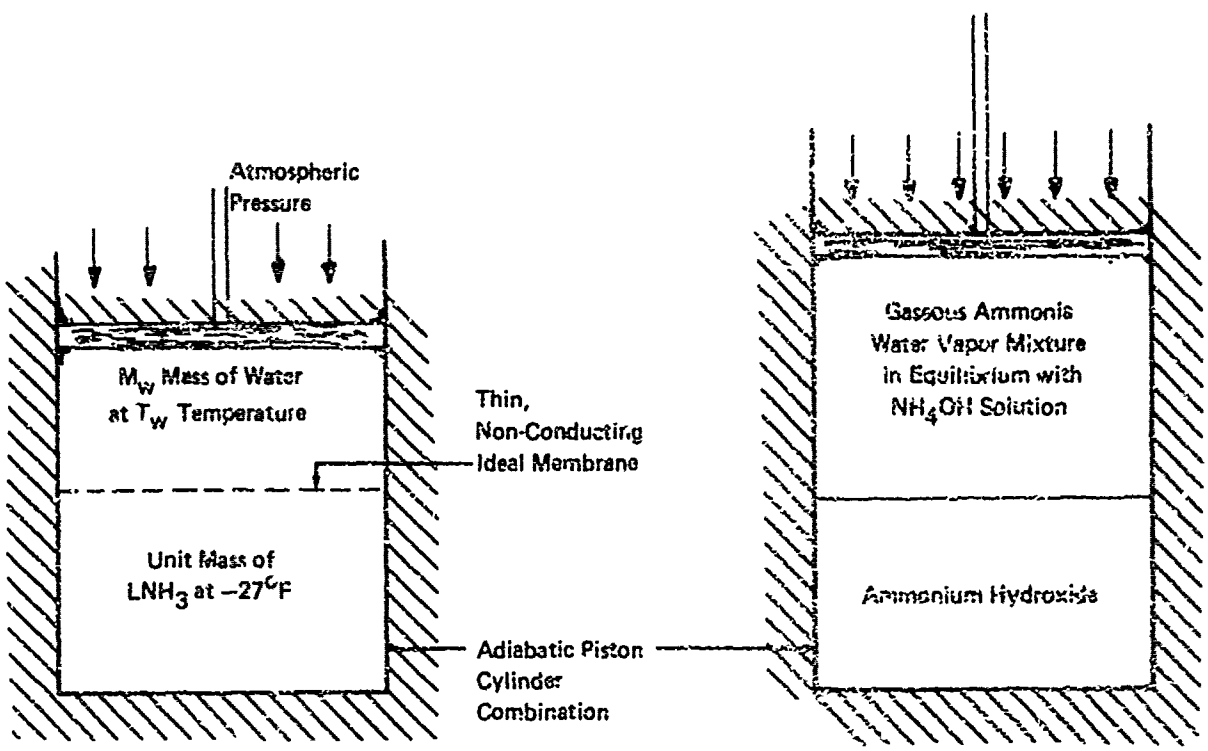

Figure 6–5a

Figure 6–5b

FIGURE 6–5 SCHEMATIC ILLUSTRATION OF THE THERMODYNAMIC MIXING MODEL 2

the cylinder pressure maintained at atmospheric value. At some instant, the membrane is punctured and the LNH_3 and water are allowed to mix, react, and come to equilibrium to form an NH_4OH solution of a desired concentration. It is desired to find what initial mass of LNH_3 is needed to attain a specified concentration and to determine the mass of ammonia in the solution at the final condition.

Since the process is adiabatic and at constant pressure, it can be shown that it is also isenthalpic. If,

x = mass of LNH_3 to be taken initially to obtain a final concentration c

m_w^{ℓ}, m_w^{v} = mass of water in the liquid phase and vapor phase, respectively, in the equilibrium mixture at c

and m_a^{ℓ}, m_a^{v} = mass of ammonia in the liquid and vapor phases, respectively,

then we can write the following enthalpy balance equations.

If no vapor is formed

$$m_x = \left(\frac{c}{1-c}\right) \tag{6-14}$$

in which case, the NH_4OH solution formed is not saturated; and if vapor is formed

$$m_x I_{LNH_3} + I_w = (m_w^{\ell} + m_a^{\ell})\, I(c) + (m_w^{v} + m_a^{v})\, I_{vapor}(c) \tag{6-15}$$

To evaluate the value of x from equation (6-15), the following additional equations are used:

$$\left.\begin{aligned} m_a^{\ell} &= \left(\frac{c}{1-c}\right) m_w^{\ell} \\ 1 &= m_w^{\ell} + m_w^{v} \\ m_x &= m_a^{\ell} + m_a^{v} \end{aligned}\right\} \tag{6-16}$$

and $m_w^{v} = K(c)\, m_a^{v}$

where R(c) is a factor obtained from property data. In general, $R \ll 1$, so that for all practical purposes one can assume $m_w^v = 0$ (hence $m_w^\ell = 1$)

Substituting the set of equations (6-16) in (6-15), and knowing all the enthalpy values from property data, the value of m_x can be evaluated. Partition ratio can then be calculated by

$$p = \frac{m_a^\ell}{m_x} \tag{6-17}$$

When no vapor is formed (which happens when small amounts of ammonia mix with large quantities of water) the final solution obtained is not saturated. In such a case, the temperature of the mixture can be calculated from

$$T = T^{sat}(c) + \frac{1}{c_p}\left[\frac{(m_x I_{LNH_3} + I_w)}{(1+m)} - I(c)\right] \tag{6-18}$$

where m_x is given by equation (6-14). The temperature of the solution which is in equilibrium with the vapors at any concentration is equal to the saturation temperature corresponding to that concentration.

The results calculated for two water temperatures are shown in Figures 6-6 and 6-7. Figure 6-6 shows the total mass of water necessary to make the necessary concentration solution, starting with a unit mass of LNH_3, and gives the total NH_3 vapor produced at any equilibrium concentration. Figure 6-7 shows the dependence of the equilibrium temperature and partition ratio on the final concentration. It is noteworthy that a substantial temperature increase (above water temperature) can result if the final concentration is between 15 and 25%.

6.3.4 Continuous LNH_3 Mixing (Case 3)

One can visualize a situation where increasing amounts of LNH_3 mix with a given quantity of water. An idealized experiment, similar to the one mentioned for Case 1, can be performed where instead of

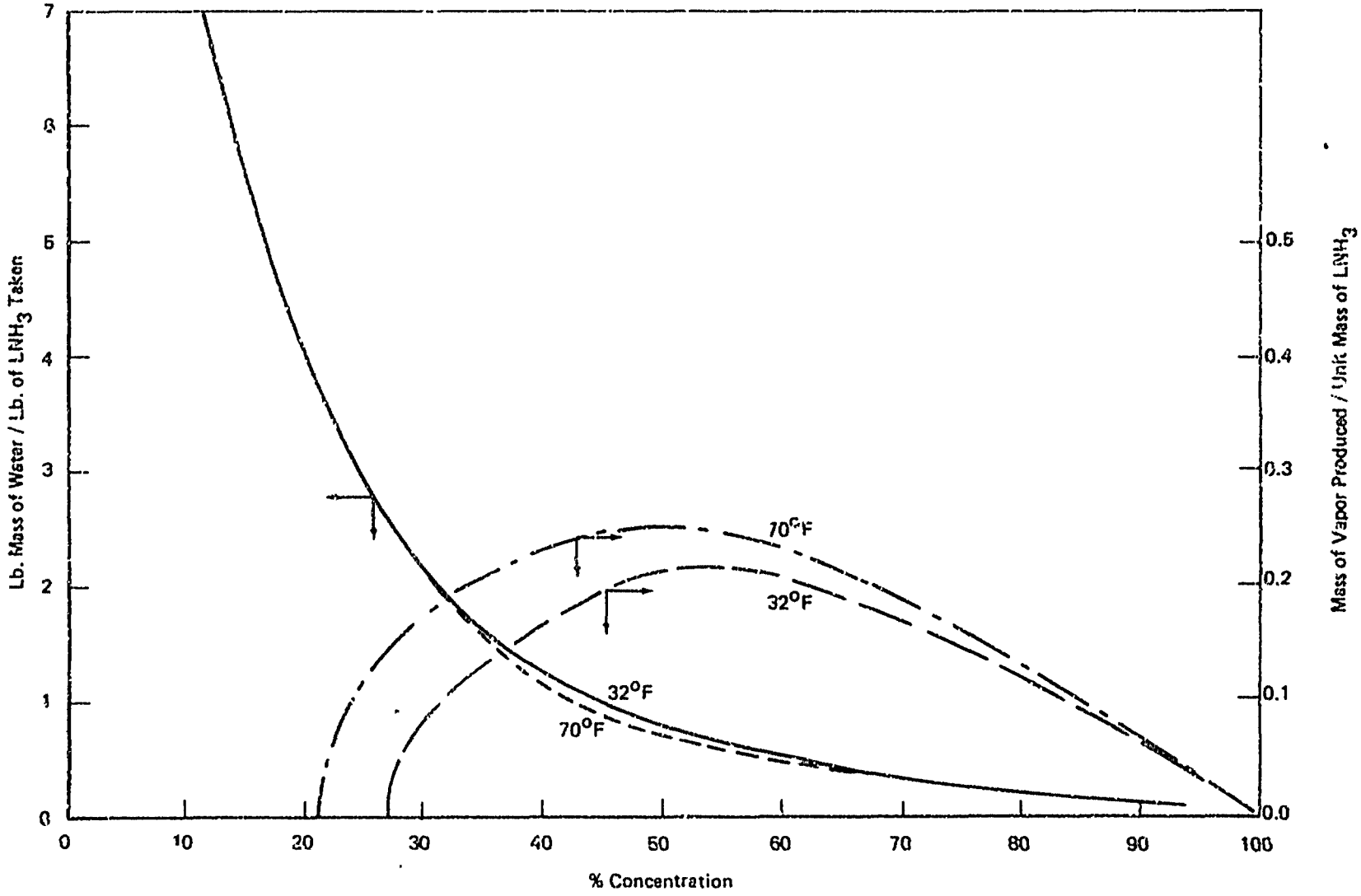

FIGURE 6–6 MASS OF VAPOR PRODUCED AND MASS OF WATER NEEDED TO PRODUCE A GIVEN CONCENTRATION OF AMMONIUM HYDROXIDE BY ADIABATIC MIXING WITH UNIT MASS OF LNH_3

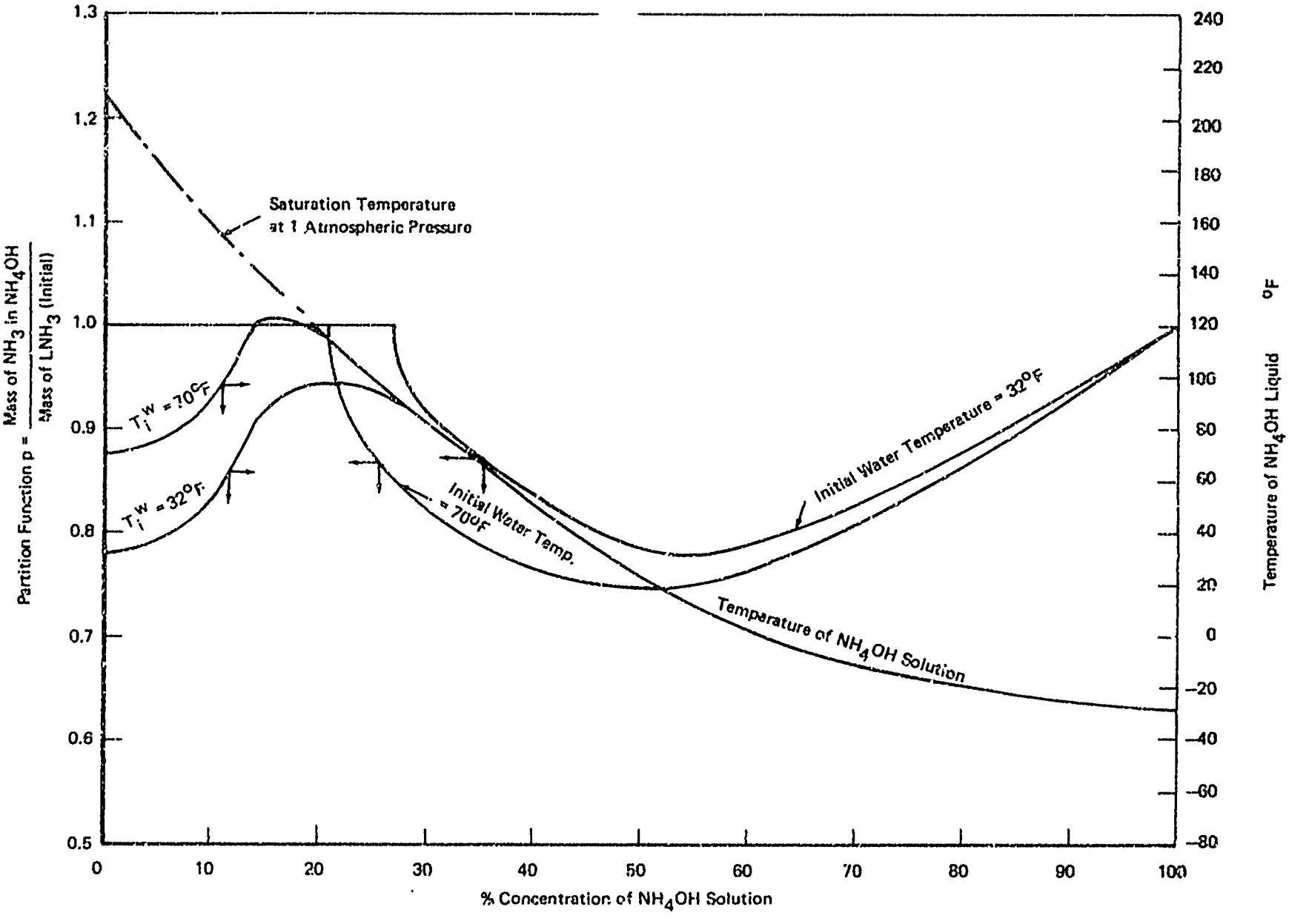

FIGURE 8–7 RESULTS OF ADIABATIC MIXING MODEL 2

water mixing with NH_4OH, LNH_3 mixes with NH_4OH solution, starting with pure water (i.e., 300% NH_4OH solution). The other conditions (adiabatic, immediate vapor removal, etc.) remain the same as those given for Case 1.

An enthalpy balance equation can be written, and expressions can be obtained for the mass of vapor produced, temperature of NH_4OH solution, etc. Detailed derivations are omitted, but the results are shown in Figure 6-8.

The results of this model show that even though the total mass of vapor liberated increases as the total mass of LNH_3 added increases, the partition ratio first decreases and then increases. This indicates that up to a certain concentration (about 45% for 70°F water) the mass of vapor produced per unit mass of LNH_3 added first increases and then decreases. However, the main difference between this model and the model for Case 1 is that in the latter case the concentration of the mixture continuously decreases, and after a certain concentration no more vapor is liberated. However, in the model for Case 3, there is a continuous increase in the mass of vapor liberated, even though the partition ratio itself reaches a minimum, then rises back to unity. This is because of the increasing quantity of LNH_3 that is added.

6.4 HAZARDS CAUSED BY SINKING AN LNH_3 BARGE

6.4.1 Introduction

A major quantity of ammonia is carried on U.S. inland waterways in refrigerated barges in amounts exceeding 2500 tons. A typical 2500-ton barge built by National Marine Service by Bethlehem Steel is shown in Figure 6-9. The barge has two, 40-foot-long, 18-foot-diameter tanks, insulated by three-inch-thick urethene foam and an 18-gage galvanized steel cover. The tanks are equipped with six-inch-diameter pressure relief valves, preset to open at 10 psig. The valves are pilot operated and have no flutter when operating at the set pressure.

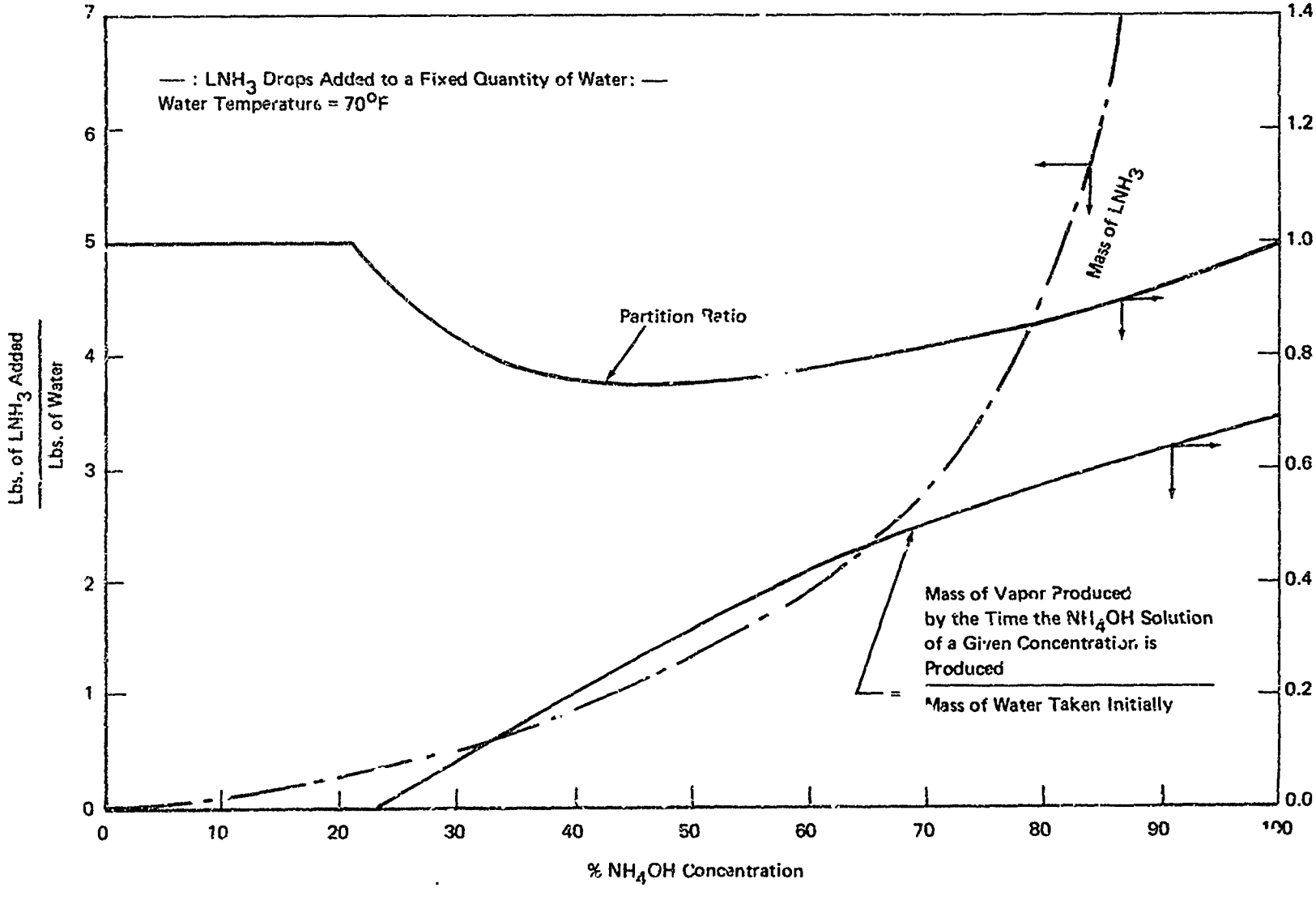

FIGURE 6--8 RESULTS OF MIXING MODEL 3

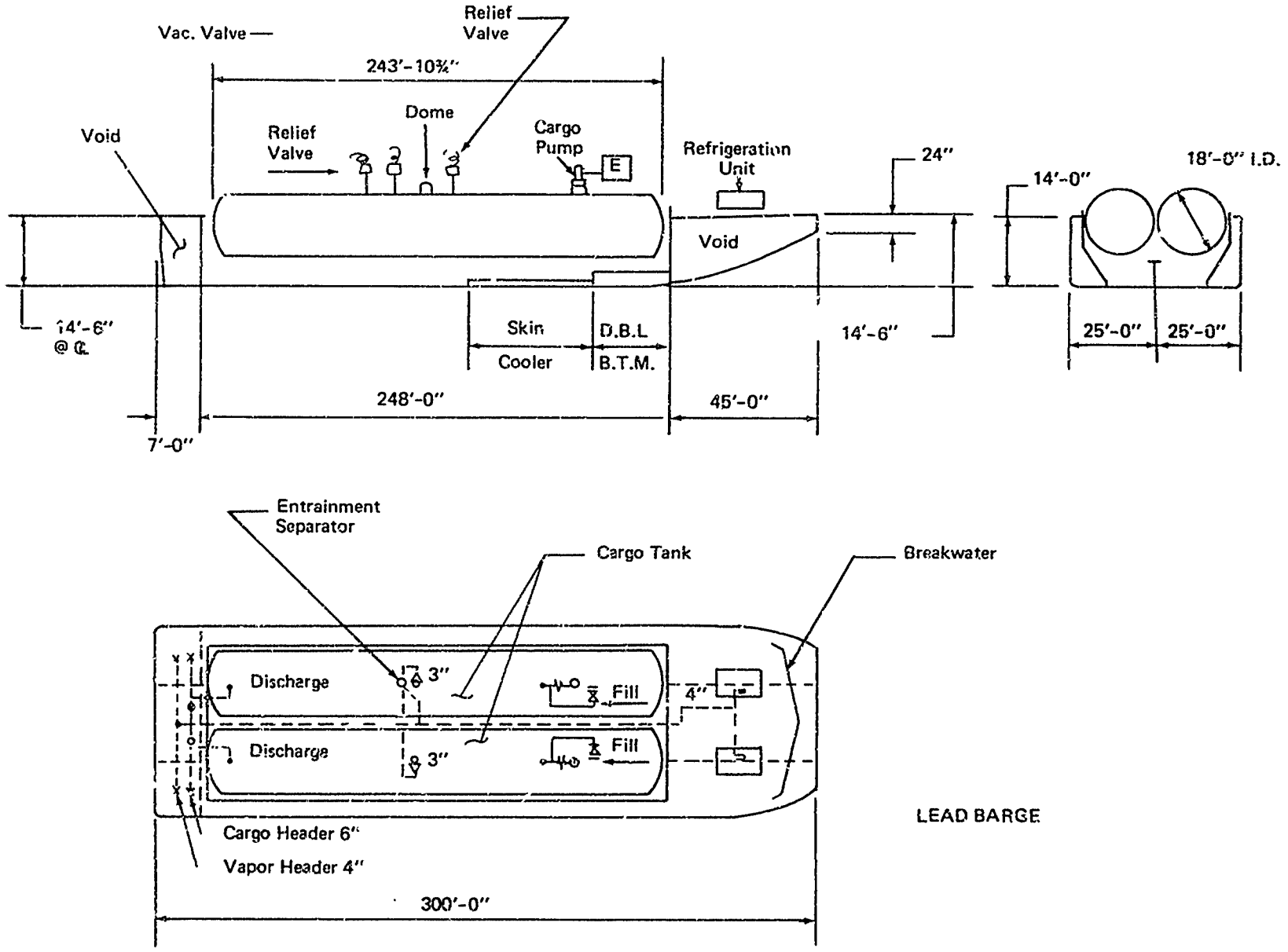

FIGURE 6–9 DETAILS OF A REFRIGERATED LIQUID AMMONIA BARGE

If such a barge is involved in an accident, and then sinks with the LNH_3 tank, a serious problem exists. Depending on the amount of tank insulation lost in the accident, a tremendous amount of heat leaks into the LNH_3 from the water. The sudden heating of the LNH_3 causes an increase in tank pressure and venting of liquid or gaseous ammonia (depending on the orientation of the barge).

The analysis presented here concerns the consequences of such a disaster and whether the venting capacity normally provided is adequate to prevent the tank over-pressure and possible rupture. The consequences of an explosion releasing all of the remaining LNH_3 at once underwater are not yet very clear.

6.4.2 Problem Description

To evaluate the potential hazard posed by a submerged tank filled with LNH_3, we considered the "worst" of the several possible cases. As shown in Figure 6-10, a sunken tank can assume a variety of orientations. The particular orientation depends on the position of the barge after sinking (note that a full tank of LNH_3 is buoyant, by itself). The worst case is the situation where the tank has been inverted during the sinking so that the relief valves are on the bottom of the tank and must pass liquid to relieve the tank pressure. In such a case, the dissolution of liquid ammonia in water takes place around the tank, heats the water around the tank, and increases heat transfer rate to the tank. A temperature rise of 60° to 70°F has been observed in a few instances in the test program. We also considered a situation where the urethene foam insulation on the tank was nullified by detachment or permeability to water, and the relief valves were malfunctioning.

The parameter of interest in this analysis is the tank pressure as a function of time subsequent to immersion in water. Such auxiliary information as ullage volume, thickness of ice on the tank outer wall, temperature of the tank contents, etc., was also generated. Two specific cases have been evaluated:

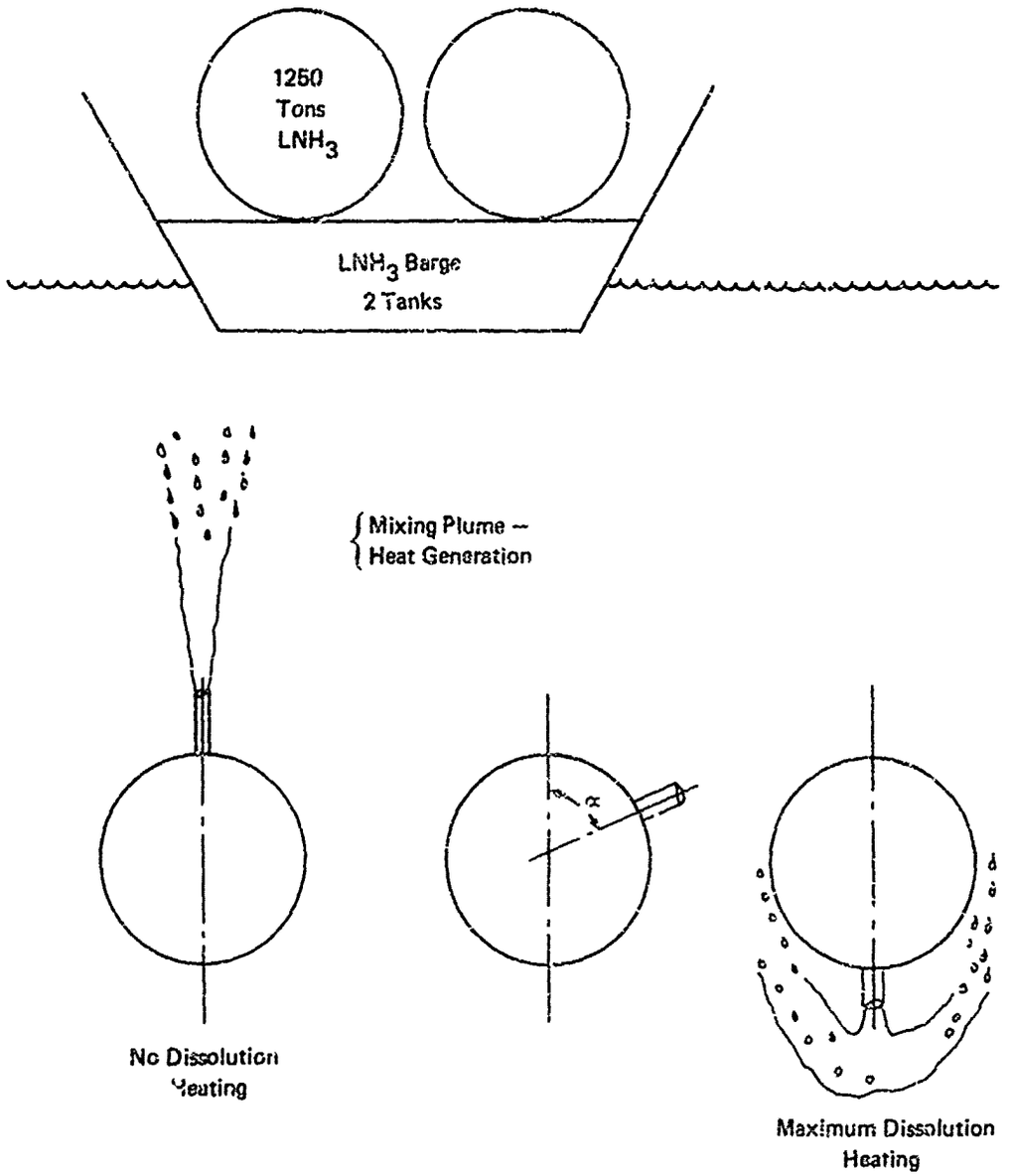

FIGURE 6–10 SCHEMATIC ILLUSTRATION OF THE POSSIBLE ORIENTATIONS OF THE SUNKEN TANK

- Initially, contents are saturated at 14.7 psia. After sinking, the tank is inverted and releases liquid from the relief valves at 10 psig. The outside water temperature is 100°F, and all of the insulation is inoperative.

- A second case supposes that the relief valves do not open at all and the tank eventually ruptures.

6.4.3 Model Formation

6.4.3.1 Assumptions

We have stated previously that the principal output from the model is a tank pressure profile versus time subsequent to immersion in 100°F water. In assembling a model of the tank's physical behavior, we made the following assumptions:

- tank contents are always saturated at uniform pressure;
- static head of liquid is ignored;
- heat transfer to contents is uniform over the exposed area of the tank outer wall;
- ambient water is at 100°F;
- flow through each of the two six-inch relief valves is modelled as turbulent flow through a sharp-edged orifice downstream from a long contraction region;
- relief valves are fully open at 11% over set pressure; and
- thermal capacity of the steel tank is ignored in comparison with the thermal capacity of the contents.

6.4.3.2 Energy Equation

Three distinct physical situations might occur during the transient temperature rise of the tank contents:

1. Relief valves are closed and both vapor and liquid phases present within the tank;

2. Relief valves are closed with the tank full of liquid;

3. Relief valves are open and mass flows out of the tank with both vapor and liquid phases present within the tank.

For each of the above cases, the energy equation is written in terms of the heat input rate and the increase in the internal energy of the contents. These are given below, using the following nomenclature.

A = surface area of the tank (ft^2)

c_p = specific heat of water (Btu/lbm-°F)

E_{cv} = energy contained within the control volume (Btu)

h_f = specific enthalpy of liquid (Btu/lbm)

h_v = specific enthalpy of vapor (Btu/lbm)

h_w = heat transfer coefficient, water to ice(Btu/hr - ft^2 - °F)

h_{sf} = heat of fusion of water (Btu/lbm)

k_i = thermal conductivity of ice (Btu/hr - ft - °F)

ℓ_i = thickness of the ice layer (in)

m_f = liquid mass within the tank (lbm)

m_v = vapor mass within the tank (lbm)

P = contents pressure (psia)

$\dot{P}$ = $\left(\frac{\partial P}{\partial t}\right)$ time derivative of pressure (psia/min)

$\dot{Q}$ = rate of heat transfer to tank (Btu/min)

t = time (min)

T = contents temperature (°F)

T_w = temperature of ambient water (°F)

u_f = specific internal energy of the liquid (Btu/lbm)

u_v = specific internal energy of the vapor (Btu/lbm)

v_f = specific volume of liquid (ft^3/lbm)

v_v = specific volume of vapor (ft^3/lbm)

V = tank volume (ft^3)

β = volume fraction of vapor (dimensionless) $0 \leq \beta \leq 1$

$\dot{\beta} = \left(\frac{\partial \beta}{\partial t}\right)$ time derivative of vapor volume fraction (min^{-1})

ρ_i = density of ice (lbm/ft^3)

Situation 1 Relief valves are closed and both vapor and liquid phases present within the tank. For this case, we define a control volume as shown in Figure 6-11, and write the First Law of thermodynamics for the closed system.

$$\frac{\partial}{\partial t}\,(E_{cv}) = \dot{Q}$$

Expanding this we get

$$\frac{\partial}{\partial t}\,(m_v\,u_v + m_f\,u_f) = \dot{Q} \tag{6-20}$$

$$\frac{\partial}{\partial t}\left[\frac{\beta V}{v_v}\,(h_v - Pv_v) + \frac{(1-\beta)\,V}{v_f}\,(h_f - Pv_f)\right] = \dot{Q} \tag{6-21}$$

In terms of the time derivatives of vapor volume and pressure, $\dot{\beta}$ and $\dot{P}$ respectively, First Law equation becomes

$$\dot{\beta}\left[\frac{h_v - \frac{P_v}{\rho_v}}{v_v} - \frac{h_f - Pv_f}{v_f}\right] + \dot{P}\left[-\frac{\beta\frac{dv_v}{dP}}{v_v^2}\,(h_v - Pv_v) + \frac{\beta}{v_v}\left(\frac{dh_v}{dP} - P\frac{dv_v}{dP} - v_v\right)\right.$$

$$\left. - \frac{(1-\beta)\frac{dv_f}{dP}}{v_f^2}\,(h_f - Pv_f) + \frac{(1-\beta)}{v_f}\left(\frac{dh_f}{dP} - P\frac{dv_f}{dP} - v_f\right)\right] = \frac{\dot{Q}}{V} \tag{6-22}$$

where we have an equation in terms of $\dot{\beta}$, $\dot{P}$, $\dot{Q}$ and the thermodynamic properties of ammonia at saturation conditions. This is the most useful formulation in terms of our interest in the vapor volume fraction β and in the pressure P as functions of time.

We need an additional equation to make the problem amenable to solution. Assuming we can later formulate the heat transfer $\dot{Q}$, an additional relationship between β and P is necessary. Conservation of mass within the control volume requires that

$$\frac{\partial}{\partial t}(m_v + m_f) = 0 \tag{6-23}$$

i.e., the total system mass is invariant in time. We can rewrite this equation as

$$\frac{\partial}{\partial t}(m_v + m_f) = \frac{\partial}{\partial P}(m_v + m_f)\frac{\partial P}{\partial t} = 0 \tag{6-24}$$

We know that $\frac{\partial P}{\partial t} = \dot{P}$ may not be constrained to be zero, so

$$\frac{\partial}{\partial P}(m_v + m_f) = 0 \tag{6-25}$$

This expression may be expanded to yield

$$\frac{\partial}{\partial P}(m_v + m_f) = V\left[\frac{1}{v_v}\frac{\partial \beta}{\partial P} - \frac{\beta}{v_v^2}\frac{\partial v_v}{\partial P} - \frac{1}{v_f}\frac{\partial \beta}{\partial P} - \frac{(1-\beta)}{v_f^2}\frac{\partial v_f}{\partial P}\right] = 0 \tag{6-26}$$

or, in another form,

$$\frac{\partial \beta}{\partial P} = \left[\frac{\beta}{v_v^2}\frac{dv_v}{dP} + \frac{(1-\beta)}{v_f^2}\frac{dv_f}{dP}\right] \Bigg/ \left(\frac{1}{v_v} - \frac{1}{v_f}\right) \tag{6-27}$$

Now, we can relate $\dot{\beta}$ and $\dot{P}$ as follows:

$$\dot{\beta} = \frac{\partial \beta}{\partial t} = \frac{\partial \beta}{\partial P}\frac{\partial P}{\partial t} = \frac{\partial \beta}{\partial P}\dot{P} \tag{6-28}$$

Given an expression for $\dot{Q}$, we can solve for β and P as functions of time, given the two first-order differential equations in $\dot{\beta}$ and $\dot{P}$.

Situation 2 Relief valves closed with the tank full of liquid. In this situation, any heat added will only serve to expand the liquid further in the absence of vapor. The assumption of saturated contents requires that there be a finite vapor fraction existing to have two phases in equilibrium, but we may simplify the results of Situation 1 for $\beta << 1$ in the interests of a simpler solution. The equations then reduce to

$$\dot{\beta} = 0$$

and

$$\dot{P}\left[-\frac{\frac{dv_f}{dP}}{v_f^2}(h_f - Pv_f) + \frac{1}{v_f}\left(\frac{dh_f}{dP} - P\frac{dv_f}{dP} - v_f\right)\right] = \frac{\dot{Q}}{V} \qquad (6\text{-}29)$$

Strictly speaking, the use of property values for the saturated liquid state is not entirely valid, because we'll be considering the compressed liquid region when the tank becomes full of liquid. But this formulation will presume two-phase equilibrium in its use of property values for the saturated liquid, while at the same time allow easier solving for the case when $\beta << 1$.

Situation 3 Relief valves are open and liquid flows out of the tank. Here, we must consider an open system (mass crossing the system boundary) analysis of the tank. The First Law formulation is now

$$\frac{\partial}{\partial t}(E_{cv}) = \dot{Q} - \dot{m}_{out} h_f \qquad (6\text{-}30)$$

where

$$\dot{m}_{out} = -\frac{\partial}{\partial t}(m_v + m_f) \qquad (6\text{-}31)$$

The left side of the equation, $\frac{\partial}{\partial t}\ (E_{cv})$, becomes after some manipulation,

$$V\left\{\left[\frac{\beta}{v_v}\left(\frac{dh_v}{dP} - P\frac{dv_v}{dP} - v_v\right) + \frac{(1-\beta)}{v_f}\left(\frac{dh_f}{dP} - P\frac{dv_f}{dP} - v_f\right)\right.\right.$$

$$\left.\left. - \frac{\beta\frac{dv_v}{dP}}{v_v^2}(h_v - Pv_v) - \frac{(1-\beta)\frac{dv_f}{dP}}{v_f^2}(h_f - Pv_f)\right]\dot{P}\right.$$

$$\left. + \left[\frac{h_v - Pv_v}{v_v} - \frac{h_f - Pv_f}{v_f}\right]\dot{\beta}\right\} \qquad (6\text{-}32)$$

The right side of the equation, $(\dot{Q} - \dot{m}_{out}\ h_f)$ may be expanded in the form

$$\dot{Q} + \frac{\partial}{\partial t}\ (m_v + m_f)h_f = \dot{Q} + V\left\{\left(\frac{1}{v_v} - \frac{1}{v_f}\right)\dot{\beta} - \left[\frac{\beta\frac{dv_v}{dP}}{v_v^2} + \frac{(1-\beta)\frac{dv_f}{dP}}{v_f^2}\right]\dot{P}\right\}h_f \qquad (6\text{-}33)$$

If the right and left sides are combined in expanded form, the energy equation yields

$$\dot{\beta}\left\{\frac{h_v - Pv_v}{v_v} - \frac{h_f - Pv_f}{v_f} - \left(\frac{1}{v_v} - \frac{1}{v_f}\right)h_f\right\} + \dot{P}\left\{\frac{\beta}{v_v}\left(\frac{dh_v}{dP} - P\frac{dv_v}{dP} - v_v\right)\right.$$

$$+ \frac{(1-\beta)}{v_f}\left(\frac{dh_f}{dP} - P\frac{dv_f}{dP} - v_f\right) - \frac{\beta\frac{dv_v}{dP}}{v_v^2}(h_v - Pv_v) - \frac{(1-\beta)\frac{dv_f}{dP}}{v_f^2}(h_f - Pv_f)$$

$$\left. + \left[\frac{\beta\frac{dv_v}{dP}}{v_v^2} + \frac{(1-\beta)\frac{dv_f}{dP}}{v_f^2}\right]h_f\right\} = \frac{\dot{Q}}{V} \qquad (6\text{-}34)$$

6.4.3.3 The Pressure Drop Equation

An additional equation is needed to relate $\dot{\beta}$ and $\dot{P}$, and can be obtained from an analysis of liquid flow through the relief valves.

If we model flow through the two relief valves to be similar to a turbulent flow through a sharp-edged orifice, downstream of a "long" ($L/D \geq 3$) contraction region, we have for the pressure drop ΔP across the orifice

$$\Delta P = 1.45 \frac{v_f}{2A_o^2}\left[-\frac{\partial}{\partial t}(m_v + m_f)\right] \qquad (6\text{-}35)$$

where the factor 1.45 is an orifice coefficient, and the term $-\frac{\partial}{\partial t}(m_v + m_f)$ is the negative of the rate of change of mass within the tank. Since the rate of change is negative for flow out of the tank, a negative sign inserted above yields a positive ΔP as

$$\Delta P = P - 14.7$$

where P is, of course, the absolute (uniform) pressure of the tank contents, and 14.7 represents the absolute pressure of the surrounding water (also assumed uniform). After some manipulation, the equation becomes

$$\dot{\beta} = \frac{-\left[\frac{2}{1.45}(P - 14.7)\frac{A_o^2}{v_f}\right]^{\frac{1}{2}}}{V\left(\frac{1}{v_v} - \frac{1}{v_f}\right)} + \frac{\left[\beta\frac{dv_v}{dP} + (1-\beta)\frac{dv_f}{dP}\right]}{\left(\frac{1}{v_v} - \frac{1}{v_f}\right)}\dot{P} \qquad (6\text{-}36)$$

This, along with the expanded energy equation, constitutes two first-order differential equations relating the time derivatives of vapor-volume fraction, β, and tank pressure, P. Given a functional form for the rate of heat transfer, $\dot{Q}$, we may solve for β and P as functions of time in Situation 3, when relief valves are open and liquid flows out of the tank.

6.4.3.4 Heat Transfer from Water

When a tank containing cold (-28°F) LNH_3 is immersed in water, ice begins to form on the outer walls of the bare portions of the tank. Figure 6-12 illustrates the ice layer and the temperature distribution of this situation. Because of the high conductivity of the metal wall, we assume negligible temperature gradient in the wall. Heat is liberated due to water freezing and the subcooling of both water and ice and the heat is transferred to the LNH_3. By ignoring the heat capacity of the ice layer and wall, we can write the following equation for the rate of heat transfer per unit area of the wall†

$$\dot{Q} = \frac{k_i A}{\ell_i} (32-T) \tag{6-37}$$

where T is the temperature of the tank contents at any instant of time.

An additional equation is necessary to quantify the ice thickness as a function of time. Considering an energy balance on the ice layer, we have

$$\dot{Q} = \dot{Q}_{\text{fusion}} + \dot{Q}_{\text{from water}}$$

This equation can be written in terms of ice layer thickness, heat of fusion, etc., as

$$\frac{k_i A}{l_i} (32 - T) = A\rho_i \frac{dl_i}{dt} \left[h_{sf} + C_p (T_w - 32) \right] + h_w A (T_w - 32) \tag{6-38}$$

The equation can be rearranged to give an expression for the rate of growth of the ice layer, in terms of the temperature of the tank contents, as

$$\frac{dl_i}{dt} = \frac{\frac{k_i}{l_i} (32 - T) - h_w (T_w - 32)}{\rho_i \left[h_{sf} + c_p (T_w - 32) \right]} \tag{6-39}$$

†All properties are expressed in British thermal units.

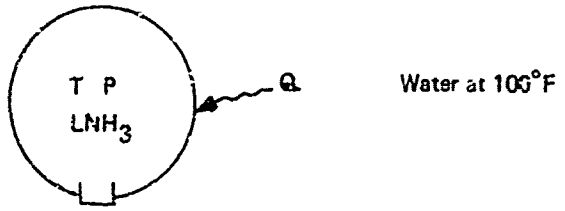

FIGURE 8–11 CONTROL VOLUME FOR ENERGY EQUATIONS

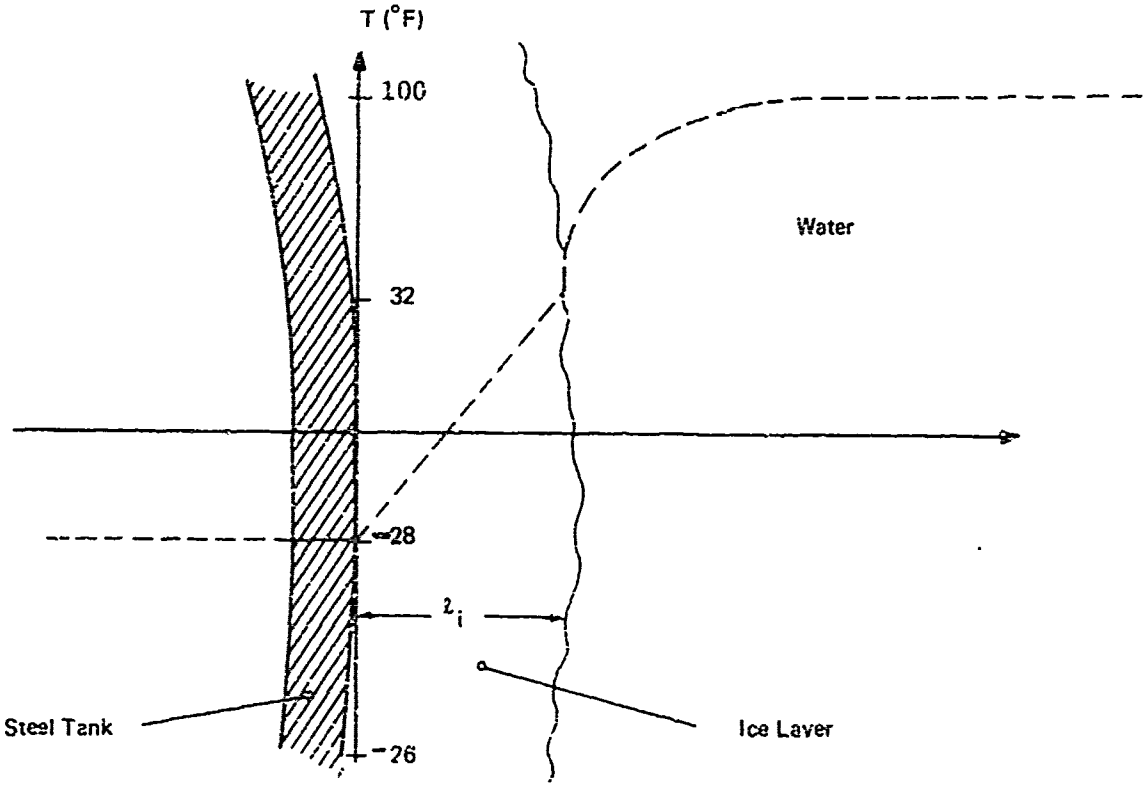

FIGURE 8–12 SCHEMATIC DIAGRAM OF THE ICE FORMATION ON THE OUTER WALL OF THE SUNKEN LNH_3 TANK

6.4.3.5 Governing Equations

In obtaining a pressure profile in time for the contents of the tank, we need to solve simultaneously for the time dependence of the vapor volume fraction, β, as well as the ice layer thickness, ℓ_i. In general, then, the solution reduces to that of a set of three simultaneous, first-order differential equations of the form:

$$\dot{P} = \frac{\partial P}{\partial t} = f_i (P, \beta, l_i, P, T, v_v, v_f, h_v, \ldots t) \tag{6-40}$$

$$\dot{\beta} = \frac{\partial \beta}{\partial t} = f_2 (P, \beta, l_i, \beta, T, v_v, v_f, h_v, \ldots t) \tag{6-41}$$

$$\frac{\partial l_i}{\partial t} = f_3 (P, \beta, l_i, T, v_v, v_f, h_v, \ldots t) \tag{6-42}$$

where each time derivative is a function of values of all three variables (but not their time derivatives), plus the thermodynamic properties of ammonia at saturation. The thermodynamic properties may be correlated as functions only of the saturation pressure, P, with the result that each time derivative is a function of only the three dependent variables and of time. This system of equations is readily amenable to solution on a digital computer using one of many numerical techniques. The following section describes the particular computer program chosen.

6.4.4 Solution to the Governing Equations

The governing equations that describe the pressure behavior within the tank as a function of time involve the thermodynamic properties of anhydrous ammonia. These physical properties were obtained from reference (19) and are listed in Appendix A. Unfortunately, tabular data is not readily amenable to use in a numerical solution of the governing equations in the preceding section; rather, an analytical correlation is far more useful, particularly when calculating derivatives of properties along the saturation curve.

In deference to computational ease, the temperature, specific volumes of the vapor and liquid, and specific enthalpies of the vapor and liquid

were correlated by curve-fitting the property value in a series of Chebyshev polynomials in saturation pressure. This technique is a standard one and yields smooth approximations of the functional dependence of the property with respect to saturation pressure. F[illegible]ty was fitted to the 5th degree in the Chebyshev polynomials [illegible]actory reproduction of the property value as well as p[illegible]ation of smooth derivatives through the range of pressure (7.67 to 128.8 psia) over which the correlation is valid. Accuracy of the computer calculated property values was checked. Smoothness of the derivative was assured, because the calculated first derivatives with respect to pressure are monotonic, with the second derivatives (curvature) unchanging in sign over the range of pressure for which the correlation is applicable. SUBROUTINE APROP contains the coefficients yielded by the curve fitting, and serves to calculate property values and first derivatives for a given value of the absolute pressure.

The system of three simultaneous first-order differential equations from Section 6.4.3.5 which describe the transient characteristics of a submerged liquid ammonia tank, were solved via a computer program invoking one of the standard predictor-corrector techniques for numerical integration of such a system. The program involves a short main program and four subroutines, in addition to SUBROUTINE APROP. The program is extremely flexible in that it has the capability to vary the (time) step size during the integration to keep the numerical errors within specified bounds. The program elements are:

SUBROUTINE APROP - Calculates property values and derivatives given a pressure input.

SUBROUTINE FUNCT - Evaluates time derivatives of vapor-volume fraction, pressure, and ice layer thickness at a particular time step, given the property values from APROP.

SUBROUTINE RUKU - Using a Runge-Kutta technique, RUKU performs a single-point integration of the three dependent variables, given derivatives from FUNCT.

SUBROUTINE MILNE - Using the Milne predictor-corrector method, MILNE integrates based on a three-point technique using derivatives at three points to find function values at a fourth.

SUBROUTINE DE - This subroutine is called from the MAIN program. Its basic function is error control during the integration. At the start of the integration, DE calls FUNCT (which calls APROP) for values of the derivatives of vapor volume fraction, pressure, and ice layer thickness at the origin. It then calls RUKU which performs a single-point Runge-Kutta integration of this derivative to obtain the pressure, etc. at the first, second, and third time steps. DE then calls MILNE for a calculation of the dependent variables at the fourth and all succeeding time steps, and checks the error in the predicted versus corrected values. Should this error exceed that maximum acceptable error specified in MAIN, DE will halve the step size, employ RUKU to get started again, and proceed. In the case where the error yielded by MILNE is sufficiently low (as specified in MAIN), DE will double the step size to speed up subsequent integration. Again, since the step size is changed, RUKU will need to be used to start the integration procedure again.

Figure 6-13 is a flow chart for the program that solves the governing equations.

6.4.5 Results and Discussion

The results of the numerical solutions to the various cases are discussed in this section. In all of the cases, it was assumed that the heat transfer from water to the tank was over the entire surface area of the tank (no insulation).

Figure 6-14 shows the pressure-time history for various initial ullage volumes. After the pressure in the tank reaches 10 psig, the relief valve opens. The important observation that can be made from the Figure is the duration of time (about 6-7 hours) it takes for the tank pressure to reach 10 psig. This is indeed an important result

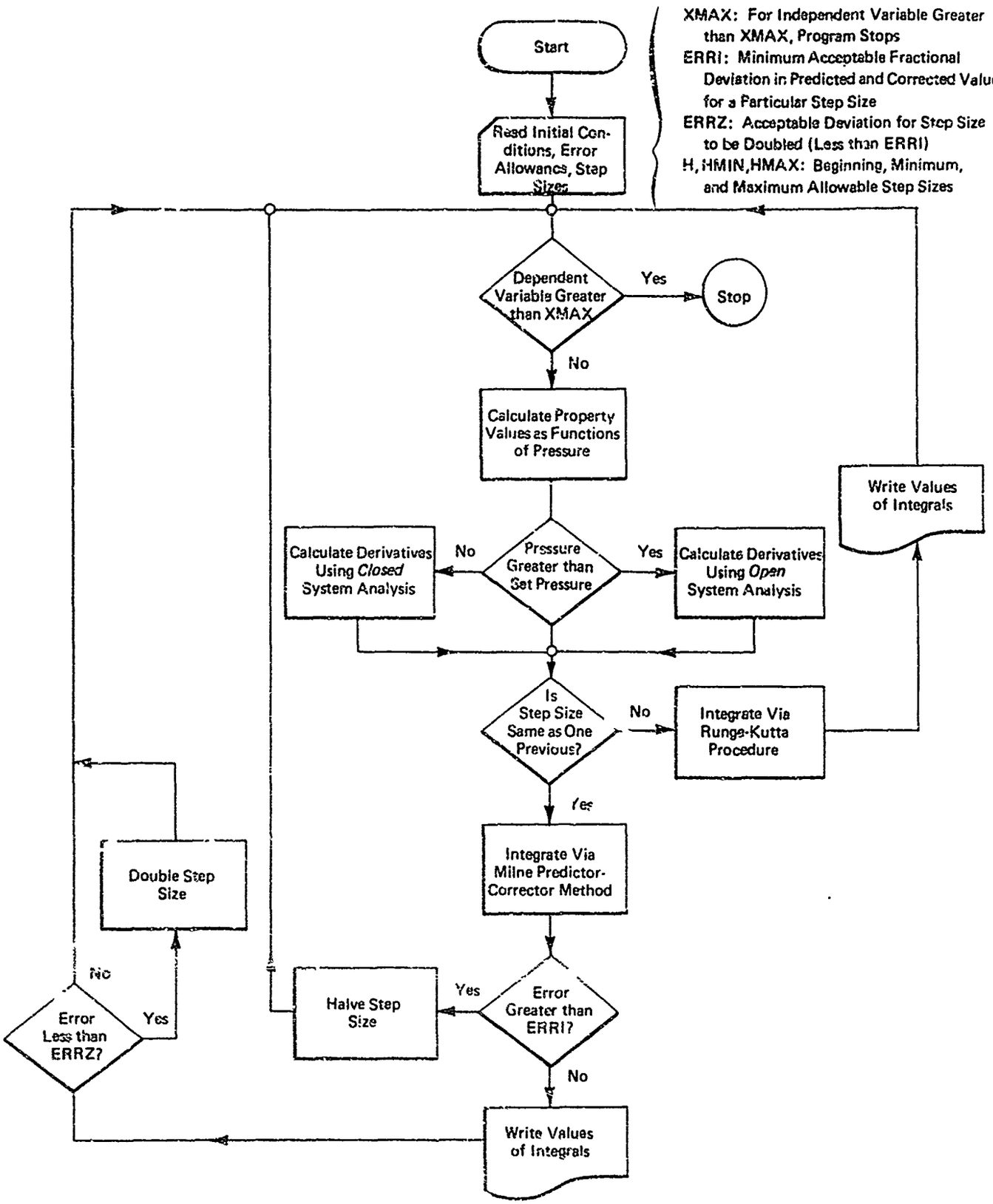

FIGURE 6–13 FLOW CHART FOR THE NUMERICAL SOLUTION OF THE EQUATIONS TO OBTAIN SUBMERGED TANK PRESSURE AS A FUNCTION OF TEMPERATURE

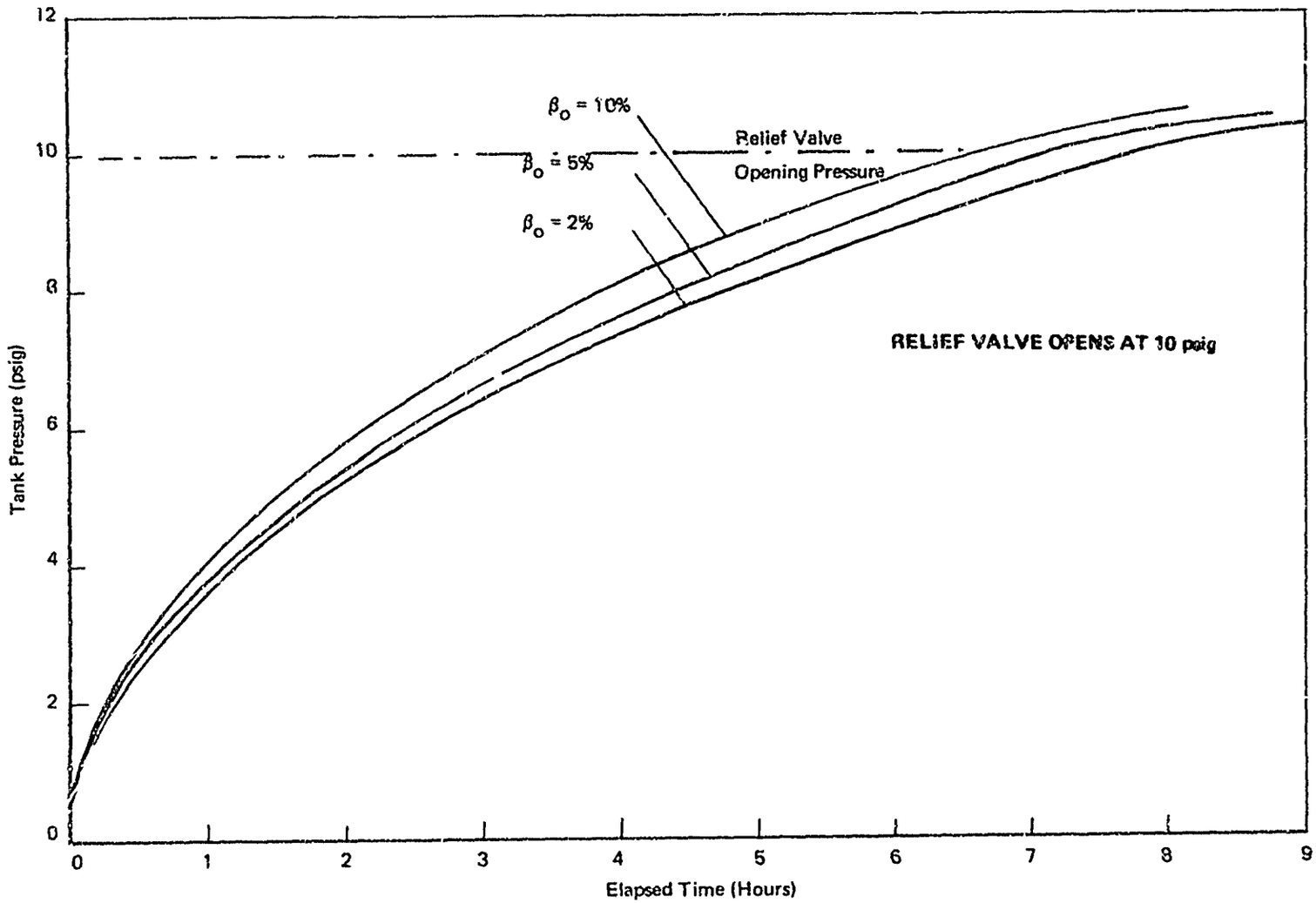

FIGURE 6–14 PRESSURE RISE IN TANK AFTER IMMERSION.

in that it allows considerable amount of time in which to take action following an accident and barge sinking. Also notice from the Figure that for larger ullage volumes the rate of pressure rise is higher. This is explained as due to the higher heat capacity of the liquid compared to that of the vapor. The larger the amount of liquid, the greater its ability to absorb heat, and the slower the rise in pressure.

The liquid expands due to heating and tends to occupy the ullage volume. Figure 6-15 shows the variation of the ullage volume with time for different initial vapor volumes. If the initial ullage volume is a very small fraction of the total volume, there occurs a time during the heating process when the liquid expands to completely fill the tank volume. This is shown clearly in Figure 6-15 for the case of 2% volume. However, in practice the vapor-phase volume is generally never less than 10%.

In the event the relief valve fails to open, the pressure-time history is as indicated in Figure 6-16a, assuming of course that the tank structure does not fail. One can see that after the pressure inside the tank reaches a value corresponding to which the saturation temperature is 32°F, the ice layer outside the tank completely disappears, resulting in a sudden increase in heat transfer. This has detrimental effects in that the pressure rise becomes extremely rapid and eventually the tank ruptures. The pressure rise in the post-ice-melt period is shown in Figure 6-16b. Observe the time scales involved before rupture.

6.4.6 Conclusions

A theoretical analysis of the consequences of the submergence of a 2500-ton ammonia barge has been made. The main result of the analysis is the tank pressure-time history. The analysis has been carried out for the worst possible case, that of the tank inverting after submerging with the relief valve at the bottom. Also assumed in the analysis was the total loss of the urethene insulation around the tank and the formation of an ice layer on the outside of the tank wall. The follow-

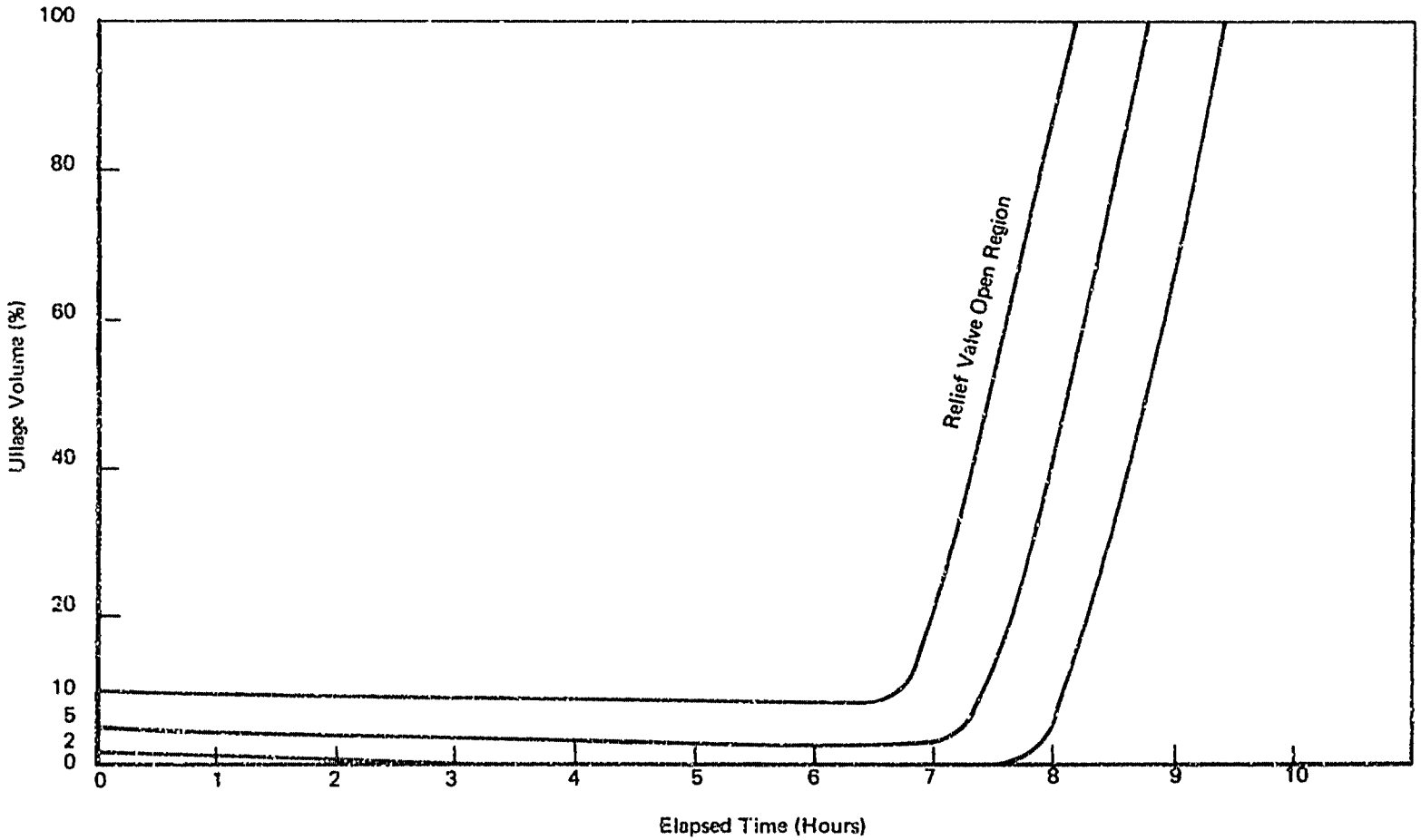

FIGURE 6–15 VARIATION IN ULLAGE–VOLUME AFTER TANK IMMERSION

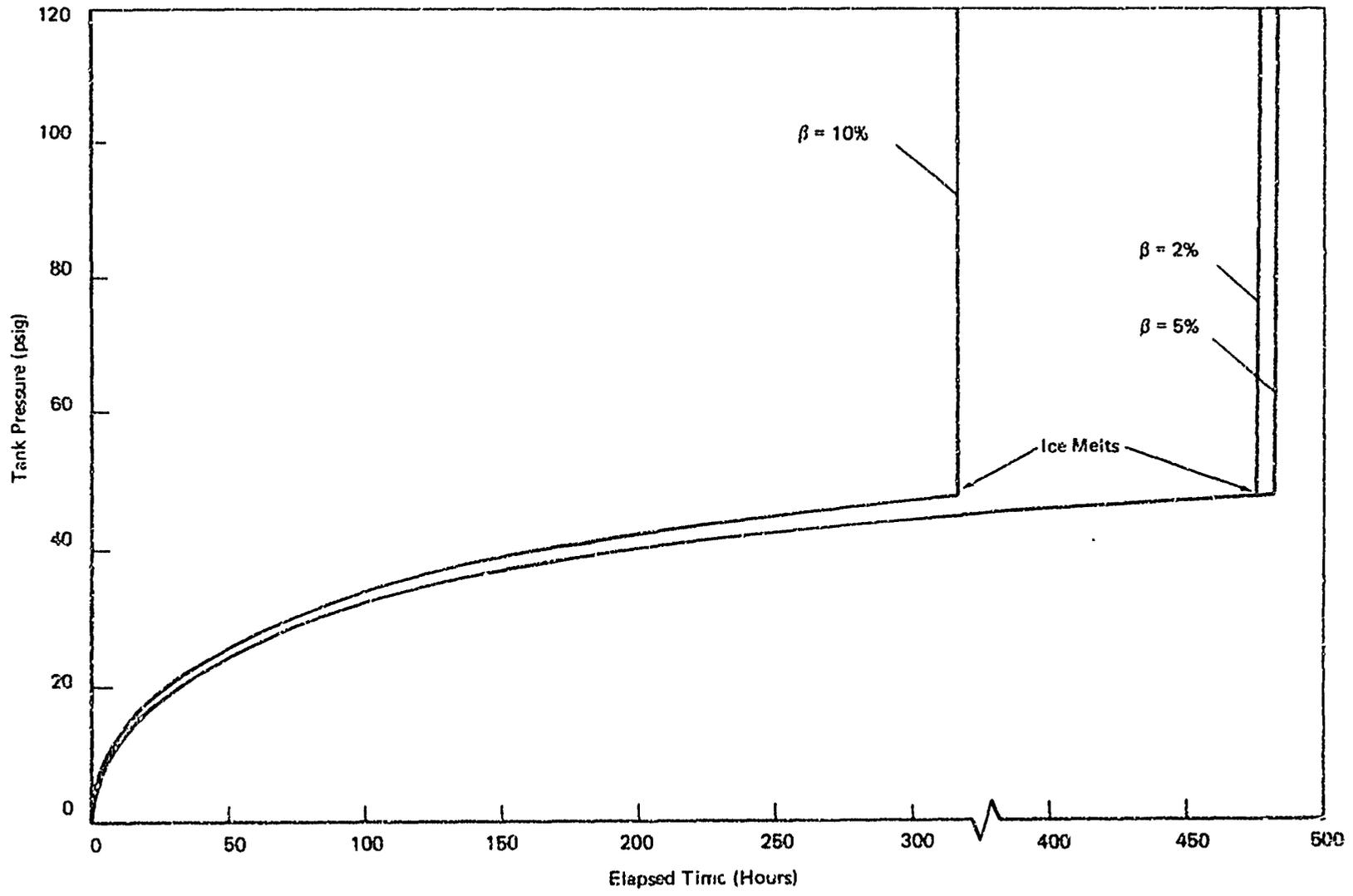

FIGURE 8–18a PRESSURE PROFILE IN TANK – RELIEF VALVE CLOSED – IN 100°F WATER

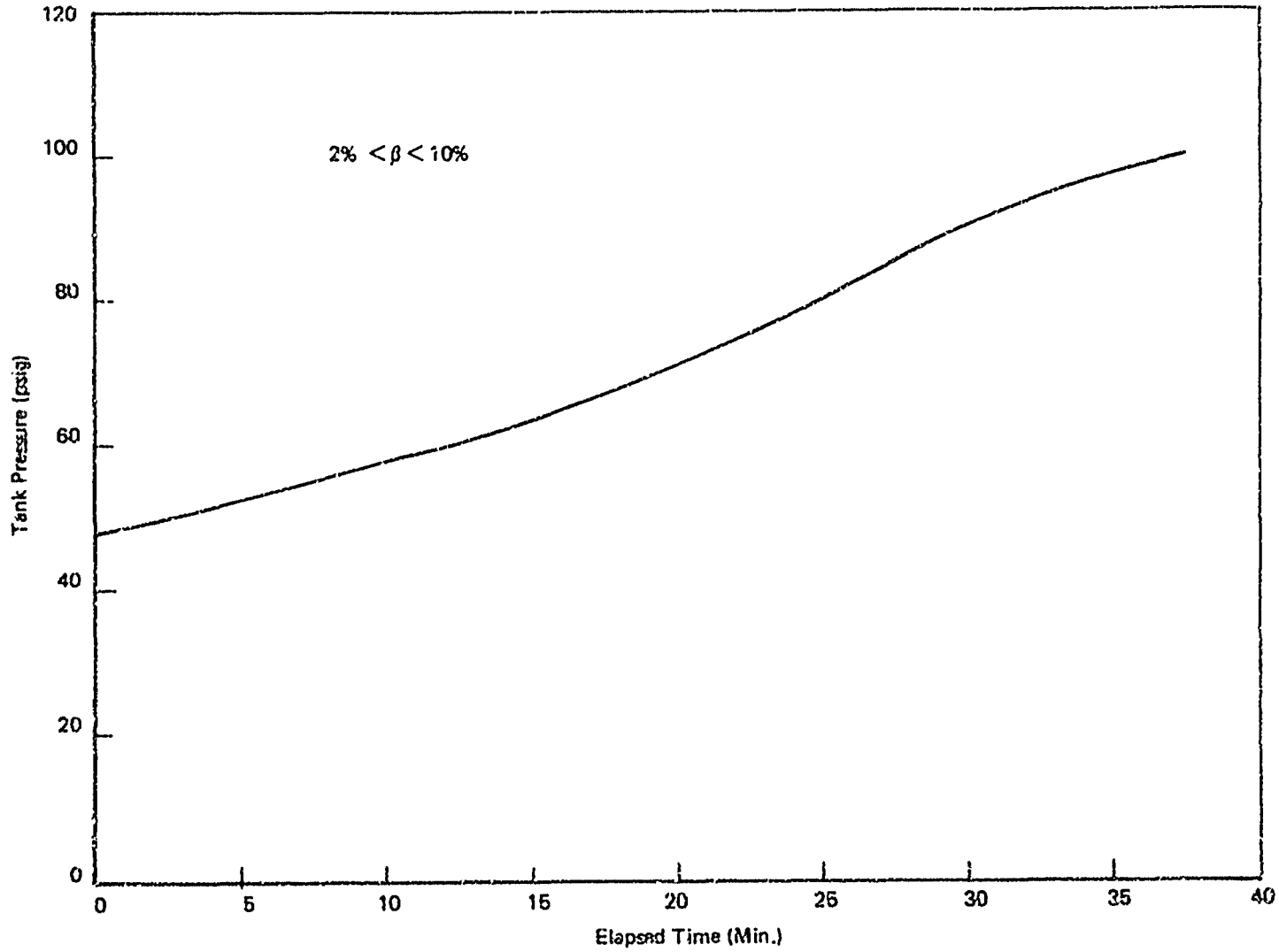

FIGURE 6–16b PRESSURE RISE AFTER ICE MELTS

ing conclusions can be drawn from the results:

- The pressure rise inside the tank, even when no venting is taking place in the initial stages, is very low.
- The relief valve opening pressure (10 psig) is reached only after 6 to 8 hours, depending on the initial ullage volume. The larger the initial ullage volume, the quicker the time in which this set pressure is reached. Even so, the time scale is of the order of several hours.
- If the relief valves open at the above pressure, the rate of pressure rise drops, eventually reaching zero, and even negative values. That is, the relief vents provided are sufficient to cope with the problem.
- If the relief valves are stuck and do not open at all, there results a time (after a long period) at which the pressure increases very rapidly and reaches values higher than the maximum allowable pressure (45 psig) for the tank, within a matter of minutes. This may lead to disasterous results. However, even in this case, there is sufficient lead time (of the order of 300 to 400 hours) within which remedial measures can be taken.

In short, the design of the tank is such that it can withstand several hours of submergence even without any insulation. However, a word of caution is expressed in relation to the above analysis. The whole analysis rests on the assumption that a uniform layer of ice forms on the outer wall of the tank. If for some reason the ice does not form and there is a large rate of heat to the tank, conditions will become worse much sooner.

6.5 VAPOR DISPERSION

6.5.1 Introduction

Saturated ammonia vapor is lighter than air and therefore rises rapidly when released into the atmosphere. While rising, the vapor is

also carried downwind by the prevailing wind. The latter phenomenon is dealt with in this section. The parameter of interest is the downwind ground level concentration of ammonia vapor.

Two models are given, one of which is applicable to the vapor dispersion in a small-scale spill. In this, the lateral dispersion caused by the air-vapor mixing at the plume edges is important and is taken into account. The second model is applicable to large-scale spills where the size of the cloud initially is so large that lateral dispersion can be neglected in comparison with vertical mixing. In both models, we assume that the concentrations within the vapor cloud can be represented by Gaussian profiles. Also used are the Pasquill-Gifford curves[6.8] for the description of the variances of these Gaussian curves. The effects of local topology, variations in wind velocity and direction during the cloud dispersion, meteorological condition variations, etc. are neglected. (The rise of ammonia vapor in air has been modeled and discussed in Section 5.)

6.5.2 Description of the Models

6.5.2.1 Continucus Spills (Model 1)

The concentration at any point downwind can be represented by

$$C(x,y,z,t) = \begin{cases} \dfrac{\dot{m}(t-\frac{x}{U})}{2\pi U \sigma_y \sigma_z} e^{-\frac{y^2}{2\sigma_y^2}} \left[\mathrm{Exp}\left\{-\dfrac{(z-h)^2}{2\sigma_z^2}\right\} + \mathrm{Exp}\left\{-\dfrac{(z+h)^2}{2\sigma_z^2}\right\} \right] & \text{for } x \leq Ut \\ 0 & \text{for } x > Ut \end{cases} \qquad (6\text{-}43)$$

where

$\dot{m}(t - \frac{x}{v})$ = mass rate of generation of ammonia vapor

U = mean wind velocity

h = height of the center of the plume above the ground (or water)

z = coordinate measured from the ground surface.

$\dot{m}$ can be obtained if we assume a constant boiling rate of LNH_3 on water and a linear increase in area of spread with time. (See Section 5.) z_o is determined from the plume theory (Section 6.7), while σ_y and σ_z are obtained from the Pasquill-Gifford curves shown in Figure 6-17a and Figure 6-17b.

In deriving the above equation, it has been assumed that the vapor is generated from a point source. Hence the equation is applicable at large distances compared to the diameter of the spill.

The concentration in equation (6-43) is expressed in density units. The relationship between vapor concentration and the concentration in density units (c) is expressed in mole fraction (χ) of the air vapor mixture.

$$\chi = \frac{1}{\left[1 + \frac{\rho_a}{c}\,\frac{\mu_v}{\mu_a}\right]} \tag{6-44}$$

where

μ_a = molecular weight of air ≡ 28.9 gm/mole

μ_v = molecular weight of vapor ≡ 17.0 gm/mole

The mass of vapor collected (M_v) by an impinger with a volume suction rate of air of q is given by

$$M_v = \frac{m_v}{\pi\sigma_y\sigma_z}\,\frac{q}{U}\,e^{-\frac{y^2}{2\sigma_y^2}}\left[e^{-\frac{(z-z_o)^2}{2\sigma_z^2}} + e^{-\frac{(z+z_o)^2}{2\sigma_z^2}}\right] \tag{6-45}$$

where

m_v = total mass of vapor liberated

and y,z = the cordinates of the impinger with respect to cloud center (z = 0 is on the ground, and y = 0 is at the cloud center)

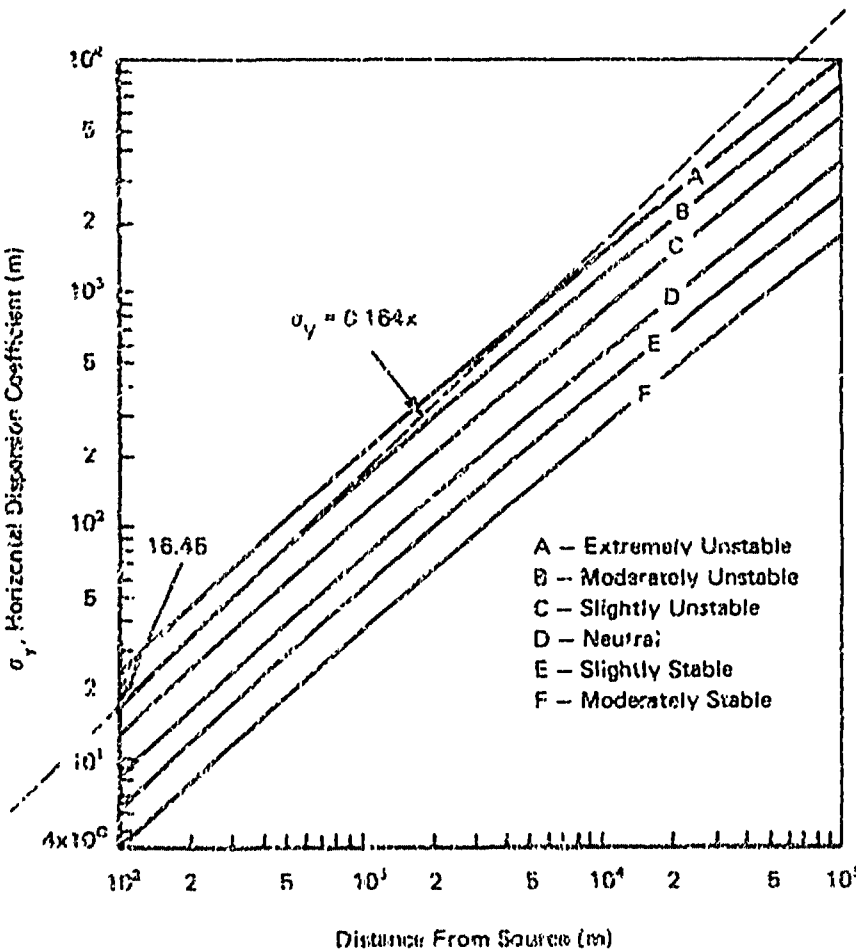

Figure 6–17a Lateral Diffusion, σ_y, Versus Downwind Distance from Source for Pasquill's Turbulence Types

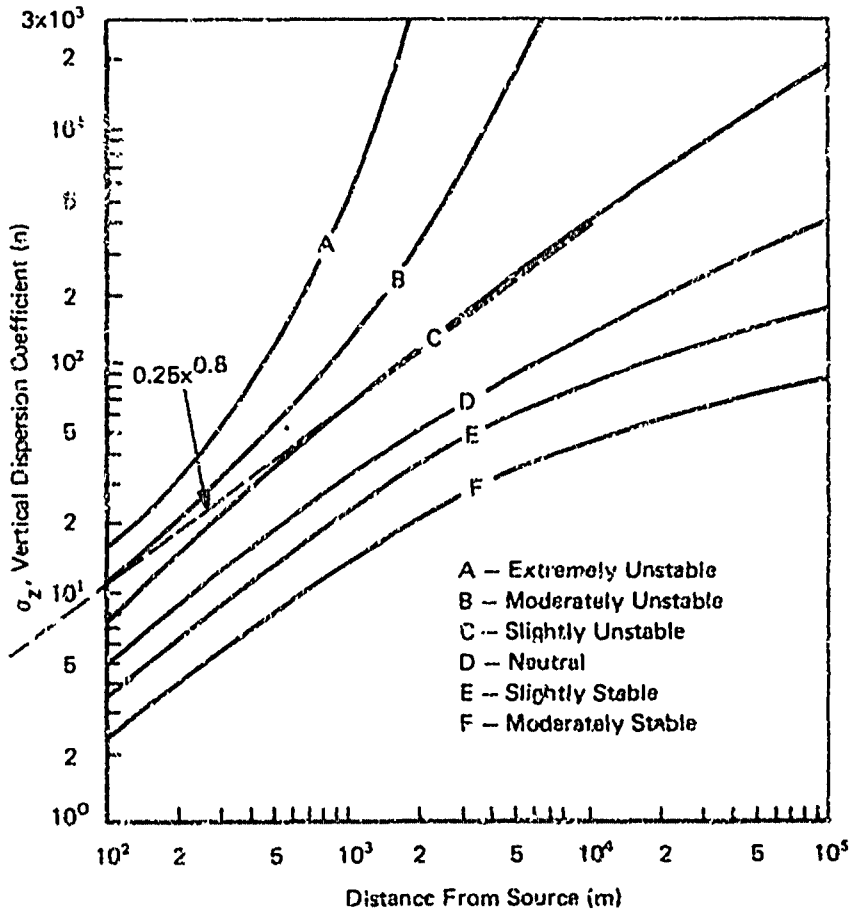

Figure 6–17b Vertical Diffusion, σ_z, Versus Downwind Distance from Source for Pasquill's Turbulence Types

FIGURE 6–17 PASQUILL-GIFFORD DISPERSION COEFFICIENT CURVES FOR VARIOUS ATMOSPHERE TYPES

6.5.2.2 Large Spills (Instantaneous Spills)

In large instantaneous spills, the vapor cloud formed is so massive that under ordinary wind conditions (less than, say, 10 mph) the mixing with ambient air is slow. Consequently, vapors from larger spills will rise to greater heights than the vapors from smaller spills, during the same time duration.

The dispersion of vapors from large spills depend to a great extent on the atmospheric condition. In neutral and unstable atmospheres, the vapor cloud rises continuously as it disperses downwind. In stable atmospheres ("inversion") the cloud center reaches a ceiling height and from then on disperses almost entirely in the horizontal directions only. This will occur because of the lack of atmospheric mixing process above this ceiling height. From the point of view of ground level concentrations of vapor, the worst condition during stable atmospheric conditions occur when there is fumigation[18] taking place (that is, when good mixing occurs between the ground level and the ceiling height, resulting in a uniform vertical distribution).

Because of the relatively short duration in which even massive (instantaneous) spills of LNH_3 evaporate and the comparatively long time it takes for the cloud to reach distances of the order of a kilometer or more (in low wind velocities), the spill can be assumed to generate all of the vapor instantaneously. To take this finiteness of the source size into consideration, it is assumed that the vapor is generated from a "virtual point source" located 5 pool diameters upwind. Therefore, in the formulae given below the dispersion parameters (σ's) have to be estimated from the location of this virtual point source.

The following formulae are used for the two types of atmospheric conditions:

(i) neutral and unstable atmospheres (See Figure 6-18)

$$c(x, y, z, t) = \frac{m_v}{(2\pi)^{3/2}\,\sigma_y^2\,\sigma_z}\left[\exp - \left(\frac{(x-ut)^2 + y^2}{2\sigma_y^2}\right)\right]\left[\exp - \frac{(z-h)^2}{2\sigma_z^2} + \exp - \frac{(z+h)^2}{2\sigma_z^2}\right] \qquad (6.46a)$$

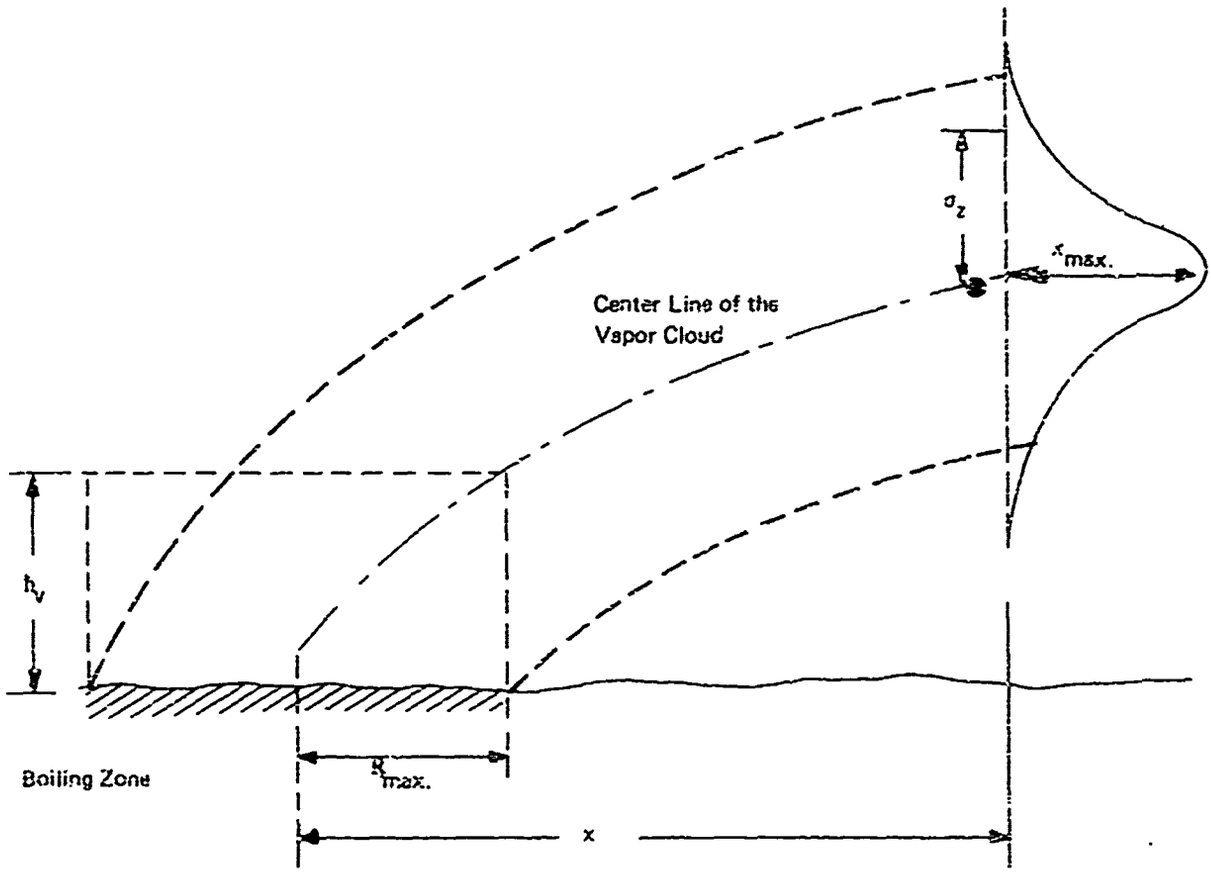

FIGURE 6–18 SCHEMATIC DIAGRAM SHOWING THE FEATURES OF THE VAPOR DISPERSION MODEL FOR LARGE SPILLS

i.e., maximum ground level concentration at any x is

$$c_{ground} = \frac{2m_v}{(2\pi)^{3/2}\sigma_y^2\sigma_z} e^{-\frac{h^2}{2\sigma_z^2}} \qquad (6\text{-}46b)$$

where

h = the height of the center line of the plume at downwind distance x, calculated by the method discussed in section 6.7.2.1

m_v = mass of vapor liberated in the spill

(ii) Stable Atmosphere

There are several types of stable atmospheres. An excellent review of the different types and their consequences on atmospheric dispersion of pollutants is given in reference 18. The different types arise because of the variety of mixing process that takes place in the atmosphere depending on the time of day, solar insolation, location of the area of concern (over water or land) etc. To calculate the ground level ammonia vapor concentrations in stable atmospheres, it is necessary to know the exact type of stability. In the discussions below two extreme types of stable atmospheres are treated and methods for estimating the ground level concentrations are given.

a) Stable: Fanning

In this type of stable atmosphere the temperature in the atmosphere increases continuously from the ground up. The ammonia vapor released from a spill rises to a certain height and then spreads horizontally, with virtually no vertical dispersion. The ground level vapor concentration in such a case is very small. This concentration is estimated by using the same equation 6-46b, after substituting the ceiling height h_c (calculated from equation 6-61) for the parameter h. The values of σ_y and σ_z correspond to those in stable atmospheres.

b) Stable: Fumigation

In this type of stable atmosphere there is good mixing between the ground and a certain height (ceiling height). Above this height the atmosphere is inverted. Because of this mixing process below the ceiling height the pollutants tend to disperse and increase the ground level concentrations. In the case of ammonia vapor liberated from a ground level spill, the vapor rises till it reaches the ceiling height. Later on the dispersion is primarily in the horizontal direction with the vertical concentration distribution being practically uniform from the ground to the ceiling height. From the point of view ground level NH_3 vapor concentrations, this situation is by far the worst condition. Given below is an equation to estimate this ground level concentration.

$$c_{ground}^{max} = \frac{m_v}{2\pi \sigma_y^2 h} \qquad (6\text{-}47)$$

where

h = ceiling height

σ_y = horizontal dispersion parameter for unstable condition (generally atmosphere C is used)

It is to be noted that the above ceiling height is an atmospheric parameter and has to be known before ground concentration can be evaluated. The maximum duration for which the ground concentration level persists above any tolerable concentration C*, is given by:

$$t = \frac{2\sqrt{2}\,\sigma_y}{U} \sqrt{\ell n \frac{c_{ground}^{max}}{c^*}} \qquad (6\text{-}48)$$

Specific example are worked out in Appendix C to illustrate the value of ground level concentrations obtained for a 3000 ton ammonia spill, during different kinds of atmospheric conditions.

6.5.3 Discussion

The dispersion models presented are often used for predicting the concentrations downwind from a vapor source. However, most previous applications have been to describe the dispersion of gases that are either neutrally buoyant or are heavier than air. In the sections just presented, we have attempted to describe the dispersion of ammonia vapor - a lighter-than-air gas - by using the same formulae, but including the vertical rise of the vapor. The procedure essentially retains the same turbulent mixing characteristics of the atmosphere while allowing for the buoyancy driven rise of the vapor cloud. The method of calculation of the latter has been presented in Section 5.4.3.

Two models of vapor dispersion were presented: a model that should be used to describe the dispersion of vapor from a continuous spill, and a model for instantaneous (large) spills. The model to be used in a particular situation depends on not only the nature of the spill but also the relative times of concentration observation and evaporation of spill. The finiteness of the source area is accounted for by assuming the vapor to be released from a point source located five pool diameters upwind from the spill point. This origin shift does not significantly affect the estimation of safe distances for toxic concentration levels, as these distances are expected to be large compared to the maximum pool size. However, if the concentrations are very close (within one or two diameters) to the spill desired, more appropriate area source models have to be used. One of these methods is described in reference 17.

Two extreme examples of stable atmospheres have been discussed. The need to distinguish amongst the various classes of stable atmospheres arises due to the buoyant nature of ammonia vapor. It is because of this phenomenon together with the variability of stable atmospheres that a single equation can not adequately describe the ground level concentrations. As a consequence of the low vertical mixing during fanning stability the ground concentrations will be extremely small. However, the concentration predicted by equation 6-47 for the fumigation case are high and should be construed as being extremely conservative.

In most realistic situations, the ground level concentrations are expected to be lower (perhaps by as much as an order of magnitude) than that predicted. This should be so because, in nature, the vertical concentration distribution is rarely uniform and is more likely to be peaked at the ceiling height. Also, there will be some, though not much, dispersion into regions above the ceiling height. Together, these two phenomena will contribute to lessen the ground level concentration predicted by the fumigation theory.

It is to be noted here that no test was conducted during the present program in a stable atmosphere and consequently the predictions by the above equations could not be tested against experiemntal data from the present series.

6.6 WATER DISPERSION

6.6.1 Introduction

When liquid ammonia is spilled on water, a considerable portion of the spilled quantity goes into solution with water, forming ammonium hydroxide (NH_4OH). This NH_4OH formed is hot and lighter than water. Therefore, it tends to spread out on the water surface (a spread velocity of about 0.22 ft/sec was observed in the laboratory-scale spill tests). However, NH_4OH is readily miscible with water and thus any mixing or stirring of the two liquids result in a diluted ammonium hydroxide solution. If the ammonia spill occurs in a river or an estuary, the flow-created stream-turbulence or the wave action is sufficient to rapidly mix the ammonium hydroxide with water and dilute it.

The phenomenon of mixing is generally described theoretically by the classical diffusion equations with one or more diffusion coefficients. A comprehensive survey of literature and the derivations of the equations from first principles are described in references (21) and (22). Several investigators (Fisher[23], Holley and Harleman[24], Thatcher and Harleman[21]) have correlated, from experimental data, the dispersion and turbulent diffusion coefficients for dispersion in rivers, estuaries and other regions. The dispersion equations derived are strictly correct for neutrally buoyant, conservative (or at best first order decay) substances. Though concentrated ammonium hydroxide

is lighter than water, the density of water containing low concentrations of it will be very close to that of pure water. Also, even though some vapor is generated during the dilution of NH_4OH, the quantity of vapor produced is so small as to make the dilution process a mass conserved one.

The equations presented below predict the concentration of the NH_4OH solution. The spill is assumed to be instantaneous. The two regions of water considered are a non-tidal river and a tidal river.

6.6.2 Description of the Models

6.6.2.1 Dispersion in a Non-Tidal River

When LNH_3 dissolves in water and spreads radially, the NH_4OH formed has a concentration gradient in the vertical direction. Figure 6-19 shows the distribution of NH_4OH solution concentration at the instant the LNH_3 spread is a maximum. Dye distribution observed in the laboratory experiments indicates that a high concentration of NH_4OH is at the water surface, decreasing to a very low value within a few inches depth (three to four inches). The water dispersion models all assume an initial uniform concentration (in fact, infinite concentration for instantaneous spill) condition. For such a hypothetical, uniform concentration region, we define

$$h = \frac{m_\ell}{\rho_\ell \pi R_{max}^2} \qquad (6\text{-}49)$$

where

m_ℓ = mass of LNH_3 that dissolves in water

ρ_ℓ = LNH_3 density (0.628 gms/cm^3)

R_{max} = maximum radius of spread of LNH_3

h = thickness of a hypothetical, 100% concentrated radius-of-spread equal to R_{max}

In general, the value of h is very small (1.3 inch for a 3000-ton spill with 50% partition) compared to the depth of rivers. Hence

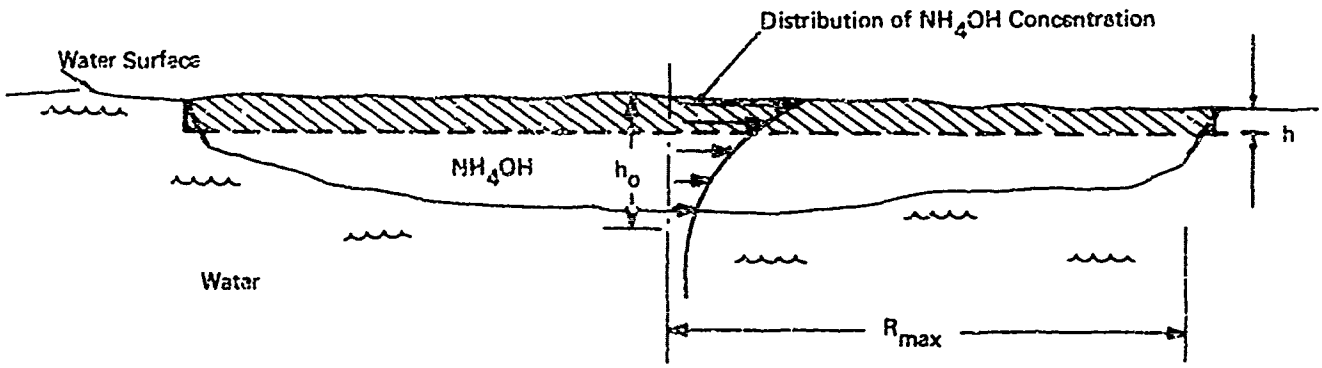

FIGURE 6–19 SPREADING POOL OF NH_4OH SOLUTION AT THE INSTANT THE LNH_3 SPREAD IS A MAXIMUM

the source can be essentially treated as an instantaneous area source. Two models are discussed below.

The dispersion of NH_4OH can be visualized as follows. During the initial stages, the spill pool of NH_4OH is moving downstream at about the same velocity as the surface velocity of the river. During this period the NH_4OH is getting diluted by dispersion, essentially in the vertical direction only. (The lateral and longitudinal dispersions can be neglected if the spill diameter is of the same order as the width of the river.) After some time, the vertical distribution of NH_4OH concentration becomes essentially uniform. Beyond this stage the dispersion is essentially longitudinal. Given below are two models to describe the above two different regions of dispersion. In the first case -- called the near field analysis -- the finite area of the source is accounted for. In the second case -- called the farfield analysis -- the concentration is assumed to be uniform throughout the cross section of the river and dispersion to be predominently longitudinal.

(i) Near Field Analysis:

In the near field analysis we first propose a model in which the area source is taken into account together with the dispersion in all three directions. This model is amenable to solution only on a computer. Subsequently, we give a simplified version of this model in which the longitudinal and transverse dispersions of NH_4OH are neglected.

General Model: The concentration at any point within the river at time t after the spill is given by

$$c(x,y,z,t) = \frac{2\,m''}{(4\pi t)^{3/2}\sqrt{e_x e_y e_z}} \int_{x_o=-R_{max}}^{R_{max}} dx_o \int_{y_o=-R_{max}}^{R_{max}} dy_o \left\{ e^{-\frac{(x-Ut-x_o)^2}{4e_x t}} \right.$$

$$\left[e^{-\frac{(y-y_o)^2}{4e_y t}} + e^{-\frac{(y-y_o-w)^2}{4e_y t}} + e^{-\frac{(y-y_o+w)^2}{4e_y t}} \right]$$

$$\left. \left[e^{-\frac{z^2}{4e_z t}} + e^{-\frac{(z-2d)^2}{4e_z t}} \right] \right\} \qquad (6\text{-}50)$$

where

m'' = mass of NH_4OH per unit area of spill = $\frac{m_\ell}{\pi R^2_{max}}$

d = depth of the river

w = width of the river

y_o = location of the centre of spill from the mid stream

$e_x e_y e_z$ = turbulent diffusion coefficients respectively in x, y & z (i.e., longitudinal, lateral and depthwise) directions.

The turbulent diffusion coefficients e_x, e_y, and e_z are obtained from the characteristics of the river. Harleman suggests the use of the coefficients given in Table 6-3. The concentration given in equation (6-50) is in density units.

Table 6-3

Turbulent Diffusion Coefficients in a River †

Diffusion Coefficients	Very wide rivers (w/d > 100)	For narrow rivers (w/d < 100)	Remarks
e_z	$0.067\ u^* d$	$0.067\ u^* R_h$	The e_z value is the mean of the vertical distribution given by $e = u^* z(1-z/d)$
e_x	$0.1\ e_z$	$0.1\ e_z$	
e_y	$0.1\ e_z$	$0.23\ u^* R_h$	

where

u^* = shear velocity = $3.3\ n\ U\ R_h^{-1/6}$

R_h = hydraulic radius = $\frac{\text{stream crossectional area}}{\text{wetted perimeter}}$

n = manning factor $0.01 < n < 0.04$

U_f = mean stream velocity

† all quantities are in F.P.S. units

Simplified Model: Neglecting the longitudinal and lateral dispersion and assuming no edge effects and using equation 6-49, equation 6-50 can be simplified to the following equations.

With

$$t_1 = (x - R_{max}) / U$$

$$t_2 = (x + R_{max}) / U$$

U = mean stream velocity

and for $t_1 \leq t \leq t_2$

$$c_{water\ surface} = \begin{cases} \dfrac{h \rho_\ell}{\sqrt{\pi e_z t}} & \text{if } \sqrt{\pi e_z t} < d/2 \quad (6\text{-}51) \\ \rho_\ell \left[h/d + \dfrac{2}{\pi} \sum_{n=1}^{\infty} \sin\left(n\pi \dfrac{h}{d}\right) \dfrac{e^{-n^2 \pi^2 \left(\frac{e_z t}{d^2}\right)}}{n} \right] & \quad (6\text{-}52) \end{cases}$$

and $c = o$ for $t < t_1$ or $t < t_2$

At any point x downstream this concentration would last for a time of about $2R_{max}/U$. It should be noted that the minimum concentration predicted by this above equation is equal to h/d. However, in the river the concentration goes below this value due to the longitudinal dispersion. This is discussed below.

(ii) Far Field Analysis

In order to calculate the far field concentration value the following equation can be used. Far field analysis results can be used when in equation 6-52 the term involving the summation of the expontially decaying sine series is very small compared to h/d.

$$c = \frac{m_{\ell}}{2wd\sqrt{\pi E t}} \qquad (6\text{-}53)$$

where

c = NH_4OH concentration (maximum)

ℓ = $77\ n\ U\ R_h^{5/6}$ = longitudinal dispersion coefficient

t = time from the instant of spill

and other quantities are defined in Table 6-3.

6.6.2.2 Dispersion in a Tidal River

When ammonia spills occur at the mouth of a harbor or in the esturine regions, one must consider the tidal character of the waterway in dispersing the ammonium hydroxide formed.

For a constant cross-sectional area region with a sinusoidal variation in the tidal velocity, superimposed on a stream velocity, the following equation can be used to predict the concentration downstream.

$$C(x,t) = \frac{M}{A\sqrt{4\pi E t}}\ e^{-\left\{\frac{(x-U_f t)+\frac{U_T}{\sigma}[\cos\sigma(t-\delta)-\cos(\sigma\delta)]}{\sqrt{4Et}}\right\}^2} \qquad (6\text{-}54)$$

where

M = total mass of NH_4OH that is dispersing

U_f = constant stream velocity

U_T = amplitude of sinusoidal wave velocity

δ = phase lag between spill time and high water slack time

σ = frequency of oscillations

E = longitudinal dispersion coefficient

A = cross-sectional area of the channel

The concentration given by equation (6-54) is the cross-sectional area mean value. Local concentrations can be obtained by a much more complicated formulation of the dispersion problem. Also, the mass of NH_4OH generated is assumed to be uniformly distributed across the cross-sectional area of the stream at the initial time. Because of these assumptions, equation (6-54) can be used to predict the concentration far downstream from the spill position. The longitudinal dispersion coefficient, E, is an empirically determined parameter that depends on the flow characteristics of the river. In general, it can be determined from the following formula:

$$E = 6u^*d \qquad (6\text{-}55)$$

6.6.3 Discussion

The character of navigable waterways varies so much from place to place that no one general water-dispersion model can be applied to all places. We have presented three models; two for non-tidal rivers, and the other for tidal regions. In all the models, we have assumed that the primary mixing agency is stream turbulence. The equations can be used to predict the temporal averages of ammonium hydroxide concentration in a stream for instantaneous spills. Different equations must be used for continuous spills, and many such equations have been published elsewhere (reference [17]). The values of the turbulent coefficients, or the longitudinal-dispersion coefficient, are based on the empirical correlations which seem to correlate several experimental results, both in the laboratory and in the field [25].

The models presented have, in some cases, taken into account the finite area on the water surface from which NH_4OH spreads and mixes In spite of the initial lower density of NH_4OH solution (hence its tendency to stay on the water surface), because of its extreme miscibility and the mixing process in the stream, the concentration of NH_4OH is rapidly decreased by dispersion in all directions. The dilution process results in the liberation of ammonia vapor. However, the quantity of vapor is small and dilution of concentration less than 50% NH_4OH does not release ammonia vapor. Therefore, we have assumed that the process of dilution takes place with the total mass of ammonium hydroxide as a constant.

It is pointed out here that during the present series of experiments ammonium hydroxide concentrations were not measured. Consequantly, the results of the models suggested cannot be compared to any experimental data. However, these models have been well established in the literature and have been verified against experimental data.

6.7 VAPOR CLOUD RISE

6.7.1 Introduction

When liquid ammonia spills on water, rapid boiling ensues, resulting in the liberation of a cloud of NH_3 vapor. The cloud is lighter than air and rapidly rises into the atmosphere, while at the same time drifting horizontally on the prevailing wind. Vapor liberation can be continuous, as in a continuous spill, or more or less in a puff, in the case of an instantaneous spill. The two models given below describe the motion of a maintained plume and that of a puff of vapor.

The plume rise model was developed by Slawson and Csanady[26] refined recently by Hoult et al.[27]. The theory was developed primarily to describe the behavior of chimney plumes. The puff model is due to Morton et al.[28], and describes the motion of a suddenly released cloud of buoyant gas. In both the theories, the motion of a uniform density vapor in a stably stratified atmosphere is considered.

6.7.2 Vapor Cloud Motion Models

6.7.2.1 Plume Theory

A continuous stream of buoyant gas released from a maintained source rises into the atmosphere. The gas mixes with atmospheric air and is diluted, resulting in a continuous decrease of buoyancy. In the initial stages, the plume is carried vertically by the momentum of exit gases. During the second stage, buoyancy forces dominate the plume rise.

If the atmosphere were of constant density, theoretically the plume would keep on rising. However, at a certain height in a stably stratified atmosphere, the plume, which is being constantly diluted due to turbulent mixing with air, attains a mean density that is equal to the outside air density. Above this height, the plume rise is retarded by a negative buoyancy, but it continues to rise because of upward momentum. However, after the plume has risen a small distance, upward velocity drops to zero and the plume falls down, finally reaching an equilibrium height. During vertical motion, the plume is being dispersed horizontally by the wind.

The following equations describe plume motion. In deriving them, Slawson et al.[26] and Hoult et al.[27] assumed that the rate of turbulent entrainment of the ambient air was proportional to the vertical velocity of the plume. Also, the plume was assumed to be circular in cross section and have uniform density and velocity.

The following nomenclature describes the definitions of the various symbols used in the equations.

b = radius of the continuous plume at any position

b_i = radius of plume at the place of generation

B_i = initial buoyancy volume released in the puff = $Vg\Delta$

c = fraction of actual size for evaluating the position of the virtual source ($0.005 < c < 0.01$)

d = distance along the plume beyond which the initial momentum has no effect on the plume size

F_p = buoyancy flux in the continuous plume = $b_i^2 u_i g\Delta = \frac{Vg\Delta}{\pi t}$

g = acceleration due to gravity

ℓ = buoyancy length (used with a subscript)

ℓ_c = buoyancy length in the case of cloud rise = $\frac{\sqrt{B_i}}{U}$

ℓ_p = buoyancy length in the plume rise = F_p/U^3

R = radius of the sperical cloud at any position

S = stratification parameter = $\frac{U}{\ell\omega}$

t = duration over which a volume V of vapor is released

T = absolute temperature of the ambient air

u_i = initial vertical velocity of vapor at release

U = mean wind velocity

V = volume of vapor initially generated

x = downwind distance

x^* = downwind distance where the cloud becomes neutrally buoyant

z = vertical coordinate

z = maximum height reached by the vapor cloud (or plume)

α = empirical parameter in equation (6-62) (generally - 0.093)

β = empirical parameter occuring in equation (6-56) ($0.5 < \beta < 2.0$)

Δ = fractional density defect = $\left(1 - \frac{\rho_v}{\rho_a}\right)$

$\frac{\partial\theta}{\partial z}$ = abaolute value of the potential temperature gradient in the atmosphere

$\varkappa$ = parameter in equation (6-62)

ρ_a = density of ambient air at the position of vapor release

ρ_v = density of vapor at release

ω = Brunt Vaisalla frequency = $\sqrt{\frac{g}{T}\frac{\partial\theta}{\partial z}}$

The Plume trajectory (in a constant density region of the atmosphere) can be written as

$$\frac{z}{\ell_p} = \left(\frac{3}{2\beta^2}\right)^{1/3} \left(\frac{x}{\ell_p}\right)^{2/3} \tag{6-56}$$

$$\text{or} \quad z = (1.5/\beta^2)^{1/3} \; x^{2/3} \; F_p^{\frac{1}{3}} \; U^{-1} \tag{6-57}$$

where β is an empirical parameter found to be in the range $0.5 \leq \beta \leq 2$. (Fay [29] suggests the use of $\beta = 1$, based on the analysis of a large volume of chimney plume data.)

Physically, the buoyancy length, ℓ_p, indicates the minimum distance along the plume, measured from the exit, at which the entrained fluid, rather than the ejected fluid, is balancing the buoyant impulse of the exit gases. The distance, d, along the plume up to which initial gas momentum dominates the plume rise is given by [29],

$$\frac{d}{\ell_p} = \left[\frac{U^2}{b_i g \Delta}\right]^2 \tag{6-58}$$

Equation (6-56) was derived assuming that the radius of the "chimney" at the exit of the gases is small. Essentially, the source was assumed to be a point. However, if the vapor source is an area source (as in the case of LNH_3 spill on water) the equation can be easily modified to account for the release from a virtual source. The height above the ground of the center line of the plume can be represented by the equation for the virtual source by

$$\frac{z}{\ell_p} = -\frac{\bar{z}}{\ell_p} + \left(\frac{3}{2\beta^2}\right)^{1/3}\left(\frac{x}{\ell_p}\right)^{2/3}\left(1 + \frac{\bar{x}}{x}\right)^{2/3} \tag{6-59}$$

where

$$\left.\begin{aligned} \bar{x} &= \sqrt{\frac{2(b_i c)^3}{3\beta U}} \\ \text{and } \bar{z} &= c b_i/\beta \end{aligned}\right\} \tag{6-60}$$

c = effective radius fraction, for the finiteness of the source ($.005 < c < .01$).

When the atmosphere is stably stratified, the limiting height reached by the plume is given by

$$\frac{z_\infty}{\ell_p} = S^{2/3} \tag{6-61}$$

where S is the stratification parameter related to the potential temperature gradient in the atmosphere.

Equation (6-56) describes the trajectory of the plume center fairly close to the source, while equation (6-61) describes the maximum height reached by the plume.

6.7.2.2 Puff Theory

When a puff of buoyant gas is released into the atmosphere, it behaves very much like a buoyant gas plume. However, in the case of a gas cloud, mixing with ambient air takes place over the entire surface area of the cloud. This leads to much more rapid mixing that that in a continuous gas stream.

Morton et al. [28] have derived the following equations to describe the behavior of a buoyant cloud in the atmosphere. The cloud shape is assumed to be spherical, and the initial momentum and size of the cloud at release are ignored. The cloud trajectory, in the constant density region of the atmosphere, is

$$\frac{z}{\ell_c} = \left[\frac{3}{2\pi(\alpha\kappa)^3}\right]^{1/4} \left(\frac{x}{\ell_c}\right)^{1/2} \tag{6-62}$$

or in dimensional form

$$z = \left[\frac{3}{2\pi\ (\alpha\kappa)^3}\right]^{1/4} x^{1/2} B_i^{1/4} U^{-1/2} \tag{6-63}$$

while the radius of the spherical cloud is

$$\frac{R}{\ell_c} = \left[\frac{3\alpha\kappa}{2\pi}\right]^{1/4} \left(\frac{x}{\ell_c}\right)^{1/2} \tag{6-64}$$

where the value of the parametric group $\alpha\kappa$ has been experimentally determined to be in the range of $0.27 < \alpha\kappa < 0.34$. Morton suggests the use of $\alpha = 0.093$.

For the rise of a cloud in a stably stratified atmosphere, the following formulae are used:

$$\frac{z_\infty}{\ell_c} = \left(\frac{3}{\pi}\right)^{\frac{1}{3}} \left[\frac{\kappa}{(\alpha\kappa)^3}\right]^{\frac{1}{4}} S^{\frac{1}{2}} \qquad (6\text{-}65)$$

and for the distance downwind at which the vapor cloud first reaches neutral buoyancy the expression is

$$\frac{x^*}{\ell_c} = \frac{\pi\sqrt{\kappa}}{2} S \qquad (6\text{-}66)$$

The vapor cloud reaches the equilibrium height given by equation (6-65) after several oscillations. For practical purposes, the steady-state height is a distance about five times the distance indicated in equation (6-66).

6.7.3 Discussion

The plume model is used to describe a continuous plume, and for this model the height of the center line of the plume decreases inversely with the wind velocity for a fixed observation position downwind. The results presented by this theory have been found to correlate all of the observed data for chimney plumes from power plants. The theory indicates that the maximum height reached depends on both the wind velocity and the temperature gradient.

The second puff model describes the ascent of a suddenly released buoyant vapor mass. The height of rise of the center of the cloud at a given downwind distance is proportional to the inverse square root of the wind velocity. However, the maximum height reached is independent of the wind velocity, and depends only on the initial buoyancy

volume and the potential temperature gradient in the atmosphere. It has been reported[18] that the result of equation (6-65) under predicts by 30% the actual peak height reached by clouds generated by atomic blasts. It has been argued by Morton et al.[28] that such an effect is due to the strong initial turbulent motion in the interior of a cloud whose surface is relatively smooth and because of this, there is very little mixing with ambient air. In effect, the cloud rises as a bubble rather than as a mixing mass. Similar observations have been made in the case of vapor liberated during quiescent conditions from the instantaneous spill of 50 gallons on LNH_3 on water.

6.8 UNDERWATER RELEASE OF LIQUID AMMONIA

6.8.1 Introduction

A liquid ammonia barge that sinks in water may eventually release ammonia underwater. Depending on the orientation of the tank, liquid ammonia or gaseous ammonia may be released. When the liquid is released, a plume of liquid ammonia rises towards the water surface and during this rise a considerable quantity of LNH_3 reacts with water. The primary concern of this section is to predict a "critical depth" deeper than the depth at which all of the liquid reacts with water before reaching the water surface if the liquid ammonia is released.

Trying to model in all its entirety the above process of rising ammonia plume which continuously reacts with water producing vapor (which itself may dissolve in water at a site far removed from the site of generation) is much too complicated. The fraction of the released liquid ammonia reaching the water surface might be a function of the release depth, release rate underwater currents, mixing rate between the water and the ammonia plume, turbulence level in the stream and the plume, effect of vapor bubbles on the mixing process, etc. The physical model presented below is based on the similarity between a liquid ammonia plume rising in water and a turbulent diffusion flame. The model is based on simple dimensional arguments and gives a method of calculating the "critical depth" to an order of magnitude only.

6.8.2 Details of the Model

6.8.2.1 Analogy with Turbulent Diffusion Flame

The physical processes associated with the ammonia plume bear striking resemblance to th iffusion flame. If one conceives of NH_3 as a fuel, H_2O as an oxidiz ., and NH_4OH as the combusion product, the similarity is apparent. Water diffuses into the LNH_3 plume forming a mixture of NH_4OH and NH_3. LNH_3 diffuses into the water forming a solution of NH_4OH and H_2O. The mixing process also involves a release of heat though the magnitude of heat release per mass of NH_3 is clearly much less than that associated with a combustion process.

The modeling procedure becomes especially convenient because of the analogy with flame. For the turbulent flame, it has long been known that the flame height is a function only of the burner diameter for a given fuel. The height is independent of volumetric flow rate[30].

If the flame height is considered as the length of the reaction zone, then by analogy the mixing height of the ammonia plume would be the height at which the ammonia would have achieved complete solution in the water. If the release depth were greater than this mixing height, one would expect no ammonia to escape into the atmosphere. In the following section an order of magnitude estimate calculation is given for calculating the mixing height.

6.8.2.2 Derivation of Mixing Height Relation

The dimensional arguments for estimating the height of turbulent mixing height start with the mass conservation equation:

$$U \frac{\partial c}{\partial z} = D \frac{\partial^2 c}{\partial y^2} \qquad (6\text{-}67)$$

where

c = some specie concentration

D = turbulent diffusion coefficient

U = velocity of flow in the axial direction of the discharge tube

z = axial co-ordinate

z = cross axial cooridinate

The solution of the above equation will result in the definition of a "boundary layer thickness of reaction zone" δ, which is of the following order of magnitude

$$\alpha \sim O \left(\frac{D z}{U} \right) \tag{6-68}$$

Assuming that the reaction zone dimension at the mixing height is of the same order of magnitude as the pipe diameter, we have

$$\delta \backsim O\,(d) \backsim O \left(\sqrt{\frac{D h}{U}} \right) \tag{6-69}$$

i.e.,
$$h \backsim O \left(\frac{U d^2}{D} \right) \tag{6-70}$$

In the case of turbulent jet from a pipe, the turbulent diffusivity varies as

$$D \backsim O\,(U d) \tag{6-71}$$

Substituting 6-71 in 6-70, we have

$$h \backsim O\,(d) \tag{6-72}$$

Of course, application of the turbulent flame concept requires that the flow from the pipe be turbulent. Calculations of the liquid ammonia Reynolds number at the exit of a two-inch diameter pipe for release from a 10 psig tank indicate the flow is quite turbulent. Therefore, we can write a relation for the plume mixing height "h" as

$$h = A d + B \tag{6-73}$$

where A and B are experimentally determined constants.

6.8.3 Discussion

The result derived in equation (6-72) indicates that the length of the LNH_3 plume, before it is completely converted to NH_4OH is of the same order of magnitude as the diameter of the pipe from which it is released. Within the scope of the assumptions made, this is an interesting result. It implies that if the mouth of the discharge pipe is at a depth greater than about 5 to 10 diameters of the release pipe, all of the LNH_3 would be converted to NH_4OH and no vapor would be liberated.

Also the analysis presented has tacitly assumed that the turbulent mixing in the jet is characterized by the turbulence in the pipe. However, this may not always be true. During the discharge of LNH_3 into a stream, the stream turbulence itself may be very important. Also to be considered is the turbulence caused by the rapid boiling phenomenon during the heating of LNH_3 by water.

Many other phenomena that may occur in an underwater release have not been considered. These include possible explosions, limitation of water quantity, water currents, etc. Further refinements of the model will have to include one or more of these phenomena.

7. NEUTRALIZATION

7.1 INTRODUCTION

The general characteristics of a spill of refrigerated (-28°F) ammonia on water may be described as follows. A spreading pool of liquid, boiling ammonia forms on the water. About half to three-fourths of the total amount of ammonia spilled dissolves in the water by the time the liquid has completely boiled away, forming a layer of ammonium hydroxide which is elevated in temperature between 5°F and 15°F above the ambient water temperature. After the liquid ammonia has disappeared, more ammonia will be generated from the ammonium hydroxide layer and vaporize into the atmosphere. However the quantity of vapor produced is small compared to the amount of vapor liberated during the boiling. The thickness of the ammonium hydroxide layer is in the neighborhood of a few inches, and the rate of spread is roughly a few inches per second (radial increase), depending on the rate of spill. The maximum spread radius is proportional to the three eights power of the quantity of spill. For example, if 3,000 tons of refrigerated ammonia were spilled instantaneously, the rate of spread would be 2-1/2 inches per second, the maximum thickness of the ammonium hydroxide layer would be about 5 inches, and the maximum radius of the liquid pool would be approximately 475 feet. The characteristics of underwater leaks are determined by the leak rate and depth under water.

The dispersion of the ammonia vapor in the atmosphere depends on the wind velocity and atmospheric conditions. Because of the extremely buoyant nature of the ammonia vapor, there results a rapid rise of the vapor cloud, following the spill. It is estimated that within about 1000 feet of downwind travel, the center of the vapor cloud from a 3000 ton spill would reach a height of between 1500 to 1800 ft.

Estimate of the time of vaporization of a 3000 ton instantaneous spill indicates that the entire boiling process lasts only for about 120 seconds. If therefore the time of spilling of this 3000 tons is larger than about 10 minutes, it should be assumed that evaporation of the spilled mass occurs as soon as the spill touches the water.

The approaches which can be taken towards corrective action may be enumerated as follows:

A. Ammonium hydroxide solution in water
   1. Dispersal
   2. Containment
   3. Air sparging
   4. Sorption
   5. Chemical neutralization

B. Ammonia vapors
   1. Dispersal
   2. Water fog

7.2 AMMONIUM HYDROXIDE SOLUTION

The preferred method of treatment for the ammonia dissolved in the water depends on the specific situation. If the principal hazard is due to the presence of ammonium hydroxide in the water, and the presence of ammonia vapor in the air is of secondary importance, containment of the ammonium hydroxide while allowing evaporation of ammonia from the water to occur, or stripping of the ammonia from the water by subsurface air sparging, may be desirable. If the reverse is the case and the significant hazard is ammonia vapor in the air, it is important to prevent evaporation by dilution, neutralization or absorption of the ammonium hydroxide in the water.

7.2.1 Dispersal

If the spill is on a river or any body of water where rapid water movement occurs, the NH_4OH in the water will be carried away with the current. If mixing occurs, which is likely under such conditions, the dispersal will be enhanced by occurring in depth as well as horizontally, particularly in the case where there is significant wave action.

The effects of the NH_4OH will be felt along the entire swept-out path, although the severity of these effects may decrease with distance downstream due to the reduction of the NH_4OH concentration as a result of evaporation of NH_3 from the water surface and the mixing with larger volumes of uncontaminated water.

In the case of a confined channel, however, a plug of NH_4OH may sweep down the river with only a slight decrease in concentration with downstream distance.

In lakes or harbor areas where currents may be small, dispersal may be enhanced by running small vessels through the spill, utilizing the turbulence caused by the propellers and wake of the vessel to promote mixing with the water. Care should be taken, however, to temporarily block off water intakes, and it should be remembered that the NH_4OH is highly corrosive to copper, copper alloys, and galvanized surfaces. Smaller spills in still bodies of water may be dispersed with fire hoses (or any high pressure, high volume water hose) played onto the NH_4OH layer from dock or shipboard facilities.

Since prompt action is required for dispersal of an LNH_3 spill, the use of water hoses or the turbulent wake of a boat or vessel is the only practical means of achieving rapid dispersal.

7.2.2 Containment

In lakes, ponds, or other less active bodies of water, the NH_4OH layer may remain intact near the spill location. If it is important to localize the adverse impact due to the NH_4OH on aquatic life floating boom such as is used to contain oil spills may be deployed to contain the NH_4OH layer. The instantaneous spill considered above does not represent a realistic situation. In most cases, a 3,000 ton spill would be the result of a tanker barge or vessel accident, and the ammonia would most likely be released over a period of time ranging from minutes to hours. Consequently, the maximum spill diameter would be substantially less that 1,000 feet. The NH_4OH spreading could probably be contained by 2,000 feet of boom. Placement of a boom would allow a substantial fraction of the ammonia to evaporate from the NH_4OH layer, and would allow the use of a neutralizing agent or of absorption or removal of the NH_4OH or NH_3.

There are a large number (more than 65) of different types of floating booms for containment of oil spills,[31] some of which would

be suitable for containing an LNH_3 spill. In the case of an LNH_3 spill, it is important to use a boom which is rapidly deployable and is constructed of materials which are inert to NH_4OH and NH_3. It has been observed that the currents in sheltered areas where most spills occur, such as at piers, in ships, at bulkheads and in coves, are much smaller than the high velocity currents which occur in midstream at peak flow periods.[32] It was found that a boom having a freeboard barrier of 6 inches and a submerged skirt of 12 inches would suit many spill situations and be rapidly deployable.

The following general performance characteristics are desirable for an LNH_3 containment boom:

1. The boom's fabric should contain the flotation pods, ballast and vertical stiffeners, and be capable of withstanding total tension stresses up to 6,000 lbs without additional chain or cable tension members.

2. The fabric must be resistant to NH_4OH, NH_3 abrasion, solar heat and ultraviolet radiation, salt water and anticipated environmental temperature extremes.

3. The boom must be towable from one end at speeds up to 5 knots without damage.

4. The boom should weigh less than 2 lbs per running foot and cost less than $12 per foot with a minimum life expectancy of five years. It should be bright yellow in color to reduce accidental damage by uninformed vessels in harbors. Grab handles should be provided on the top edge.

5. The ballast and float configuration should give stability in 15 knot winds, 0.5 to 1.0 knot currents and 2 ft waves.

Although none of the manufacturers of oil containment booms appear to meet all of the above specifications, several of them[32] could be

considered for containment of LNH_3 spills: Acme O. K. Corral Boom; Bennett 20-inch Harbor Oil Boom; Jaton Boom, Centri-Spray Corp.; Reynolds Aluminum Oil Boom; Sea Curtain, Kepner Plastics Fabricators, Inc.

In cases of currents above the retention capability of the floating boom, it may be desirable to divert the LNH_3 spill to keep it from vulnerable shoreline locations or to guide it into an area where it can be controlled and further corrective action can be taken.

Mooring of the floating boom should not be as critical for LNH_3 spills as for oil spills, since the duration of the spill is limited by evaporation, and the full, twelve hour tidal variation will probably not have to be accommodated by the mooring.

Bubble barriers or air curtains are not usually rapidly deployable and are not likely to be available in time to contain LNH_3 spills. The effect of such barriers would be to enhance evaporation of NH_3 from the water into the air.

7.2.3 Air Sparging

Once the LNH_3 spill has been contained, it may be allowed to evaporate from the water over a period of time, or a more active course may be taken. If it is important to remove the contained ammonia from the water rapidly and there is no significant hazard associated with transferring the NH_3 to the atmosphere, air sparging may be used.

Ammonia can be stripped from water through the use of large quantities of air. Since the NH_4OH layer is only a few inches deep and the power required for air ejection is directly proportional to the depth of air ejection, the air bubble pipes should be suspended only a few feet below the surface. For a four foot pipe depth, 2 psig air is required, and the horsepower requirement is:

$$HP = 0.024\ Q$$

where Q is air volume in cfm (cubic feet per minute), and compressor efficiency and pipe and fitting losses have been accounted for. For example, if the NH_4OH layer were 4 inches deep and 475 feet in radius (3,000 ton spilled instantly), a 100 HP internal-combustion-engine driving a compressor unit would pass one cubic foot of air through each cubic

foot of NH_4OH every 56 minutes. This type of self-contained compressor unit is common in construction work.

7.2.4 Sorption

In some cases it is important to remove the ammonia from the water without releasing it into the atmosphere. One way of accomplishing this is by absorption or adsorption with solids. Absorption refers to the containment of the ammonia in the bulk of the solid; adsorption refers to the adherence of the ammonia on the surface of the solid. Both methods are included in the term sorption.

At least half a dozen different sorbent booms have been developed for oil spill removal; similar principles can be applied to ammonia. The advantage of configuring the sorbent in the form of the boom is two-fold: it may be towed over the spill repeatedly, which effectively circumvents the problem of dispensing the sorbent; and it may be placed on board ship or towed to a clean-up area after use, which reduces the difficulty of collecting the used sorbent. Since the depth of the NH_4OH layer is only a few inches, the sorbent boom will penetrate the entire layer and practically all of the NH_4OH should come into contact with the sorbent material.

When the sorbent boom is saturated with ammonia, it must be removed to a clean-up area where the ammonia can be removed and the boom be readied for further use as required. Ammonia removal may be accomplished by washing the boom with water, squeezing the sorbent material to remove NH_4OH, allowing the NH_3 to evaporate into the atmosphere, or heating the sorbent material to promote evaporation of ammonia. If the sorbent material is low cost and readily available, it may be disposed of in sealed containers or by chemical treatment.

The sorbent material in sorbent booms is generally contained in porous bags, cloth or netting. The sorbent materials must have a preference for absorption or adsorption of NH_3 or NH_4OH rather than water.

The practical difficulties in the use of a sorbent for large spills lies in the quantity of sorbent, or number of sorbent boom deployments required. Sorbent capacity is generally stated in terms of a retention ratio, or ratio of weight of NH_3 taken up to weight of sorbent. With a

retention ratio of 2, a 3,000 ton spill which dissolved 2,000 tons in the water would require 1000 tons of sorbent or 500 passes with a 2 ton sorbent boom. For this reason, the use of a sorbent may only be practical for small spills. It should be noted, however, that the sorbent is generally inactive chemically, and should not present a hazard in storage, handling, or transport.

7.2.5 Chemical Neutralization

The NH_4OH layer may be chemically neutralized by the addition of an appropriate chemical to the water. However, there are major difficulties associated with this type of corrective action, and these are discussed below.

Quantity. The neutralizing agent must be used on a mole for mole basis with the ammonia to completely neutralize it. For a 3,000 ton ammonia spill of which only 2,000 tons dissolves in the water, 4,300 tons of HCl would be required. Neutralizing chemicals are not normally available in these quantities.

Dispensing method. The neutralizing chemical must be dispensed in a uniform and controlled manner throughout the NH_4OH layer. If this is not accomplished, additional neutralizing agent may be required and concentrations of excess neutralizing agent may occur and cause additional adverse conditions in the body of water. It is difficult to dispense the agent uniformly dispensed over the water surface, it must still mix or diffuse through the NH_4OH layer to achieve optimum effect; uniform mixing may be inhibited by density differences between the neutralizing agent and NH_4OH or by the kinetics of the chemical reaction.

Heat generation. Most of the neutralizing agents that could be used with NH_4OH would cause exothermic reactions, and create a significant temperature rise in the surface layer of water. Although some of this heat may be removed by evaporation, convective air cooling and radiation, some of the heat will be removed by water convection. The adverse effects of the increase in water temperature must be taken into account.

Reaction products. The most likely product of a neutralizing reaction is a salt, i.e.: NH_4Cl if HCl is used. Most of the ammonium salts that would result from use of a neutralizing agent are soluble in water, and would be difficult to remove from a large body of water. The adverse effects of the dissolved salts must be considered in the use of a neutralizing agent.

7.2.6 Safety

Most neutralizing agents are hazardous chemicals which must be stored, transported and handled with caution. The circumstances surrounding an LNH_3 spill allow little time for adequate practice of safety procedures; the use of a neutralizing agent can represent a new hazard comparable in potential adverse impact to the original LNH_3 spill.

It appears, from the above discussed difficulties, that the use of a neutralizing agent is not the preferred corrective action for an LNH_3 spill, except perhaps for very small, confined spills.

7.3 AMMONIA VAPORS

Depending on the particular situation, it may be desirable to disperse the ammonia vapor into the atmosphere, or conversely, to trap the ammonia vapor by water (or other means) and remove it from the atmosphere. For a 3,000 ton spill of LNH_3 on water during a one hour period, about 1,000 tons of ammonia will be generated during a period of 120 seconds. Subsequent to the complete evaporation of the liquid ammonia pool, provided no corrective action is taken with respect to the NH_4OH in the water, ammonia will continue to evaporate from the water surface to the extent of 1,000 tons during the next few minutes, for quiescent water conditions.

7.3.1 Dispersal

If a strong wind is blowing, the ammonia vapor will be dispersed into the atmosphere, leaving little alternative as to any possible correction actions. This is true regardless of wind conditions since the cold ammonia vapor is always lighter than air. Little can be done to prevent rapid dispersal of the vapor cloud.

7.3.2 Water Fog

If atmospheric conditions are such that the ammonia vapor is not rapidly and naturally dispensed, it may be desirable to attempt to remove it from the atmosphere. Probably the most effective way of achieving this goal is by the use of a water fog or water spray. Equipment for generating substantial quantities of a dense water fog could be developed utilizing the principle of the cooling (to near ambient temperature) of a warmer, water saturated air mass, and using mechanical blowers or fans to direct the fog through the ammonia vapor. The result would be the formation of a NH_4OH fog which, as it cooled, would condense and fall into the water surface where further corrective action could be taken.

If specialized water fog generating equipment is not available, fire hoses could be utilized (with spray nozzles, if possible) to play streams of spray or water through the ammonia vapor cloud. This would not be as effective as a water fog, and might create the additional problem of forming a liquid ammonia aerosol by splashing the LNH_3 (if the liquid ammonia pool has not yet completely evaporated), which is more difficult to remove with the water spray than is the ammonia vapor.

7.3.3 Sorption and Chemical Neutralization

The use of solids to absorb or adsorb the ammonia vapor may be unreasonably difficult. The only possibility would be the use of a pulverized or dust-like sorbent which could be projected through the ammonia vapor cloud by a mechanical blower. However, large quantities of sorbent would be required (on the order of 500 to 1,000 tons for a 3,000 ton spill), and the problems of availability, transport, and subsequent clean-up of the sorbent from the water appear to be major objections to this type of corrective action.

The use of a chemical neutralizing agent is even more unlikely considering the difficulties discussed above in Section 7.2.5. The hazards associated with spraying large quantities of a neutralizing chemical through the ammonia cloud appear to be greater than the benefit that might be gained by neutralizing the ammonia vapor.

8. REFERENCES

1. Creelman, W.A., Marine Technology, 69, (January 1971).

2. Husa, H.W., and Buckley, W.L., CEP Technical Manual, Vol. 7, 41, AIChE, (1965).

3. Atallah, S., and Allan, D.S., Fire Technology, 7, 47, (1971).

4. Buckley, W.L., and Husa, H.W., Chemical Engineering Progress, 58 , 81, (1962).

5. National Safety Council Data Sheet 251A, National Safety Council, Chicago, Ill., (1970).

6. Nakanishi, E., and Reid, R.C., Chemical Engineering Progress, (1971).

7. Prof. R.C. Reid, Dept. of Chem. Eng., Massachusetts Institute of Technology. (Private Communication) (1972).

8. AGA Sponsored Test Program, "A Report on LNG Safety Research," Vol. II by Arthur D. Little, Inc. (1971).

9. AGA Sponsored Test Program, "LNG Safety Program," Vol. III, by Battelle Memorial Institute and University Engine s. (1971).

10. Burgess, D.S., et al, "Hazards of LNG Spillage in Marine Transportation," Final Report by the Bureau of Mines, Pittsburgh, Pennsylvania, (1970).

11. Shell Research Ltd., "Laboratory Investigations into the Characteristics of LNG Spills on Water - Evaporation, Spreading, and Vapour Discharge," March 1973, Available through American Petroleum Institute.

12. Esso Research and Engineering Co., "Spills of LNG on Water - Vaporization and Downwind Drift of Combustible Materials," May 1972, (revised May 1972), Available through American Petroleum Institute.

13. Resplandy, A., Chemie et Industrie - Génie Chimique, 102, 691, (1969).

14. Ball, W.L., AIChE, Ammonia Plant Safety Manual, Vol. 12, 1, (1970).

15. Morgan, G.O., and Reed, J.D., CEP Technical Manual, Vol. 7, 38, AIChE, (1965).

16. Apfel, R.E., "Vapor Cavity Formation in Liquids," Ph.D. Thesis, Harvard University, (February 1970).

REFERENCES (cont)

17. "Analytical Models in Support of Hazard Assessment Handbook" - CHRIS Manual 3, prepared for U.S.C.G. by Arthur D. Little, Inc., Cambridge, Mass. (July 1973).

18. "Meteorology and Atomic Energy," D.H. Slade, Editor, Div. of Tech. Information, Atomic Energy Commission, (1968).

19. "Physical and Thermodynamic Properties of Ammonia - Water Mixtures," Research Bulletin #34, Institute of Gas Technology, I.I.T. Centre, Chicago, Ill., (September 1964).

20. Fay, J., "Dispersion of LNG Vapor Clouds," a supplement to the paper, "Unusual Fire Hazard of LNG Tanker Spills," Fay, J., Combustion Science and Technology, Vol. 7, 47-49, (1973).

21. Thatcher, L., and Harleman, D.R.F., "A Mathematical Model for the Prediction of Unsteady Salinity Intrusion in Estuaries," Department of Civil Engineering, Massachusetts Institute of Technology, Report No. 144, (February 1972).

22. Harleman, D.R.F., "Transport Processes in Water Quality Control," Massachusetts Institute of Technology course lecture notes, (1972).

23. Fischer, H., "Dispersion Predictions in Natural Streams," Proc. ASCE, J. Sanitary Eng. Division, 927-943, (October 1968).

24. Holley, E. R., Harleman, D.R.F., and Fischer, H., "Dispersion in Homogeneous Estuary Flow," J. Hyd. Div., Proc. ASCE, 1691-1709, (August 1970).

25. Tracor, Inc. - Austin, Texas, "Estuarine Modeling - An Assessment," Report prepared for the Water Quality Office of the Environmental Protection Agency, (February 1971).

26. Slawson, P.R., and Csanady, G.T., "On the Mean Path of Buoyant, Bent-Over Chimney Plumes," J. Fluid Mech, Vol. 28, Part 2, 311-322, (1967).

27. Hoult, D.P., Fay, J.A., and Forney, L.J., "A Theory of Plume Rise Compared with Field Observations," Paper #68-77, Air Pollution Control Association, Pittsburgh, Pa., (1968).

    Fay, J.A., Escudier, M., and Hoult, D.P., "A Correlation of Field Observations of Plume Rise," Publication #69-4, Fluid Mechanics Laboratory, Massachusetts Institute of Technology, Cambridge, Mass. (April 1969).

REFERENCES (cont)

28. Morton, B.R., Taylor, G.I., and Turner, J.S., "Turbulent Gravitational Convection from Maintained and Instantaneous Sources," Proc Roy Soc (Lond), Vol 234.A, 1-23, (January 1956).

29. Fay, J.A., "Plume Rise Measurements at Industrial Chimneys - DISCUSSIONS," Atmospheric Environment, Vol. 3, 311-315, (1969).

30. Hottel, H.C., "Burning in Laminar and Turbulent Fuel Jets", 4th International Symposium on Combustion, 97-113, (1953).

31. "Oil Spill Containment Systems," Second Edition, U.S. Environmental Protection Agency, Surveillance and Analysis Division, Region II, Edison, New Jersey, (January 1973).

32. "A Rapidly Deployable Oil Containment Boom for Emergency Harbor Use," Office of Research and Monitoring, U.S. Environmental Protection Agency, EPA-R2-73-112, (February 1973).

APPENDIX A

This appendix contains the thermodynamic properties of anhydrous ammonia. Table A-1 (taken from reference 33), gives the important property values. Tables A-2, A-3 and A-4 (from reference 19) give respectively the boiling points and the liquid and vapor enthalpies, all as functions of pressure. Figure A-1 is the enthalpy concentration diagram[19] for an ammonia-water system.

Table A-1 Important Properties of Anhydrous Ammonia

Chemical Formula	NH_3
Molecular Weight	17.03
Boiling Temperature at Atmospheric Pressure, F	-28.0
Freezing Temperature at Atmospheric Pressure, F	-108
Critical Temperature, F	271.4
Critical Pressure, psia	1657
Critical Density, lb per cu ft	14.6
Density of Liquid at -28.0 F, lb per cu ft	42.56
Specific Volume of Saturated Vapor at -28.0 F, cu ft per lb	18.00
Specific Heat of Liquid at 86 F, Btu per (lb) (F)	1.143
Specific Heat Ratio (c_p/c_v) of Vapor at 86 F and One Atmosphere Pressure	1.29
Thermal Conductivity, (Btu) (ft) per (sq ft) (hr) (F):	
Saturated Liquid at 32 F	0.29
Saturated Liquid at 86 F	0.29 (Avg.)
Vapor at One Atmosphere Pressure at 32 F	0.0128
Vapor at One Atmosphere Pressure at 86 F	0.0145
Viscosity, Centipoises:	
Saturated Liquid at 5 F	0.250
Saturated Liquid at 86 F	0.207
Vapor at One Atmosphere Pressure at 5 F	0.0085
Vapor at One Atmosphere Pressure at 86 F	0.0102
Relative Dielectric Strength of Vapor at 84 F and One Atmosphere Pressure (Nitrogen = 1)	0.82
Color	Clear and water white
Odor and Detection	Irritating odor, readily detectable by smell. Burning sulphur used for locating leaks.
Flammability Limits (Per cent by volume)	16 to 25
Toxicity, Underwriters' Laboratories Classification	Group 2

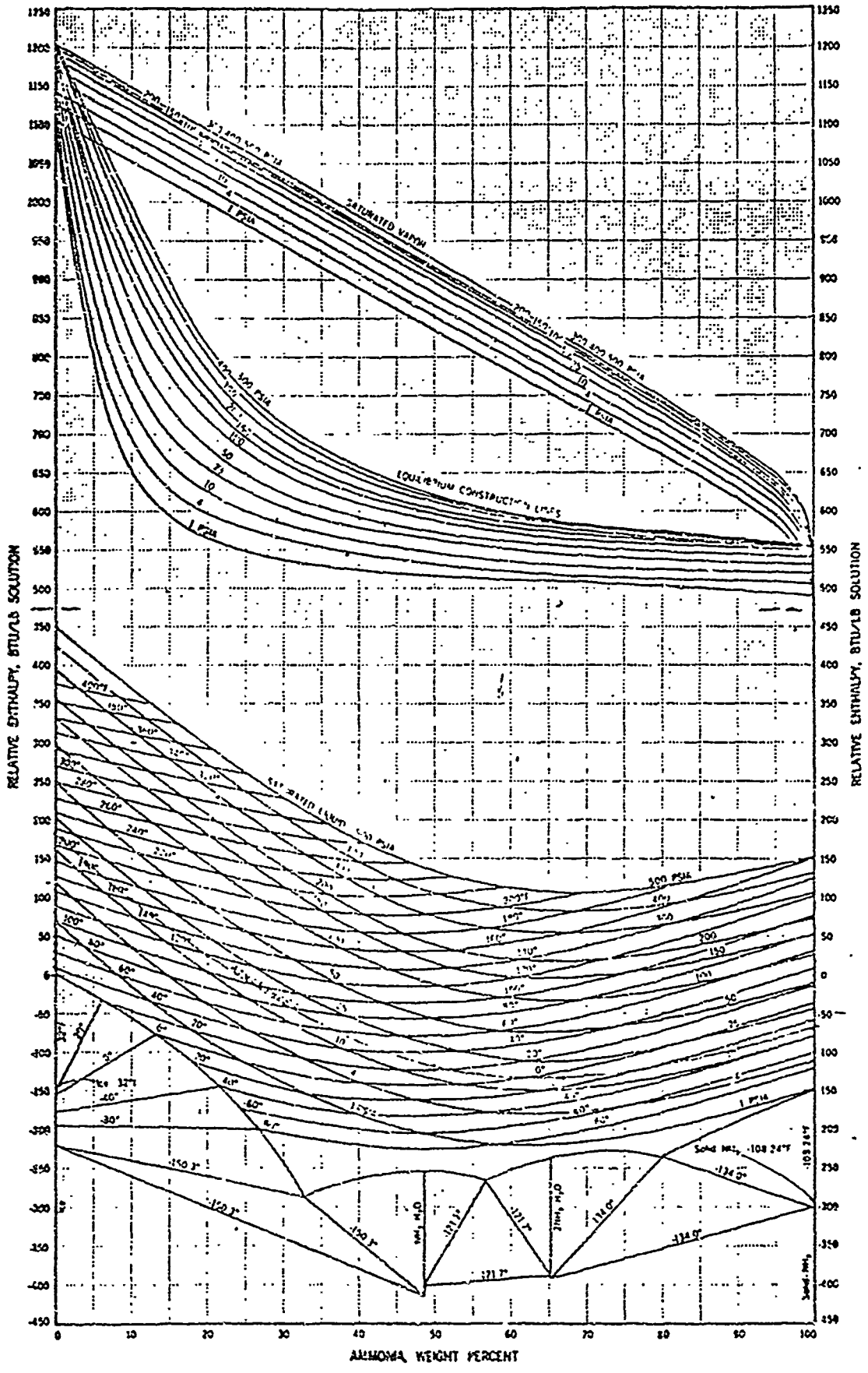

FIG A-1 ENTHALPY-CONCENTRATION DIAGRAM FOR AMMONIA-WATER MIXTURES

Table A-2—BOILING POINTS OF AMMONIA-WATER MIXTURES AS A FUNCTION OF SATURATION PRESSURE

Saturation Pressure, psia	Ammonia in Liquid, wt %										
	0	10	20	30	40	50	60	70	80	90	100
	Saturation Temperature, °F										
1	101.7	49.5	12.5	-16.5	-40.5	-64.0	-83.5	-95.0	-99.5	-102.5	-105.0
2	126.1	72.5	35.0	4.5	-21.5	-45.5	-65.0	-76.5	-82.0	-85.5	-88.2
4	153.0	99.0	61.0	29.5	0.5	-24.5	-44.5	-55.0	-62.5	-66.5	-69.6
6	170.1	116.0	77.5	45.5	16.0	-10.0	-31.0	-43.0	-50.5	-55.0	-57.6
8	182.9	128.5	89.0	56.5	26.5	0.0	-21.5	-33.5	-41.0	-46.0	-48.5
10	193.2	138.0	98.0	65.0	34.5	8.0	-13.5	-26.0	-33.5	-38.5	-41.3
12	202.0	146.5	107.0	73.0	42.0	15.0	-6.5	-19.0	-27.0	-32.5	-35.2
15	213.0	158.0	117.5	83.5	52.5	24.5	2.0	-10.5	-18.5	-24.0	-27.3
20	228.0	173.0	132.0	97.0	65.0	36.5	14.5	1.5	-7.5	-13.0	-16.6
25	240.1	184.5	143.5	108.0	75.5	46.5	24.5	11.0	1.5	-4.5	-8.0
30	250.3	195.5	153.0	117.0	84.5	55.0	32.5	18.5	9.5	3.5	-0.6
35	259.3	204.5	162.0	125.5	92.0	62.5	40.0	25.5	16.5	10.0	5.9
40	267.3	213.0	169.5	132.5	98.5	69.0	46.5	32.0	22.5	16.0	11.7
50	281.0	226.0	182.5	145.0	111.0	80.5	58.0	43.0	33.0	26.0	21.7
60	292.7	238.5	193.5	156.0	121.5	90.5	67.5	52.5	42.0	35.0	30.2
70	302.9	248.0	203.5	165.5	130.5	99.5	76.0	60.0	49.5	42.0	37.7
80	312.0	258.0	212.5	173.5	138.5	107.5	83.0	67.5	57.0	49.0	44.4
90	320.3	267.0	220.5	181.5	146.0	114.5	90.0	74.5	63.5	55.5	50.6
100	327.8	276.0	229.5	188.5	153.0	121.5	97.0	80.5	69.5	61.5	56.0
110	334.8	282.5	236.0	195.0	158.5	126.5	102.5	86.0	74.5	67.5	61.2
120	341.3	289.0	242.0	201.0	164.0	132.5	108.5	91.0	79.5	71.5	66.0
130	347.3	295.0	248.0	206.5	169.0	137.5	113.5	96.0	84.5	76.5	70.5
140	353.0	301.0	254.0	212.0	174.0	142.5	118.0	100.5	89.5	81.0	74.8
150	358.4	306.5	259.5	217.0	179.0	147.0	122.5	105.0	93.5	85.0	78.8
160	363.5	312.0	264.5	222.0	183.5	151.5	127.0	109.5	97.5	89.0	82.6
170	368.4	317.0	270.0	226.5	187.5	156.0	131.0	113.5	101.5	93.0	86.3
180	373.1	322.0	274.5	230.5	192.0	160.5	135.0	117.0	105.0	96.5	89.8
190	377.5	327.0	279.5	234.5	196.0	164.0	139.0	121.0	108.5	99.5	93.1
200	381.8	331.5	284.0	238.5	200.0	168.0	142.5	124.5	112.0	103.0	96.3
210	385.9	335.5	288.0	242.5	203.5	172.0	146.0	128.0	115.5	106.5	99.4
220	389.9	339.5	291.5	246.0	207.5	175.5	149.5	131.5	118.5	109.5	102.4
230	393.7	343.0	295.0	249.5	211.0	178.5	153.0	134.5	121.5	112.5	105.3
240	397.4	346.5	298.5	253.0	214.0	182.0	156.0	137.5	124.5	115.5	108.1
250	401.0	350.0	301.5	256.5	217.5	185.0	159.0	141.0	127.5	118.5	110.8
260	404.4	353.0	304.5	259.5	220.5	188.0	162.0	143.5	130.5	121.0	113.4
270	407.8	356.0	307.5	262.5	224.0	191.0	164.5	146.5	133.5	123.5	116.0
280	411.1	359.0	310.5	266.0	227.0	193.5	167.5	149.5	136.5	126.0	118.4
290	414.2	362.0	313.0	268.5	230.0	196.5	170.5	152.0	139.0	128.5	120.9
300	417.3	364.5	316.0	271.5	232.5	199.0	172.5	154.5	141.5	131.0	123.2
310	420.4	367.5	319.0	274.5	235.5	202.0	175.0	157.0	144.0	133.5	125.6
320	423.3	370.0	321.5	277.5	238.0	204.5	177.5	159.5	146.5	135.5	127.1
330	426.2	372.5	324.0	280.0	241.0	207.0	180.0	162.0	148.5	138.0	129.2
340	429.0	375.5	326.5	282.5	243.5	209.5	182.5	164.0	151.5	140.0	131.2
350	431.7	378.0	329.0	285.0	246.0	212.0	185.0	166.5	153.0	142.0	132.5
360	434.4	380.5	331.5	287.5	248.5	214.5	187.0	169.0	155.0	144.0	134.9
370	437.0	383.0	334.0	290.0	251.0	217.0	189.5	171.0	157.0	146.0	137.1
380	439.6	385.5	336.5	292.5	253.5	219.0	191.5	173.0	159.5	148.0	139.2
390	442.1	388.0	339.0	295.0	255.5	221.5	193.5	175.5	161.5	150.0	141.4
400	444.6	390.5	341.5	297.5	258.0	223.5	196.0	177.5	163.5	152.0	143.5
410	447.0	392.5	343.5	299.5	260.5	226.0	198.0	179.5	165.5	154.0	145.6
420	449.4	395.0	346.0	302.0	262.5	228.0	200.0	181.5	167.0	155.5	147.5
430	451.7	397.5	348.5	304.5	264.5	230.5	202.0	183.5	169.0	157.5	149.4
440	454.0	399.5	351.0	306.5	267.0	232.5	204.0	185.5	171.0	159.5	151.3
450	456.3	402.0	353.0	309.0	269.0	234.5	206.5	187.5	173.0	161.5	153.1
460	458.5	404.5	355.5	311.0	271.0	236.5	208.5	189.5	175.0	163.0	154.9
470	460.7	407.0	357.5	313.0	273.0	238.5	210.0	191.5	177.0	164.5	156.7
480	462.8	409.0	359.5	315.5	275.5	240.5	212.0	193.0	178.5	166.5	158.4
490	464.3	411.5	362.0	317.5	277.5	242.5	214.0	195.0	180.5	168.5	160.0
500	467.0	413.0	364.0	319.5	279.5	244.5	216.0	197.0	182.0	170.0	161.6

Table A–3–SATURATED LIQUID ENTHALPY OF AMMONIA-WATER MIXTURES AS A FUNCTION OF SATURATION PRESSURE

Table A–4–ENTHALPY OF SATURATED VAPOR OF AMMONIA-WATER MIXTURES AS A FUNCTION OF SATURATION TEMPERATURE AND SATURATED LIQUID COMPOSITION

APPENDIX B

BUOYANCY OF AMMONIA VAPOR - AIR MIXTURE WITH AEROSOL FRACTION AS A PARAMETER

Introduction

Whether a gas cloud rises in air (and if so, its rate of rise) is determined by the relative densities of the gas cloud and the surrounding air. The information about the buoyancy of the cloud is important in determining its dispersion in the atmosphere.

Pure ammonia vapor is lighter than ambient air, even at the low saturation temperature (-28°F). However, when the ammonia vapor is liberated from a boiling pool of liquid ammonia on water, or on land, liquid droplets of LNH_3 are thrown into the vapor phase in the form of aerosols. The density of such an aerosol laden ammonia vapor is more than that of pure vapor. Also because of the affinity of ammonia for water and its reaction with water, several phenomena take place when moist air mixes with aerosol laden ammonia vapor. The air is cooled, because of the vapor's low temperature, resulting in the possibility of water vapor condensation. Ammonia may go into solution with water, liberating heat. A part of this heat goes to heat the mixture of the gases and another part to evaporate the liquid droplets of ammonia. The final equilibrium condition depends on the relative amounts of aerosol, humidity, the air temperature, and the mass ratio of vapor to air.

To obtain the final mixture condition for NH_3, vapor mixing with moist air for any given initial conditions, is an extremely difficult and involved process. However, to obtain some basic understanding of the buoyant nature of the gas with different aerosol fractions, a simplified problem is worked out, wherein only dry air is considered. Finally, equations are developed to describe the mixing process with moist air and an approach to the solution is discussed.

1) Mixing of Saturated Ammonia Vapor with Bone Dry Air

To obtain the gaseous mixture density, the mass balance equation and energy balance equations are written and solved for the final equilibrium mixture temperature. Knowing this temperature, the mixture density is obtained. In deriving the equations, the following assumptions are made:

- All equations are derived on the basis of one unit mass of bone dry air;
- The gases are considered to be perfect gases;
- The final mixture is in a pure gaseous state (no droplets);
- Total pressure is one atmosphere.

Let F = Mass of cold ammonia vapor (including the aerosol) mixing with unit mass of air;

F_L = Fraction of the mass of ammonia vapor which is in the form of aerosol;

I = Enthalpy per unit mass of any substance (subscripted);

T_a = Air temperature

T_i = Initial vapor temperature (saturation temperature)

T_{mix} = Temperature of the air vapor mixture.

a) Mass Conservation

Mass of air + mass of vapor = mass of final mixture

b) Energy Conservation

Since the total pressure is a constant, the energy conservation equation becomes the enthalpy conservation equation, i.e.,

$$I_a(T_a) + F\,[F_L\, I_{liq}^{(sat)}\,(T_i) + (1-F_L)\, I_{vap}^{(sat)}\,(T_i)] = I_a\,(T_{mix}) + F\, I_{vap}^{(sat)}\,(T_{mix}) \qquad (B1)$$

The air-vapor mixture temperature is obtained from the above equation.

c) Equation of State

$$p = \rho_a \frac{R_u}{\mu_a} T_i = \rho_{mix} \frac{R_u}{\mu_{mix}} T_{mix} \tag{B2}$$

where

$$\mu_{mix} = \frac{(1 + F)\, \mu_a \mu_v}{(\mu_v + F\, \mu_a)} \tag{B3}$$

R_u = universal gas constant

p = atmospheric pressure

μ = molecular weight

If the gases can be assumed to have constant specific heats, then equation B1 can be rearranged to give

$$T_{mix} = \frac{[c_{p,a} T_a + F\, (c_{p,v} T_i - F_L \lambda)]}{[F\, c_{p,v} + c_{p,a}]} \tag{B4}$$

where c's are the constant pressure specific heats and λ is the average latent heat of vaporization of liquid ammonia.

Also from equations B2 and B3 we get

$$\text{Fractional Density Deviation} = \Delta = \left(\frac{\rho_{mix}}{\rho_a} - 1\right) = \left[\frac{T_a}{T_{mix}} \frac{(1 + F)}{(1 + \frac{\mu_a}{\mu_v} F)} - 1 \right] \tag{B5}$$

It is noted that physically the mixture temperature cannot be less than the saturation temperature of ammonia at atmospheric pressure. This condition imposes an upperbound on the acceptable value of the mass ratio of vapor to air (F) for a given fractional aerosol mass in vapor.

By substituting $T_{mix} = T_i$ in equation B4 and rearranging we get for the critical F,

$$F_c = \frac{c_{p,a}\ (T_a - T_i)}{\lambda F_L} \tag{B6}$$

and $F \leq F_c$

Substituting B6 in B5 and using the numerical values for the molecular weights of air and ammonia

$$\Delta_c = \left[\frac{T_a}{T_i} \frac{(1 + F_c)}{(1 + 1.6985\ F_c)} - 1 \right] \tag{B7}$$

Figure B-1 shows the fractional density deviation as a function of vapor air ratio (F) with the aerosol fraction (F_L) as a parameter. The critical F value and the Critical Δ values are indicated for each F_L. The buoyant and nonbuoyant regions (i.e., Δ negative and Δ positive, respectively) are indicated as also the forbidden region consistent with the mixture temperature condition.

Figure B-2 indicates the mixture temperature for different F and F_L values.

2) Mixing of Saturated Ammonia Vapor with Moist Air

In formulating this problem we assume that:

- The mixing of air and vapor is adiabatic.
- At equilibrium condition after mixing, the mixture contains air, ammonium hydroxide solution, water vapor and ammonia vapor. The last two components are in equilibrium with the ammonium hydroxide solution.
- The ammonium hydroxide solution is in the form of aerosols and does not precipitate out.
- The volume occupied by NH_4OH drops is very small.
- The total pressure is constant.
- A unit mass of dry air basis is used.

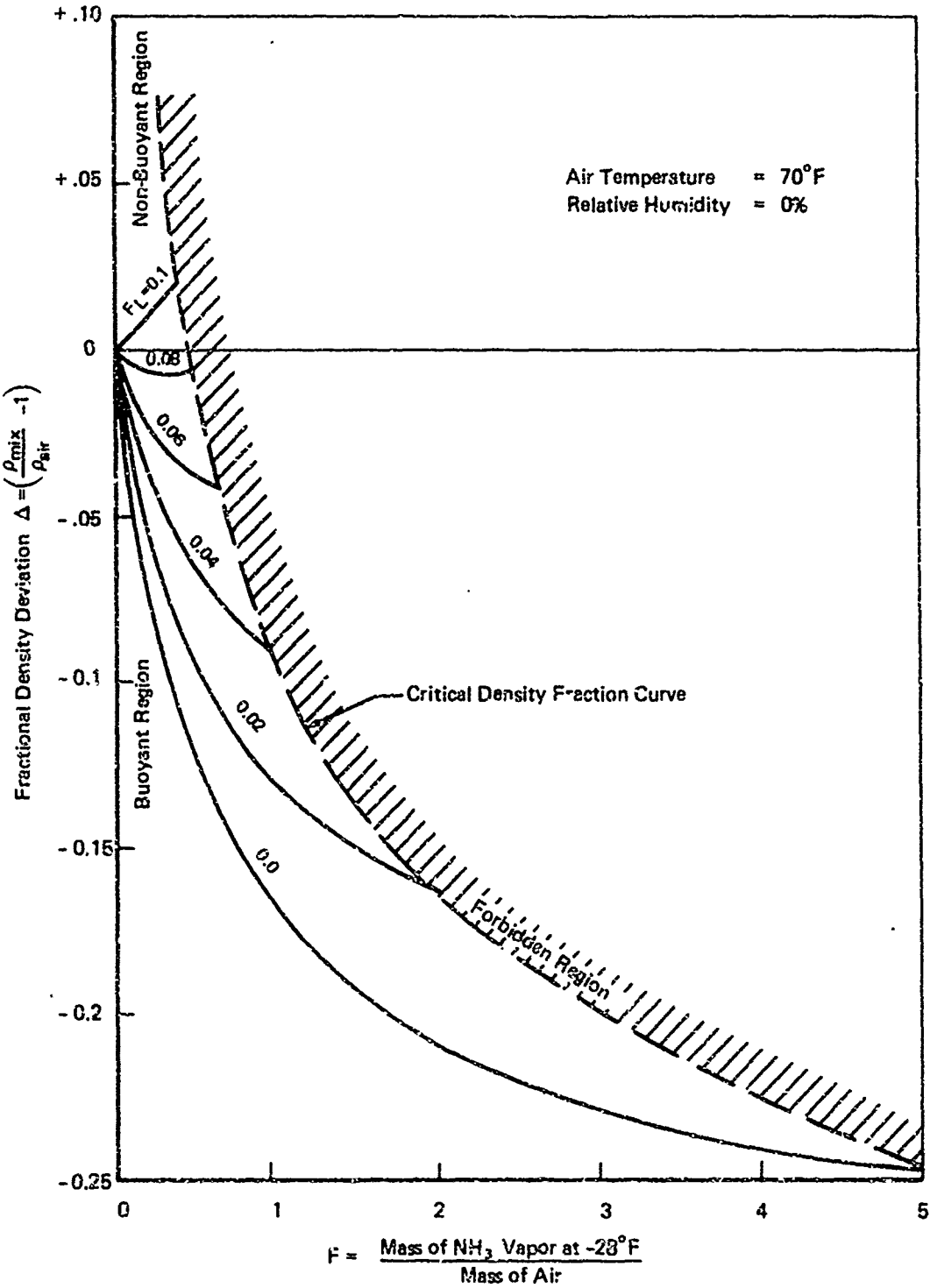

FIGURE B–1 FRACTIONAL DENSITY DEVIATION OF AMMONIA VAPOR–AIR MIXTURE WITH AEROSOL FRACTION AS A PARAMETER

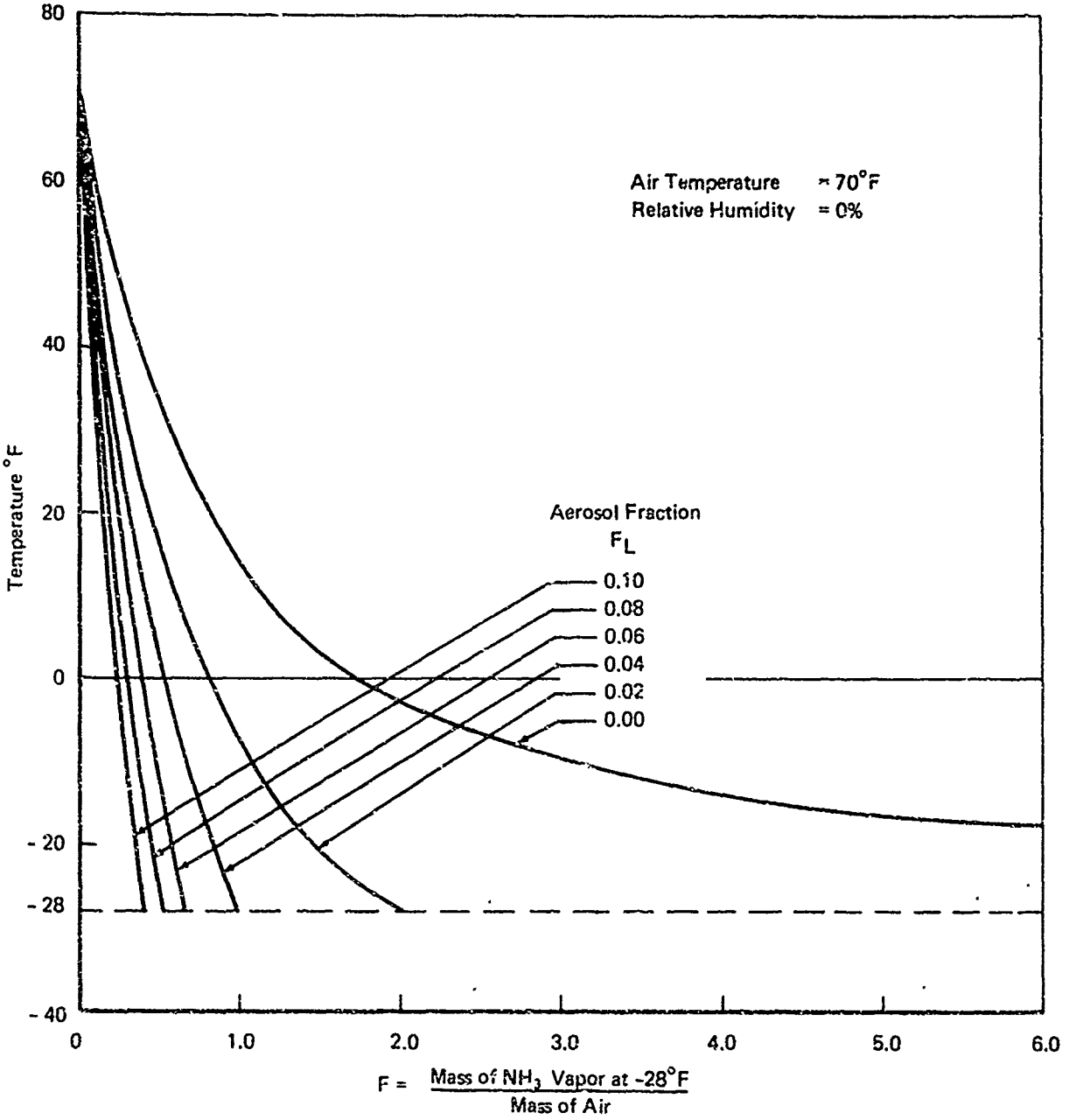

FIGURE B–2 TEMPERATURE OF AMMONIA VAPOR–AIR MIXTURE WITH AEROSOL FRACTION AS A PARAMETER

Let

M_v = mass of gases other than air in the vapor phase (only water and ammonia)

M_L = mass of NH_4OH liquid droplets formed

x = mass fraction of water in the liquid

y = mass fraction of water vapor in the water vapor ammonia vapor mixture (air excluded)

w_i = initial mass of water vapor in air

P_a = partial pressure of air in the mixture of gases

V = volume of the mixture

a) Ammonia Mass Balance

$$(1 - x)M_L + (1 - y)M_v = F$$

b) Water Mass Conservation

$$x M_L + y M_v = w_i$$

c) Phase Equilibrium Relation

$$y = f(x, T_{mix}, p - p_a)$$

d) Partial Pressure of Air

$$p_a V = \frac{R_u}{\mu_a} T_{mix}$$

e) Volume Relation

$$V = \frac{M_v}{\rho_v}$$

where

$$\rho_v \equiv \rho_v(x, T_{mix}, p - p_a)$$

f) Relation Between Mass of Vapor and Mass of Liquid

$$\frac{M_v}{M_L} = f(x, T_{mix}, p - p_a)$$

g) Energy Equation

Initial enthalpy of air + Initial enthalpy of saturated ammonia vapor = Final enthalpy of mixture

The above form a set of seven coupled equations for the seven unknowns: M_L, M_v, T_{mix}, p_a, x, y and V. The solution of these equations for given initial values of F, w_i and T_a is extremely difficult. However, in principle the solution can be obtained provided the functional relationships connecting the various parameters for an ammonia-water system are known completely.

APPENDIX C

HAZARD ASSESSMENT PROCEDURES AND APPLICATION TO SEVERAL SPILL SIZES

Introduction

The procedures for calculating the hazards caused by a spill of liquid anhydrous ammonia (LNH_3) are presented in this appendix. The procedures are illustrated with specific numerical examples for the spill of 3,000 tons of LNH_3 on water. The examples include the calculation of vapor concentration at ground level in section 1, and in section 2 the calculation of ammonium hydroxide concentration in water. At the end of each section, plots are given which facilitate quick hazard assessment for several spill quantities and environmental conditions.

Section 1: Vapor Dispersion

The procedure for calculating the ground level vapor concentration can be summarized by the following steps:

1. Calculate the maximum radius of spread (Figure 5-7) R_{max}.
2. Calculate the mass and volume of saturated vapor liberated using the value of the partition function, the mass of liquid spilled, and the density of vapor.
3. Calculate the fractional density deviation of the vapor.
4. Calculate the buoyancy flux (section 6.7.2.1) and then the buoyancy length. Knowing this and the downwind distance, the vapor plume rise can be obtained.
5. Knowing the value of the potential temperature gradient in the atmosphere, calculate the stratification parameters (see section 6.7.2.1). From this the ceiling height z_∞

to which the cloud rises can be obtained. Note that cloud reaches a ceiling height only in stable atmospheres (atmospheres E and F). Also, in the case of fumigation type of atmospheres, the atmosphere should be considered to be unstable up to the ceiling height. This latter ceiling height should be obtained from weather data (see section 6.5.2.2 ii).

6. For the height of rise of cloud, use the smaller of the values obtained in steps 4 and 5.

7. Obtain the effective downwind distance x_{eff} by adding to the actual distance 10 times the maximum radius of spread.

8. Obtain the dispersion parameter values (σ's) for the appropriate atmospheric type, at the effective distance, from Figures 6-17a and 6-17b.

9. Using the appropriate formula depending on the type of atmosphere, obtain the ground level concentrations.

The procedure is illustrated below with a specific numerical example.

Data

Density of liquid ammonia at -28°F		42.56	lbs/ft^3
Density of saturated vapor at -28°F		0.05556	lbs/ft^3
Ambient temperature		68.0	°F
Density of air at 68°F		0.07488	lbs/ft^3
Mass of LNH_3 spilled instantaneously	H_ℓ	3000	tons
		$= 6 \times 10^6$	lbs
Volume of liquid	V_ℓ	1.056×10^6	gallons
Partition ratio (assumed)	p	0.6	
Liquid regression rate (see page 126)	$\dot{y}$	3.89×10^{-3}	ft/s

Calculations

Maximum radius of spread (Figure 5-7)	R_{max} =	$2.5\ (gal)^{0.375}$ =	453.75	ft
Mass of vapor liberated	M_v =	$(1-p)M_\ell$ =	2.4×10^6	lbs
Volume of vapor liberated	V_v =	=	4.32×10^7	ft^3
Fractional density deviation of LNH_3	Δ_ℓ =	$(1-\frac{\rho_\ell}{\rho_w})$ =	0.318	
Fractional density deviation of vapor	Δ_ℓ =	$(1-\frac{\rho_v}{\rho_{air}})$ =	0.259	
Maximum vapor liberation rate	$\dot{m}_e$ =	$\pi R_{max}^2 \rho_\ell \dot{y}(1-p)$ =	1.713×10^4	lbs/s
Time for complete evaporation of LNH_3 (equation 5-5)	t_e =	$\left[\frac{V_\ell}{g \dot{y}^2 \Delta_\ell}\right]^{1/4}$ =	123.4	sec

a) Dispersion of Vapor Under Unstable Atmosphere (c)

Wind velocity (assumed) U = 20 knots = 33.8 ft/s

Downwind distance at which ground level concentration is needed: x = 5 km = 2.7 nautical miles

Buoyancy flux F_p (see section 6.7.2.1) = $\frac{4.32 \times 10^7 \times 32.2 \times 0.259}{\pi \times 123.4}$

= $9.29 \times 10^5\ ft^4/s$

Buoyancy length $\ell_r = \frac{F_p}{U^3}$ = 24.0 ft

Height of rise of center line of vapor cloud (equation 6-56 with x in feet): $z = 3.3x^{2/3}$ ft

Hence: $z = 3.3 \times (16400)^{2/3}$ = 2130 ft

Effective source distance = $x_e = x + 10\ R_{max}$ = 20936 ft

Dispersion parameters for x_e, in atmosphere c (see Figures 6-17a and 6-17b):

σ_y = 1837 ft

σ_z = 1050 ft

Ground level concentration (see equation 6-46b)	c	$= \frac{2 \times 2.4 \times 10^6 \; e^{-1/2\left(\frac{2130}{1050}\right)^2}}{(2\pi)^{1.5} \; 1837^2 \times 1050}$	
		$= 1.1 \times 10^{-5}$	lb/ft^3
Concentration in ppm		$= 1.1 \times 10^{-5} \times (22.825 \times 10^6)$	
		$= 251$	ppm

b) Dispersion in Stable Atmosphere (F)

Potential temperature gradient in the atmosphere (assumed)		5	°K/km
Wind velocity	U	5	mph
		7.3	ft/s
Atmospheric temperature		288	°K
Buoyancy length (ℓ_p)	$\frac{F_p}{U^3}$	2389	ft
Height of rise of center line of vapor cloud in a distance of x feet (see equation 6-56)	z	$15.3 \; x^{2/3}$	ft
Brunt Väisalla frequency (see page 193)	ω	1.304×10^{-2}	rad/s
Stratification parameter (see page 193)	S	$\frac{7.3}{2389 \times 1.304 \times 10^{-2}}$	$= 0.234$
Hence the maximum height reached by the vapor cloud (equation 6-61) given by the plume theory†	z_∞	$2389 \times (.234)^{2/3}$	= 989 ft
Downwind distance at which this maximum height is reached	x^*	$\left(\frac{989}{15.3}\right)^{1.5}$	= 520 ft
Downwind distance at which ground level concentration is needed (assumed)	x	10	nautical miles
		60,800	ft
Effective distance	x_e	$x + 10 \; R_{max}$	= 65,337 ft
Dispersion parameters for atmosphere F at the distance x_e (from Figures 6-17a and 6-17b)	σ_y	1640	ft
	σ_z	197	ft

†As already discussed in section 5.5 (page 128), the behavior of a vapor cloud liberated by a massive spill is likely to be more accurately described by the puff theory. However, because of the lack of data for massive spills of LNH_3 and in order to conform to the findings of the present test program, we use the more conservative value given by the plume theory; that is, z_∞ is assumed to be 989 ft (instead of z_∞ = 1710 ft given by puff theory).

Therefore ground level concentration (equation 4-46b)

$$= \frac{2 \times 2.4 \times 10^6 \, e^{-1/2\left(\frac{989}{197}\right)^2}}{(2\pi)^{3/2} \times 1640^2 \times 197}$$

$$= e^{-20.0625} \quad \text{lbs/ft}^3$$

$$= 0.044 \quad \text{ppm}$$

c) Dispersion Under Stable (F): Fumigation Condition

Assuming a ceiling height (this has to be obtained from weather data)	h	1,000	ft
Downwind distance - same as in case b)	x	10	nautical miles
Dispersion coefficient at effective distance (x_e) for fumigation condition (atmosphere C) from Figures 6-17a and 6-17b)	σ_y	4,900	ft

Hence ground level concentration (see equation 6-47)

$$= \frac{2.4 \times 10^6}{2\pi \times 4900^2 \times 1000}$$

$$= 1.59 \times 10^{-5} \quad \text{lbs/ft}^3$$

$$= 361.0 \quad \text{ppm}$$

The ground level concentrations for various atmospheric conditions are plotted as functions of downwind distances in Figures C-1, C-2, C-3, and C-4 respectively for 100, 500, 1000, and 3000 ton spills. The curves for atmosphere F indicate the fumigation condition, which is the worst condition as can be seen from the examples in b) and c). In calculating these stable atmosphere curves, the ceiling height for each value of spill was evaluated from the plume theory assuming a temperature gradient of 5°K/km. It is recalled here that under fumigation conditions, the ceiling height depends on the weather and as such has to be obtained from weather data. Therefore, the curves given for atmosphere F are to be used with care and where necessary have to be recalculated using the proper ceiling height data.

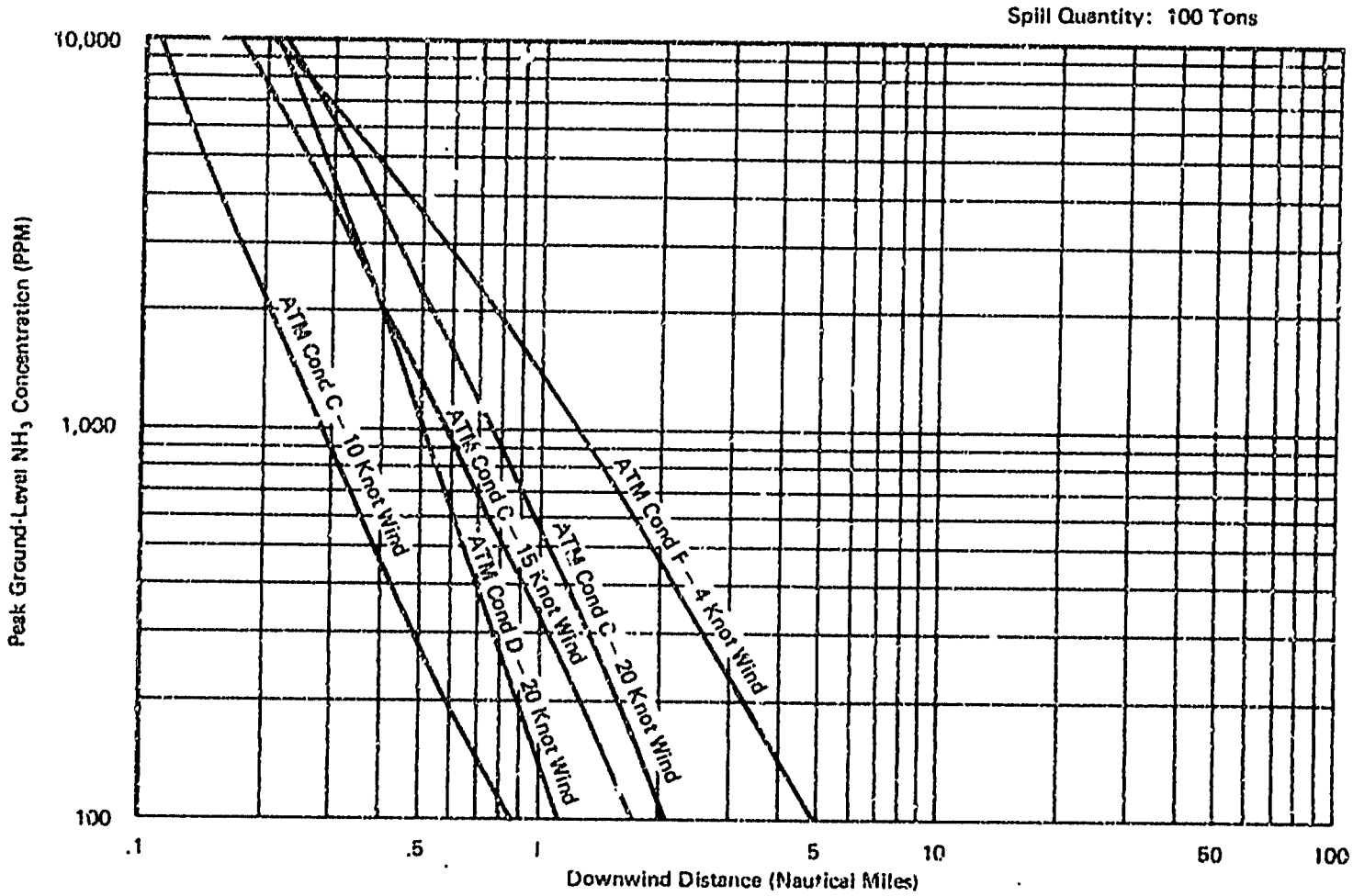
Spill Quantity: 100 Tons
10,000
1,000
100
Peak Ground-Level NH_3 Concentration (PPM)
.1
.5
1
5
10
50
100
Downwind Distance (Nautical Miles)
ATM Cond C – 10 Knot Wind
ATM Cond C – 15 Knot Wind
ATM Cond C – 20 Knot Wind
ATM Cond D – 20 Knot Wind
ATM Cond F – 4 Knot Wind

FIGURE C-1

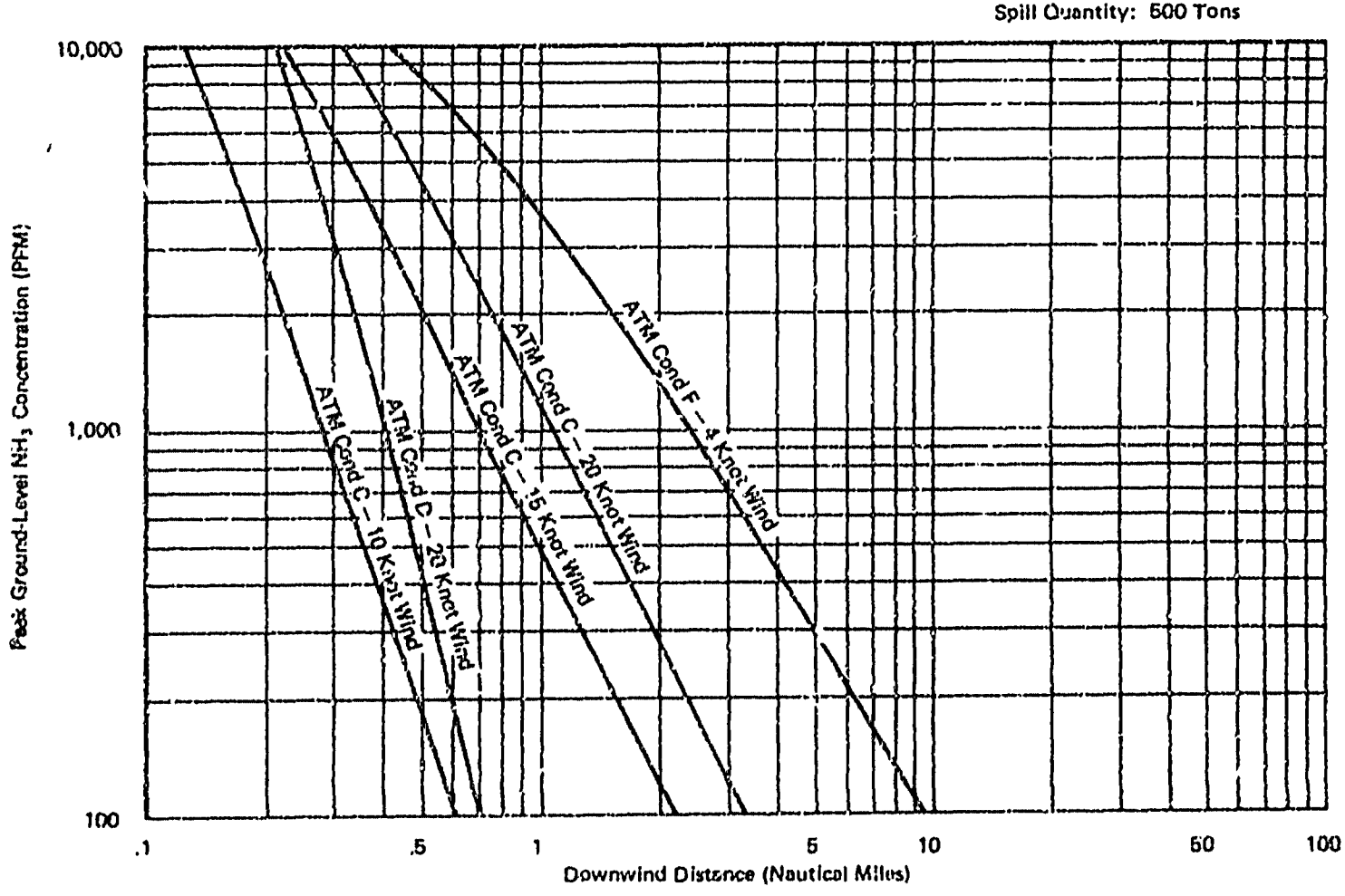
Spill Quantity: 500 Tons
10,000
1,000
100
Peak Ground-Level NH3 Concentration (PPM)
.1
.5
1
5
10
50
100
Downwind Distance (Nautical Miles)
ATM Cond F — 4 Knot Wind
ATM Cond C — 20 Knot Wind
ATM Cond C — 15 Knot Wind
ATM Cond C — 23 Knot Wind
ATM Cond C — 10 Knot Wind

FIGURE C-2

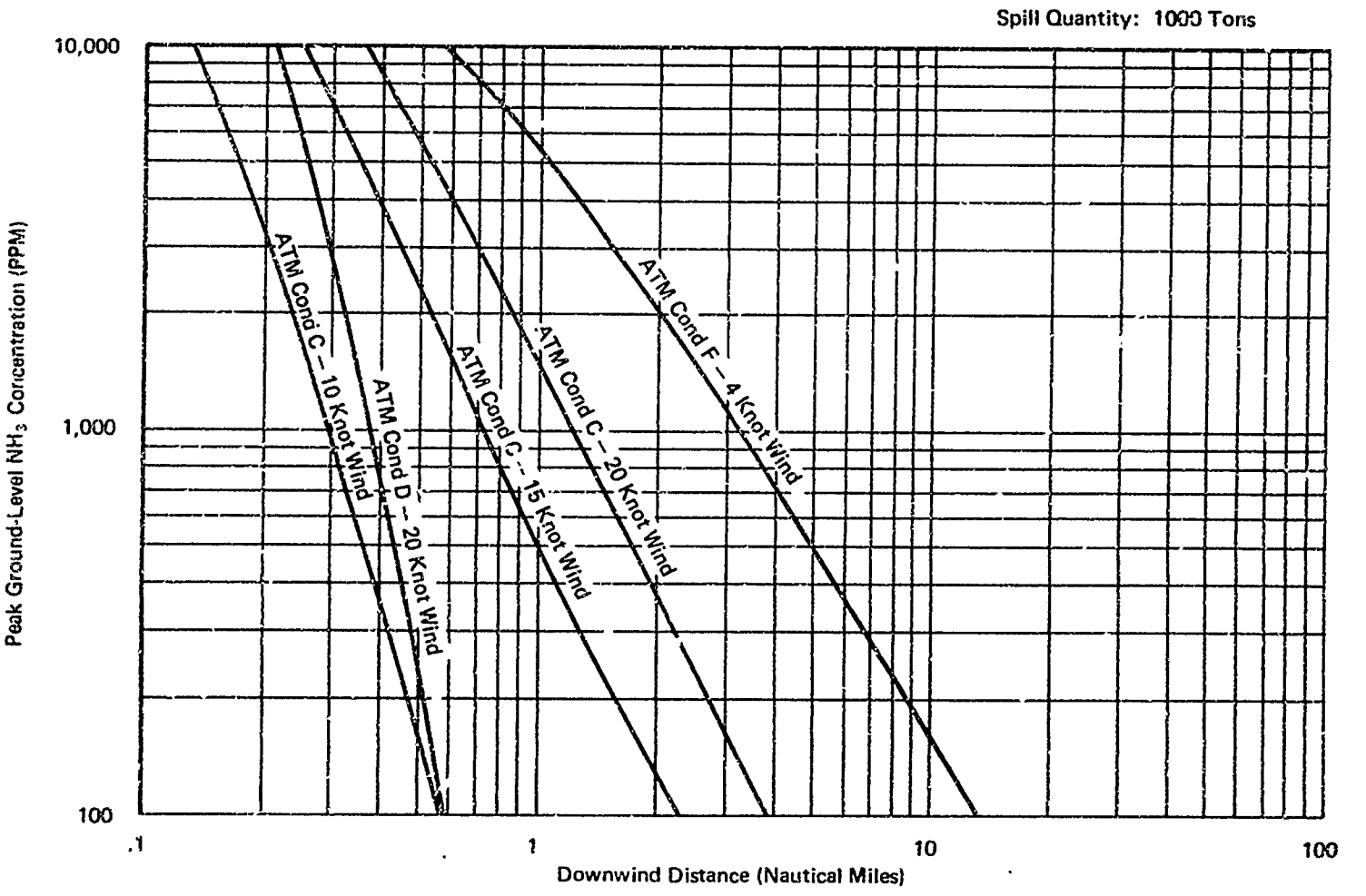
Spill Quantity: 1000 Tons
10,000
1,000
100
Peak Ground-Level NH_3 Concentration (PPM)
.1
1
10
100
Downwind Distance (Nautical Miles)
ATM Cond C – 10 Knot Wind
ATM Cond D – 20 Knot Wind
ATM Cond C – 15 Knot Wind
ATM Cond C – 20 Knot Wind
ATM Cond F – 4 Knot Wind

FIGURE C-3

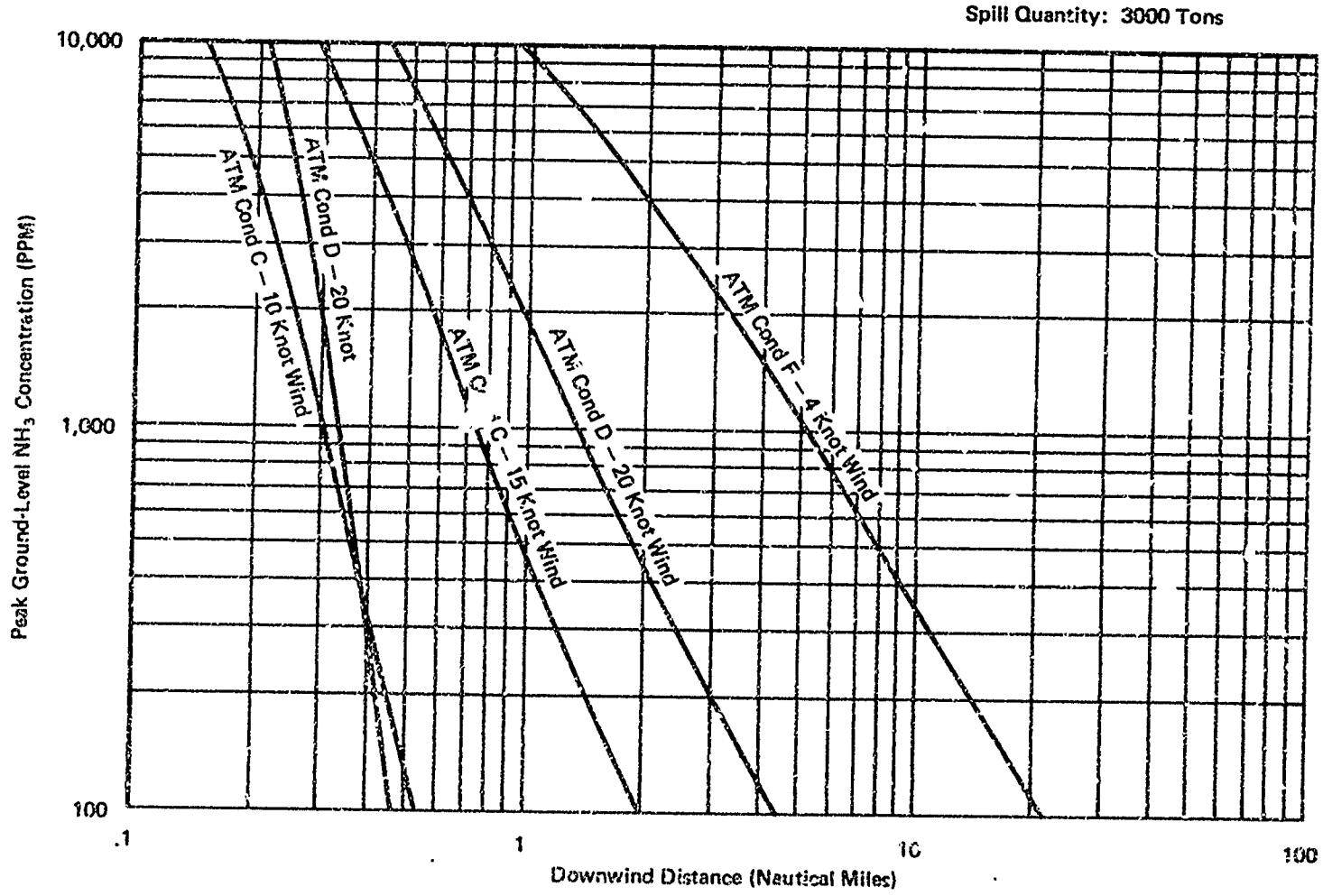
Spill Quantity: 3000 Tons
10,000
1,000
100
.1
1
10
100
Peak Ground-Level NH_3 Concentration (PPM)
Downwind Distance (Nautical Miles)
ATM Cond C — 10 Knot Wind
ATM Cond D — 20 Knot
ATM C
C — 15 Knot Wind
ATM Cond D — 20 Knot Wind
ATM Cond F — 4 Knot Wind

FIGURE C-4

Section 2: Water Dispersion

Introduction

The ammonium hydroxide (NH_4OH) formed by the dissolution of LNH_3 in water is dispersed by molecular diffusion in quiescent water and by turbulent mixing in flowing streams. In the case of flowing rivers and streams, the downstream NH_4OH concentration is calculated by using the water dispersion models.

In this section, numerical examples are given, indicating the calculating procedure to obtain the NH_4OH concentration. A 3,000-ton surface spill of LNH_3 is considered.

In the examples shown below, both the near field and far field calculations are indicated. The near field approximation gives NH_4OH concentrations in the immediate vicinity of the spill. The far field model is used for distances beyond which there is no appreciable vertical mixing. Because of the nature of the assumption made in the derivation of these two models, there is bound to be some discontinuity in the values of NH_4OH concentrations predicted by the models in the common regions of applicability. Hence, proper judgment has to be exercised in interpreting the concentration values obtained in these regions.

Calculations

In the calculations shown below, the following assumptions are made:

- Even though ammonium hydroxide is lighter than water, we assume that this does not have any significant effect on the dilution process.
- No evaporation of the ammonium hydroxide takes place during dilution.
- The spill is instantaneous.

Spill and environmental conditions:

Quantity of Spill	= 3,000 tons = 6×10^6 lbs ≅ 10^6 gallons
Density of LNH_3	= 42.56 lbs/ft^3
Partition Ratio	= 0.6
Location of Spill	= In the middle of a nontidal river
River width	= 1,000 ft
River depth	= 50 ft
Roughness factor for riverbed	= 0.03
Mean velocity in the river	= U = 3 ft/sec
Downstream distance at which maximum concentration is to be known for near field approximation	= 0.5 nautical miles ≅ 3,000 ft
Downstream distance at which maximum concentration is to be known for far field approximation	= 10 nautical miles ≅ 60,000 ft
Total quantity of 100% ammonium hydroxide generated in a surface spill	= $0.6 \times 6 \times 10^6 = 3.6 \times 10^6$ lbs
Hydraulic depth of stream R_h	= $\frac{1000 \times 50}{1000 + 2*50} = 45.45$ ft
Shear velocity (see Table 6-3) u^*	= $3.3 \times .03 \times 3 \times (45.15)^{-1/6}$ = 0.16 ft/s

The concentration at any point downstream of a surface spill is a maximum on the water surface. For the near field analysis, the source is considered to be an area source because of the rapid spread of LNH_3 on water. For underwater releases, at sufficient depths all of the LNH_3 should be assumed to dissolve in water. The location of the maximum NH_4OH concentration downstream for underwater release is not necessarily at the level of the release. This is because of the buoyant nature of NH_4OH. However, for large downstream distances, the location of release hardly influences the concentration.

Near Field Approximation

Time at which concentration is maximum at x = 3000 ft

$$= \frac{x}{U} = \frac{3000}{3} = 100 \text{ sec}$$

Estimated turbulent diffusion coefficient (e_z) (see Table 6-3) for narrow river

$$= 0.067 \times 0.16 \times 45.45$$
$$= 0.49 \text{ ft}^2/\text{sec}$$

Maximum radius of spill, R_{max}

$$= 2.5 \text{ (gallons spilled)}^{0.375}$$
$$\cong 454 \text{ ft}$$

Equivalent thickness of 100% concentration NH_4OH layer (see Figure 6-19 and equation 6-49)

$$= \frac{3.6 \times 10^6}{42.56 \times \pi \times (454)^2}$$

Maximum NH_4OH concentration (see equation 6-52)

$$= 0.144 \text{ lb/ft}^3$$
$$= 2300 \text{ ppm} = 2300 \text{ mg/l}$$

Far Field Approximation

It can be seen that the near field approximation gives a constant concentration for sufficiently large time. This occurs because the derivation of the equation neglects longitudinal dispersion - the only mechanism by which dilution will take place once the vertical distribution of NH_4OH in the water becomes uniform.

Therefore, for concentration predictions at long times, equation 6- is used to allow for longitudinal dispersion.

Longitudinal dispersion coefficient (see equation 6-55) (E)

$$= 23.3 R_h U^*$$
$$= 23.3 \times .16 \times 45.45$$
$$= 169.4 \text{ ft}^2/\text{sec}$$

Time at which concentration is maximum at x = 61,000 ft

$$= \frac{x}{U} \cong \frac{60,000}{3} = 20,000 \text{ sec}$$

Maximum NH_4OH concentration (see equation 6-53)

$$= \frac{3.6 \times 10^6}{1000 \times 50\sqrt{4\pi \times 169.4 \times 20,000}}$$
$$= .011 \text{ lb/ft}^3$$
$$= 177 \text{ ppm} = 177 \text{ mg/l}$$

Discussion

To facilitate a rapid hazard assessment of the water pollution from an LNH_3 spill on water, Figures C-5 through C-8 are drawn. These Figures indicate the maximum NH_4OH concentration as a function of the downstream distance in nontidal rivers. The stream width is treated as a variable in addition to the spill quantity. The stream depth is kept a constant at 50 feet.

The plots were generated using the two models illustrated earlier. However, in the overlapping regions, continuity between the two models is provided using subjective judgment (to give conservative concentration estimates).

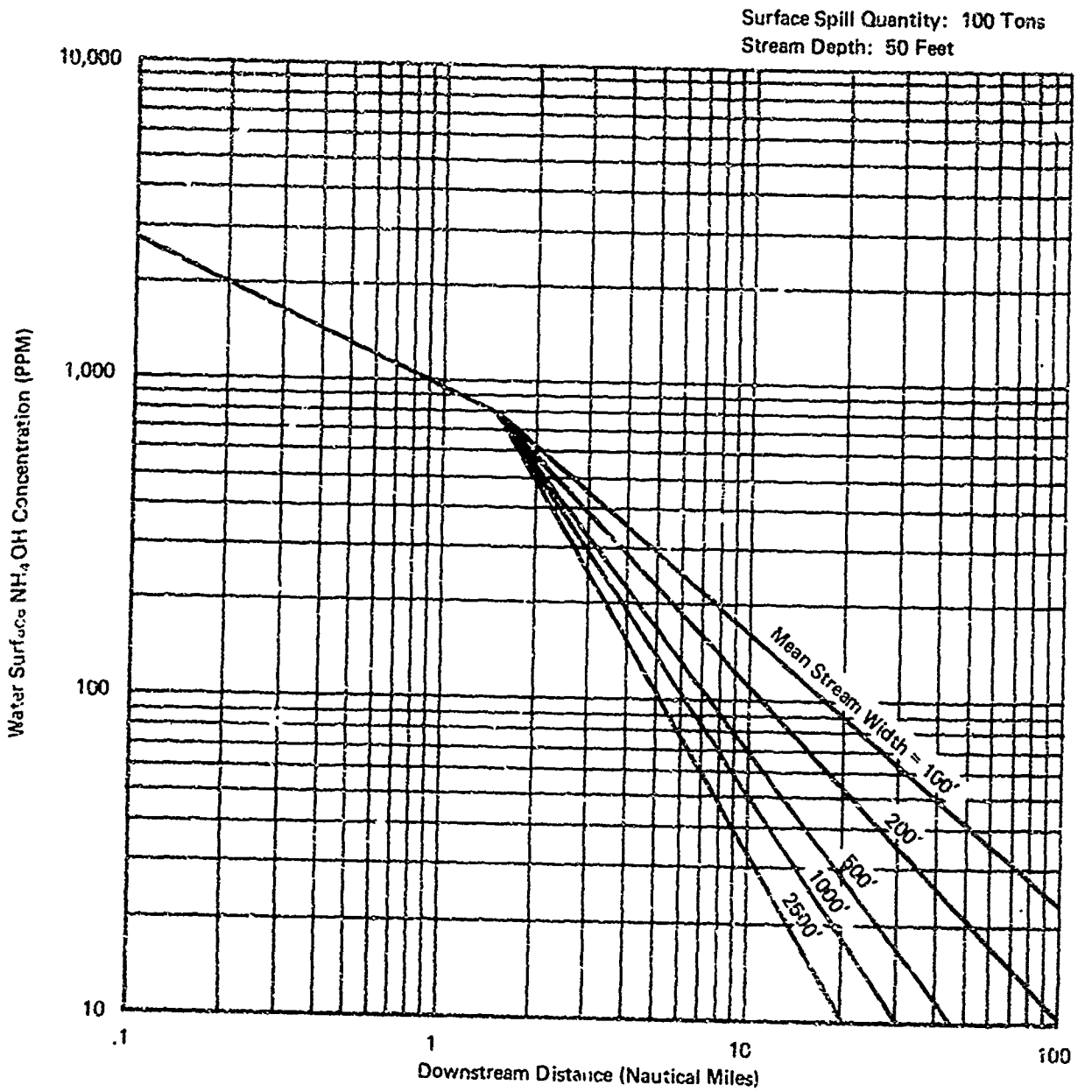

FIGURE C-5

Water Dispersion Hazard Assessment Plot for
Surface Spill Quantity of 100 Tons

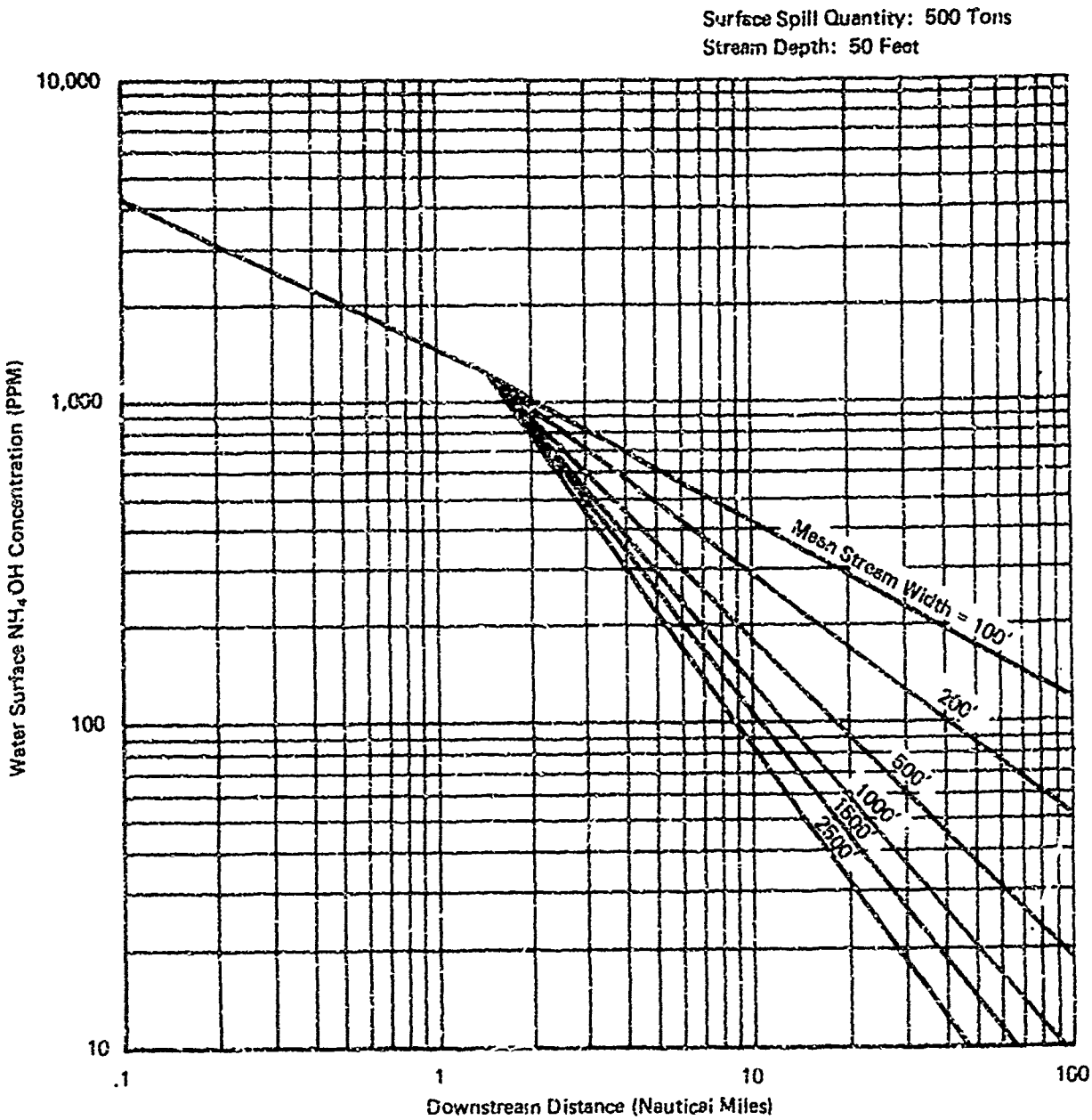

FIGURE C-6

Water Dispersion Hazard Assessment Plot for
Surface Spill Quantity of 500 Tons

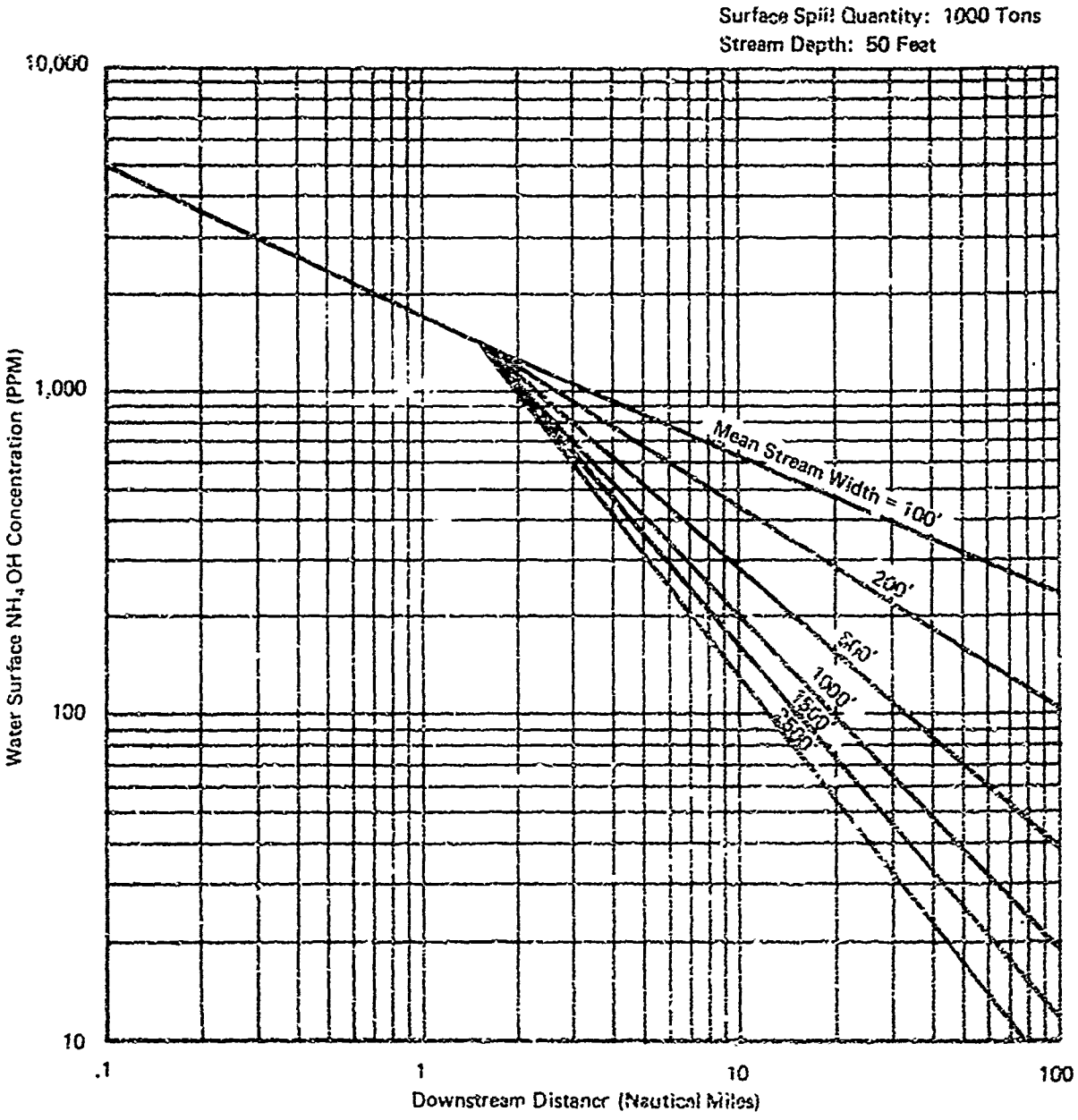

FIGURE C-7

Water Dispersion Hazard Assessment Plot for
Surface Spill Quantity of 1000 Tons

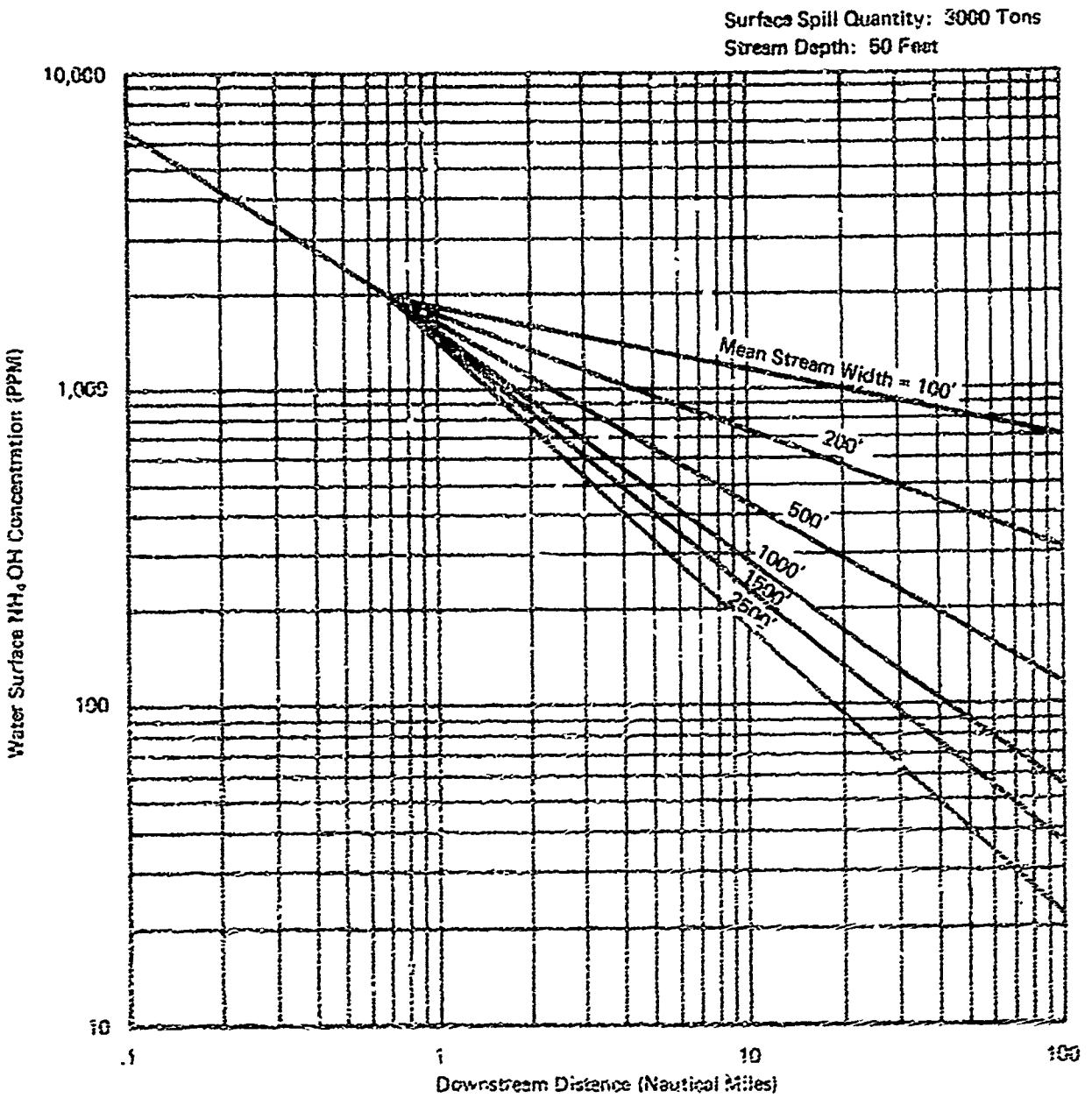

FIGURE C-8

Water Dispersion Hazard Assessment Plot for

Surface Spill Quantity of 3000 Tons